Porcupines for river training

A study on the near-field effect of porcupines

G.E. Nientker

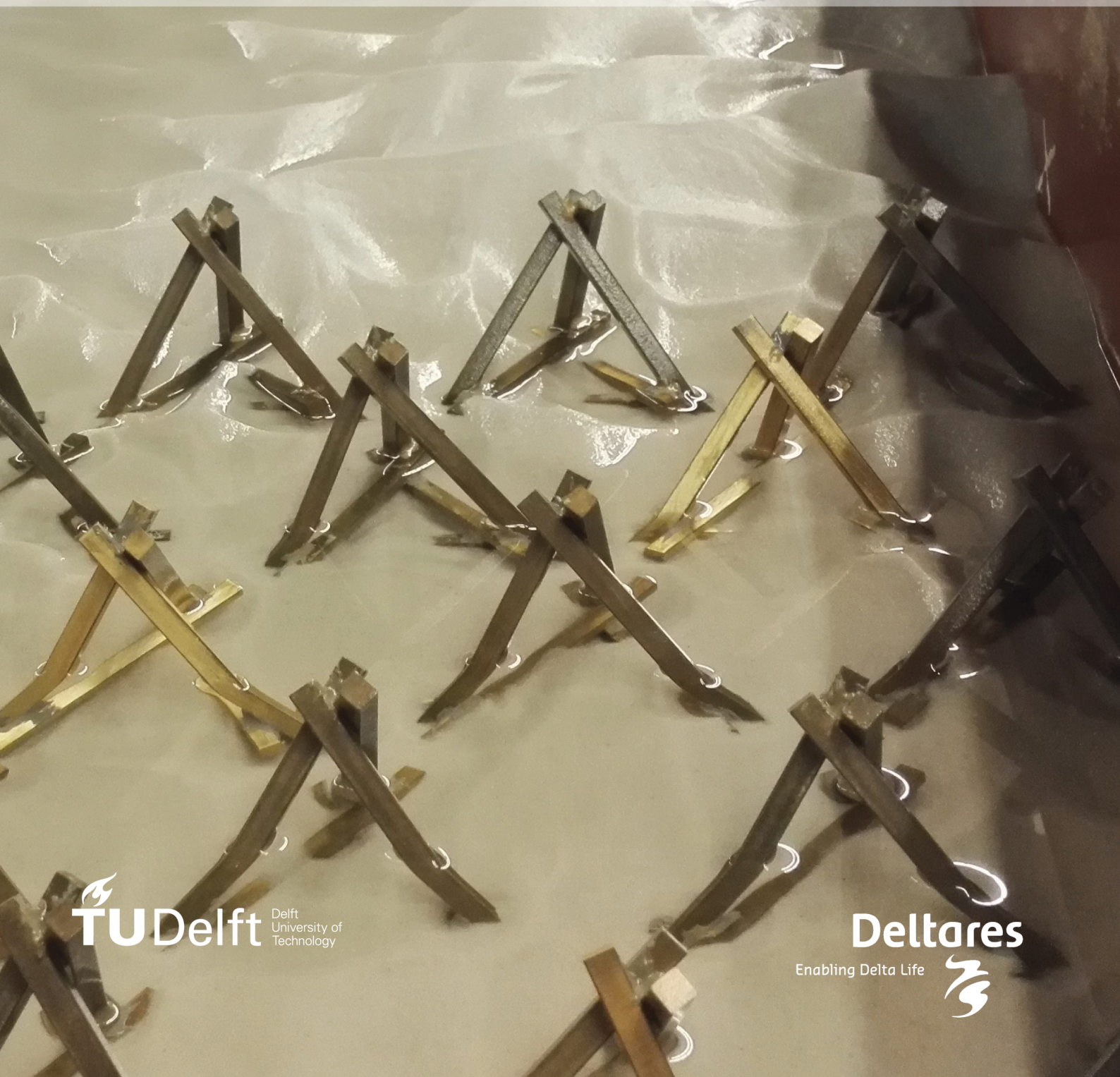

TU Delft Delft University of Technology

Deltares
Enabling Delta Life

Porcupines for river training

A study on the near-field effect of porcupines

by

G.E.Nientker

in partial fulfilment of the requirements for the degree of

Master of Science
in Civil Engineering

at the Delft University of Technology (TU Delft)
to be defended publicly on Tuesday July 10th, 2018 at 10:30 AM.

Student number:	4156293	
Project duration:	October 1, 2017 – July 10, 2018	
Thesis committee:	Prof. dr. ir. W. S. J. Uijttewaal,	Delft University of Technology
	Dr. ir. C. J. Sloff,	Delft University of Technology & Deltares
	Dr. ir. E. Mosselman,	Delft University of Technology & Deltares
	Dr. F. Schuurman,	Royal HaskoningDHV

An electronic version of this thesis is available at http://repository.tudelft.nl/.

Cover: Porcupines in a drained flume after an experiment, Fluid Mechanics Laboratory at Delft University of Technology, Photography by Gustav Nientker

TU Delft Delft University of Technology

Deltares Enabling Delta Life

Acknowledgement

This thesis concludes the Master of Science program in Hydraulic Engineering at Delft University of Technology. This research was partly conducted at the fluid mechanics laboratory at Delft University of Technology and partly at the research institute Deltares. I would like to thank Deltares for the opportunity to execute this project in their open and inspiring environment. I appreciate the willingness of each colleague to make some time and help when needed. Also, I would like to thank the skilled staff in the lab for always being available to work out problems in the flume, both big and small.

Special thanks go to my graduation committee, whose guidance was invaluable in executing my laboratory experiments. I would like to thank the committee members, Wim Uijttewaal, Kees Sloff, Erik Mosselman and Filip Schuurman for all their effort. My sincere gratitude goes to Wim Uijttewaal for your profound knowledge in the environmental fluid mechanics and your contribution in improving the experimental measurements during our fruitful discussions. Kees, your practical viewpoint always helped me to focus on what was most relevant in this study. Thank you for your ability to always put things into perspective. I enjoyed your weekly surprising visits at the laboratory and the interest you showed in the newest findings. Erik, thank you for your enthusiasm and critical feedback. You have always helped me to better understand the underlying theoretical background. I am also very grateful for your experience in writing a good report. Filip, your close involvement in the project from a practical point of view made me realise that the findings in the laboratory can be extremely valuable. Thank you for your contributions and the valuable comments you provided from an engineering perspective.

Furthermore, I would like to thank my fellow graduate students at Deltares for their advice and relaxing discussions during coffee breaks. You were great sparring partners as well as a very welcome distraction whenever I needed it. I would also like to specially thank my laboratory buddies Raoul and Roland who were always there during exhausting and endless days, evenings and weekends of measurements. Without your presence the time spent in the laboratory would have been less joyful. Your willingness to help each other out when needed was much appreciated.

Last, but certainly not least, this achievement would not have been possible without the support of my close family and friends, for which I am ever grateful. To all my housemates, thank you for enduring my endless whining and for carrying me through the tough moments I have experienced. You guys helped me wherever possible. Especially Daan, thank you for your dedicated help with Matlab. Without you I would still be processing data. To my mother and sister: Ingrid and Laura, thank you for believing in me, for your unconditional support and for providing the opportunity to study in Delft. I think dad would be proud. Finally I would like to express my gratitude towards my girlfriend, Thysia. I would like to thank you for being the patient and loving girlfriend you are. You always put everything aside to try and help me however you can and therefore I am forever grateful. You put my mind at ease and give me the strength and motivation to continue. Without you the past 7 years in Delft would not have been the same.

G.E. Nientker
Delft, July 2018

Summary

Braiding rivers are characterised as highly dynamic, and experience annual morphological changes in planform. This dynamic nature of the river leads to navigational hindrance and risk of unstable bifurcation points where discharge distributions might switch. In pilot studies, porcupines have shown promising results in retarding the flow and cause sediment deposition near river banks to prevent bank erosion. However the aim now becomes to apply the porcupines on a much larger scale to increase the channel roughness and influence discharge distributions of bifurcation points such that the flow is mainly diverted to the channel where the highest discharge is required. This way the main channel receives the largest discharge and therefore sedimentation in these channels is prevented. Currently it is not known how porcupines should be modelled in a numerical model. It is simply assumed that porcupines can be modelled similar to vegetation which is schematised as rigid cylinders with a certain density, drag coefficient and resulting representative roughness. No measurements are available to validate the assumed roughness of porcupines and if the hydro- and morphodynamic behaviour, represented by the model, is true.

In this thesis laboratory experiments are conducted to assess the near-field hydro- and morphodynamic effect of porcupines and generate more knowledge about their behaviour. Experiments with a concrete bottom give a detailed insight in the hydrodynamic behaviour of porcupines without the interference of bedforms and morphological developments. Experiments with a sediment bottom give more insight in the morphological development and flow patterns over time which clearly influenced the initial hydraulic behaviour. Experiments are conducted in a 12 metre long and 0.8 metre wide flume with a recirculating pump. The water level, discharge, density of the porcupine field and configuration of the field are systematically varied to identify the dependences on the drag and sedimentation/erosion volumes in the near-field domain of the porcupines. Additionally, general observations are performed, describing the flow structures and sedimentation patterns in and around the porcupine field.

From fixed-bed experiments it is observed how the flow is retarded by the presence of porcupines. Flow is pushed around the field in both transverse and vertical direction. Behind the porcupines, longitudinal flow vectors are downward directed and the flow velocity near the bed is significantly reduced. It is observed that staggered porcupine grids help to retard the flow stronger and captures sediment behind the field in wider strokes. Non-staggered grids only work effectively in the line of porcupines. Between those lines barely any retardation is observed and therefore only narrow strokes of sedimentation are observed behind the lines of porcupines. The reduction in flow velocity behind the porcupines is similar to the velocity reductions observed in experiments with vegetation. The velocity retardation is gradually restored in longitudinal direction where the effect of porcupines gradually diminishes. For different experiments this deceleration of the flow has been observed and it follows a linear trend line, that by means of extrapolation can be used to quantify the effective retardation length in longitudinal direction. Water level differences over the porcupine field are observed indicating loss of energy, and pushing up the water level upstream. Porcupines can effectively influence bifurcation points in braiding rivers this way. The local water level gradient over the porcupine field, combined with the velocity measurements, is used to determine the drag and representative roughness of the porcupines by using the equations of Baptist. The obtained values for the roughness are validated by simulating the flume in SOBEK with the corresponding roughness coefficients. Comparing the measured water levels with the computed water levels by the model gave a relatively good fit indicating that porcupines can be schematised by the equations of Baptist with a few adjustments. The Reynolds stresses give an indication of the height of the bed shear stresses. Measurements show that the shear stress in the near-bed region behind the porcupines is lower or the same compared to the undisturbed velocity profile. Lower bed shear stresses indicate a reduction in sediment transport and is therefore an important mechanism to reduce the bedload sediment transport.

Mobile-bed experiments show clear erosion patterns inside the porcupine field due to the increased turbulence intensity generated by the porcupines themselves. For the experiment with low water levels and high flow velocities erosion is observed to be most severe, whereas in experiments with lower field density an

overall sedimentation is observed inside the porcupine field. Due to the erosion porcupines sink into the bed significantly reducing their effectiveness on retarding the flow. To prevent scour larger spacing between the porcupines seems beneficial. A growing sedimentation ridge behind the porcupines is observed that influences the flow retardation even stronger, enhancing further sedimentation. Once maximum sedimentation height is reached, the ridge will migrate downstream as a growing sedimentation bar gradually sloping down towards its initial bed level. This length scale of the sedimentation bar is comparable with the retardation length scale. Combined with the migration rate of the sedimentation bar an estimation of the time scales can be obtained. Based on the mobile-bed experiments it is concluded that least erosion within the field is beneficial and therefore low water levels and high flow velocities should be avoided.

Although initial results show that porcupines show similar behaviour compared to vegetation and that the roughness can be estimated by using the equations of Baptist it has become clear that there are still major differences between the behaviour of vegetation and porcupines. Therefore further research is required to improve schematisations of porcupine behaviour, especially to improve the schematisation of the sediment transport around porcupines since no descriptions are yet available.

Contents

List of symbols

Symbol	Description	Unity
A	frontal area of porcupines	[m^2]
B	river width	[m]
b	degree of non-linearity of sediment transport versus depth-averaged flow velocity	[-]
C	Chézy coefficient	[$m^{1/2}/s$]
C_b	bed roughness Chézy coefficient	[$m^{1/2}/s$]
C_D	drag coefficient	[-]
C_p	representative porcupine Chézy coefficient	[$m^{1/2}/s$]
C_r	representative vegetation Chézy coefficient	[$m^{1/2}/s$]
c_f	friction coefficient	[-]
D_i	median grain size of the sediment fraction	[m]
D_{50}	median sediment grain size	[m]
D_{90}	sediment size for which 90% is smaller	[m]
d_*	dimensionless particle diameter	[m]
E_{spir}	calibration coefficient of the spiral flow	[-]
Fr	Froude number	[-]
g	gravitational acceleration	[m/s^2]
H	energy head	[m]
h	water depth	[m]
I	spiral flow intensity	[m/s]
i	longitudinal bed slope	[-]
K	total kinetic energy in turbulent flow	[m^2/s^2]
k	porcupine height	[m]
k_d	erodibility coefficient	[m^2s/kg]
k_r	Nikuradse roughness	[m]
L	length scale	[m]
m	bar mode	[-]
n	Manning coefficient	[-]
n_x	scale of parameter x	[-]
Q	discharge	[m^3/s]
q	specific discharge	[m^2/s]
Re	Reynolds number	[-]
r	relative fluctuation intensities	[-]
s	specific sediment discharge	[$m^3/s/m$]
T	bed-shear stress parameter	[-]
u	flow velocity in x direction	[m/s]
$\overline{u}$	mean flow velocity	[m/s]
$\overline{\overline{u}}$	depth-and time averaged flow velocity	[m/s]
u'	fluctuating part of flow velocity	[m/s]
u_*	shear velocity	[m/s]
$u_{*,c}$	critical shear velocity	[m/s]
u_p	flow velocity in porcupine field	[m/s]
u_0	flow velocity of main flow	[m/s]
v	flow velocity in y direction	[m/s]
w	flow velocity in z direction	[m/s]
x	longitudinal distance	[m]
x_m	model value of parameter x	[-]

Continued on next page

Symbol	Description	Unity
x_p	prototype value of parameter x	[-]
x_{sf}	location of sedimentation front in longitudinal direction	[m]
Z	Rouse number	[-]
z	vertical distance	[m]
z_0	zero-velocity level	[m]
z_b	bed level	[m]
Δ	relative density	[-]
δ	thickness of boundary layer	[m]
ϵ	erosion rate	[m/s]
κ	von Kármán constant (≈ 0.4)	[-]
λ_p	bed porosity	[-]
μ	variance	[-]
ν	kinematic viscosity	[m^2/s]
ξ	hiding and exposure factor	[-]
ρ_w	density of water	[kg/m^3]
ρ_s	density of sediment	[kg/m^3]
σ	standard deviation	[-]
τ	shear stress	[N/m^2]
τ_b	bed shear stress	[N/m^2]
τ_c	critical bed shear stress	[N/m^2]
$\tau'_{b,c}$	grain-related bed-shear stress	[N/m^2]
τ_p	porcupine shear stress	[N/m^2]
τ_t	total shear stress	[N/m^2]
ϕ_r	direction of bed load transport relative to primary flow direction	[°]
ϕ_s	direction of sediment transport due to bed slope effect	[°]
ψ	Shields mobility parameter	[-]
ψ_c	critical Shields mobility parameter	[-]

1 Introduction

This chapter gives the problem description for the thesis based on the situation in the Ayeyarwady river in Myanmar in section 1.1. Elaboration on the problem definition is given in section 1.2, from which the research itself is extracted. The research objectives and research question are described in section 1.3. Section 1.4 describes the method applied for this research and in the final section the outline of the report is given.

1.1. Background information

The Ayeyarwady river is a large braided river system in Myanmar and passes one of the major cities of the country, Mandalay. The key characteristics of the Mandalay/Sagaing section of the Ayeyarwady are determined by geological 'fixed' points. A few kilometres north of Mandalay the Ayeyarwady river is trifurcated after such a geological fixed location into the Mandalay channel (left), a middle channel and the Sagaing channel (right). The current main navigational channel towards the harbour of Mandalay is the Mandalay channel and is hampered by annual siltation and bar migration in front of the port which is one of the two important risks at this location (Commandeur et al., 2017).

Figure 1.1: Mandalay/Sagaing section

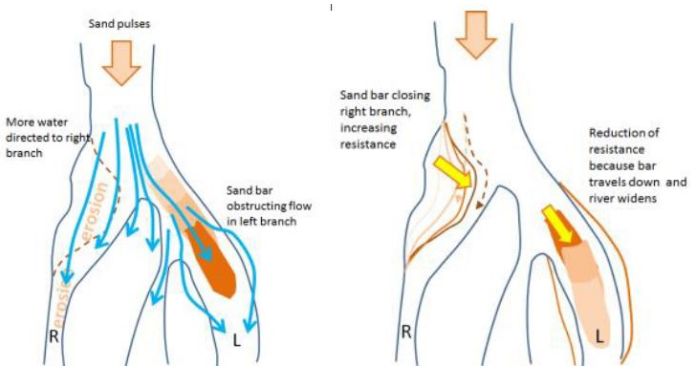

Figure 1.2: Schematic representation of the causes for a channel switch, adopted from (Commandeur et al., 2017)

The second risk for the Mandalay port is the possibility of a main channel shift towards the Sagaing channel visualised in figure 1.2. During the past couple of years the Mandalay channel has been the dominant channel, but satellite images show that this has not always been the case. In 1993 the Sagaing channel was the dominant channel indicating that channel shifts happen in this part of the river. This is the effect of the sudden widening of the river reach where the sediment transport capacity reduces which results in sedimentation. The generated sand bar inside the channels causes blockage of the flow which enhances the switch towards the other channel. After such a migration a counteracting evolution may take place. The curved flow lines from upstream can generate a sandbar at the head of the Sagaing branch that gradually pushes eastward. The off-take angle gradually increases resulting in larger flow curvature at the entrance generating a

spiral flow. This helical flow will bring most of the sediment towards the inner bend, and pushes the water outwards resulting in a growing sandbar and a gradual shift towards the Mandalay channel again. Historical satellite images show that this channel shift occurs with a frequency of 10-30 years.

The Ayeyarwady Integrated River Basin Management Project (AIRBM) is aiming to control the river and proposes river training works along the river near Mandalay. The objective is to achieve a least available depth for shipping towards the harbour of Mandalay, by partly blocking the flow towards the secondary channels. The plan is to implement 'flexible' solutions that are able to be relocated if necessary, since the river is highly dynamic. Creating enough resistance by placing porcupines in the secondary channels may result in a re-distribution of the discharge over the bifurcation points upstream and therefore pushes a larger discharge through the main channel. Solutions such as dams are expensive and may become obsolete over time and are therefore not considered.

Flexible measures can easily be adjusted to fit the new situation. Besides, in the model study by Ostanek Jurina (2017) it has been shown that closing off a channel within a braiding river requires a lot of effort with hard structures. Numerical models can be used to determine the impact of river training measures although permeable structures such as porcupines can not be modelled accurately, since no correct schematisation is present in the model. Currently, porcupines are schematised as vegetation with the equations derived by Baptist (2005) since it is assumed that their effect on flow is similar. For long-term solutions, porcupines were recommended for an effective use. However it is largely unknown if the numerical model represents all the processes correctly and if its outcome is the correct effect of porcupines. It has been shown with experiments that porcupines cause sedimentation and a reduction of flow velocities (Aamir & Sharma, 2015b; Lu et al., 2011), and perform extremely well to prevent bank erosion in the Brahmaputra river (Sarma & Acharjee, 2012). However, these porcupines are not yet applied, nor tested, for large-scale river training measures to stimulate channel closure or to affect bifurcation points.

1.2. Problem description

The origin of this research is based on the applicability of porcupines to gain more control over large braided rivers, such as the Ayeyarwady river. So far no model concepts are present that can determine the amount of sedimentation in or around a porcupine field accurately. The grid resolution in rivers is generally too low to capture individual porcupines, and is therefore parametrized as a sub-grid effect, for example in the bed roughness. It remains largely unknown how the hydrodynamic and morphodynamic effects of the porcupines can best be parametrized. Porcupines are not yet applied on large scale and application of the structures is limited to only a few locations in the world. In these small scale pilot studies the porcupines are solely used as a measure to prevent bank erosion, and not to affect large scale river behaviour. Only a single field configuration has been applied that dates from the work of Brown (1985) while other configurations may be more efficient. Knowledge about the evolution of sedimentation and erosion patterns coupled with certain configurations are desired which are not present at the moment.

Only a small amount of flume experiments have been performed to study the effectiveness of porcupines to prevent bank erosion (Aamir & Sharma, 2014, 2015b; Khaund et al., 2015). However the scientific basis of these studies is lacking. In many experiments the Reynolds number and Froude number are very low. This indicates that the amount of turbulence behind the porcupines might be too small to accurately represent the reality where they will be applied. Furthermore, no analytical relation is present that can predict the amount of sedimentation. To obtain predictive formulas on the amount, location and rate of sedimentation/erosion systematic research is needed on how flow conditions and geometric conditions are of influence. Data analysis performed on the results from flume experiments could be used to further improve numerical models and measurements from real river applications could be used to calibrate such models.

Porcupines are often assumed to have similar behaviour compared to aquatic vegetation. In recent modelling exercises the effect of porcupines is therefore parametrized by adjustign the local bed roughness, applying a methodology that is commonly used for modelling vegetation. Vegetation models are mainly based on the hydraulic effect around stiff cylinders with a certain height. However porcupines are much larger than vegetation and a porcupine field is less dense than a vegetation patch. Therefore it is important to understand their behaviour and identify their difference in schematisation for numerical models. The schematisation by Baptist (2005) only takes into account the hydrodynamic effect without solving for the effect of turbulence. The turbulence contribution is very important for the morphological development however. Nepf (2012a) studied the effect on the turbulence distribution around vegetation. It remains questionable if the formulations for solving turbulence in numerical models represent the effect of vegetation or porcupines correctly.

1.3. Research objective & questions

This research aims to better understand the hydraulic and morphological implications of a porcupine field in a river and predict erosion and sedimentation patterns around the porcupine field. Moreover, it is aimed to better understand porcupines as a measure to counteract bank erosion. Furthermore a description for the roughness is sought that effectively pushes the water upstream from the porcupines to influence the discharge distribution at bifurcation points in braiding rivers. Therefore, the main objective of this thesis is to gain more insight in the near-field hydrodynamic and morphodynamic responses of porcupines and their effect on the river bed. It is aimed to quantify the roughness exerted by the porcupines and erosion/sedimentation volumes on the short term after placement. To achieve the objective of this research the following research question will be central in the thesis:

> *What is the effect of porcupines on the water level and the river bed in the-near field region, and can the behaviour be schematised?*

The following sub-questions have been specified to find an answer to this question:

1. What is the hydrodynamic effect of porcupines?
2. What is the morphodynamic effect of porcupines?
3. What are the dominant processes that cause sedimentation?
4. Can the hydrodynamic effect of porcupines be schematised by the concept of Baptist?
5. Under which conditions is a porcupine field the most efficient to create additional roughness and result in sedimentation?

1.4. Methodology

In order to reach the objective and find the answers to the research questions laboratory flume experiments are used to systematically study the influence of the average velocity, water depth and porcupine field density on the development of the morphology. Additionally, the effect of staggering of the porcupine field is studied. During the experiments three-dimensional velocity measurements are performed to get more insight in the direction of the flow and the amount of generated turbulence. The flow retardation is quantified and water level measurements indicate the energy loss and amount of roughness exerted by the porcupines. Water levels are measured at a fixed upstream and downstream point of the flume to determine water level gradients. Additionally the water level is measured over a transect along the flume to identify the local effect of porcupines on the water level. Finally, underwater measurements of the bathymetry are performed at fixed time intervals to observe the morphological development over time and to identify the amount of erosion and sedimentation in the near field of the porcupines. The sedimentation and erosion volumes are quantified and related to experimental variables. Sedimentation rates are also linked with flow retardation to perform predictions on the equilibrium sedimentation lengths. Finally a relation is sought between the schematisation of Baptist and the observed behaviour of the experiments to check if it is possible for numerical models to schematise porcupines as vegetation.

1.5. Outline of the report

Chapter 2 gives an overview of literature on general flow characteristics related to the laboratory experiments with porcupines. Furthermore the relevant knowledge about porcupines is given and their effect on the hydrodynamics. Finally the fundamental theory about vegetation is given. The experimental set-up is discussed in chapter 3 and chapter 4 elaborates on the results from the fixed-bed experiments. The results from the mobile-bed experiments are discussed in chapter 5. Chapter 6 contains analysis on the experimental data followed by a discussion on the experimental results and the executed analysis in chapter 7. Conclusions and recommendations for further research are given in chapter 8.

2

Literature review

In this chapter the relevant literature is discussed for this research, starting with the consequences of laboratory experiments on reduced scale in section 2.1. Subsequently the most important properties of the flow are discussed in section 2.2 and an overview of permeable structures and further characteristics of porcupines are given in section 2.3. A brief overview of the behaviour and schematisation of vegetation is mentioned in section 2.4 followed by a discussion on the literature and general assumptions for the research based on the findings in the literature in sections 2.5 and 3.4 respectively.

2.1. Scale experiments

The two most important dimensionless numbers for describing flow are the Froude number and the Reynolds number. For scaling down a real river into a flume model one has to account for scale effects related to these two numbers. The Froude number describes the importance of gravitational forces, as given in equation 2.1. From the Froude number it can be derived whether a flow is sub- or supercritical. Flow is subcritical when Fr<1 and supercritical when Fr>1.

The Reynolds number indicates the imporatnce of the viscous forces, as described in equation 2.2. The Reynolds number indicates whether the flow is laminar or turbulent and gives an estimate on the amount of turbulence as well. Flow is significantly turbulent when Re≫1000 (Uijttewaal, 2003).

$$Fr = \frac{u}{\sqrt{gL}} \tag{2.1}$$

$$Re = \frac{uL}{\nu} \tag{2.2}$$

in which

Fr = Froude number [-]
Re = Reynolds number [-]
u = flow velocity [m/s]
g = gravitational acceleration [m/s^2]
L = length scale [m]
ν = kinematic viscosity [m^2/s]

For scaling down a river and the porcupines it is important that the flume is scaled according to a Froude number that remains small enough to prevent supercritical flow. On the other hand however, the Reynolds number is very important for scaling down the porcupines. The length scale applied there is very small, but turbulence is required to remain as close to the reality as possible.

2.1.1. Scale effects

To assure that the experiments behave similarly as the prototype situation, concerning flow and morphology, the ratio of forces should be equal between the model and the prototype. Scale effects arise due to the inability to keep each relevant force ratio constant between the scale model and its real-world prototype (El Kadi

Abderrezzak et al., 2014; Heller, 2011). The most general equation describing scale is given below in equation 2.3 where the scale of a physical quantity is determined as the value of the prototype divided by the value of the model.The inverse of this equation is herein defined as the scale 1:n_x

$$n_x = \frac{x_p}{x_m} \tag{2.3}$$

in which

n_x = scale of parameter x [-]
x_p = prototype value of parameter x
x_m = model value of parameter x

With decreasing model size, increasing scale effects are expected and the up-scaled model results may deviate from real-world prototype observations. The appropriate selection of n_x is therefore an economic and technical optimization and the scale may intentionally be selected in a range where scale effects cannot fully be neglected.

A physical scale model is completely similar to its real-world prototype and involves no scale effects if it satisfies mechanical similarity implying the following three criteria (Heller, 2011):

- geometric similarity
- kinematic similarity
- dynamic similarity

Geometric similarity requires similarity in shape such that all length dimensions in the model are n_x times shorter than of its prototype value. Lengths, areas and volumes therefore scale with n_x, n_x^2 and n_x^3 respectively. *Kinematic* similarity implies geometric similarity and in addition indicates a similarity of motion between model and prototype particles. It requires constant ratios of time, velocity, acceleration and discharge in the model and its prototype at all times. *Dynamic* similarity requires that all force ratios in the two systems are identical. The most important forces are: inertia, gravitation, viscosity, surface tension, pressure and elastic compression. The inertial force is normally the most relevant in fluid dynamics and is therefore included in all common force ratio combinations. In morphodynamics however, inertia can often be ignored as long as $Fr < 0.8$ to 0.9.

Water flow

A large number of force ratios have been defined of which two have already been mentioned in equations 2.1 and 2.2, which are the most important for open water scaling problems. As mentioned previously a model has no scale effects if all three similarities are fulfilled, including all scaled fluid properties and characteristics of the structures and atmospheric pressure. However once the model fluid is identical to the real-world prototype, which it normally is, only one of the two force ratios can be identical between model and it's prototype, and dynamic (and mechanic) similarity is impossible. Besides, the following relations also show that the Froude number and Reynolds number can only both be true on full scale.

$$Fr = \frac{u}{\sqrt{gh}} \rightarrow \frac{n_u}{\sqrt{n_g n_h}} = 1 \rightarrow \frac{n_u}{n_h^{1/2}} = 1 \rightarrow n_u = n_h^{1/2} \tag{2.4}$$

$$Re = \frac{uh}{\nu} \rightarrow \frac{n_u n_h}{n_\nu} = 1 \rightarrow n_u = \frac{n_\nu}{n_h} \tag{2.5}$$

These two relations result in the following condition: $1/n_h = n_h^{1/2}$ since n_ν is 1 where we use normal water. The resulting relation can only be valid if n_h is 1 which means full scale model.

sediment transport

Similarity in sediment transport is established by similarity in Shields number, particle Reynolds number and the relative particle fall velocity. The relative fall velocity is commonly not used when only bedload is examined. All relevant equations on sediment transport are discussed in appendix A.7.

$$\Psi_c = \frac{\rho u_{*,c}^2}{(\rho_s - \rho) g d} \rightarrow n_{\Psi_c} = \frac{n_i n_h}{n_{\rho_s - \rho} - n_d} = 1 \tag{2.6}$$

$$Re_* = \frac{u_* d}{\nu} \rightarrow n_{Re_*} = n_{u_*} n_d = n\tau^{1/2} n_d = n_i^{1/2} n_h^{1/2} n_d = 1 \tag{2.7}$$

To ensure similarity on sediment mobility, the critical Shields number should be equal in both prototype and model. This can be obtained by maintaining a relatively high particle Reynolds number to remain significantly turbulent (El Kadi Abderrezzak et al., 2014). In laboratory models the shear velocity is often relatively low. To obtain an equal Shields number it is possible to use other particles than sand e.g. polystyrene or PVC.

2.2. Flow properties

Flow processes in a river are not constant and do therefore rarely develop a fully logarithmic velocity profile over the water depth. The turbulence is affected by local acceleration and deceleration and consequently determines the sedimentation processes. The sediment transport is highly dependent on the amount of shear stress that is generated by the flow and by the roughness of the bottom. To get a general understanding of these important processes, they will be elaborated below.

2.2.1. Flow type

Uniform flow

A situation with constant speed and no changes in depth is called uniform flow. An equilibrium exists between the bottom shear stress and the component of the fluid pressure on the slope as illustrated in figure 2.1. The slope causes a continuous transformation of potetial energy, via kinetic energy in the main flow and in the turbulent eddies, into heat (Schiereck & Verhagen, 2012). Besides the balance of the acting forces the logarithmic flow profile is given together with its fluctuations in the flow and the amount of turbulence.

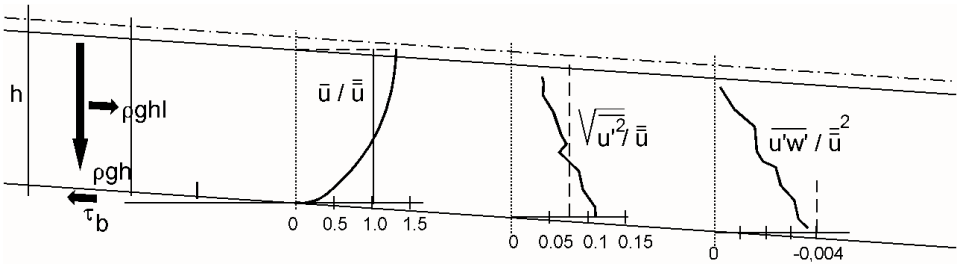

Figure 2.1: Uniform flow with the acting forces (left), followed by the logarithmic profile and turbulence intensities (right), adopted from (Schiereck & Verhagen, 2012)

Normally, river flow is fully developed which indicates that the boundary layer has grown over the entire water depth, resulting in a logarithmic velocity profile, which is elaborated in section 2.2.2. The boundary layer is defined as the region which is influenced by the presence of the wall. In stationary, uniform flow, the boundary layer is fully developed and takes up the entire water depth, leading to the logarithmic velocity distribution as illustrated above. This boundary layer is the part of a water column which is influenced by viscous shear stress created by the bed and results in the relation between the bed shear stress and flow velocity given in equation 2.8. The growth of this boundary layer is a result of the presence of a bed which causes exchange of momentum due to the shear stress along the bed that decelerates the flow locally.

$$\tau_b = \rho g h i = c_f \rho \overline{\overline{u}}^2 = \rho u_*^2 \tag{2.8}$$

in which

τ_b = bed shear stress [N/m^2]
ρ = density of water [kg/m^3]
g = gravitational acceleration [m/s^2]
h = water depth [m]
i = bed slope [-]
c_f = friction coefficient [-]
$\overline{\overline{u}}$ = depth- and time averaged flow velocity [m/s]
u_* = shear velocity ($=\sqrt{\frac{\tau_b}{\rho}}$) [m/s]

The growth of a boundary layer that has not yet been fully developed is illustrated in figure 2.2, where an infinitely thin plate is placed in a flow. When water suddenly flows along a wall, a boundary layer will start to grow (Schiereck & Verhagen, 2012). The growth rate of the boundary layer can roughly be estimated with $\delta(x) \approx 0.02x$ to $0.03x$.

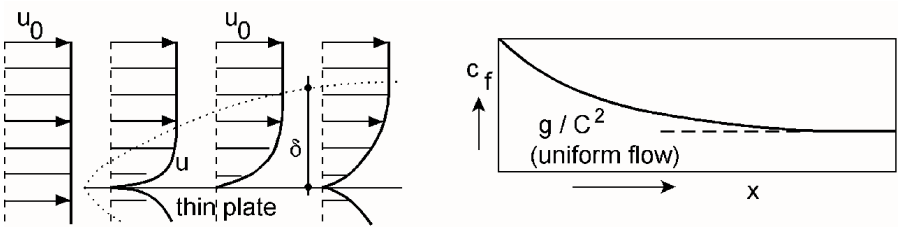

Figure 2.2: Growth of a boundary layer, adopted from (Schiereck & Verhagen, 2012)

With uniform flow conditions, no accelerations or decelerations are allowed. This requirement is important in order for Chézy to be valid. The C (Chézy) coefficient is used to relate the sediment bed roughness to the so-called equivalent roughness according to Nikuradse-Colebrook. The value can be computed for 3 different scenarios: hydraulic smooth, rough or intermediate situations. This will be elaborated in section 2.2.2.

Non-uniform flow

In practice, flow is never uniform. Accelerations and decelerations influence the boundary layer and the turbulence in the flow. In figure 2.2 there are no accelerations or decelerations on a macro level; the thin plate only creates a new boundary layer. When accelerations and decelerations are present, another situation arises. The accelerations are generated by pressure gradients in the flow direction and decelerations are the result of gradients in the opposite direction. Both cause changes in the boundary layer thickness, described by the following equation.

$$\frac{\mathrm{d}\delta}{\mathrm{d}x} = \frac{-(4 \text{ to } 5)\delta}{u_0} \frac{\mathrm{d}u_0}{\mathrm{d}x} \tag{2.9}$$

in which

δ = thickness of boundary layer [m]
u_0 = velocity of main flow [m/s]
x = distance along horizontal axis [m]

The accelerations and decelerations alter the velocity profile for the non-uniform case. If accelerations are dominant the velocity profile becomes fuller, increasing $\partial u/\partial z$ and hence increasing the shear stress. The opposite holds for the case with decelerations.

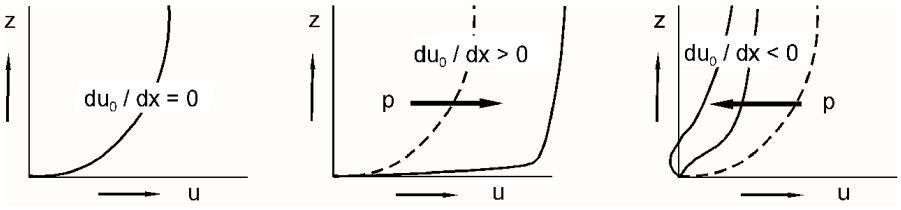

Figure 2.3: Changes to the velocity profile for acceleration (middle) and deceleration (right), adopted from (Schiereck & Verhagen, 2012)

2.2.2. Velocity profile

Assuming uniform stationary flow such that there are no vertical velocities and that no longitudinal accelerations are present, a constant shear stress is acting on the flow. This shear stress can be expressed as a shear velocity as described in equation 2.8. By using this shear velocity a logarithmic velocity profile can be constructed. The velocity at the bed is assumed zero, so a constant zero-velocity coordinate at the bottom (z_0) is

required. This zero-velocity level should be interpreted as a computation parameter without physical meaning (van Rijn, 1993). The position of z_0 depends on the roughness of the bed. The equation that describes the velocity profile is given below.

$$u(z) = \frac{u_{*,c}}{\kappa} \ln\left(\frac{z}{z_0}\right) \tag{2.10}$$

in which

$u_{*,c}$ = critical shear velocity ($= \frac{u_0\sqrt{g}}{C}$)[m/s]
u_0 = average velocity [m/s]
κ = von Kármán constant (≈ 0.4) [-]
z = vertical coordinate [m]
z_0 = zero-velocity level ($u = 0$ at $z = z_0$) [m]

For the zero-velocity level there are three different regimes, hydraulic smooth, rough or intermediate which depend on the ratio between the viscous sublayer and the Nikuradse roughness (k_s) as given below.

smooth flow regime:	$z_0 = 0.11\frac{\nu}{u_{*,c}}$	for	$\frac{u_{*,c}k_r}{\nu} \leq 5$
rough flow regime:	$z_0 = 0.033k_r$	for	$\frac{u_{*,c}k_r}{\nu} \geq 70$
intermediate flow regime:	$z_0 = 0.11\frac{\nu}{u_{*,c}} + 0.033k_r$	for	$5 < \frac{u_{*,c}k_r}{\nu} < 70$

Consequently the bed shear stress described in equation 2.8 and the bed roughness described by the Chézy value are related to the regimes described above, since $c_f = \frac{g}{C^2}$. In turbulent flow the C coefficient can be derived and results in the following expression.

$$C = 18\log\left(\frac{0.37h}{z_0}\right) \tag{2.11}$$

By combining this with the given three expressions above for the different flow regimes determined by the amount of roughness, this results in the following roughness definitions for smooth, rough and intermediate flow conditions.

smooth flow regime:	$C = 18\log\left(\frac{12h}{3.3\nu/u_{*,c}}\right)$
rough flow regime:	$C = 18\log\left(\frac{12h}{k_r}\right)$
intermediate flow regime:	$C = 18\log\left(\frac{12h}{k_r + 3.3\nu/u_{*,c}}\right)$

2.2.3. Turbulence

Turbulent fluid motion is a flow condition in which large irregularities appear and where various quantities show a random variation with time and space coordinates. Because of these large variation over time and space, statistically distinct average values can be discerned. Turbulence is created when kinetic energy is high and capable to overpower viscous forces which decelerate fluid (Uijttewaal, 2003). Turbulence will appear in flows where energy can be transferred from the mean motion to the turbulent fluctuations. A turbulent fluctuation will induce a turbulent shear stress in the presence of a velocity gradient providing the conditions for energy transfer . Two types of turbulence can be distinguished depending on the origin of a velocity gradient. Close to the wall a no-slip condition produces a large velocity gradient, which leads to wall turbulence. Free turbulence exists where adjoining flows have different velocities, creating a gradient on the interface between both flows. Mass and momentum transfer occurs in these, so called, mixing layers (Uijttewaal, 2003). The existence of turbulence leads to energy loss. Energy is shifted from mean motion to smaller turbulent motion. From the really small scales, at the so-called Kolmorogov length scales, turbulent energy is dissipated and converted into heat.

The effect of turbulence can be observed in all aspects of river morphology. It plays an important role on large scale river dynamics, but also affects the sediment transport on very small scale due to increased turbulence of small ripples or dunes on the bed. Turbulence plays a part in the energy dissipation in flow expansions after a river constriction. On a large scale it influences the dispersion of flow patterns and consequently affects the erosion and deposition processes in a braided river. It enhances scour processes by locally

increasing velocities, affecting the local morphological response to various structures (Ostanek Jurina, 2017). On a small scale the amount of turbulence is determined by the effective roughness of the bed topography. Turbulence and roughness will increase as the water depth and, therefore, all bedform dimensions increase. Consequently it affects the sediment transport capacity of the flow and results in higher or smaller amounts of erosion and sedimentation.

As stated before, turbulent motion is highly irregular and chaotic and therefore it is essential to use statistical quantities to describe turbulence. Turbulent fluctuations are by definition deviations from the mean motion such that the value for velocity can be written as a mean velocity ($\overline{u}$) and a fluctuating part (u'). The fluctuating part is represented by the variance which is a measure of kinetic energy (Uijttewaal, 2003).

$$u = \overline{u} + u' \tag{2.12}$$

$$\sigma^2 = \mu = \overline{(u' - \overline{u})^2} \tag{2.13}$$

in which

$\overline{u}$ = mean velocity [m/s]
u' = fluctuating part of velocity [m/s]
σ = standard deviation [-]
μ = variance [-]

For the velocities the variance is a measure of the present kinetic energy in the turbulent fluctuations. To obtain statistically distinct average values of the velocity fluctuations the squares of the velocities are used, since a simple average of the fluctuations are 0 by definition (Schiereck & Verhagen, 2012). The intensity is defined as the square root of this average as can be seen in equation 2.13.

Turbulent fluctuations in the x, y and z direction combined represent the total turbulent kinetic energy per unit mass. This is described by the following equation.

$$K = \frac{1}{2}(\overline{u'^2} + \overline{v'^2} + \overline{w'^2}), \quad r_u = \frac{\sqrt{\overline{u'^2}}}{\overline{u}}, \quad r_v = \frac{\sqrt{\overline{v'^2}}}{\overline{u}}, \quad r_w = \frac{\sqrt{\overline{w'^2}}}{\overline{u}} \tag{2.14}$$

n which

K = total kinetic energy in turbulent flow [m^2/s^2]
u', v', w' = flow velocity of fluctuations in x, y and z-direction [m/s]
$\overline{u}, \overline{v}, \overline{w}$ = average flow velocity in x, y and z-direction [m/s]
r_u, r_v, r_w = relative fluctuation intensities of u,v and w [-]

The Reynols averaged Navier-Stokes (RANS) equation governs the evolution of turbulent fluid motion whereby an instantaneous quantity is decomposed into its time-averaged and fluctuating quantities. Equation 2.15 represents the RANS-equation for a two dimensional situation with uniform flow. The left hand side of the equation represents the change in mean momentum of the fluid. This is balanced by the mean body forces, pressure, viscous stresses and the apparent Reynolds stresses representing the turbulence part of the fluid motion.

$$\underbrace{\rho\left(\frac{\partial \overline{u}}{\partial t} + \overline{u}\frac{\partial \overline{u}}{\partial x} + \overline{w}\frac{\partial \overline{u}}{\partial z}\right)}_{\text{inertia}} = \underbrace{-\frac{\partial \overline{p}}{\partial x}}_{\text{pressure forces}} + \underbrace{\mu\frac{\partial^2 \overline{u}}{\partial z^2}}_{\text{viscous forces}} \underbrace{-\rho\left(\frac{\partial \overline{u'^2}}{\partial x} + \frac{\partial \overline{u'w'}}{\partial z}\right)}_{\text{Reynolds stresses}} \tag{2.15}$$

According to this equation, the shear stress in a steady uniform turbulent flow at a height z can be described as equation 2.16. In case of turbulent flow conditions ($Re > 1000$), the second part of this equation becomes dominant. The first part only becomes dominant in the viscous sublayer close to the bed where turbulent fluctuations are respectively small.

$$\tau = \underbrace{\rho\nu\frac{du}{dz}}_{\tau_\nu} \underbrace{-\rho\overline{u'w'}}_{\tau_t} \tag{2.16}$$

As depicted in figure 2.1 in the far right, the dimensionless Reynolds stress is given over the vertical. It can be noted that close to the bottom the viscous shear stress is neglected. Especially in turbulent regions this

viscous shear stress is negligible. Therefore the Reynolds stress is mainly composed of the turbulent motion and can be described as:

$$\tau = -\rho\overline{u'w'} \tag{2.17}$$

2.3. Permeable training measures

The classic training measures such as groynes, weirs and dams have been extensively studied and monitored in lots of rivers around the world. Their effect is more or less known, and many construction guidelines are available for the use of bank protection, channel deepening or other applications. However, this kind of training works are expensive for countries such as Bangladesh, India and Myanmar. Therefore many countries have developed other cost-efficient measures to protect their banks and gain control over the river. In India many different pilot studies have been performed to test the applicability of porcupines and jack jetties. In Bangladesh other smart engineering works such as falling aprons and bandal structures have been tested. In general the research that has been performed so far can be separated into two categories: research that is solely focused on the effect of the flow around certain training measures, and research that is focussed on the short-and long term morphodynamic effect of certain measures.

Bandals and jack jetties are interesting structures that have shown to be effective for different applications. However, each has its own drawback, as is elaborated in appendix A.1, where their behaviour and applications are explained. For this research the primary focus is on porcupines since little studies have been performed on these structures yet. Porcupines are relatively cheap and easy to construct. They can be constructed out of wood or concrete and are very flexible in their application. Furthmore, when applied as bank protection they have shown to have no significant adverse effect in the upstream and downstream region or on the opposite bank (Kharya & Kumar, 2012).

2.3.1. Porcupines

Just like jack jetties, porcupines are flow altering devices in the form of permeable structures. It is found that the main and most dominant mixing mechanism of the flow adjacent to the permeable structure is the vortex generated by the inflectional velocity profile (Lu et al., 2011). The structures are developed and tested in the early 1970's where their main function was to retard and divert the flow away from river banks (Brown, 1985). Different types of spurs were tested in his work and it was found that porcupine like structures were the most versitile in retarding and deflecting flow. However, they are no longer effective in high flow regimes and in environments with lower sediment concentration. This is further elaborated in appendix A.1. Permeable structures permit through-flow and cause velocity reduction, thereby minimizing scour and causing sediment deposition. Experiments by Lu et al. (2009) show a scour depth reduction up to 83% with the use of porcupine-like structures (tetrahedron frames). Tetrahedron frames are basically the same as porcupines except for the extending spikes at the bar joints. An illustrative sketch of a porcupine is given in figure 2.4 and for a tetrahedron frame in figure 2.5.

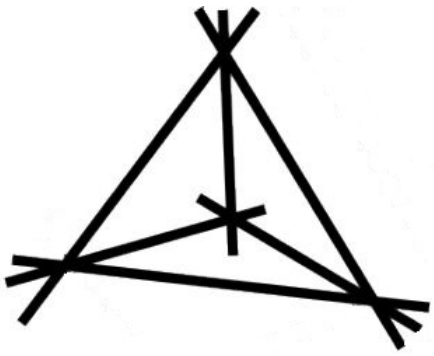

Figure 2.4: Porcupine construction, adopted from (Aamir & Sharma, 2015b)

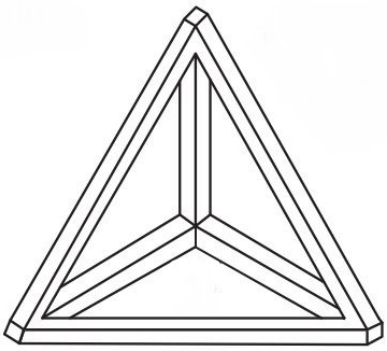

Figure 2.5: Tetrahedron frame construction, adopted from (Lu et al., 2011)

Although porcupines and jack jetties show similar initial results in the field, the focus of this thesis will be on porcupines. They are stronger construction-wise and are preferred in larger river pilot studies such as the Ganga, Brahmaputra-Jamuna, the Kosi and in the Ayeyarwady. Porcupines systems are now seen as one of

the novel techniques that are both flexible, simple and cost-effective. Although they have been sparsely used in real rivers, they do show a lot of potential.

Previous research by Lu et al. (2011) focussed on the turbulence characteristics of flows passing through a porcupine and observed that it reduces the probability of sediment entrainment by retarding the flow and reducing the boundary shear stress. In addition it may induce sediment deposition in a sediment laden flow by changing the flow direction and increasing the energy dissipation. Zhu et al. (2009) carried out studies on three dimensional numerical hydrodynamic models of porcupines based on computational fluid dynamics. Furthermore, the effect of bank protection by porcupines has been studied as well (Aamir & Sharma, 2015a,b; Khaund et al., 2015). Observations in the Brahmaputra show sedimentation where a porcupine screen of about 1 km long was laid out in 2005 (Sarma & Acharjee, 2012). A screen was made of 3 metre high porcupines in 3 numbers of staggering rows from the embankment to a sand bar. Large erosion patterns were observed before placing the screen, but since the porcupines were placed the chronic and severe erosion problem was completely stopped. It functions extremely well in holding the porcupine-generated bed level at that location till date after facing many flood waves. In 2009 more porcupine fields have been placed along the Brahmaputra, and performed extremely well either. In addition to bank protection, porcupines may also be used for protection of bridge piers against scouring (Tang et al., 2009).

Most of the previous research clearly indicates that sedimentation does occur in or behind the porcupine fields, although no clear statement has been made about what happens to the sediment transport further downstream of the porcupine field. Parameters that influence the amount of sedimentation are the field density, the spacing between the porcupines and the submergence ratio (Aamir & Sharma, 2015b).

2.3.2. Flow patterns around porcupines

Although there is a lack of detailed measurements around porcupines and porcupine systems, some numerical modelling of the hydraulics has been performed by Zhu et al. (2009) to predict velocity fields and drags. In figure 2.6 some important results are shown. It was found that the patterns of turbulence intensity distribution for different cases were very similar and were maximum in the rear of the two upstream poles (fig 2.6b), and minimal at some locations close to the bed (fig 2.6c).

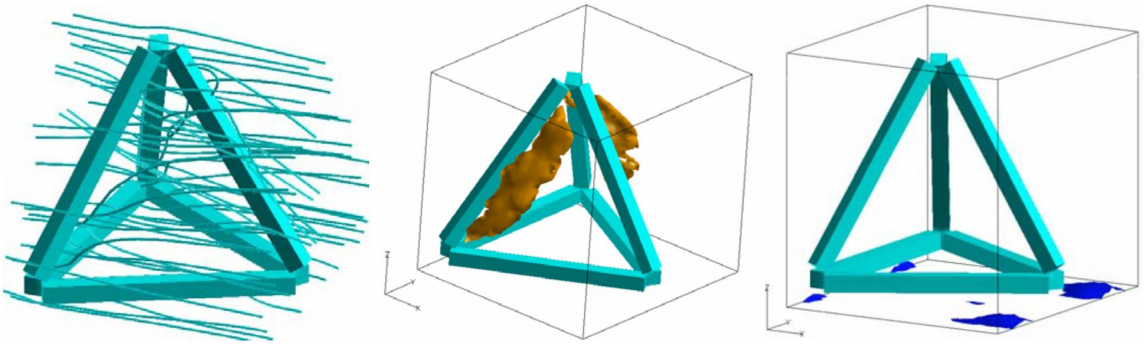

(a) Streamlines around a porcupine

(b) Position of maximum turbulence intensity occurrence

(c) Position of minimum turbulence intensity occurrence

Figure 2.6: Numerical porcupine model results, adopted from (Zhu et al., 2009)

Drag and lift forces on the structure have been computed, resulting in a C_D value of approximately 1.4-1.6 and a C_l of approximately -0.29. The latter means that the lift force acts in the negative z-direction (downwards) and thus improves stability of the porcupines. This observed downward vertical lift force is confirmed by Lu et al. (2011) who also found downward vertical velocities in his study on the turbulence characteristics of flow around a porcupine structure. Furthermore, he observed that with the porcupine structure the mean longitudinal velocity decreased in the retardation zone. However, both the longitudinal and the vertical turbulence intensities were larger than those for the undisturbed approach flow. Because of the retarded flow pattern behind the porcupines a reduced probability of sediment entrainment is achieved resulting in sediment deposition for sediment laden flow (Lu et al., 2009).

The flow field around a single porcupine is also observed and it is noted that the flow is more sensitive to the retardation for un-submerged situations compared to fully submerged conditions. In case of submergence, the flow is diverted upwards and plunges down further downstream resulting in acceleration flow in the upper section of the channel. The evolution of the flow field is summarised in figure 2.7 for the submerged

scenario. It can be seen that the gradient of the longitudinal velocity in the retardation zone decreases as the flow passes through the frame, especially at location (C), as shown by the two dashed circles in the figure. The result of this larger gradient is that the viscous shear stress in the retardation zone also decreases.

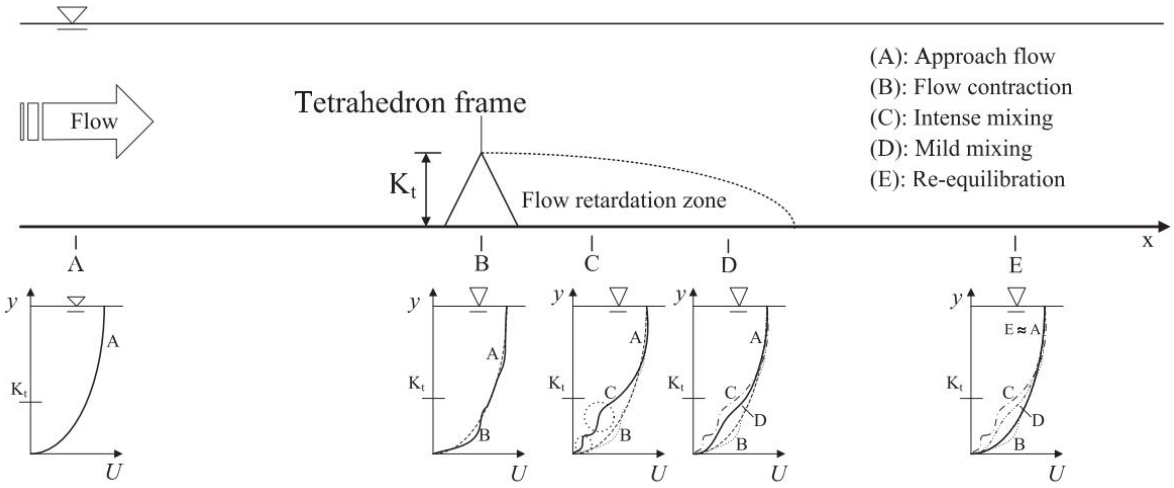

Figure 2.7: Flow field for 2D case around single porcupine, adopted from (Lu et al., 2011)

Finally, Lu et al. (2011) observed that the dimensionless Reynolds Stresses ($-\overline{u'v'}/u_*^2$) at the location where the flow passes through the porcupine decreases close to the bed. The combined effect of a reduced Reynolds stress, reduced velocity gradient and turbulent mixing results in a reduction of the total shear stress close to the bed as well. Measurements show that the total shear stress values close to the bed are smaller than theoretically derived values. It is stated that this is one of the major reasons that scour can be significantly reduced with the placement of the porcupine-like structures.

Scour

Due to the presence of objects in the flow additional scour mechanisms are induced. A common known phenomenon is the bridge pier scour as described in figure 2.8. The basic understanding is that down-flow occurs in front of the object. Behind the object wake vortices are generated, and together with the down flow horseshoe vortices are generated around the object resulting in scour holes around the pier. For slender objects the scour depth is mostly proportional to the pier diameter. For wider objects this proportionality does not seem to apply.

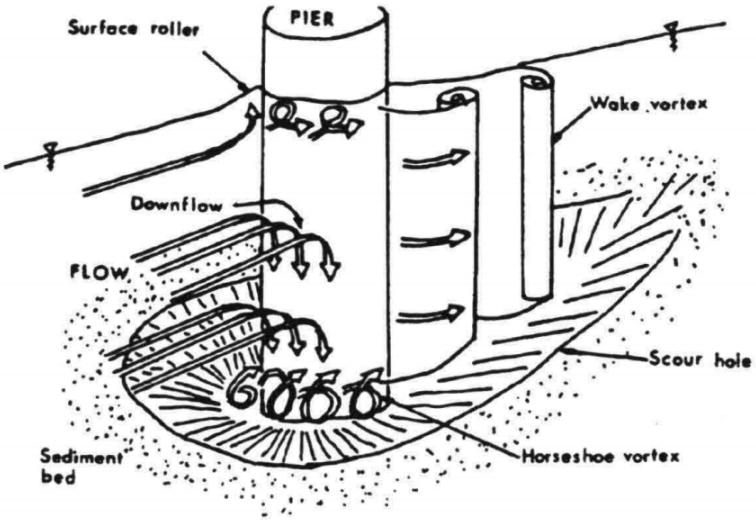

Figure 2.8: Flow patterns around bridge piers, adopted from (Schiereck & Verhagen, 2012)

Porcupines have a far more complicated structure and will therefore induce more complex vortex patterns around the structure. The bridge pier scour effect may partly be present, but also pipeline scour underneath the bottom triangle may arise. No literature exists for scour processes around complex objects like porcupines and therefore no relations exist.

On larger scale there is a relation that describes the amount of erosion or sedimentation over time based on the sediment characteristics and hydraulic conditions. Flow velocities change constantly over the course of a river reach due to shallow areas, curvature or other structures in the flow. This increase or decrease in flow velocity has an effect on the sediment transport rate, causing erosion and sedimentation. The transport of sediment is highly non-linear, which can be observed in the sediment transport formulas, which are discussed in appendix A.7. Large spatial and temporal differences in the flow velocity in rivers are present, and even larger fluxes can be found in the sediment transport. The fluxes in sediment transport lead to deposition and erosion, causing changes in the bed. This can be explained by evaluating the Exner equation:

$$\frac{\partial z_b}{\partial t} = \frac{1}{1-\lambda_p}\frac{\partial s}{\partial x} \tag{2.18}$$

Where,

z_b = bed level [m]
λ_p = bed porosity [-]
s = specific sediment discharge, discussed in section A.7 [$m^3/s/m$]

The equation shows that the bed level change is determined by fluxes of sediment transport. If more sediment enters a certain domain than is being transported out of the domain the bed level increases. The opposite is also true, and leads to erosion. Two types of erosion can be distinguished: bank erosion (horizontal direction) and scour of the channels bed (degradation, vertical direction), whereas deposition of sediment occurs mainly on the channel bed (aggradation, vertical direction) (Jagers, 2003).Both mechanisms will be discussed in appendix A.2.4.

2.4. Flow around vegetation

For the Ayeyarwady morphodynamic simulation with porcupines, using Delft3D, an approach has been used that is developed for modelling vegetation. It assumes that a field of cylindric sticks affect te velocity profile as shown in fig 2.9. This assumption is based on the findings of Baptist (2005) where schematisations for vegetation are derived. Therefore it is important to understand the effect of vegetation on flow and morphology. In the laboratory experiments by Baptist (2005) and Nepf (2012a) velocity profiles inside the vegetation are observed. For sparse vegetation patches the bed roughness and near-bed turbulence are enhanced, but the velocity profile remains logarithmic.

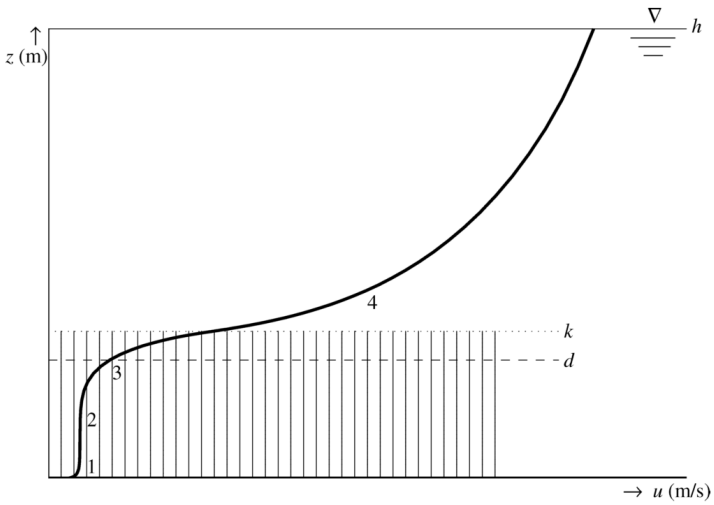

Figure 2.9: Velocity profile inside a vegetation field, adopted from (Baptist et al., 2007)

Only for higher-density vegetation patches the velocity profile transforms to a mixing layer form with four distinct zones as is illustrated in figure 2.9. In the first zone near the bed, the velocity is highly influenced by the bed, and its vertical profile joins the logarithmic boundary layer profile. In the second zone, which corresponds to the zone inside the vegetation sufficiently away from the bed and from the top of the vegetation, the velocity is uniform. In the third zone, near the top of the vegetation, there is a transitional profile between the uniform velocity inside the vegetation and the logarithmic profile above it. The profile in this zone can be approximated by an exponential function. Finally, the fourth zone corresponds to the zone above the vegetation, where a logarithmic profile is observed, which has a zero-plane displacement below the top of the vegetation layer (Baptist et al., 2007).

These vegetation patches generate two distinct scales of turbulence: canopy-scale turbulence generated by the flow instability at the top of the vegetation and stem-scale turbulence generated within the vegetation field. Canopy-scale turbulence penetrates the vegetation only over a length scale dependent on the canopy drag (δ_e). This length scale determines both the zero-plane displacement level for the logarithmic velocity profile above the vegetation and the decay of stress within the vegetation (Nepf, 2012a). Furthermore the canopy drag separates a dense canopy into two regions of distinct transport. The upper part where energetic vertical transport and high levels of turbulent diffusion are present, controlled by canopy-scale vortices. The lower part where significantly slower transport is observed is associated with the smaller stem-scale turbulence.

Formulations to schematise the overal roughness of vegetation have been derived by Baptist (2005) and are elaborated in appendix A.5. The flow velocities inside the vegetation are assumed to be completely uniformly distributed and a developed logarithmic velocity on top of the vegetation is assumed. Finally it is assumed that the total shear stress is composed of the bed shear stress plus the resulting vegetation shear stress. By means of theoretical and analytical derivations, supplemented by genetic programming, the following equation is derived and confirmed to fit measurements from laboratory experiments on vegetation.

$$C_r = \sqrt{\frac{1}{\frac{1}{C_b^2} + \frac{C_D m D k}{2g}}} + \frac{\sqrt{g}}{\kappa} \ln\left(\frac{h}{k}\right) \tag{2.19}$$

in which

C_r = representative vegetation Chézy coefficient [$m^{1/2}/s$]
C_b = bed roughness Chézy coefficient [$m^{0.5}/s$]
C_D = drag coefficient [-]
m = number of vegetation stems [$1/m^2$]
D = stem diameter [m]
k = vegetation height [m]
g = gravitational acceleration [m/s]
κ = von Kármán constant (≈ 0.4) [-]
h = water depth [m]

For vegetation it is shown that the approach with cylinders works well for a range of vegetation types, in which different shapes and flexibilities are introduces through empirical coefficients. It is likely that also for porcupines such extensions for the formulation may work. Introducing this formulation in numerical models is usually done as a sub-grid effect. Deriving the grid-all average requires solving the effects on momentum and continuity using these formulations.

Similar equations have been derived by multiple researchers but it has been shown that this formulation represents the behaviour of vegetation the best in the work of Vargas-Luna et al. (2015). This equation has been fitted to both artificial and real vegetation, submerged and emerged conditions. Although no formulation performs perfectly in all conditions, the equation of Baptist (2005) works best.

2.4.1. Drag

In most studies on aquatic submerged vegetation it is assumed that the drag coefficient is 1, especially when schematised as rigid cylinders for numerical computations. In appendix A.6 the physical explanation of a drag force is elaborated where it is explained that a drag coefficient should not be larger than 2 since this is the result of maximum pressure difference over a certain object.

$$F_D = \frac{1}{2}\rho u^2 C_D A \tag{2.20}$$

in which

F_D = drag force [N]
ρ = density of water [kg/m^3]
u = flow velocity [m/s]
C_D = drag coefficient [-]
A = frontal area [m^2]

Equation 2.20 describes the drag force on an object from which it becomes clear that the drag coefficient, C_D is proportional to the velocity squared. This holds for flow conditions with high Reynolds numbers which is generally the case in rivers. Sukhodolova & Sukhodolov (2012) have found a formulation that describes the drag coefficient for vegetation over the depth where it becomes clear that due to gradients in turbulent shear stress and velocity difference over the depth the drag coefficient is not constant any more. Especially for flexible vegetation, the drag significantly changes near the top of the vegetation patch. although porcupines are rigid structures, they do have a different shape near the top due to the confluence of the different rods that come together.

$$C_D = \frac{2\left(g i_0 + \frac{1}{\rho}\frac{\mathrm{d}\tau_{xz}}{\mathrm{d}z}\right)}{A u^2(z)} \tag{2.21}$$

in which

C_D = drag coefficient [-]
i_0 = mean water level slope [-]
τ_{xz} = turbulent shear stress [N/m^2]
A = frontal area [m^2]
u = flow velocity [m/s]

2.5. Discussion on literature review

Most of the previous studies on porcupines or porcupine-like structures by for example Lu et al. (2011); Zhu et al. (2009) focussed on the hydraulic response and the amount of turbulence around the structure. Other research has been performed on the general response of a sediment bed in laboratory flumes. However only a single layout has been applied dating from the work of Brown (1985) who describes the use of porcupines and jack jetties for the first time. In these experiments the focus was on the prevention of bank erosion and bank accretion by applying porcupines in a certain configuration. For this thesis the focus will be on the generation of enough friction in a river channel to cause a significant water level increase upstream and sedimentation over a complete river channel. Different configurations and circumstances will be tested to identify both the hydraulic and morphological effect of porcupines. Besides, the effect op porcupines fields that partly block the flow will be studied as well, similar to previous research on the prevention of bank erosion. Doing this helps to indicate the differences and similarities between the different application techniques for porcupines.

From experimental measurements and pilot studies in rivers such as the Brahmaputra it is known that the porcupines work and that they can effectively reduce flow velocity and cause sedimentation. Extensive research on the effect of a complete porcupine field is limited however and data is lacking on both the hydraulic and morphological effect. In Myanmar certain channels in the braided river will be tried to be narrowed by means of a porcupine field across the whole channel. They should cause enough sedimentation and push the water level up to result in a new discharge distribution over bifurcation points.

Although some experiments have been performed on the morphological response to porcupines, the documentation of their results is very poor. No accurate velocity measurements have been performed and no indication of the roughness is given. In many experiments the Reynolds number and Froude number are very low. This indicates that the amount of turbulence behind the porcupine might be too small to accurately represent the reality where they will be applied in fast flowing rivers. Finally, the porcupine rods of the scale models in previous research by Aamir & Sharma (2014, 2015b) were round bars while in practice square bars are applied. Whether the cross section is a square or a circle determines the size of the wake vortex behind the rod and thus the amount of turbulence. The amount of turbulence is an important indicator of the generated energy loss. The loss of energy reduces the sediment transport capacity and therefore results in sedimentation (Lu et al., 2011).

3

Experimental set-up & calibration

Laboratory experiments are performed to gain more insight in the behaviour of porcupines. In this chapter it is explained how the experimental flume is set up and which measurement equipment is used. The goal of these experiments is to find correlations between characteristic river parameters and the quantification of the sedimentation or erosion near a porcupine field, and to get detailed insight in the mechanisms that induce the sedimentation or erosion. In order to obtain these results two types of experiments have been conducted, experiments without sediment (fixed bed), and experiments with sediment (mobile bed). The experiments have been executed at the Fluid Mechanics Laboratory at Delft University of Technology.

3.1. Approach

In this section the approach for the experimental set-up is given, where the general layout of the flume is described, the procedure of porcupine construction is given and an elaboration on the measurement equipment is provided. Furthermore the choice for the type of sediment used in the experiments is explained and the approach for calibration of the equipment is described, the actual calibration results are given in section 3.2

3.1.1. Flume characteristics

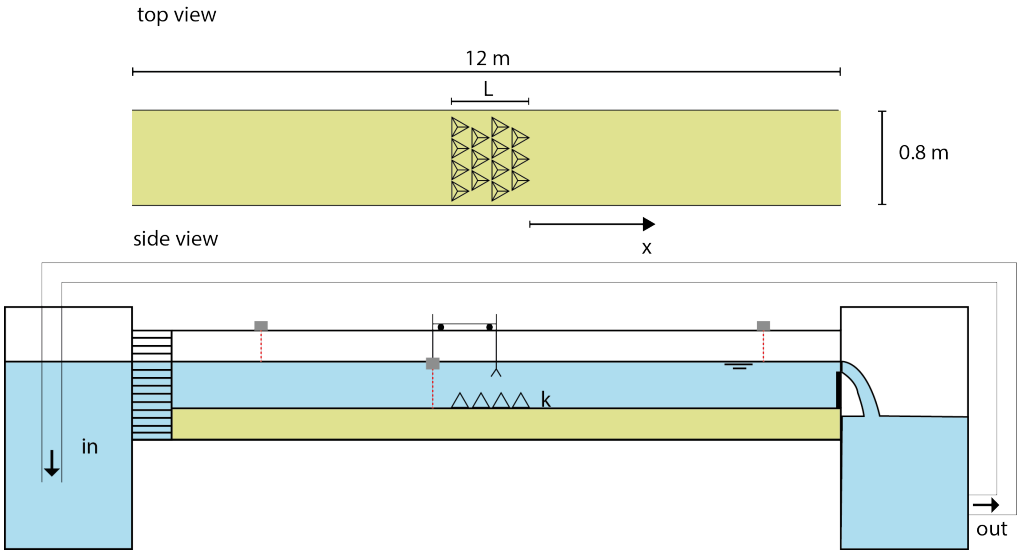

Figure 3.1: Schematization of flume set-up in side view and top view

In figure 3.1, a schematic overview of the flume set-up is given. The water is recirculated from left to right in the 12 metre long and 0.8 metre wide flume. The recirculation was necessary for the experiments with a mobile bed since it enables sediment to be transported out of the flume, and re-enter at the inflow point again.

The sediment layer was approximately 15 centimetres thick but varied during the experiments due to formation of ripples. At the inflow point hydraulic smoothers were present to eliminate some inflow disturbances and calm the water. A foam board was used to reduce the surface irregularities, and small pipes were used to straighten the flow. They are shown in figure 3.2. At the end of the flume a weir was used to control the water level and remove disturbances generated by the pump. Due to the critical flow velocities over the weir these disturbances could not migrate upstream. This is shown in figure 3.3.

Besides the general layout of the flume, also the measurement devices are depicted in the schematic overview. Two water level meters are placed along the flume, one upstream and one downstream to measure the water level gradient. An additional water level laser is mounted on the cart to capture the water level along the flume. Besides this measurement device there is a laser that measures the bed level from this cart. Finally there is an ADV Vectrino Profiler mounted on the cart as well to measure flow velocities at multiple positions along the flume.

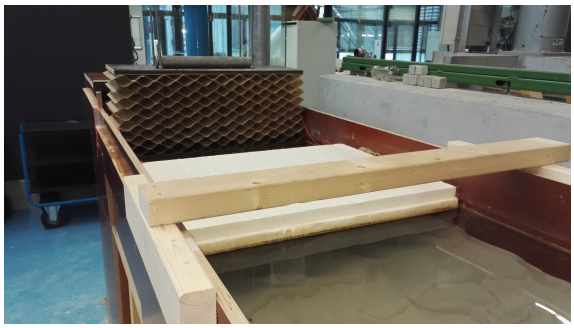

Figure 3.2: Hydraulic smoothers at inflow of the flume to reduce inflow disturbances

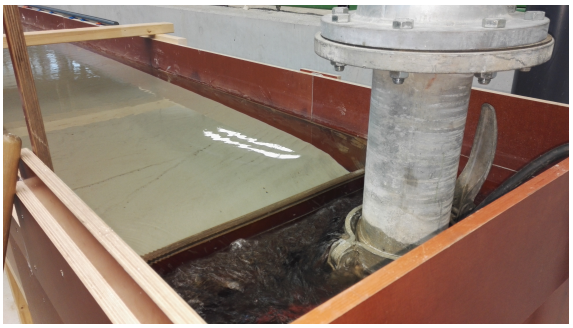

Figure 3.3: Downstream weir to control water level and remove disturbance from pump

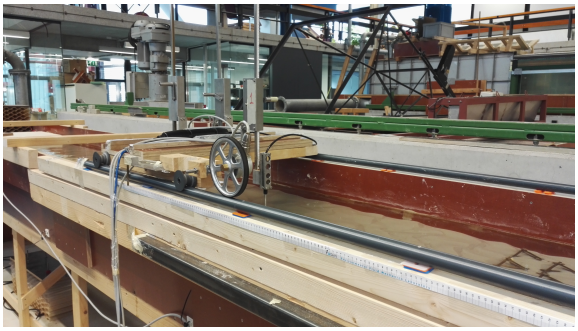

Figure 3.4: Multiple measurement devices mounted on a cart that can move in longitudinal direction

The cart with measurement equipment can be moved in longitudinal direction over a distance of 5 metres such that the bed evolution and velocity profiles can be measured over the same distance along the flume. The rail of this cart starts approximately 3.5 metres downstream from the inflow point to capture the near-field response of the porcupines both upstream and downstream of the field. During the analysis of the experiments in the following chapters, the positions of velocity profiles are related to the distance from the porcupine field. In order to do so the longitudinal distance x from the porcupines is defined to start from the end of the porcupine field. The length (L) of the porcupine field and height (H) are also defined. In this way relative distances such as $[x/L]$ and $[x/H]$ can be used.

The porcupines were placed approximately 5 - 6 metres downstream from the inflow point of the flume to ensure a fully developed flow is reached. This means that the boundary layer is present over the entire water depth as calculated with equation 3.1 for representative cases of the experiments conducted for this thesis.

$$\delta > h_{flume} \quad \text{for} \quad x > 45R \quad \Longrightarrow \quad x > 45\frac{A}{P} \approx 3.6 \sim 6 \text{ [m]} \tag{3.1}$$

in which

δ = width of boundary layer [m]
h_{flume} = water depth in flume ($\approx$ 0.1 - 0.2) [m]
R = hydraulic radius [m]
A = conveyance area [m^2]
P = perimeter [m]

Porcupines

The porcupines that are used for this study have been manually constructed of 10 centimetre long brass square beams with a diameter of 7 millimetres. They should be heavy enough to remain at the bottom of the flume, hence no wood has been applied. Normal steel would start to rust over time which could affect the glue, which is something that does not happen to brass. Before putting the porcupines together the elements had to be roughened up by using sanded paper in order for the glue to attach better. In total 38 porcupines have been constructed on top of a foam board by first setting up the base triangle with tooth pickers as is illustrated in the figures below. Once the base triangle was fixed, the vertical elements were placed one-by-one again fixed with tooth pickers. Finally the top joint was held together by an elastic band after which the porcupines could be glued together by special two-component glue for steel.

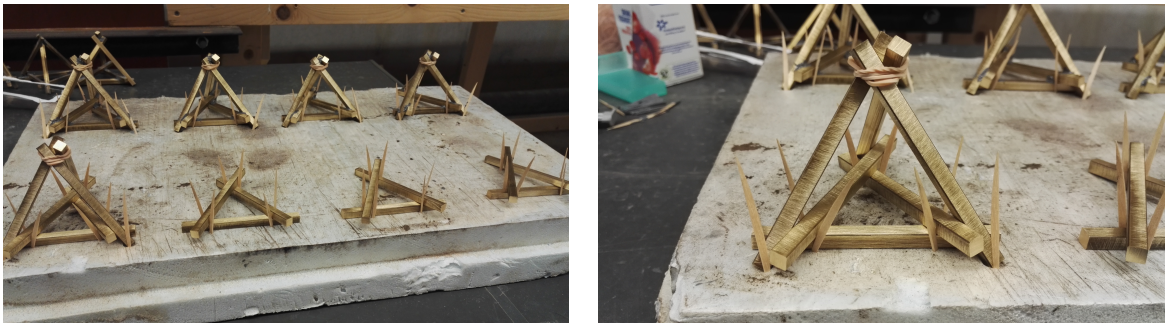

Figure 3.5: Construction of porcupines

Sediment

For the experiments a quartz sediment type (Silica M32) has been used with a d_{50} of 260 μm and a density of 2650 kg/m^3. The application of sediment is difficult for scale experiments since sediment cannot be scaled down as much as other scaling parameters for the experiment such as the porcupines. This is due to the fact that sediment behaves differently once the particles become too small. Cohesive forces between sediment particles arise once the sediment particles become very small and then the sediment does not represent the real river sediment any more. Therefore this problem should be avoided.

The choice for the sediment type used in the experiments is described in detail in appendix B where an elaboration is given on the different types of important behaviour that have to be taken into account. The first important property of the sediment is the size of the generated ripples and dunes according to the bed-shear stress parameter (T) (van Rijn, 1993). Secondly the amount of suspended sediment should remain as small as possible and this is checked with the use of the Rouse number.

Table 3.1: Sediment characteristics

Type of sand	d_{50}[μm]	D^*[m]	Ψ_c[−]	u_c[m/s]	T [−]	Z [−]
M32	260	6.58	0.042	0.215	0.565	5.707

3.1.2. Measuring equipment

Below a description is given about all the measurement devices used for the experiments. Although the devices work perfectly out of the box, they do need to be calibrated such that all devices give an accurate outcome. The results of these calibrations are given in section 3.2.

Velocity measurements

The Vectrino Profiler used in this experiment uses Acoustic Doppler Velocimetry to determine velocities in three dimensions over depth of approximately 2 centimetres. The smallest resolution is 1 mm, and it has a sampling frequency up to 100 Hz. Furthermore it measures its own distance to the bottom and the temperature of the water. The ADV can be moved along the flume in Additionally it is possible to change the height accurately by the pulley device.

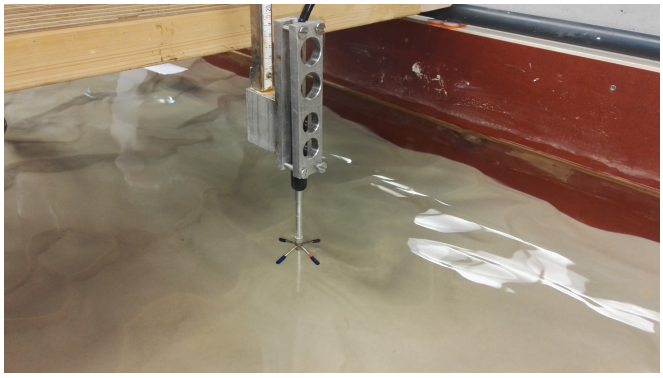

Figure 3.6: ADV Vectrino Profiler

To ensure reliable velocity profiles, only measurements with a correlation above 85% are used. To improve the measurement quality the Signal to Noise Ratio (SNR) should be as high as possible, with a minimal value of 15%. If more particles are in suspension within the water column there are more objects where the sound of the Vectrino can reflect on, thus improving the measurement. Although an SNR of 15% is sufficient, higher is better and in most experiments performed it was above 30%.

The ADV has a limited range in which it can perform accurate measurements. According to Nortek (2012) there is a sweet spot in which the measurements are most accurate, at a distance of approximately 5 centimetres from the device. However there is a larger range in which it could perform measurements it is advised to remain within this sweet spot range for most accurate results. Once the full range is used for measurements it can be observed that the measured values start to deviate from the actual values. The first 4 centimetres from the central transmitter of the device are not measurable due to the angle under which the beam transmitters are positioned as is illustrated below. The sweet spot ranges from 4.5 to 5.5 centimetres underneath the ADV and therefore this range is chosen for the measurements during the experiments, which implies that only 1 cm per measurement is captured.

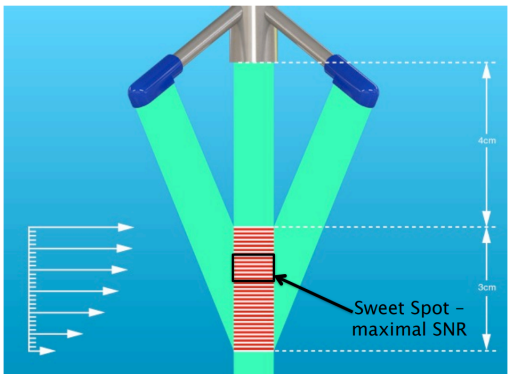

Figure 3.7: Measurable range of the ADV, adopted from (Nortek, 2012)

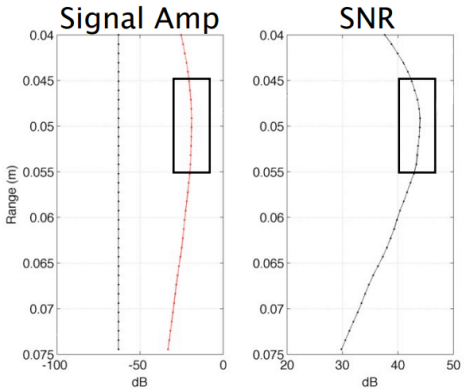

Figure 3.8: Most accurate measurements are within the sweet spot from 4.5 to 5.5 centimetres underneath the central receiver, adopted from (Nortek, 2012)

Bed and water level measurements

Both the bed level and the water level are measured with the same laser equipment. It measures the distance to a surface within the range of 6 to 26 centimetres corresponding with 2 to 10 Volts. The lasers have an accuracy of ± 0.001 Volt which corresponds with an accuracy of 0.04 [mm]. But since the laser cannot detect

the surface of the water, a piece of tape is positioned such that it floats atop the water surface underneath the laser. Three of these lasers are installed on the flume, one upstream, one downstream and one on the cart. The two on either side of the flume measure the water surface at a stationary position and are used to determine the gradient along the flume, while the laser on the cart measures the water level in longitudinal direction at the same location of the underwater laser to determine the exact water depth over the area of interest. Additionally this laser provides a detailed measurement of the water level along the flume. By measuring the water level over the area of interest it is possible to measure water level differences over the porcupine field and the area in front and behind.

Figure 3.9: Laser measurement in a special boat such that it can measure under water

Figure 3.10: Laser measurement that determines the water level by using a piece of paper

To measure the surface under water the laser is positioned in a 'boat' that enables to measure from underneath the water surface. This laser can be moved in transverse direction such that multiple transects of the bottom level can be measured in longitudinal direction. By merging these transects together a 3D bottom surface map can be generated.

The cart on which the lasers are mounted always starts at the same point and subsequently is pushed manually downstream over the area of interest. All the laser measurements are triggered by means of a trigger wheel mounted on this cart. This wheel gives a signal to the lasers when to measure as it is pushed along the flume. This way the laser devices only register the surface if the cart is moved and prevent double measurements of the same location.

Discharge measurements

To measure the discharge through the flume, and thereby the average velocity in the flume, the Proline Prosonic Flow 91W Ultrasonic flowmeter is mounted on the pipe connecting the pump on the outflow point with the inflow point. Data from this device is compared with the velocity profiles measured by the Vectrino Profile to check whether the equipment works properly.

Figure 3.11: Discharge measurement device

3.1.3. Overview of experiments

For this study two types of experiments have been performed, experiments with and without sediment. The experiments without sediment (fixed bed) are aimed to get a detailed insight in the hydraulic behaviour around porcupines without the interference of ripples and other bedforms. Findings about the hydraulic

behaviour due to the presence of porcupines are later compared to experiments with sediment (mobile bed) to check whether certain hydraulic phenomena could be related to morphological developments.

To evaluate the hydrodynamic and morphological near-field effects of porcupines, a variety of experiments has been set up. During these experiments only one parameter is changed each time while the other parameters remain approximately the same. For this thesis the experiments on the effect of staggering, flow velocity, water depth and field density are studied. Besides, the effect of asymmetrical placement is also evaluated to study the three-dimensional effect of porcupines.

The experimental range has been made as wide as possible, limited by the boundaries of the flume dimensions and capacity of the pump. Furthermore there is a minimal flow velocity required for sediment transport as given in table 3.1. Finally, to ensure sub-critical flow conditions a Froude number below 0.4 is required. A schematic overview of the experimental range is given in figure 3.12.

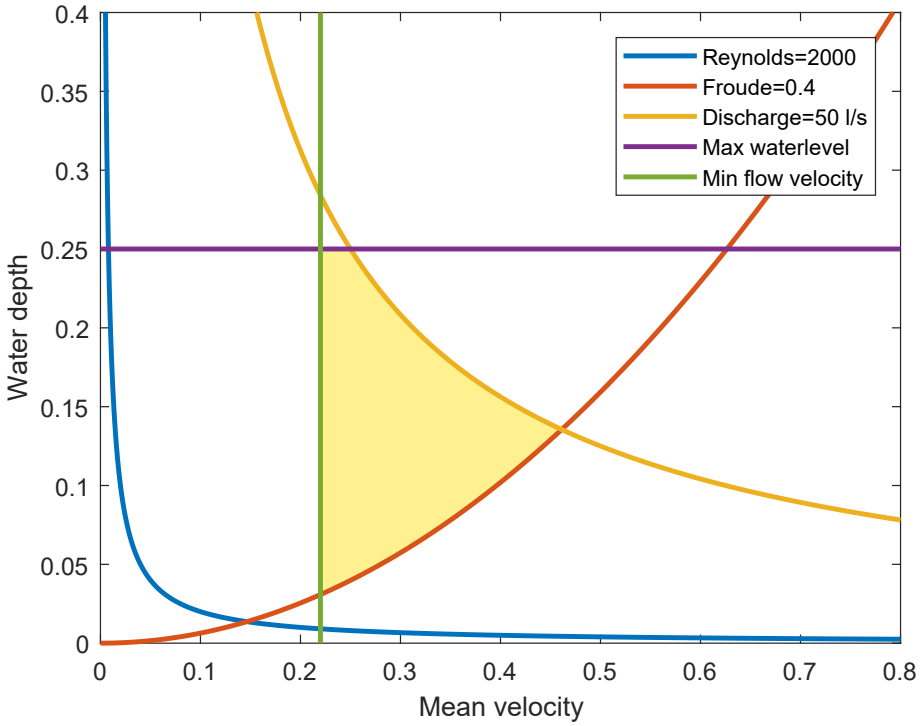

Figure 3.12: Range of valid experiment conditions

3.2. Calibration results

The measurement equipment described in the previous section had to be calibrated in order to obtain reliable data. This section will elaborate on the procedures taken to calibrate all equipment for the performed experiments. The lasers that measure the distance to a surface were calibrated as explained in section 3.2.1. Furthermore the ADV measurements were verified with theoretical values for the flow profile, elaborated in section 3.2.2.

3.2.1. Laser

The laser equipment first has to be normalised to a certain level such that all lasers are calibrated to the same value. To ensure that all lasers are calibrated to the same value the flume is filled with water to a certain level. The water level along the flume is exactly the same in case the water is not moved. All lasers have been set to zero at this level, the so called Gustav Level (GP). So for all measurements that have been performed it holds that they are relative to GP.

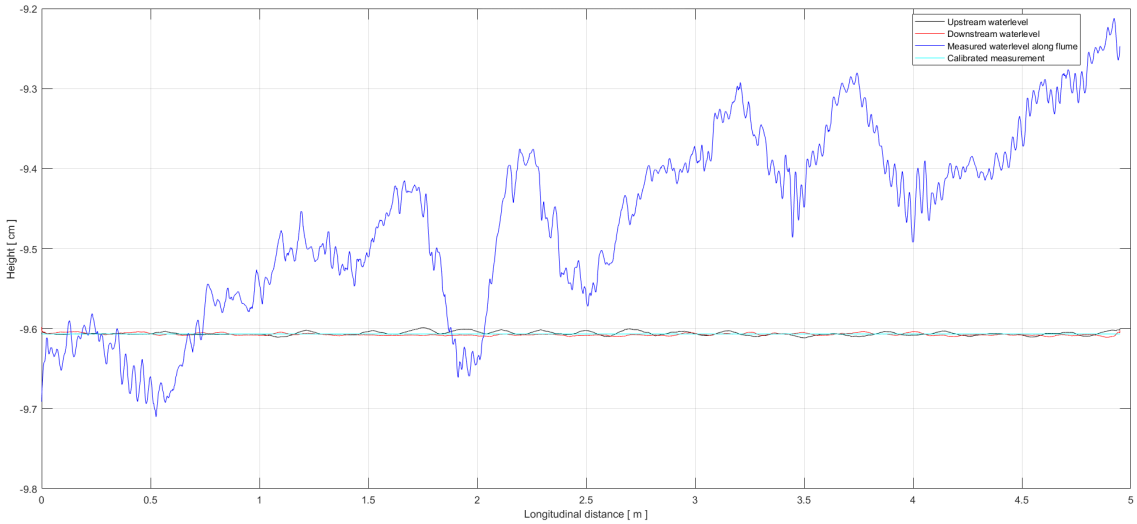

Figure 3.13: Laser calibration relative to upstream and downstream laser

However, the flume is man-made and constructed of wood a couple of years ago. Although the flume may have been perfectly straight at first, it was not any-more during my measurements. This meant that, when the cart was moved along the flume, measurement errors occurred. These errors are removed by measuring the water level along the flume while the water was standing still. Again it is known that the water level should be the same everywhere. Since both the lasers upstream and downstream are stationary and calibrated they can be used to calibrate the final lasers that move along the flume.

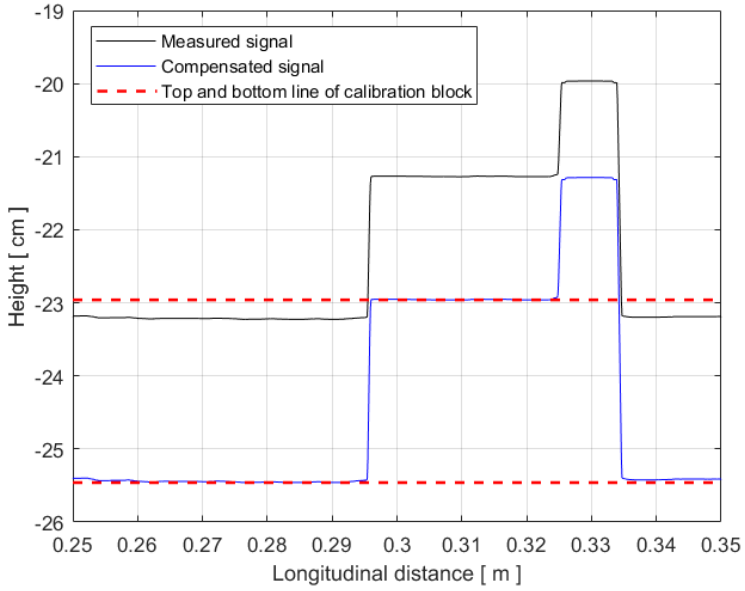

Figure 3.14: Under water laser calibration

Multiple measurements have been performed at different positions along the flume in transverse direction such that multiple error files are determined in longitudinal and transverse direction of the flume. These error files are constantly applied to the measurements in the experiments such that the lasers show the correct values. Below the result is given for one laser calibration. Multiple of these calibrations have been performed such that the water level can be obtained relatively accurate by summing all the measurements and taking the mean. This results in the most accurate measurements possible with a resulting error in the order of millimetres instead of centimetres.

3.2.2. ADV

To verify the outcome of the ADV the theoretical flow profile as explained in section 2.2.2 is plotted together with the measured values for the flow velocity. In section 3.2.3 it is described how the bottom roughness is retrieved from measurements in order to plot this theoretical line. The obtained bed roughness is applied to compute equation 2.10 and equation 2.11 for three different scenarios. For all scenarios it holds that the water level is identical. However three different discharges are applied to check whether the measured data is consequently plotted relative to the theoretical lines. It can be noted that the measured velocity profiles do not completely follow a logarithmic line as they seem to curve back at the top of the measurements. However completely uniform flow is assumed for experiments without porcupines present for calculations. It can be observed that the measured velocities also show a slight curve per cluster. This is due to the sweet spot mechanic of the ADV as mentioned earlier. Larger distances from this sweet spot result in larger deviations from the actual velocity at that location.

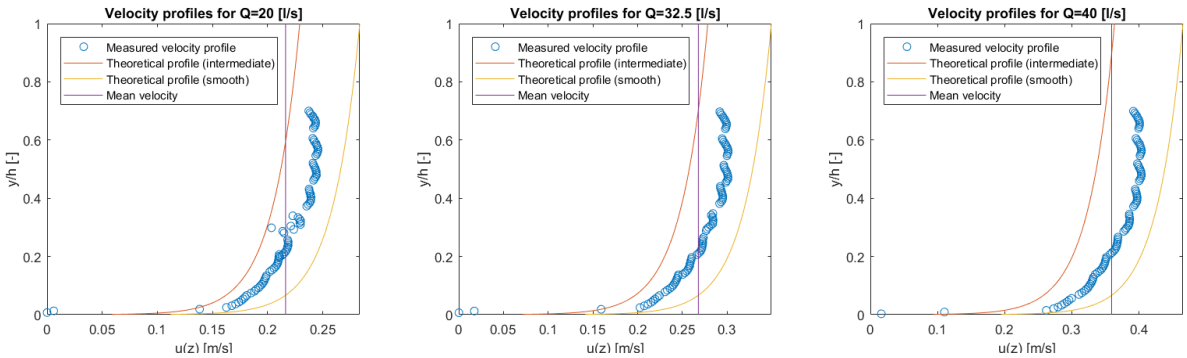

Figure 3.15: Different measured velocity profiles in relation with theoretical profiles

The velocity measurements obtained with the Vectrino Profiler show fluctuations and therefore require averaging. During the calibration experiments the required measuring time was determined by plotting the average velocity signal with a changing averaging time. In figure 3.16 it is shown that only small changes in average values are obtained after an averaging time span of approximately 2 minutes. For further velocity measurements a measurement time of 3 minutes is chosen, since the averaging time is slightly longer in case the flume is filled with sediment.

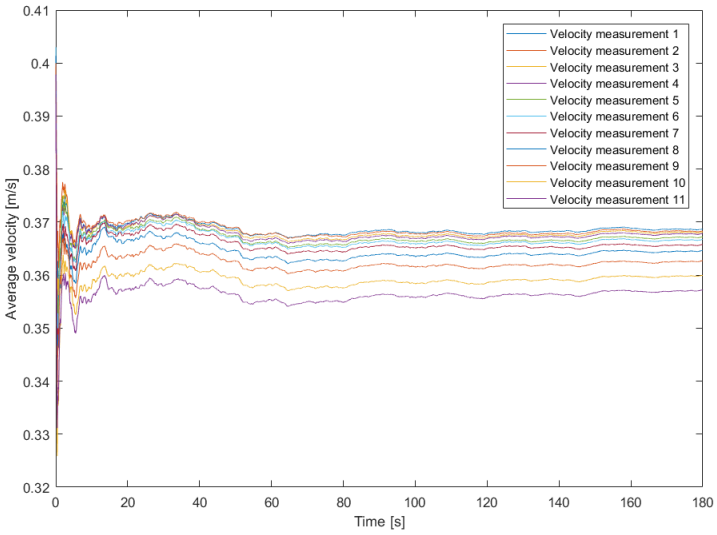

Figure 3.16: Possible averaging time

3.2.3. Bottom shear stress and bed roughness

In all experiments the water level is measured in the upstream and downstream end of the flume. Furthermore the water level is measured along the flume over different transects. With these measurements the overall water level gradient can be determined with the two water level measurements upstream and downstream. Furthermore local water level gradients can be determined with a water level laser that is moved along the flume. If a uniform flow is assumed the only resisting force on the flow is the bed shear stress exerted by the bed. This force is compensated by the water level gradient. Since the density and depth are known the bed shear stress can be determined with the following equation.

$$\tau_b = \rho g h i = 1000 \cdot 9.81 \cdot 0.17 \cdot 2.2 \cdot 10^{-4} = 0.367 \quad [\mathrm{N/m^2}] \tag{3.2}$$

The bed shear stress will become larger for increasing bed roughness. In case of a flume without sediment the bed roughness, expressed in a Chézy coefficient, can be computed from the bed shear stress. The two parameters are related by the equation below. Calculation is made for a representative experiment and the corresponding bed shear stress computed above.

$$C = \sqrt{\rho g \frac{u^2}{\tau_b}} = 39.23 \quad [\mathrm{m^{1/2}/s}] \tag{3.3}$$

For a sediment bottom the Chézy coefficient can also be determined the same way, resulting in a Chézy coefficient of 27.28 $\mathrm{m^{1/2}/s}$. By measuring the bottom with the under water laser the roughness can also be determined. As described in section 2.2.2 the roughness depends on k_r (Nikuradse roughness) of the bottom. In case of a bottom with ripples and dunes the mean height of the bedforms is applied for the roughness height (van Rijn, 1993). As can be seen in the figure 3.17 the bottom shows regular ripples along the flume of approximately 2 centimetre height. by applying the mean ripple height to equation below, the following Chézy value is obtained.

$$C = 18 \log\left(\frac{12h}{k_r}\right) = 35.17 \quad [\mathrm{m^{1/2}/s}] \tag{3.4}$$

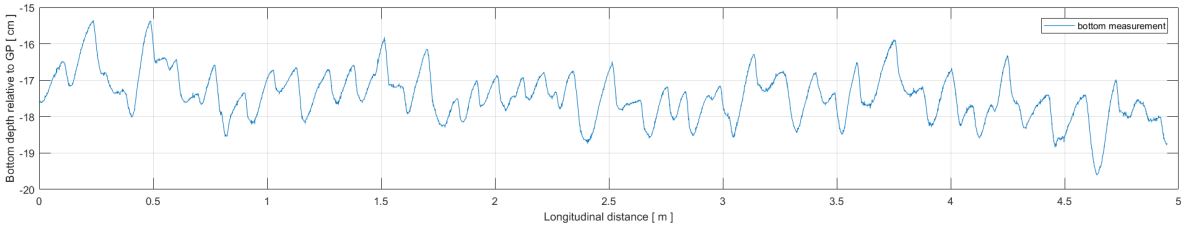

Figure 3.17: Measurement bottom of flume with sediment

The calculation of the Chézy coefficient by the method of Van Rijn underestimates the roughness compared to the method of water level gradients. For the experiments the water level method is used because the water level gradient is relatively easy to determine. However in case of flow where porcupines are present there is no longer a uniform profile, and the method is no longer valid. The same holds for the method of Van Rijn because the bed shows no constant ripple pattern any more. Therefore the amount of turbulence is used to determine the bed shear stress. This is elaborated in section 4.2.5. By determining the bed shear stress from the amount of turbulence, equation 2.8 can still be used, therefore the Chézy coefficient can still be determined.

3.3. Experiments

In this research multiple different experiments are performed to obtain insight in the behaviour of porcupines under different circumstances. The effect of different layouts of the field is tested by applying a staggered grid and non-staggered grid. Furthermore the effect of a partly blocked flume is investigated to study the effect of porcupines applied as a groyne field. This is interesting since they may be an economical attractive solution as alternative to groyne fields in braiding rivers. Not for all experiments hold that they have been tested in a set-up with a sediment bottom since these experiments were highly time consuming. Besides, the experiments

with a fixed-bed resulted in much more reliable data from the measurements that were better to use for the analysis. In table 3.2 an overview is given of all different experiments that are conducted for this research.

Table 3.2: List of all conducted experiments

	Experiment	h [m]	Q [l/s]	u [m/s]	Fr [-]	Re [-]	Longidudinal spacing [m]
Fully blocked	1	0.112	32.5	0.36	0.35	2537	0.01
	2	0.165	32.5	0.25	0.19	1726	0.01
	3	0.148	25	0.21	0.18	1483	0.01
	4	0.178	32.5	0.23	0.17	1592	0.02
Partly blocked	5	0.1305	32.5	0.31	0.28	2179	0.01
	6	0.160	32.5	0.25	0.20	1776	0.01
	7	0.162	25	0.19	0.15	1352	0.01
Fully blocked	8	0.114	32.5	0.36	0.34	2495	0.01
	9	0.173	32.5	0.23	0.18	1642	0.01
	10*	0.197	32.5	0.21	0.15	1445	0.01
	11	0.172	25	0.18	0.14	1272	0.01
	12*	0.171	40	0.29	0.23	2053	0.01
	13	0.173	32.5	0.23	0.18	1644	0.02
	14*	0.173	32.5	0.24	0.18	1646	0.03
Partly blocked	15*	0.108	32.5	0.38	0.37	2645	0.01
	16	0.173	32.5	0.23	0.18	1643	0.01
	17*	0.207	32.5	0.20	0.14	1372	0.01
	18	0.161	25	0.19	0.16	1362	0.01
	19*	0.167	40	0.30	0.23	2092	0.01

* Experiments with water level measurement only.

Besides the layout of the porcupine field, there are also different experiments that focus on the effect of different hydraulic settings. The effect of different water levels is tested which is important since rivers normally do not experience the same water level throughout the year. Experiments with different flow velocities are also set up to indicate under which circumstances the porcupines work best, which is important knowledge for practical applications. Finally the density of the porcuipne field is varied to see if the porcupine field remains effective when less porcupines are used.

3.4. Hypothesis

In this section the general assumptions, based on the literature, for the experiments are presented. First some general thoughts on the porcupines are given, with expectations on the sedimentation and erosion patterns along the flume. These general assumptions are followed by the expectations on the effect of varying water levels, different field configurations and different flow velocities

3.4.1. General

By placing porcupines over the total width of the flume it is expected that sedimentation over the total width will appear as well. The sedimentation is mainly expected inside the porcupine field and partly behind the field due to the retarded flow behind the porcupines. However at the point where the flow reattaches with the bottom downstream of the field erosion is expected. Flow is diverted upstream by the porcupine field as described by Lu et al. (2011) and will accelerate down again. While all research so far has focussed on the amount of sedimentation in or around porcupines, in this study focus will also be given to the amount of erosion downstream, which is expected to appear.

Erosion will probably be present due to the reduced sediment supply from upstream, since sediment is trapped in the porcupine field. Following the Exner equation, erosion is a logical response. Besides, the accelerating flow plunging down on the bed will also increase the shear stress and entrainment of the sediment bringing more sediment into suspension, resulting in erosion. This reattachment point is at a location ap-

proximately 7 times the height of a backward facing step(Schiereck & Verhagen, 2012). However since porcupines are permeable and momentum is carried through the obstruction it is expected that this reattachment point is further downstream.

3.4.2. Varying water level

Since the porcupines will be placed in rivers with large discharge variation, and consequently varying water levels, the effect of different water levels on porcupines is important. Preliminary research has shown that porcupines are most effective once they are not fully submerged (Aamir & Sharma, 2015b). In this case the entire flow field is affected by the porous frame structure, while in case of fully submerged scenarios part of the flow is directly affected by the frame while another part of the flow is diverted upward but largely remains undisturbed. The flow velocities slightly increase in the diverted part of the flow and plunge down again behind the porcupine. Although the un-submerged scenario will probably result in the most sedimentation, only submerged scenarios will be tested. Different submergence ratios are tested and it is expected that lower water levels are most effective. As the water level increases, the effective retardation becomes smaller. It is expected that less sedimentation is present for higher submergence ratios scenarios. Besides, it is expected that the amount of erosion further downstream increases for scenarios with lower water levels. As more sediment will be trapped behind the porcupines for lower water levels, less sediment is transported further downstream which will enhance the erosion process.

3.4.3. Varying field configuration

Until now a simple groyne-like configuration of porcupines has been tested that is composed of elements aligned with the flow (diversion lines) and elements that are positioned perpendicular to the flow (retards) as illustrated in figure 3.18. In this configuration only a part of the cross section is blocked to prevent bank erosion. In this research the difference in total blockage and partly blockage will be studied. It is expected that morphological development will be completely different. However it is expected that due to horizontal mixing also enough energy dissipation may occur to result in approximately the same amount of roughness with a smaller amount of porcupines over a smaller area.

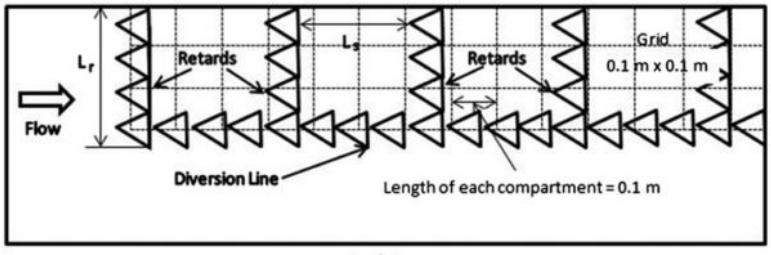

Figure 3.18: Current applied configuration for porcupines as a means for bank protection, adopted from (Aamir & Sharma, 2015b)

In case of fully blocked flow, two main different configurations will be tested, staggered and non-staggered grids. It is expected that for the non-staggered grid the flow velocities between the lines of porcupines in longitudinal direction are much higher compared to the staggered grid of porcupines. This higher flow velocity will probably reduce the sedimentation and is therefore expected to be the least effective. Besides it will be tested if the density of the porcupine field will have a significant effect. For the staggered grid it is hypothesised that the density of the field has an optimum. Increasing the longitudinal spacing of the porcupine rows might result in less sedimentation and a lower roughness of the bed, but it is expected that half the density is not half as effective.

3.4.4. Varying flow velocity

The sediment transport is directly related to the height of the flow velocity as described in appendix A.7. There it is described that sediment transport can generally be seen as the product of some sediment characteristics with the flow velocity to a certain power. As an example, in the sediment transport formula of Engelund and Hansen, the flow velocity is to the power 5. In large sand-bed rivers such as the Ayeyarwady, however, the power is known to be around 4. It means that the intensity of the flow velocity is of main importance to the sediment transport. Previous experiments on the effect of porcupines have been performed with relatively

small flow velocities, while in nature flow velocities are much higher. The low flow velocities in the flume also result in low Reynolds number which are also not realistic since the Reynolds number around the porcupines in nature is definitely larger than 2000, such that there is enough turbulence. By performing the experiment with somewhat more realistic flow velocities it is expected that the amount of sedimentation observed in other research (around 80%) will not be achieved in this study. If the flow velocity is decreased it is expected that more sedimentation will occur. The flow velocity may be too high such that no sedimentation will occur at all, or will require additional measures to ensure that it will still work.

4

Fixed-bed experiments

In this chapter, the fixed-bed experiments are elaborated and an overview of the general results is given. First the experimental approach is explained in section 4.1. In section 4.2 the effect of staggering is illustrated and the retardation of the flow and velocity profile are visualised. Furthermore the effect of porcupines on the water level is discussed. Finally the turbulence behind the porcupines is visualised.

4.1. Approach

4.1.1. Preparation

For the experiments without sediment not many preparations were required for the start of each new set-up. The porcupines needed to be positioned in the right location, and the flume was filled until the right water level was reached. The water level measurement set-up was always checked before the experiments. It was important that the pieces of tape were still floating well and were not deformed. Finally the pump was set to the right discharge, and only a couple of minutes were required for initial disturbances in water motion to dampen out.

4.1.2. Execution

In the experiments that focussed purely on the hydraulic effect, the porcupines were placed further downstream such that the velocity profile was better developed and more uniform. Due to the lower roughness the development of the boundary layer was slower compared to the experiments with sediment. Besides the placement of the porcupines in the right configuration no other preparations were needed. In table 4.1 an overview of the conducted experiments is given with a fixed bed.

Table 4.1: List of conducted fixed-bed experiments

	Experiment	h [m]	Q [l/s]	u [m/s]	Fr [-]	Re [-]	Longidudinal spacing [m]
Fully blocked	8	0.114	32.5	0.36	0.34	2495	0.01
	9	0.173	32.5	0.23	0.18	1642	0.01
	10*	0.197	32.5	0.21	0.15	1445	0.01
	11	0.172	25	0.18	0.14	1272	0.01
	12*	0.171	40	0.29	0.23	2053	0.01
	13	0.173	32.5	0.23	0.18	1644	0.02
	14*	0.173	32.5	0.24	0.18	1646	0.03
Partly blocked	15*	0.108	32.5	0.38	0.37	2645	0.01
	16	0.173	32.5	0.23	0.18	1643	0.01
	17*	0.207	32.5	0.20	0.14	1372	0.01
	18	0.161	25	0.19	0.16	1362	0.01
	19*	0.167	40	0.30	0.23	2092	0.01

* Experiments with water level measurement only.

The table indicates that not for all experiments flow velocity measurements have been performed. This is due to a limit of time. For experiments 10, 12, 14, 15, 17 and 19 only water level measurements have been conducted. by measuring the water level the energy loss can still be determined. Combined with the obtained knowledge from the experiments where velocity profiles have been measured useful analysis can be performed.

4.1.3. Measurements

For the fixed-bed experiments less measurements were required in comparison with the mobile-bed experiments. The bed has been measured once since it does not change. This measurement can therefore be used in all experiments and does not need to be repeated.

For all the experiments the flow velocities have been measured at fixed locations along the flume, with the exception of experiment 13 with a lower density. Due to the lower density the porcupine field was extended 0.2 metres upstream and therefore the first velocity profiles have shifted a bit upstream too. As mentioned in chapter 3 in the experiments with a fixed bed the porcupines have been placed further downstream such that the velocity profile was better developed. Therefore the position of the velocity profiles along the flume are further downstream compared to the experiments with a mobile bed. The velocity profiles consist of 4 consecutive measurements with an intermediate vertical distance of 1 cm from the bottom. From the fifth measurement upward the resolution has been reduced to measurements every 1.5 [cm] to reduce measurement time.

For all experiments the water level has been measured by following five transects along the flume with equal spacing over the width. This way 5 different measurements were obtained over the width of the flume. These measurements were combined and averaged out to obtain the general water level of the flume. Besides, the water level is also measured upstream and downstream of the flume and it was always checked whether the transect water level was between these measurements.

4.2. Results

In this section an overview of the findings from the hydraulic experiments will be given. First insight is provided in the retardation caused by the porcupines followed by an overview of the corresponding velocity profiles. In section 4.2.4 the general behaviour of the water level will be described followed by a section dedicated to the turbulence patterns around the porcupines. Finally some information will be given about the roughness exerted by the porcupines based on hydraulic measurements only.

4.2.1. Staggering

The flow field behind the porcupines is retarded significantly for both the staggered porcupines as the non-staggered porcupines. However, the staggered grid does seem to disturb the flow better as is illustrated in figures 4.1 and 4.2. It can be seen that the velocity between the non-staggered porcupine field remains higher and therefore results in a different flow pattern behind the field. This velocity profile through a non-staggered grid confirms the modelled velocity magnitudes described by Zhu et al. (2009).

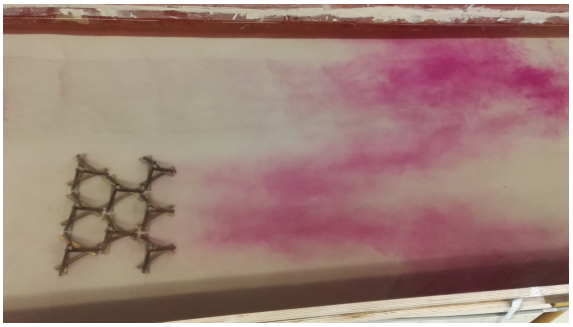

Figure 4.1: Staggered porcupines

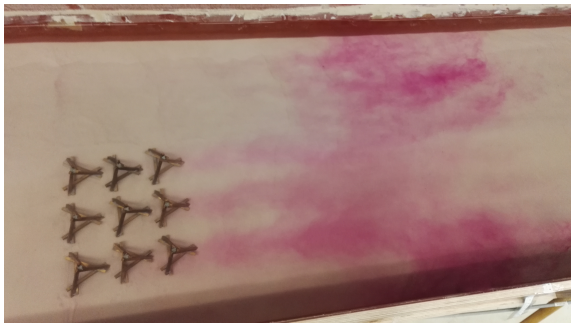

Figure 4.2: Non-staggered porcupines

This difference in the velocity field behind the porcupines has consequences for the sedimentation patterns behind the field as illustrated in figure 4.5. This schematic illustration is based on observations in the flume with remainders of sediment still present that settled in certain patterns behind the field. Figure 4.4 clearly confirms the schematic sedimentation pattern for staggered grids. In figure 4.3 the other pattern is recognizable although less clearly. Still, the single line sedimentation pattern has been observed and is in line with the research by Zhu et al. (2009).

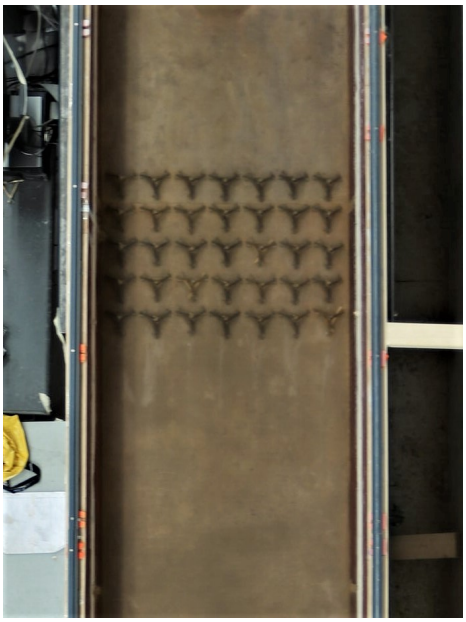

Figure 4.3: Results on sedimentation based on the staggering of porcupine

Figure 4.4: Two strokes of sedimentation behind staggered porcupines

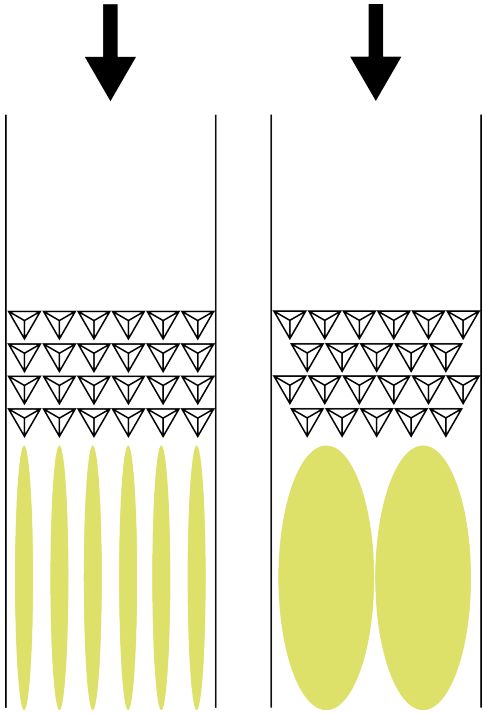

Figure 4.5: Multiple small strokes of sedimentation behind the non-staggered porcupine grid

4.2.2. Flow retardation

The presence of porcupines in the flume causes a highly dynamic and turbulent flow structures behind the porcupines. In this area the flow is strongly retarded. This is partly visualised in figures 4.1 and 4.2, where it becomes clear that the flow velocities are reduced behind the porcupines. This reduction in flow velocities is further elaborated in section 4.2.3. The three dimensional flow structure that is generated behind the porcupines is hard to capture. Based on the sedimentation patterns described in the previous section, three dimensional velocity profiles and observations with dye it is determined that rotational flow is generated. This spiralling motion of the water causes areas with higher turbulence intensities and flow velocities and areas with milder conditions where the flow structures meet each other. These locations, where vortices meet each other are the first deposition locations for the sediment. This process is illustrated below, where a distinction is made between staggered and non-staggered grids.

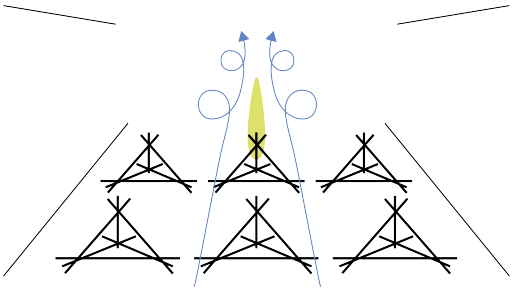

Figure 4.6: Schematic flow pattern with a non-staggered grid

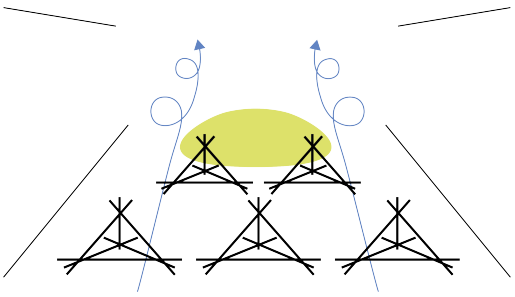

Figure 4.7: Schematic flow pattern with a staggered grid

Further downstream from the porcupine field this secondary flow intensity reduces, and the velocity profiles starts to restore to normal flow profiles. The spiralling flow structures that retard the flow behind the porcupines result in a negative vertical component such that the flow is directed downward. However the effect of the spiralling, and therefore the downward velocity component is dampened out much quicker than the retardation in longitudinal direction. From literature it is known that the reattachment point for the flow behind a backward facing step is approximately 7 times the height of the step. From this point the boundary layer start developing again until a new uniform profile is reached.

From the experimental measurements it is hard to determine from which point a boundary layer has started to develop again and if a reattachment point even exists. Due to the permeability of the obstruction a large amount of momentum is carried through the porcupines and no recirculation occurs behind the field. In contrast with a solid obstruction where recirculation does occur, this results in a continuous convection near the bottom and prevents a real reattachment at the bottom. However the vertical flow velocity does indicate that the water is pushed over the porcupine field and plunges down behind the field again, as illustrated in figure 4.8. The red lines indicate the domain of the porcupine field end the height of the porcupines. After a distance of approximately 0.7 metres from the end of the porcupine domain the vertical flow velocity is reduced significantly and it is assumed that the flow is 'reattached' at this distance. This corresponds to a distance of 8-10 $[\frac{x}{k}]$, where x is the longitudinal distance from the end of the porcupine field and k is the height of the field. This is in accordance to the observed retardation length in the experiments by Lu et al. (2011).

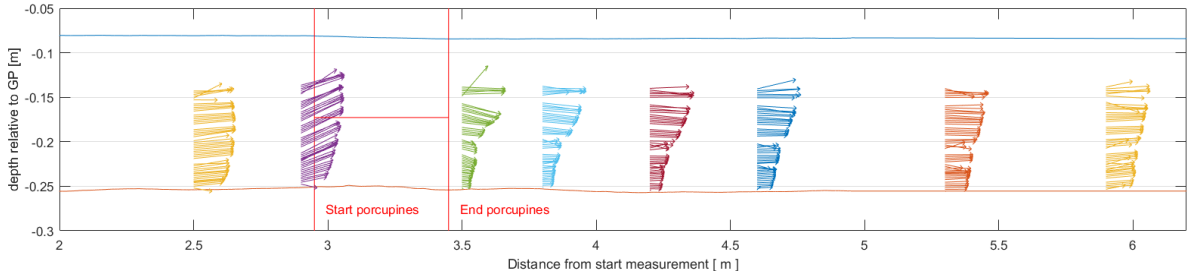

Figure 4.8: Velocity vector plots around porcupine field, Experiment 9

For the spiral flow patterns holds that approximately the same length of retardation is present since the vertical component is correlated to the spiralling flow. Below in figure 4.9 it is visualised that the velocity component in transverse direction is damped out almost completely after a distance of 0.7 metres, and is not present after a distance of 1.1 metres behind the field.

However, the retardation zone for the longitudinal mean velocity is much longer compared to retardation of the vertical velocities. This retardation zone is still present after 2.5 metres behind the field, which corresponds to a distance of 30 $[\frac{x}{k}]$. It is not known what distance is needed to restore to a completely developed logarithmic profile again due to the length of the flume. In section 4.2.3 more insight is given in the evolution of the velocity profiles along the flume.

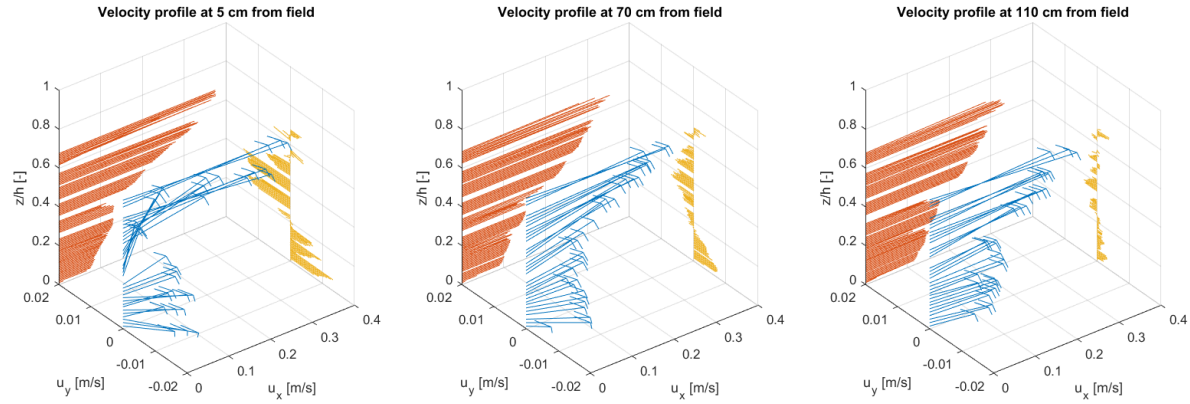

Figure 4.9: 3D velocity plots behind porcupine field, Experiment 9

Partial blockage of flow

In the experiments with partial blockage the flow pattern is completely different. The distortion is no longer uniform over de width of the flume, so three dimensional flow patterns have to be taken into account. In figure 4.10 a schematic flow pattern is illustrated for a partially blocked flume. Comparable with the fully blocked experiments, the flow is pushed over the field, but also towards the side. This means higher flow

velocities towards the unblocked part of the flume and in the top layer of the water column. Behind the porcupines the flow diverges again resulting is lots of horizontal mixing and consequently loss of energy.

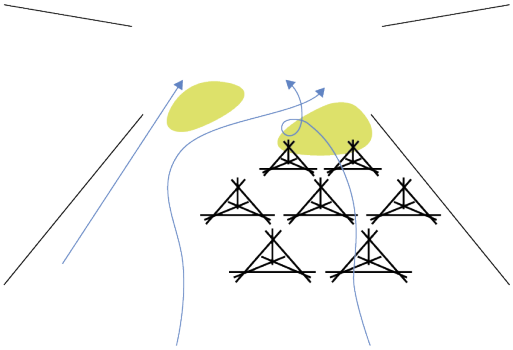

Figure 4.10: Schematic flow pattern with a partly blocked flow

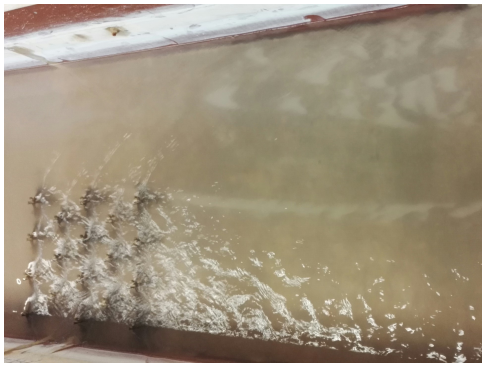

Figure 4.11: Retardation behind partly blocked flow

Behind the porcupines an area with lower flow velocities is present similar to the scenarios described previously. Flow velocities are much lower compared to the undisturbed profile and sediment deposition is likely to occur. Due to three dimensional flow pattern behind the porcupines a flow expansion occurs downstream of the unblocked part of the flume. Where the flow was pushed into the opening in front of the porcupines it is sucked back behind the porcupines resulting in a rapid drop in flow velocities behind the gap. This may result in sedimentation further downstream behind the gap and result in alternation for flow direction and sedimentation patterns.

Figure 4.12 gives a more detailed insight in the flow directions around the partly block flume. In this figure the porcupine field is positioned between column 1 and 2. All the other columns correspond to measurements further downstream from the porcupines. Furthermore, the measurements of the unblocked part of the flume are given in the top row. The middle row gives the measurements in the middle of the flume up until where the porcupines were placed. Finally the bottom row gives the measurements of the blocked part of the flume. The position along the flume is given in terms of $[\frac{x}{L}]$ where L=0.5 metres.

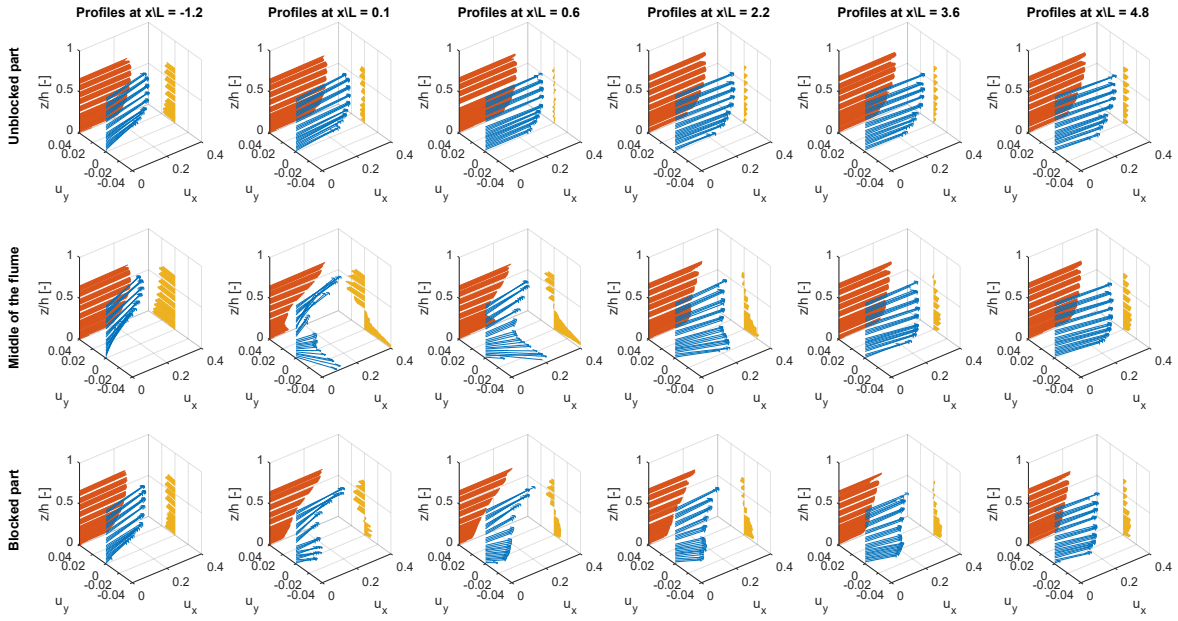

Figure 4.12: 3D velocity plots behind porcupine field, Experiment 16

Taking a closer look at the figure, it becomes clear that the flow is clearly pushed towards the left in front of the porcupines over the complete width of the flume. Even at the right hand side of the flume the flow is diverted towards the open gap. Flow velocities towards the side are highest near the bottom because the

flow higher in the water column is also pushed over the porcupines and is therefore less directed towards the left. Looking at column 2 to 6 it becomes clear that the flow direction behind the gap does not change that much although it does seem to deviate towards the right after a while indicating that the alternating pattern is present. Another notable feature is observed when taking a look at the middle row is that the water first start flowing back towards the right near the bottom. As we progress further downstream flow velocities towards the right progress closer towards the surface. The water that was pushed over the porcupines is pushed left such that a complex helical flow pattern arises behind the field that dampens out as described previously. Finally, when taking a look at the bottom row it is observed that the longitudinal flow profile is retarded the most there. Therefore most sediment deposition is expected directly behind the porcupines. This area is also subject to less transverse velocity gradients compared to the middle of the flume.

4.2.3. Velocity profiles

The velocity profiles in longitudinal direction are retarded significantly as described in the previous section. the highest amount of retardation is obtained near the bottom, where a remarkable reduction in velocity an velocity gradient is observed compared to the undisturbed flow profile. One may infer from this observation that the reduction in velocity may cause sediment deposition in a sediment laden flow. This finding, which is generally true for the different experimental settings, explain why porcupines can be successfully used as scour countermeasures or sedimentation measure. However the reduction in flow velocity is one of the main factors that determines the sedimentation process, another important quantity is the amount of turbulence as a result of generated vortices by the porcupines themselves which stir the sediment. In section 4.2.5 the result of turbulence on the bed shear stress will be discussed which mainly determines the effect on the sediment transport near the bed.

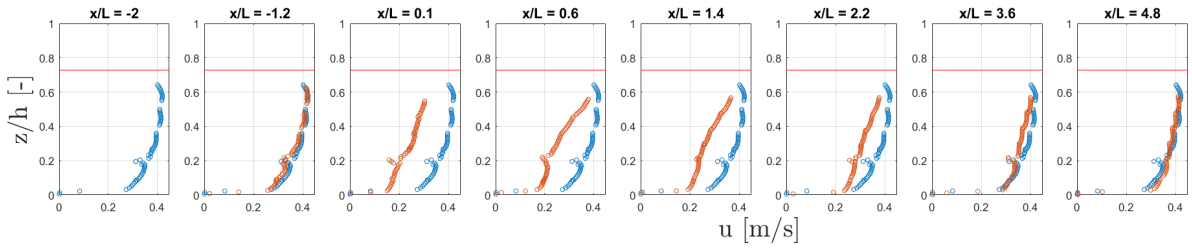

Figure 4.13: Velocity profiles along the flume at locations relative to L (=0.5[m]), Experiment 8. Blue indicates the undisturbed profile, red indicates the profile at location $\frac{x}{L}$

In figures 4.13, 4.14, 4.15 and 4.16 the development of the velocity profiles over the flume are given for experiment 8,9, 11 and 13 respectively. The position at which the velocity profiles are measured are given in terms of $[\frac{x}{L}]$, where L is the length of the porcupine field. The undisturbed profile upstream is given in blue, and the measured profile at location $[\frac{x}{L}]$ is given in red. The horizontal line indicates the top of the porcupine field.

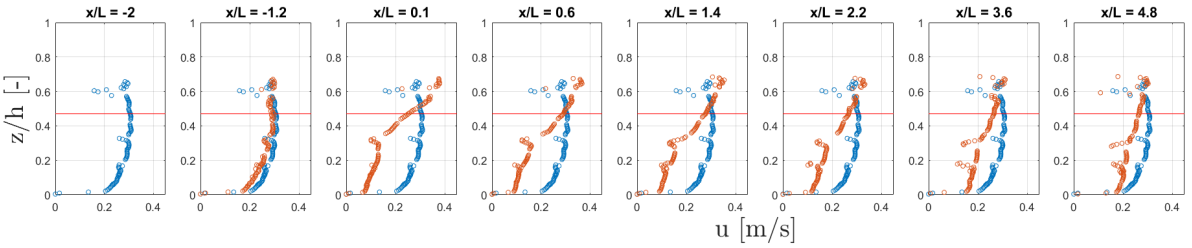

Figure 4.14: Velocity profiles along the flume at locations relative to L (=0.5[m]), Experiment 9. Blue indicates the undisturbed profile, red indicates the profile at location $\frac{x}{L}$

In figures 4.13 and 4.14 the difference between a water depth of 0.11 [m] and 0.17 [m] is given. Clearly not the complete profile is measured all the way to the water surface due to the restrictions of the ADV. In experiment 8 the water depth was reduced, however the discharge remained similar to experiment 9. Therefore the flow velocities were higher as can be noted from the plots. It does seem that the retarded velocity profile is restored much quicker with this higher flow velocity. However, experiment 11 with a lower discharge but equal water level, illustrated in figure 4.15 also shows to restore quicker to its original profile compared to experiment

9. The effect of a lower water level seems to be more dominant in reducing the retardation zone compared to different flow velocities. Since lower flow velocities reduce the momentum carried through the flume it results in quicker reduction of the length of the retardation zone.

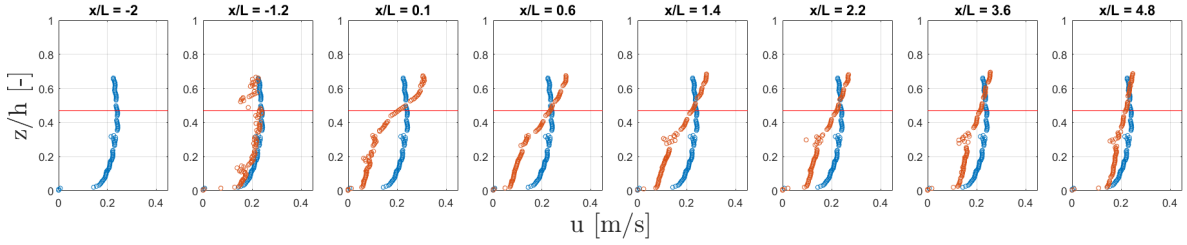

Figure 4.15: Velocity profiles along the flume at locations relative to L (=0.5[m]), Experiment 11. Blue indicates the undisturbed profile, red indicates the profile at location $\frac{x}{L}$

In figure 4.16 the effect of a lower field density on the velocity profile is given. When these results from experiment 13 are compared to the results from experiment 9 it becomes clear that a lower field density has a smaller effect on the retardation of the longitudinal flow velocities. Although the effect is still significant, the amount of retardation is less and may therefore result in less deposition of sediment behind the porcupine field

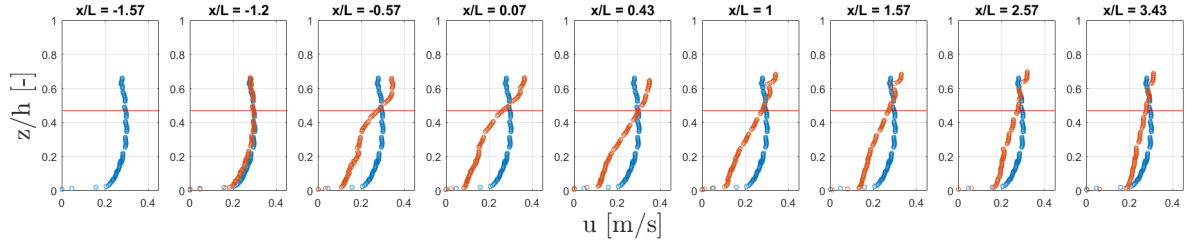

Figure 4.16: Velocity profiles along the flume at locations relative to L (=0.7[m]), Experiment 13. Blue indicates the undisturbed profile, red indicates the profile at location $\frac{x}{L}$

In the previous section it is mentioned that the porcupine field behaves partly as a weir where the water is pushed over the porcupines and plunges down behind again like a backward facing step. In the area behind the backward facing step a lot of turbulence is generated, resulting in energy losses. In analogy with this principal the flow velocities over a weir are higher due to the reduction in effective conveyance area. Based on continuity the flow velocities increase, and the water level decreases. Behind the structure the opposite happens although the water level will not completely restore to its original level due to energy losses. Both phenomena are also observed in the case of porcupines.

As described in section 2.4 the velocity profile through vegetation is more or less uniform over the depth, with the exceptions near the bottom and near the top of the vegetation. In the zone within the vegetation near the top there is a transitional profile between the uniform profile inside the vegetation and the profile above, which is observed to be logarithmic again. Taking a closer look at the measurements from experiment 11, where porcupines are placed with lower density, a velocity profile is made in the porcupine field as well at location [$\frac{x}{L} = -0.57$]. Even though the porcupine field is relatively short, and the measurement is performed after just 3 rows of porcupines an almost vertical profile is measured within the porcupine field. For all other experiments with a measurement at location [$\frac{x}{L} = 0.1$], just behind the field, a similar profile is observed. Besides, the transitional zone at the top of the porcupine field indicates that a logarithmic profile is developing although only the bottom part is observed in the measurements.

In general it can be confirmed that the assumption to schematize a porcupine field as vegetation is justified. However, due to the non-uniform shape of the porcupines the flow velocities inside the field may deviate from the theoretic uniform line. Figure 4.17 below indicates the typical velocity profile through a porcupine. Due to the top part of the porcupine, where the blockage of the flow is much more severe, the flow is pushed both up and down. Where the flow is diverted down the flow lines are constricted resulting in an accelerating flow. When porcupines are placed in a staggered grid, the reduction in flow is more or less uniform. However, when the porcupines are placed non-staggered, there are large velocity gradients in the transverse direction

of the flume like described in section 4.2.2. Furthermore the velocity profiles behind the porcupines themselves remain in the shape illustrated in figure 4.17. Therefore it remains questionable if the flow field can be described as is proposed by Baptist et al. (2007) in case of non-staggered placement.

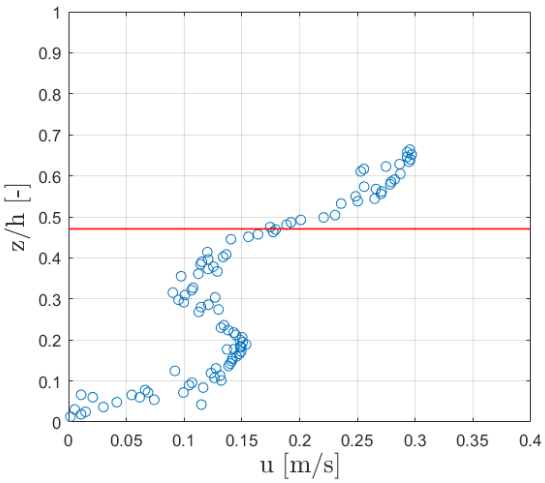

Figure 4.17: Velocity profile behind a porcupine

In figure 4.18 it can be observed how the velocity profiles for a non-staggered grid look like. The velocity gradient below the max porcupine height is much larger, indicating that the flow velocity reduction is not as uniform compared to staggered grids. The reduction in flow velocity is larger however than for staggered grids, but this is just a very local effect. Width average, the reduction is less compared to staggered grids. Furthermore, the velocity in the free flow part is not reduced at all within the porcupine field, and only shows signs of flow retardation further downstream due to compensation of horizontal velocity gradients.

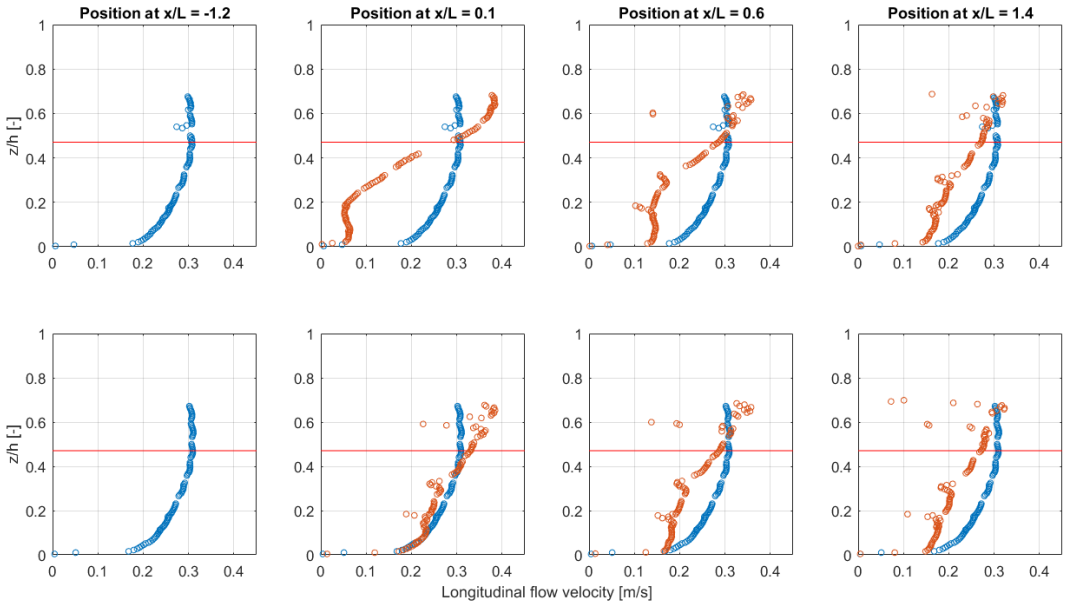

Figure 4.18: Velocity profiles behind a non-staggered grid, first row is behind the porcupines and the second row is behind the free flow line of the field. Blue indicates the undisturbed profile, red indicates the profile at location $\frac{x}{L}$

4.2.4. Water level

Taking a look at the water level around the porcupines it is observed that the water level gradient is much steeper over the porcupines. Behind the porcupines it seems like the water level gradient is slightly negative. This could be the effect of a backwater curve that is generated by the weir at the downstream end of the flume to control the water level. But as described in the preceding sections the porcupines do show behaviour of a weir where the water level restores behind the obstruction. This effect is described as the Bernoulli effect where the balance between the velocity head and water level head is restored. Although this process occurs over a smaller distance in case of a backward facing step, this longer distance of restoration of the water level could be the result of the permeable character of the porcupines. A final explanation of the negative gradient could be an error in the measurement itself. As was described in section 3.2.1 the lasers showed a significant measurement error, which has been reduced as much as possible. However, it could be the case that this error is still present and could result in deviations from the actual water level.

In figure 4.19 the water level measurement of experiment 9 is shown. In appendix C the water level measurements of all experiments are given. There are small differences between each measurement but the overall behaviour is similar. In table 4.2 an overview of the important data from these measurements is given.

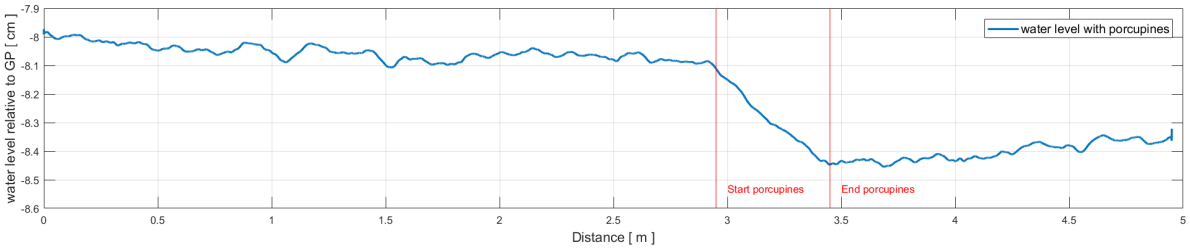

Figure 4.19: Water level, Experiment 9

Apart from the fact that the water level seems to go up slightly behind the field it is still possible to determine energy losses from these measurements. These losses are obtained by using the formulation for the energy head as described by:

$$H = h + \frac{u^2}{2g} \quad \rightarrow \quad \Delta H = h_{up} + \frac{u_{up}^2}{2g} - h_{down} - \frac{u_{down}^2}{2g} \tag{4.1}$$

in which

H = energy head [m]
h = water depth [m]
u = mean flow velocity [m/s]
g = gravitation force [m/s^2]

By using the upstream water depth and flow velocity in front of the porcupines and the depth and flow velocity downstream of the porcupines this equation can be used to calculate the energy loss over the porcupines. The mean flow velocity is computed based on the discharge that remains constant along the flume. Although the flow velocity is present in the equation, the dominant term is the water level since velocity difference are relatively small. The energy loss is therefore almost directly related to the reduction in water level and is calculated for all experiments in table 4.2.

In case of low water depth the energy loss is highest. In these experiments it was clearly visible that the porcupines pushed the water upward and large waves were generated downstream of the porcupines. In case of larger water depths the energy loss is reduced rapidly. Since the discharge remained the same for all depth dependent experiments the flow velocities changed as well. However, from the flow velocity experiments it becomes clear that an increase or reduction in flow velocity does not affect the energy loss as much as an increase or reduction of the water level. Furthermore it is observed that reducing the density of the field does influence the effectiveness of the field, however the reduction of effectiveness is not that large.

Finally, from experiment 15 to 19 it is observed that placing the porcupines only until half the flume's width reduces the effectiveness on average by a factor of 1,6. For some experiments the reduction was greater or smaller, but the important result is that that the reduction in effectiveness is less than the reduction in the amount of porcupines used. This result, combined with the results from experiment 13 and 14 indicate that effectiveness of the porcupines do not scale linearly with the amount of porcupines used.

Table 4.2: Energy losses due to the porcupines

experiment	Q [l/s]	Longitudinal spacing [m]	h_{up} [cm]	h_{down} [cm]	u_{up} [m/s]	u_{down} [m/s]	ΔH [cm]
8	32.5	0.01	12.23	10.27	0.332	0.395	1.723
9	32.5	0.01	17.54	17.13	0.232	0.237	0.401
10	32.5	0.01	19.86	19.57	0.205	0.208	0.286
11	25	0.01	17.37	17.09	0.180	0.183	0.273
12	40	0.01	17.37	16.71	0.288	0.299	0.621
13	32.5	0.02	17.52	17.15	0.232	0.237	0.359
14	32.5	0.03	17.46	17.18	0.233	0.237	0.271
15	32.5	0.01	11.31	10.02	0.359	0.406	1.107
16	32.5	0.01	17.47	17.22	0.233	0.236	0.248
17	32.5	0.01	20.86	20.70	0.195	0.196	0.156
18	25	0.01	16.21	15.99	0.193	0.195	0.211
19	40	0.01	16.95	16.55	0.295	0.302	0.382

Figure 4.20: Impoundment of water level by porcupines, Experiment 8

Partial blockage

For the experiments with a partial blocked flume the water level gradient over the porcupine area is not uniform over the width. The part of the flume with porcupines pushes the water more upward and results in a steeper gradient in longitudinal direction, whereas the unblocked part has a milder slope. In figure 4.21 it is clearly observed that the water level gradients over the porcupine area are different. The water is pushed slightly upward in front of the porcupines causing a height difference in transverse direction. Due to this gradient in transverse direction secondary flow patterns are generated, leading to hellical flow patterns behind the porcupine field. This is even further stimulated once bar patterns behind the porcupines are formed.

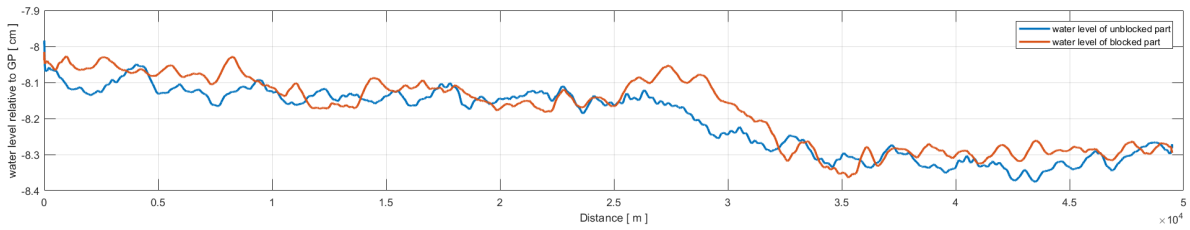

Figure 4.21: Water level gradient difference, Experiment 16

4.2.5. Turbulence

In order for the porcupines to result in deposition of sediments there should be a reduction in flow velocities, which has been shown to be present in the previous section. However sedimentation occurs when the upward turbulent fluctuation is reduced such that the sediment is able to settle easier. The turbulent fluctuations are described by u' and v' calculated as follows:

$$u' = \sqrt{\overline{u - \overline{u}^2}}, \qquad w' = \sqrt{\overline{w - \overline{w}^2}} \tag{4.2}$$

The 2-dimensional vertical distributions of dimensionless turbulence intensities, normalized as u'/u_* and w'/u_*, where u_* is the shear velocity of the approach flow ($=\sqrt{ghi}$) are shown in figures 4.22 and 4.23. For different locations along the flume it is shown how the turbulent intensity changes compared to the approach flow. For both turbulence directions, the maximum turbulence intensity occurs near the top of the porcupine field which is due to the irregular top of these frames. they result in a lot of turbulence and therefore cause energy dissipation. For the longitudinal intensity it is observed that closely behind the porcupine field the intensities are lower compared to the approach flow. In the near-bed region the vertical turbulence intensities are a little higher compared to the approach flow. The combined effect of the turbulence intensities is explained in figure 4.25. Overall the amount of turbulence behind the porcupines has significantly increased, thus dissipating an important amount of energy. Compared with the downward vertical velocity component like described in section 4.2.3, the porcupines may reduce the probability of particle suspension.

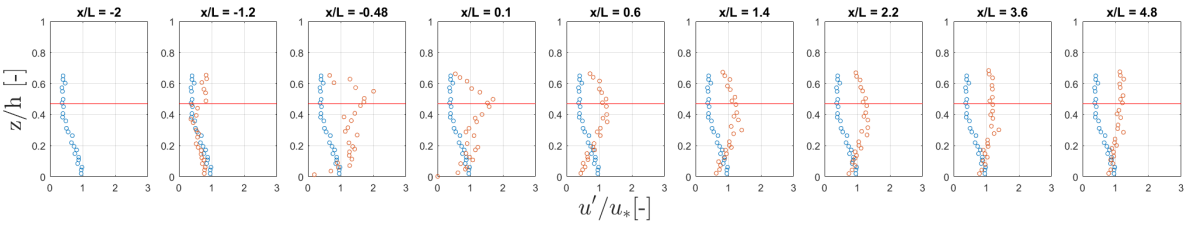

Figure 4.22: Dimensionless turbulence intensity in horizontal direction, Experiment 11. Blue indicates the undisturbed profile, red indicates the profile at location $\frac{x}{L}$

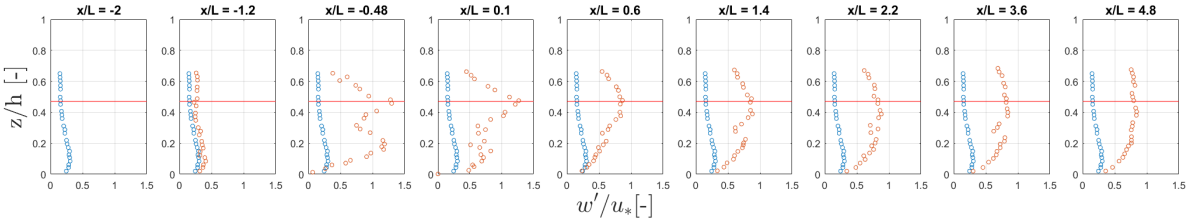

Figure 4.23: Dimensionless turbulence intensity in vertical direction, Experiment 11. Blue indicates the undisturbed profile, red indicates the profile at location $\frac{x}{L}$

By averaging over the horizontal and vertical turbulent fluctuations one can determine the shear stress($=-\rho\overline{u'w'}$) as illustrated in figure 4.24. The value for the bed shear stress is determined by the undisturbed velocity profile, by extrapolating the values close to the bottom all the way to the bottom. Besides, the bed shear stress can also be determined by equation 2.8 and should correspond to the value obtained from turbulence measurements. In figure 4.25 the dimensionless shear stresses, $\frac{\overline{u'w'}}{\overline{u}^2}$, are plotted over the vertical to get more insight in the stresses behind the porcupines.

For the undisturbed velocity profile the bed shear stress is determined by means of extrapolation of the measurements within the bottom 4 cm. This is illustrated in figure 4.24 where the extrapolated value is indicated with a red dot. For this measurement it corresponds to a bed shear stress of 0.3598. In section 2.2 it is mentioned that by calculating the bed shear stress by means of equation 2.8 the same value should be obtained. To check whether the two theoretical shear stresses correspond well with the measured data measurements have been conducted on a uniform flow field where no porcupines were present. Certain parameters were varied to receive multiple measurements, and the comparison is given below in table 4.3. The percentage of the error between the two measurement methods is given, resulting in a mean error of 13.7%.

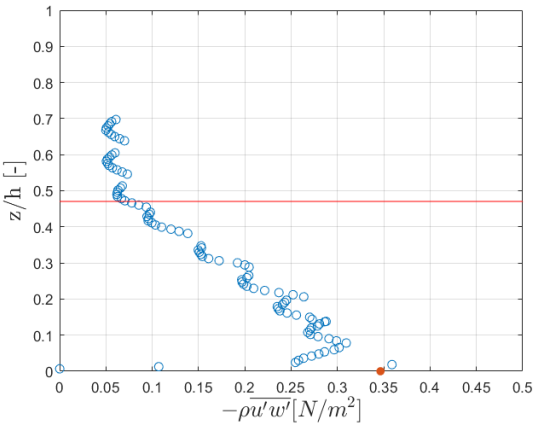

Figure 4.24: Calculation of bed shear stress by means of exptrapolation

Based on this comparison it is assumed that the turbulent measurement give a relatively good indication of the shear stress. This is important in order to give more insight in the exerted bed shear stresses behind the porcupine field.

Table 4.3: Bed shear stress based on water level gradient and turbulence

h [m]	h_{up} [m]	h_{down} [m]	Q [l/s]	i_w [-]	$\tau_{b,wl}$ [N/m^2]	$\tau_{b,ex}$ [N/m^2]	% error
20.76	20.86	20.78	32.5	1.49E-04	0.3041	0.262	13.8
17.13	17.23	17.15	32.5	2.27E-04	0.3189	0.3598	5.8
11.77	11.94	11.72	32.5	5.57E-04	0.6435	0.5657	12.1
17.80	17.90	17.82	25	1.18E-04	0.2067	0.2304	10.3
17.42	17.54	17.42	40	2.44E-04	0.4169	0.5696	26.8

Although the comparison indicates that the shear stress received by extrapolation corresponds relatively well it is noted that for further analysis inside and downstream from the porcupines, the bed shear stress is only approximated and therefore subject to a margin of error. From figure 4.25 it is observed that the total shear stress increases due to the presence of porcupines although close to the bed. From position $[\frac{x}{L}]$=0.1 to 1.4, the total bed shear stresses are less than those in the undisturbed profile. This indicates that porcupines effectively reduce the total bed shear stress close to the bed. The combined effect of a reduced velocity gradient and turbulent mixing may therefore result in a reduced sediment transport capacity. Since the height of the bed shear stress determines the sediment transport, this reduction is probably one of the major reasons that sedimentation occurs behind the porcupine field.

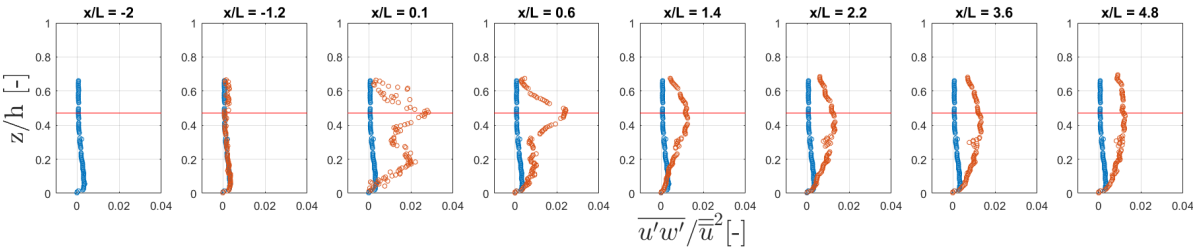

Figure 4.25: Variation of dimensionless shear stress over the vertical, Experiment 11. Blue indicates the undisturbed profile, red indicates the profile at location $\frac{x}{L}$

5

Mobile-bed experiments

This chapter elaborates the results from the mobile-bed experiments. First the preparation of the experiments and the execution are described in the approach of the experiments in section 5.1. In section 5.2 the results of the experiments are given. First a detailed overview of the morphological development is given followed by the retardation of the flow in mobile-bed experiments. Finally the flow velocities and water levels are briefly discussed to arrive at the parameter sensitivity in section 5.3

5.1. Approach

5.1.1. Preparation

For the mobile-bed experiments more preparation is required compared to the fixed-bed experiments in order to create the same starting position for each experiment. Before the experiment is started the sediment bed is flattened by using a water puller to remove all previously generated ripples and irregularities. It is tried to end up with a slightly downwards sloping bed with the exception of the first part where the bed is sloping upward to suppress generation of large dunes at the inflow point. If the bed is prepared the flume is filled with water from the upstream point until the water reaches the turning point in the bed. If this point is reached the rest of the flume is filled from the downstream point. This way of filling the flume prevents high flow velocity streams during the filling process and therefore prevents rapid erosion and bed deformation. Once the desired water level is reached the pump can slowly be turned up to the desired discharge to prevent shock waves.

5.1.2. Execution

The mobile-bed experiments have been conducted continuously without stops. This means that once the experiments were started the pump was not switched off until the end of the experiment. If the experiment needed a temporary break, for instance during the weekend, the discharge was lowered such that no sediment transport occurred. This prevented generation of algae that could influence the experiments otherwise, and it prevents the necessity to empty and refill the flume during a single experiment which could change the morphology drastically.

Before the experiments were started, first a day of morphological development without the presence of porcupines was executed under the circumstances for that specific experiment to prepare the bed. After a day the first measurement was conducted to determine the initial situation for each individual experiment. After the placement of the porcupines for the designated experiment, measurements with fixed intervals were conducted for both the bathymetry evolution and the velocity measurements. Measurements were conducted every 2, 5, 24, 48 and 72 hours after the start of the experiment. The measurements were processed immediately after completion to check whether retakes of measurements were needed. Daily observations were conducted to check if the water level remained constant. Due to evaporation water is continuously removed from the system so water is added to the system if needed.

After the experiment,s the water is removed from the flume by opening the exit valve. The porcupines are cleaned and removed from the flume in order to prepare the flume for the next experiment again. The porcupines are checked for damage and repaired if needed for the next experiment.

Since it was proven that staggered grids are more effective to retard the flow all experiments with a mobile bed are conducted with a staggered configuration. In these experiments the discharge is set to 25, 32.5 or 40 [l/s]. The water level deviates between experiments and therefore causes deviations in mean flow velocity between experiments. Although it would be better to keep flow velocities the same for different experiments, this is practically not possible. It is therefore chosen to maintain a constant discharge since this is easily controlled. Experiment 1, 2, 5, 6 determine the effect of changing water level, where a distinction is made between a fully bocked flume and partly blocked flume. Experiments 4 aims to give more insight in the effect of the density of the porcupine field by increasing the longitudinal spacing between rows of porcupines by a distance of 0.01 metres. Finally experiments 3 and 7 are on the effect of varying flow velocity.

Table 5.1: List of conducted morphological experiments

	Experiment	h [m]	Q [l/s]	u [m/s]	Fr [-]	Re [-]	Longidudinal spacing [m]
Fully blocked	1	0.112	32.5	0.36	0.35	2537	0.01
	2	0.165	32.5	0.25	0.19	1726	0.01
	3	0.148	25	0.21	0.18	1483	0.01
	4	0.178	32.5	0.23	0.17	1592	0.02
Partly blocked	5	0.1305	32.5	0.31	0.28	2179	0.01
	6	0.160	32.5	0.25	0.20	1776	0.01
	7	0.162	25	0.19	0.15	1352	0.01

5.1.3. Measurements

For the mobile-bed experiments measurements were needed at fixed time intervals to capture the bathymetry update over time. At the start of each experiment the bathymetry was measured after 1 day of morphological development. This measurement was considered to be the starting position of the bed. From this moment on the porcupines were placed at their designated position and the experiment was started. From the start of the experiment new measurements of the bottom were performed after 5, 24, 48, 72 hours after the start of the experiment. Not all experiments have been measured over the same domain however. In the first couple of experiments performed the cart on which the measurement equipment is installed was not able to go further than 3.2 metres. This distance has been extended in between experiments, resulting in non-equal measurement domains for certain experiments.

The bathymetry has been measured by performing bottom measurements over multiple transects with equal spacing between them in transverse direction of 5 cm. These different transects are put together to create a 3-dimensional representation of the bed. Measurement errors are filtered out, such that a smooth surface is plotted. The porcupines result in reflections of the laser such that the measurement equipment cannot accurately capture the dimensions of the porcupines, therefore in the area of the porcupine field the signal is filtered such that the errors due to the porcupine reflection are also filtered out to prevent large spikes.

During the bottom level measurements the water level is measured simultaneously to accurately determine the actual depth of the bed at each location. By taking the mean of these 15 water level measurements the mean water level is determined over the flume in longitudinal direction. Combined with the mean bed level, the average water depth of the flume is determined. Finally, velocity measurements have been conducted with the ADV. These measurements are less accurate near the bed compared to the measurements in the fixed-bed experiments due to the presence of ripples that retard the flow locally. Close to the bed large differences therefore arise compared to the fixed-bed experiments, but higher in the water column the flow velocities and directions are comparable.

5.2. Results

5.2.1. Bed development

The experiments 1 to 4 as listed in table 5.1 are experiments with porcupines over the total width of the flume. The variables within these experiments are in terms of flow velocity water level and density of the field. The general results of these four different experiments will be elaborated first, mainly focused on the bed evolution over time and the general hydraulic behaviour around the porcupine field. Experiments 5 to 7 are experiments with partial blockage of the flow. These experiments will be elaborated seperately from the first experiments since the morphological behaviour is different and not directly comparable with the experiments of total blockage.

Total blockage of the flow

For most measurements hold that the porcupine field starts at a distance of 1.5 metre and ends at 2 metre from the start of the measurements. Only in experiment 4, with a lower field density, the field starts at 1.5 metre and ends at 2.2 metre. In figure 5.1 the evolution of the average bed cross section of experiment 2 is given. For all 15 measured transects along the width of the flume one average cross section is determined which is used to illustrate the effect of the porcupines on the bed. The bed level is plotted relative to GP as explained in section 3.2.1.

What can be observed is that the bed erodes within the porcupine field and accretes behind the field. Besides, no clear morphological development is observed in front of the field. Due to the increased turbulence sediment is entrained in the first part of the field. As the flow velocity is reduced it is observed that the amount of erosion gradually decreased further in the field. Since the bed shear stress is lowered close to the bed behind the field, as stated in section 4.2.5, sediment settles there first as is clearly observed when taking a look at the cross section after 5 hours. The sedimentation process appears to have an equilibrium height from where the sedimentation process continues in lateral direction. After 24 hours the sedimentation front has almost migrated out of the measurement domain. The next two measurements in time show that the general shape of the sedimentation bank does not change. The sedimentation hump has a constant slope downwards under a certain angle. This indicates that the sedimentation behind the field is limited to a certain length.

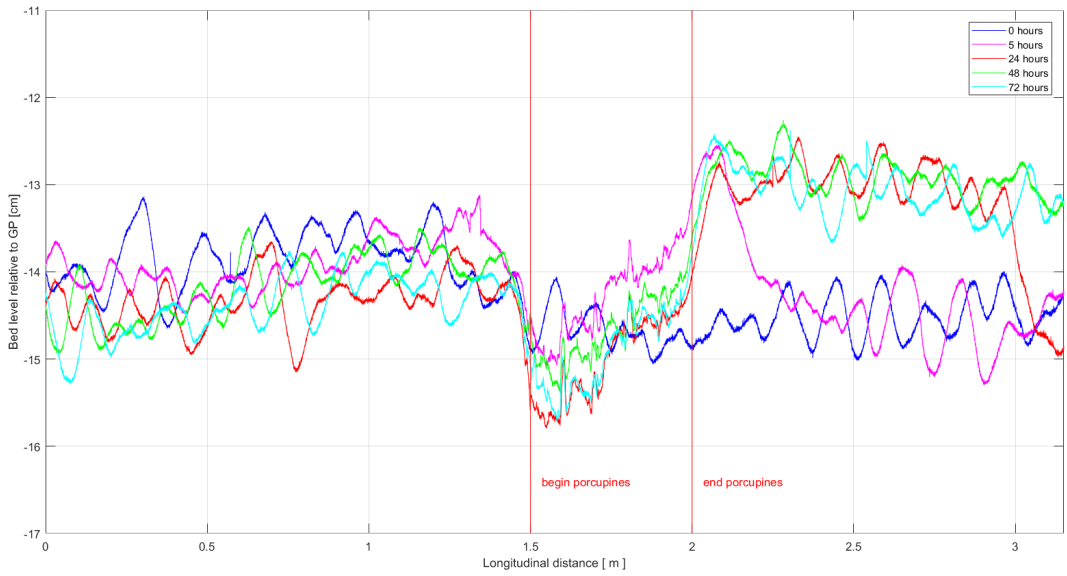

Figure 5.1: Evolution of the bed over time, Experiment 2

The actual 3-dimensional bathymetry update between the zero measurement and after 24 hours is illustrated in figure 5.2, where the position of the porcupine field is marked by the red rectangle. It becomes clear that there is no uniform bed profile over the width as is suggested by the average cross sections. In the three dimensional figures it becomes clear where sedimentation occurs exactly. Since the cross sections merely show the average of the bathymetry it could be that for some point along the flume sedimentation heights are higher or lower than given in the average cross section. In appendix D all three-dimensional figures of the bathymetry updates are given for all experiments performed.

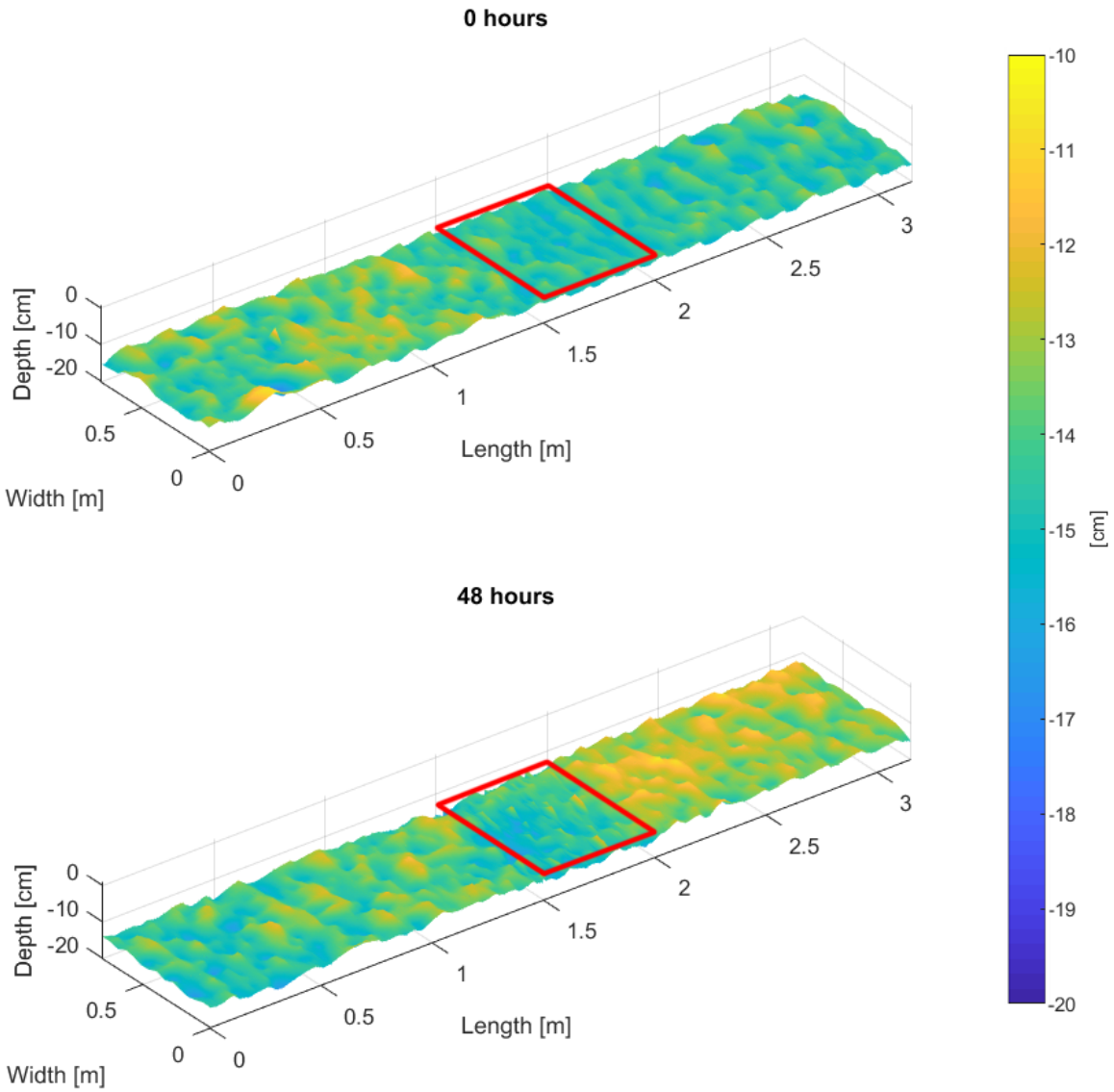

Figure 5.2: Three-dimensional evolution of the bed over time, Experiment 2

For experiment 3, with a lower discharge compared to experiment 2, the evolution of the bathymetry is given in figure 5.3. The evolution shows similar behaviour although the processes are slower. Compared to the previous experiment no large sedimentation bank is generated. Sedimentation does occur further downstream, however in smaller ridges observed in figure 5.4. Again there is a maximum sedimentation height directly behind the porcupines. The height of the sedimentation hump is determined relative to the bed height in front of the porcupines, which is assumed to be in the stable equilibrium bed height. Comparing the two experiments it is observed that the sedimentation height is significantly higher for lower flow velocities. Although the water depth has changed very little, the sedimentation height has changed relatively much, indicating that the height of the sedimentation hump is velocity-related. Clearly the critical flow velocity for which continuous sediment transport occurs is reached occurs at a smaller water depth for low flow velocities. This results in larger sedimentation humps. Although the sedimentation process is much slower, the effectiveness in terms of sedimentation height behind the field is higher for lower discharges.

For experiment 3 the bed within the porcupine field seems to stabilize after 24 hours and does not show any sedimentation or erosion after this moment in time. Like all other experiments the porcupines themselves cause scour around the bottom part of the structures. Horse-shoe vortexes near the 'feet' of the porcupines arise and the porcupines dig themselves into the bed. This erosion and digging process continues until an equilibrium is reached. It seems that the angle of the scour hole is similar for all experiments. Although the

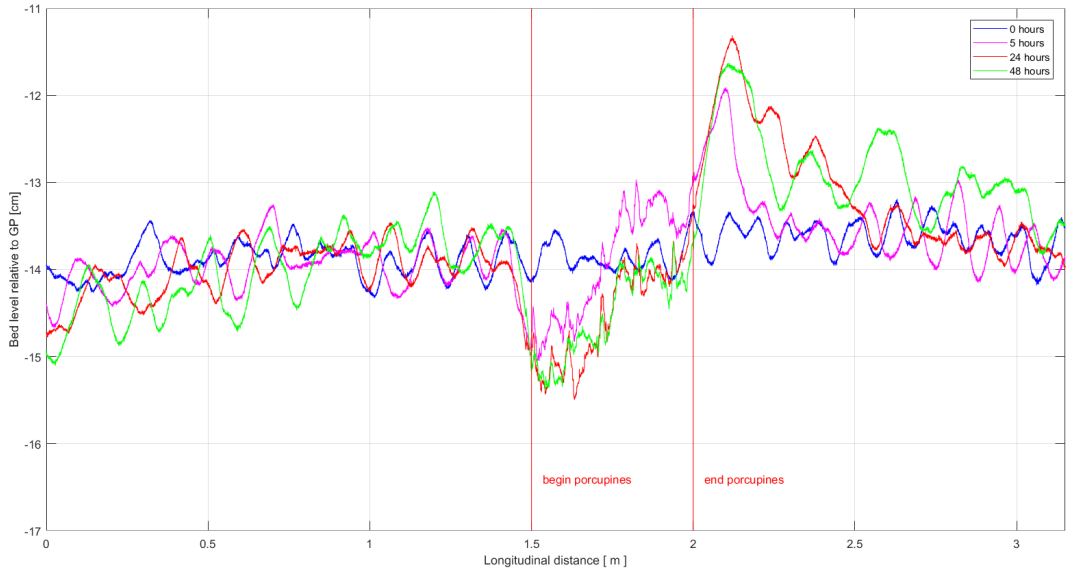

Figure 5.3: Evolution of the bed over time, Experiment 3

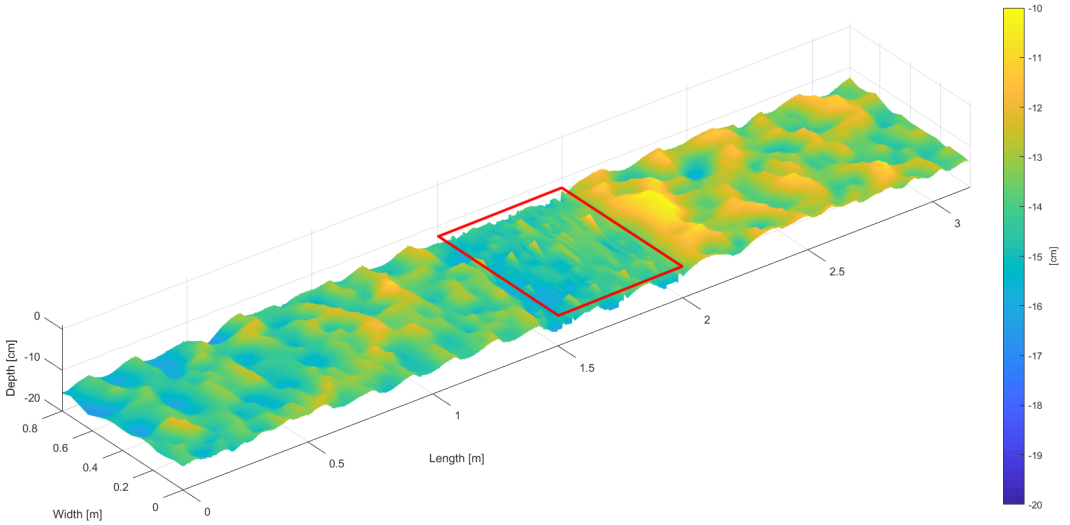

Figure 5.4: Bathymetry after 48 hours, Experiment 3

scour depth between experiments 2 and 3 seem similar, it is shown that the erosion depth is much larger for experiment 1 where a higher flow velocity is present, see figure 5.5.

In this experiment the water depth is much lower while the discharge has remained the same, therefore the flow velocities are much higher. Clearly the porcupines do not work in these circumstances. The increased amount of turbulence is not compensated by a reduction in flow velocity enough. Therefore, larger erosion depths are observed. The bed is eroded the furthest in the first 5 hours after the start of the experiment. After 5 hours the bed within the porcupine field has shown signs of sedimentation again. The porcupines have sunken into the bed enough to prevent further scour, after which ripples of sediment cover the bottom triangle of the porcupines. From that moment on they result in less turbulence near the bottom. Due to the large scour hole the porcupines have sunken into the bed and become less effective in retarding the flow behind the porcupines. Only a small amount of accretion is observed, and the length of the sedimentation bank is much smaller compared to other experiments. The maximum sedimentation height and length are already reached after 5 hours, after this moment in time only small deviations are observed.

In figure 5.6 the effect of increased longitudinal spacing between porcupines from experiment 4 is displayed. The major difference with the experiments described above is observed within the porcupine field. In previous experiments, the field as a whole 'sinks' into the bed by induced erosion of increased turbulence.

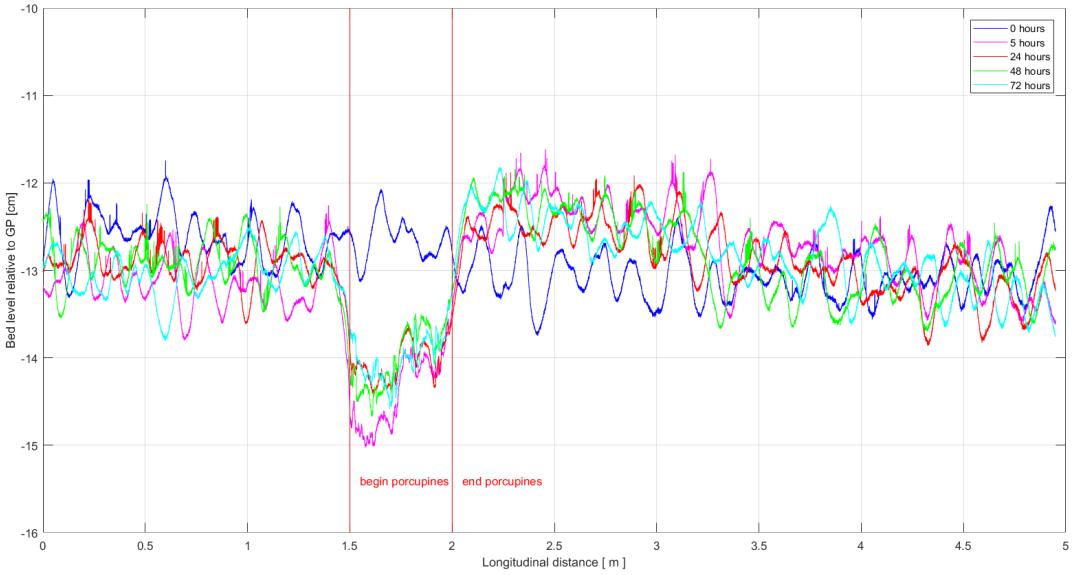

Figure 5.5: Evolution of the bed over time, Experiment 1

In experiments with lower field densities this scour effect does not occur as such. The bed around the porcupines is still eroded but a small sedimentation hump directly behind every line of porcupines diverts the flow upward and away from the bed. This prevents erosion further downstream. In this experiment sedimentation within the field is even observed at the and, so to prevent large scour development within the field increased longitudinal spacing is required. On the contrary however, the rate of sedimentation behind the field is much smaller. Where the sedimentation front has migrated approximately 0.35 metre in 24 hours for experiment 4, the sedimentation front has migrated approximately 1 metre in experiment 2 with similar conditions. Although there is a distinct reduction in erosion, the sedimentation rate is significantly lower with lower density. This indicates that the total amount of accretion is more related to positioning of the porcupines rather than the flow conditions, since the height of the sedimentation bank is similar.

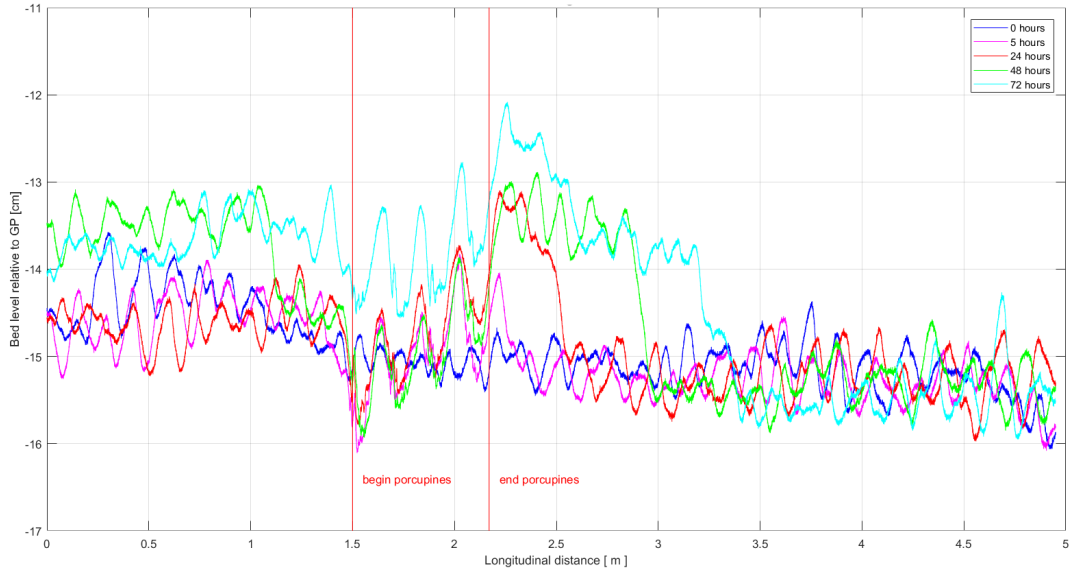

Figure 5.6: Evolution of the bed over time, Experiment 4

The final two measurements after 48 hours and 72 hours show additional sedimentation in the upstream region. This is the results of large scale instabilities of the flume. There is no relation between the sudden sedimentation upstream and the presence of the porcupines and should therefore be neglected.

Partial blockage

For experiments with partial blockage it can be noted that there is a clear difference in bathymetry changes in the transverse direction of the flume. Behind the porcupines sedimentation patterns arise as expected from previous experiments. However sedimentation does not occur in the area on the other side of the flume. since the flow is diverted to this part of the flume, the flow velocities increase and prevent sedimentation. On the contrary, increased erosion is observed in this area of the flume. This is clearly illustrated in figure 5.7.

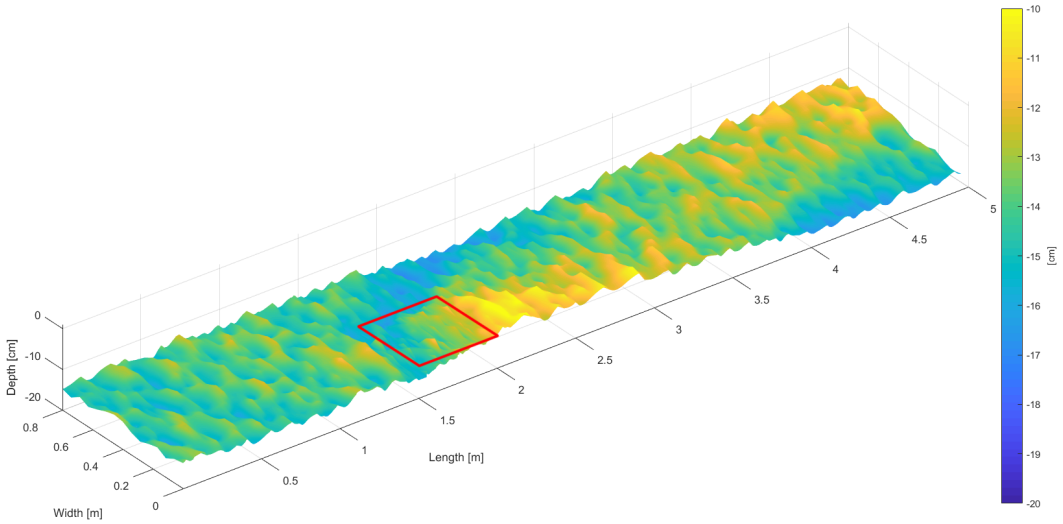

Figure 5.7: Bathymetry after 72 hours, Experiment 6

In this image the porcupines are placed on the right hand side of the flume between 1.5 and 2 metre, indicated by the rectangle. Behind the field a sedimentation hump is observed while a small erosion pit is located next to it on the left hand side. Furthermore it is observed that alternating bank patterns arise which means that some sort of helical flow pattern is generated along the flume. Even though the porcupines do not block the flow completely they still manage to cause enough resistance such that the flow is partly diverted and that helical patterns can exist. This process was explained in section 4.2.2 and is now confirmed. Looking at the shape of the sedimentation hump it becomes clear that right behind the porcupine field the flow is first a little contracted, where maximum flow velocities occur. After this point there is a flow expansion where the flow crosses over to the other side of the flume, combined with the diverted flow over the porcupine field a triangular sedimentation pattern arises which migrates slowly downstream.

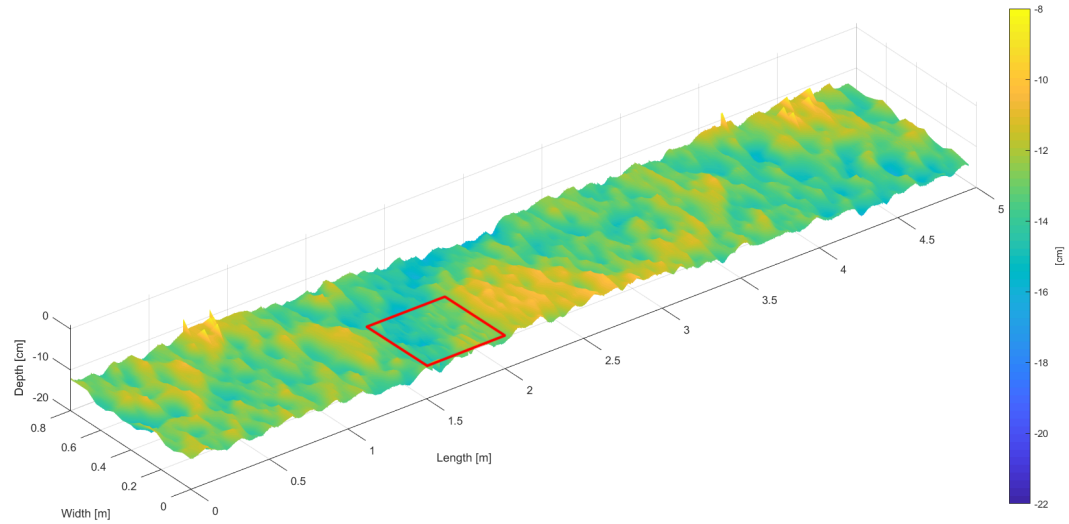

Figure 5.8: Bathymetry after 72 hours of, Experiment 5

Almost an identical sedimentation pattern arises in experiment 5 with a smaller water depth but higher flow velocities. Although experiment 1 indicated that almost no sedimentation occurred behind the porcupines in case of low water level, this experiments shows that while the flow is diverted, the flow regime behind the porcupines are good enough to still result in sedimentation. The sedimentation hight is a little lower, and the length of the sedimentation bank is also smaller, but the similarities are striking.

For the same configuration of porcupines with a lower flow velocity of 25[l/s] a different sedimentation pattern arises. Where a large bulk of sediment was trapped behind the field in the previous experiment, much less sediment is trapped there under the new flow characteristics as is illustrated in figure 5.9. The erosion/sedimentation pattern is rather different when compared with the previous experiments. In this case the erosion pit is located besides a small sedimentation ridge sloping away from the porcupine field, indicating that flow velocities are again pushed aside.

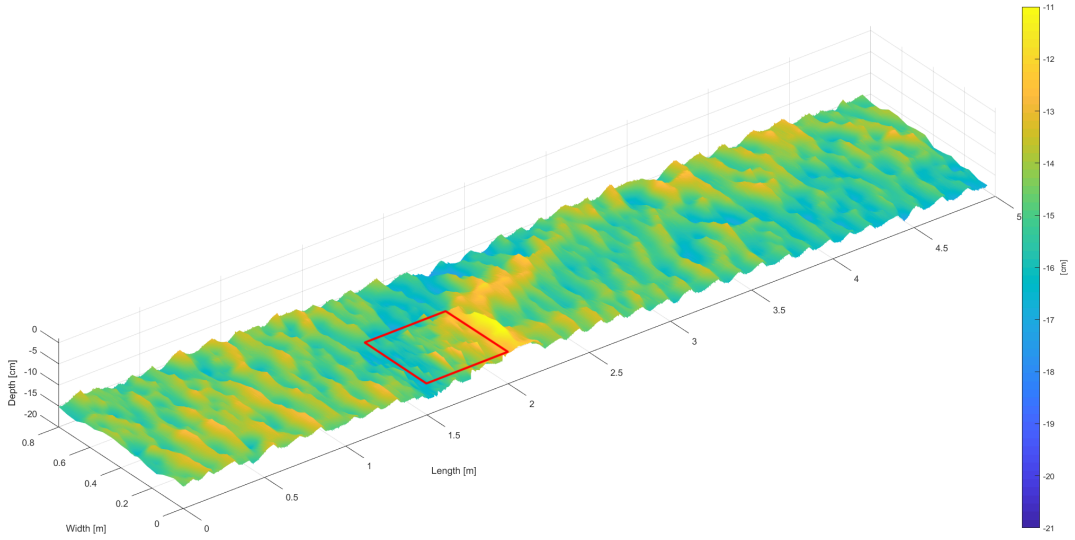

Figure 5.9: Bathymetry after 72 hours, Experiment 7

Because of the lower flow velocities less sediment transport occurs so the bed level does not change that much in the same timespan. However due to the lower velocities it seems that the hydraulics are more affected by the steep sedimentation hump directly behind the porcupine field. This sedimentation hump is generated first as can be observed in appendix D where the full bathymetry update cycle is given. Due to the steep sedimentation hump the flow is pushed even stronger towards the side, resulting in an increased velocity towards the left. This causes the erosion channel that is generated. When the flow expands again sediment is deposited directly at the expansion point. This results in the creation of sediment ridge migrating downstream. This experiment again shows signs of sedimentation on the opposite side of the flume after a certain distance, where the sediment ridge attaches to the other side of the flume.

5.2.2. Flow retardation

To illustrate the retardation in the mobile-bed experiments only the additional effect of bathymetry update is given. Al other aspects of flow retardation have already been treated in section 4.2.2. In experiments with a sediment bed the morphology itself is also an important factor that determines the retardation of the flow. Initially the flow is retarded as described earlier. But due to the scour in the front region of the porcupine field the flow is diverted downward as well as upward. Figures 5.10, 5.11 and 5.12 illustrate the general behaviour in mobile-bed experiments. In all figures it is clearly visible that flow is diverted downward at the beginning of the field.

Behind the field the retardation zone is present again at the start of the experiment comparable to experiments without sediment. Flow velocities are lower in the near bed region and the velocity is downward directed. The reduction in bed shear stress and an increase in velocity gradient combined with energy losses result in the initial sedimentation hump behind the porcupines. But this hump stimulates the retardation of the flow further by diverting the flow strongly upward resulting in additional circulation zones, increased turbulence and energy loss.
Figures 5.11 shows the clear diversion of the flow by the sediment hump. Due to this increased retardation

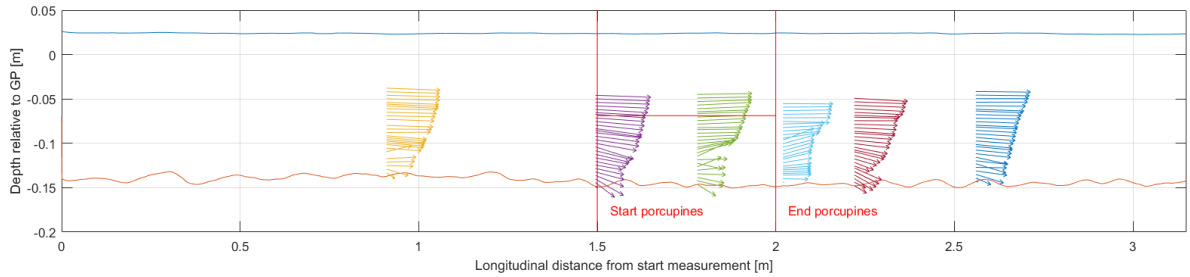

Figure 5.10: Vector plot of velocity profiles at start of experiment 2

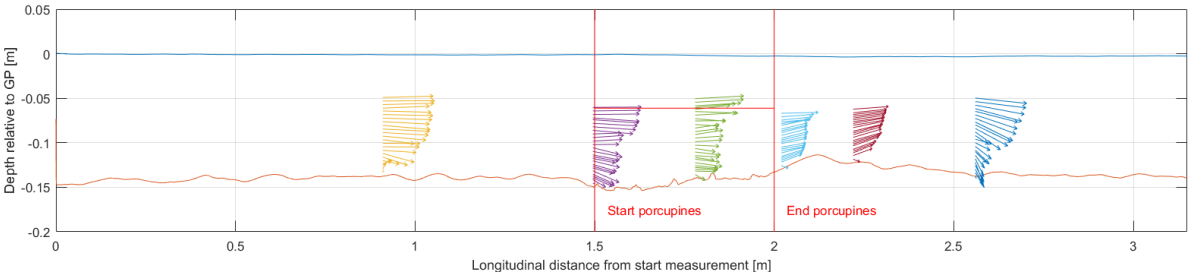

Figure 5.11: Vector plot of velocity profiles after 24 hours, Experiment 3

additional sedimentation behind the hump is stimulated and results in the migration of the sedimentation hump downstream. Over time a new equilibrium between the flow velocities that result in sediment transport, and retardation that results in sedimentation is reached. Velocity profiles restore to a normal profile again and the bed has reached a new equilibrium height behind the porcupine field. This is illustrated in figure 5.12 where the flow lines are horizontal again on top of the sill. Furhter downstream behind the sedimentation front the flow lines expand again where sedimentation occurs once again.

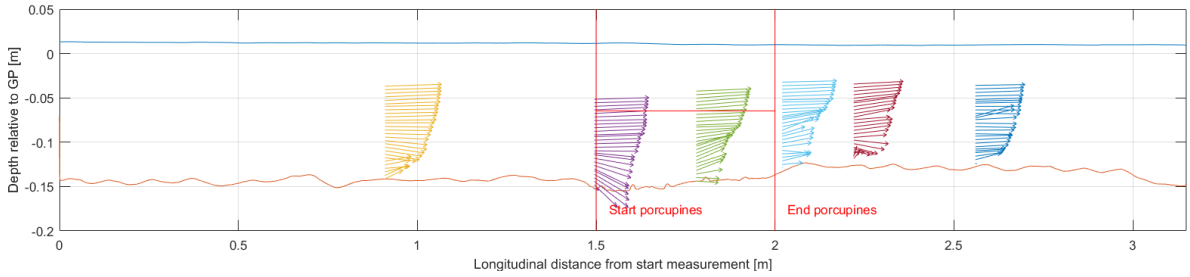

Figure 5.12: Vector plot of velocity profiles after 24 hours, Experiment 2

5.2.3. Velocity profile

Velocity measurements in the mobile-bed experiments are harder than the measurements in the fixed-bed experiments. This is explained in chapter 7 and will not be elaborated here. However some of the measurements were relatively well captured like the velocity profiles of experiment 4, see figures 5.13 and 5.14. In the first figure the velocity profiles at the start of the experiment are given, where the reduction in flow velocity is clearly visible. However the reduction is much smaller compared to the identical experiment without sediment illustrated in 4.16. This is the result of the scour hole where the porcupines have sunken into. This process where the porcupines dig themselves into the bed occurs rather quickly, therefore the effectiveness of the porcupines reduces when applied on a sediment bed. Apparently the bottom part of the porcupines is really effective in reducing the flow velocity, where this part is eliminated in experiments with sediment due to scour. Often the bottom triangle is covered with sediment over time, reducing the effectiveness even further.

What can be observed from figure 5.14 is that the velocity profiles restore to their undisturbed velocity profile

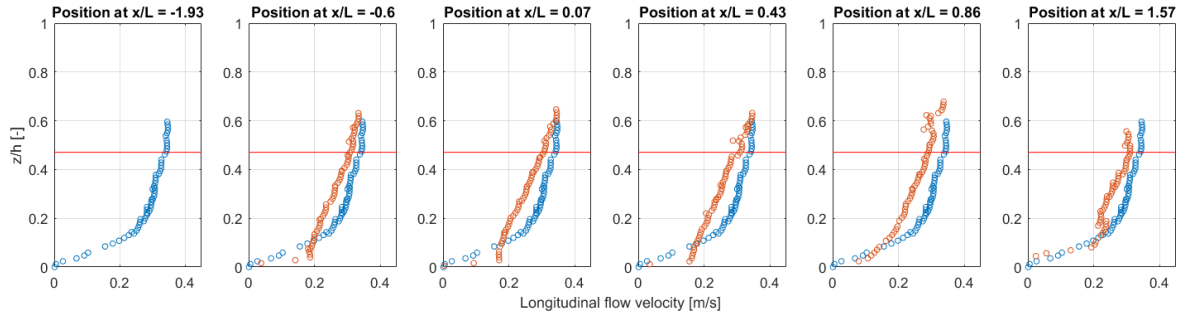

Figure 5.13: Velocity profiles at start of experiment 4

further downstream when the sedimentation front has migrated to that part of the flume. This is the main reason that no sedimentation or erosion occurs any more once the sedimentation front has migrated downstream. It is observed that at $[\frac{x}{L}]$=1.57 the fow velocities reduces again significantly. This is exactly the point of the sedimentation front after 72 hours as illustrated in figure 5.6. This rapid reduction in flow velocity is again an indicator of sedimentation.

Finally, it is observed that the flow velocity near the bottom at the start of the porcupine field at $[\frac{x}{L}]$=-0.6 increases over time. Due to the lower position of the porcupines their effective flow reduction decreases. Especially at the beginning of the field, where the porcupines sink into the bed the most. The flow velocity is higher and directed downward, only stimulating further erosion within the field.

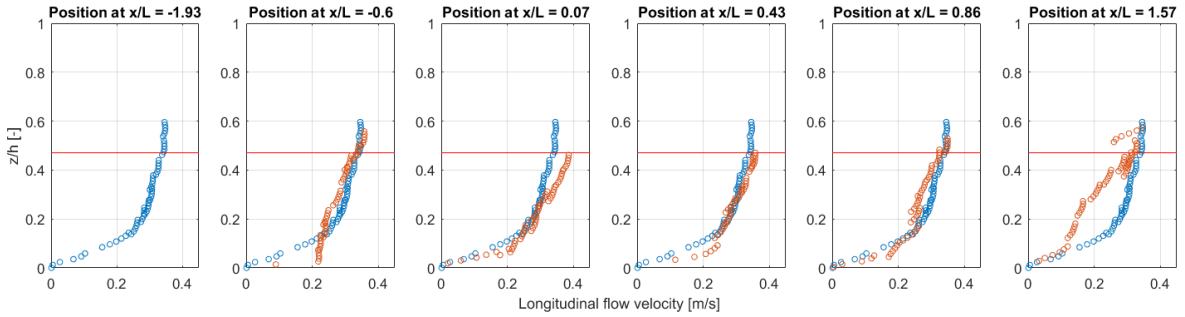

Figure 5.14: Velocity profiles after 72 hours, Experiment 4

5.2.4. Water level

In the mobile-bed experiments the water level changes over time due to the adaptation of the bathymetry. In figure 5.15 below the evolution of the water level is plotted. It is observed that the water level also decreases over time due to evaporation. Althoug it seems like the flume has not been refilled with water, after 24 hours the flume was refilled until the initial water level. However, after an additional 48 hours it has evaporated again to the level plotted in yellow. That means approximatley 0.2 cm of water evaporates every 24 hours.

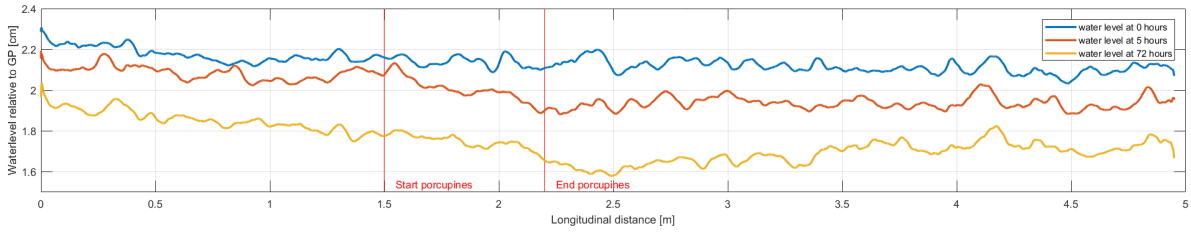

Figure 5.15: Water level development from start until 72 hours after start of experiment4

Besides the evaporation, the effect of the porcupines is visible when comparing the water level without porcupines present (in blue) and the water level after 5 hours since the start of the experiment (in red). The water level clearly reduces in the area where porcupines are present. The water level drop is slightly less compared

with the same configuration of porcupines in the fixed-bed experiments, indicating again that the full potential of the porcupines is not reached in the mobile-bed experiments as a result of the processes described previously.

Something that is observed only in the mobile-bed experiments is the reduction of the water level further downstream of the porcupines, clearly visible after 72 of the experiment. This is the result of the sedimentation bar behind the porcupines causing a contraction of the flow where flow velocities increase. As a result of increased flow velocities, the water level reduces even further, but increase again after a while, where the flow velocities gradually decrease.

5.3. Parameter sensitivity

In the experiments performed a relation was sought between the amount and location of sedimentation or erosion and the parameters that were changed between each experiment. In this section an overview is given of behaviour of the bed related to the different parameters that were changed during the experiments.

5.3.1. Water level

Changing the water level clearly results in a different behaviour of sedimentation and erosion. The amount of sedimentation has drastically been reduces and more erosion within the porcupine field is observed, illustrated in figure 5.16 below. This is the combined effect of a lower water level and higher flow velocity. Clearly these circumstances do not favour the intended goal of the porcupines.

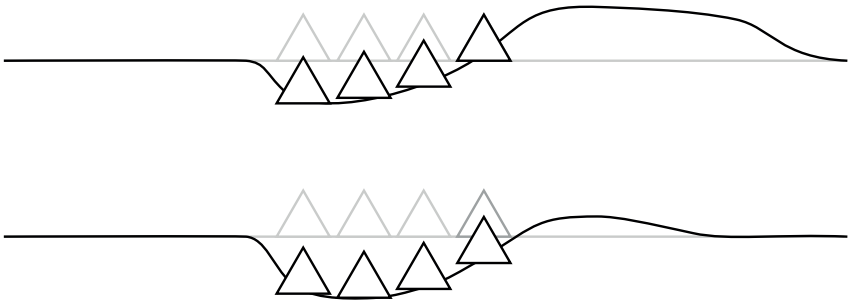

Figure 5.16: General sedimentation patterns for different water levels. Top figure represents high water level, bottom figure represents low water level.

5.3.2. Flow velocity

For experiments with higher flow velocities it seems that the area of sedimentation is more continuous compared to the are of sedimentation during low flow conditions. In figure 5.17 a schematic overview of the morhphodynamic response of the bed is given where it is illustrated that for higher velocities a larger plateau is generated mildly sloping down. In the other figure it is shown that for lower flow conditions this does not happen. In case of lower flow velocities multiple sedimentation humps or dunes are generated decreasing in size in longitudinal direction.

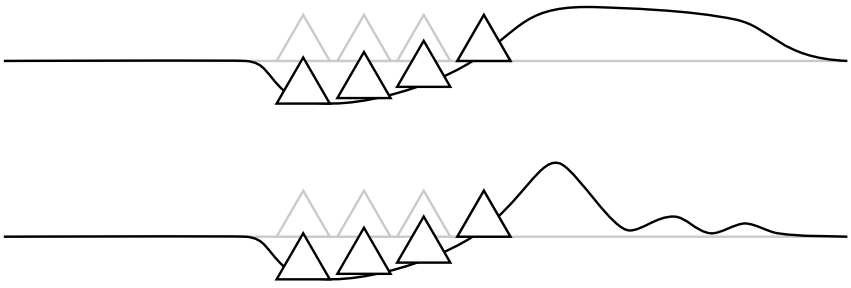

Figure 5.17: General sedimentation patterns for different flow velocities. Top figure represents high flow velocities, bottom figure represents low flow velocities.

However due to lower flow velocities the height of the sedimentation bar is larger. It is assumed that the erosion within the field is less, however this is not clearly measured in the conducted experiment. In the experiments with smaller depths, and consequently higher flow velocities larger erosion depths have been measured, so it is expected that with much lower flow velocities the amount of erosion becomes less.

5.3.3. Field density

For a denser porcupine field it is shown in the experiments that the sedimentation rate behind the porcupines is much quicker compared to the scenario with a field half the density. This may be due to the fact that in the case of lower density sedimentation also occurs within the field, which does not occur for higher density fields. The pattern of the sedimentation field behind the porcupines is similar but develops quicker for higher densities.

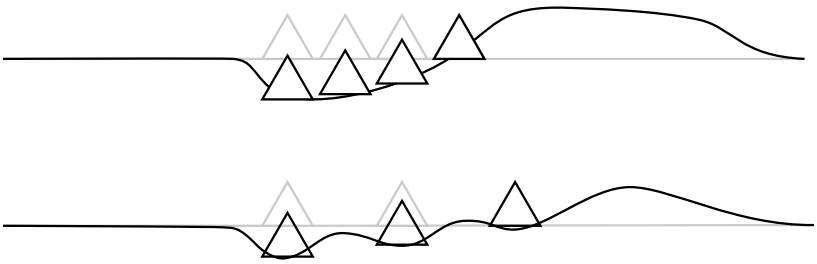

Figure 5.18: General sedimentation patterns for different field densities.Top figure represents the higher density field, bottom figure represents the lower density field.

5.3.4. Asymmetry

When porcupines are only placed to partly block the flow alternating bank patterns start to arise. The sedimentation bar behind the porcupines becomes smaller due to the horizontal retarded flow patterns that start to erode the banks from the side and cause the alternating pattern. In figure 5.19 the general cross section of the part behind the porcupines is indicated with a thick line, while the unblocked part is indicated with a thin line.

This unblocked part is subject to increased erosion at the same location where sedimentation occurs behind the blocked part. This is the result of the diverted flow towards the side, were flow velocities are higher near the bottom and result in erosion. Furhter downstream however a small amount of sedimentation is observed. it is expected that after a longer time period this bar starst developing in height.

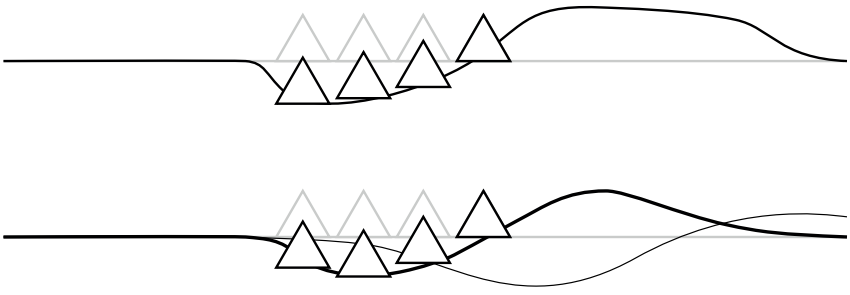

Figure 5.19: General sedimentation patterns for asymmetrical placement.Top figure represents placement over full width, bottom figure represents placement over half the width. Thick line represents the blocked part. Thin line represents the unblocked part

6 Analysis

In this chapter the analysis of the experiments are presented. In section 6.1 the hydraulic behaviour is analysed, where a relation is found for the deceleration. Furthermore the roughness is determined and tested by comparing water level measurements with model predictions. In section 6.2 the morphological processes are described, where the sedimentation volumes, rates and heights are described. Combination of the deceleration rate and sedimentation patterns lead to a description for the equilibrium time scales. Finally the sedimentation patterns around a partially blocked flume will be elaborated in more detail.

6.1. Hydraulic processes

6.1.1. Deceleration

Multiple velocity profiles have been measured in longitudinal direction in front and behind the porcupine field to observe the velocity behaviour due to the presence of porcupines. In order to quantify the effectiveness of the porcupines in different environments, a term 'deceleration rate' is introduced. This rate reflects the reduction of mean flow velocity relative to the undisturbed flow velocities. Equation 6.1 defines the deceleration rate as the undisturbed velocity minus the velocity at the point of interest divided by the undisturbed velocity. Only the velocities within the range of the porcupine height are taken into account to determine the mean velocity in that range.

$$\lambda = \frac{u_{p_{x/L=-2}} - u_{p_{x/L}}}{u_{p_{x/L=-2}}} \tag{6.1}$$

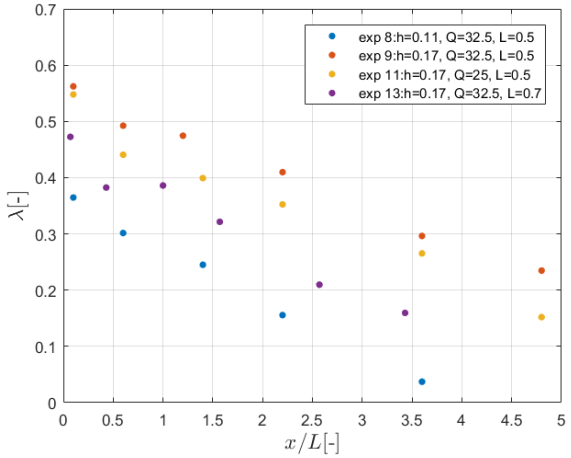

Figure 6.1: Deceleration rate of the flow

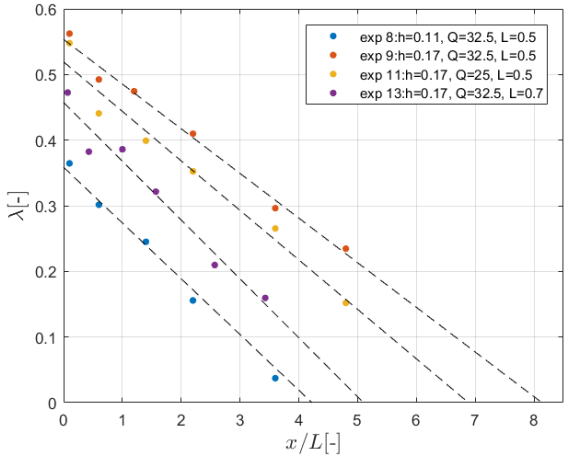

Figure 6.2: Extrapolation of the deceleration rate to λ_0

Figure 6.1 shows the variation of the deceleration rate λ over the longitudinal distance behind the porcupines x/L. It is observed that a linear trend seems to be present in all experiments. As observed in section 4.2.3

the flow profiles are restored much quicker in experiment 8 with a lower water level and it almost completely restored at the end of the measure domain. For all other experiments this restoration point is not observed, but by linear extrapolating the deceleration rates it is possible to determine the distance after which the effect of porcupines is possibly extinguished.

For all experiments hold that the initial deceleration directly behind the porcupines is approximately between 0.4 and 0.6 which can be used to estimate the expected flow velocity when no measurements are available. If the mean flow velocity in a river is known, an initial guess of the hydrodynamic response due to porcupines can now be done depending on the conditions and layout of the field. In table 6.1 the linear extrapolated values for all experiments to $\lambda = 0$ are given. It is observed that the experiments with the lower density and lower water level restore the quickest. Fields with lower density do not only result in less deceleration, they also restore quicker. Note that the length of the porcupine field with lower density is longer and therefore results in a longer distance than experiment 11 after which the velocity profiles are restored. However compared to their relative field length experiment 11 performs better.

Table 6.1: Extrapolation of deceleration rates

Experiment	L [m]	λ_0 [-]	i [-]	$(\frac{x}{L})_0$ [-]	x [m]
8	0.5	0.359	0.085	4.21	2.103
9	0.5	0.553	0.068	8.05	4.070
11	0.5	0.519	0.075	6.90	3.443
13	0.7	0.458	0.090	5.07	3.570

Denser fields with lower flow velocities work relatively best, since their distance before the velocity profiles are restored are slightly longer it is expected that these circumstance result in a larger sedimentation pattern as well. In section 6.2 the relation between the deceleration rate and sedimentation patterns will be elaborated.

6.1.2. Roughness

To determine the representative roughness of the porcupines the equation derived by Baptist et al. (2007), given in equation 6.2, is used. This equation is validated by multiple researchers who study the effect of vegetation. However, as stated in appendix A.5 the equation is derived for experiments where vegetation is present over a long distance and where uniform flow conditions are present. This entails that the depth over longitudinal distance remains the same and that uniform velocities inside the vegetation is reached such that it is more or less constant over the vertical distance. In the top part of the water column, on top of the vegetation a logarithmic velocity profile is reached again.

$$C_r = \sqrt{\frac{1}{\frac{1}{C_b^2} + \frac{C_D m A}{2g}}} + \frac{\sqrt{g}}{\kappa} \ln\left(\frac{h}{k}\right) \tag{6.2}$$

In the experiments performed in this research the porcupines have not been placed over a long distance, therefore uniform flow cannot be assumed. The problem that arises is that the water level gradient that is measured over the flume is not the actual gradient that is present. The actual water level is composed of a water level gradient over the porcupine field and the gradient over the rest of the flume. This problem is illustrated in figure 6.3 where the effect of porcupines is clearly visible, indicated with the red line.

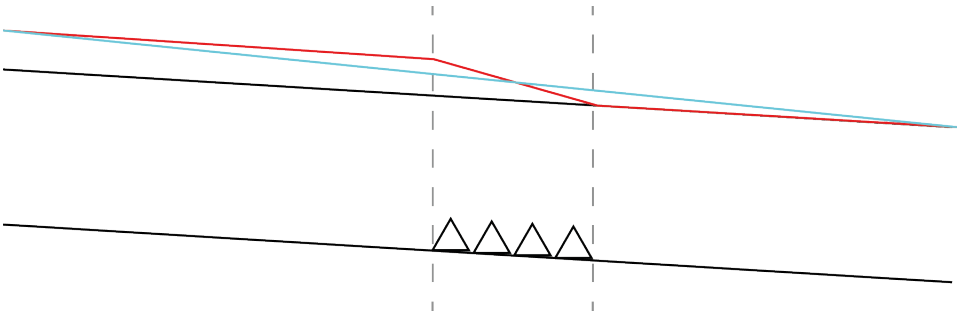

Figure 6.3: Difference in water level gradient

The total shear stress, computed as $\tau_t = \rho ghi$, does no longer represent the bed covered with porcupines. It only represents the bed with porcupines over a small distance. This water level gradient that is used in the equations now becomes the blue line in figure 6.3, which is not the true water level observed in the experiments. Therefore the porcupine shear stress can not be determined as prescribed by Baptist et al. (2007) in appendix A.5.

For this analysis however it is assumed that there is a more or less uniform constant flow velocity inside the porcupine field, which has been shown in section 4.2.3 Furthermore it is assumed that the total shear stress of the porcupines is composed of the bed shear stress of an empty flume and the porcupine shear stress, as described by Baptist et al. (2007).

$$\tau_t = \tau_b + \tau_p \tag{6.3}$$

The total shear stress should always be equal to ρghi since this is the force compensating the roughness exerted by the bed and porcupines. Although the distance is short and the gradient is relatively steep it is still assumed to be a correct approximation of the total shear stress. The bed shear stress is determined by measuring the water level gradient over an empty flume where uniform flow is present. The porcupine shear stress is determined by assuming a uniform flow profile over the porcupine height with a certain drag coefficient, C_D. The frontal area is determined as the three upright rods of the porcupine times the angle under which they are positioned, plus two times the frontal area of a single rod for the bottom horizontal triangle.

$$\tau_p = \frac{1}{2}\rho C_D m A u_p^2 \tag{6.4}$$

By assuming that the energy loss over the porcupines can be related to the total shear stress, described in equation 6.3 the measurement should follow the theoretical line given as the black line in figure 6.4. This figure illustrates the balance between the energy loss based on water level differences and the sum of bed shear stress an porcupine stress of a total blocked flume.It can be seen that there is still a large deviation from the theoretical line by approximating the porcupine field with a drag coefficient of 1. For a completely blocked flume a drag coefficient of approximatly 5.5 is required to match the theoretical stress.

This is larger than what would physically be possible since the maximum pressure difference over an object can result in a maximum drag coefficient of 2. This is elaborated in appendix A.6. Higher drag coefficient can only be described for viscosity dominated conditions in which the Reynolds number is very low. Then the drag coefficient becomes proportional to the velocity, whereas in conditions with a high Reynolds number the drag is proportional to the velocity squared. In this research Reynolds numbers are high, indicating no viscosity dominated flow. Besides, due to large velocity differences inside the porcupine field and above it is assumed that Carnot energy losses are present behind the porcupine where the velocity profile is restored. Excluding such energy losses may result in smaller drag coefficients as well. Higher drag coefficients are therefore subject to discussion which is elaborated in section 7.1.9.

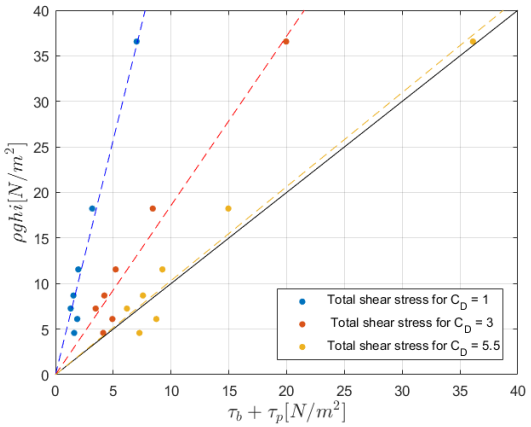

Figure 6.4: Total shear of porcupines dependant on drag coefficient, for all experiments with total blockage of the flow

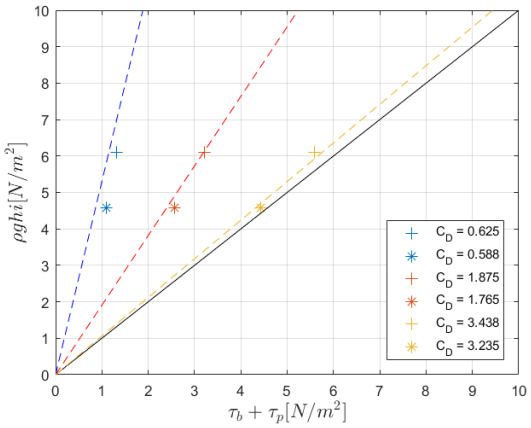

Figure 6.5: Total shear of low density porcupine fields dependant on drag coefficient, for experiments with total blockage of the flow

For all three different drag coefficients it can be observed that there are two dots below the trend line in the lower shear stress region. All other points seem to follow the trend line relatively well, which indicates that the drag coefficient does not depend that much on the different settings in the experiments. The two points that do deviate from the trend line are the experiments with lower field density. This indicates that there is a separate field drag that depends on the configuration of the field. This an additional drag on top of the individual drag of porcupines and seems to be dominate the total field roughness. It is shown in figure 6.5 that for the experiments with half the density and a third of the density of the initial field, the drag coefficient is reduced by a factor 1.6 and 1.7 respectively to match the trend line of the other experiments. Experiments with half the density are indicated by the + sign, while experiments with a quarter of the density are indicated by the $*$ sign.

Interestingly enough it is observed that for the lowest density, the drag reduces only slightly more compared to middle density. Apparently the drag significantly reduces when longitudinal spacing becomes larger. But when spacing increases more the total drag decreases less quick, implying that there is an optimum where maximum drag is created with less porcupines, or with the same amount of porcupines but over a larger distance.

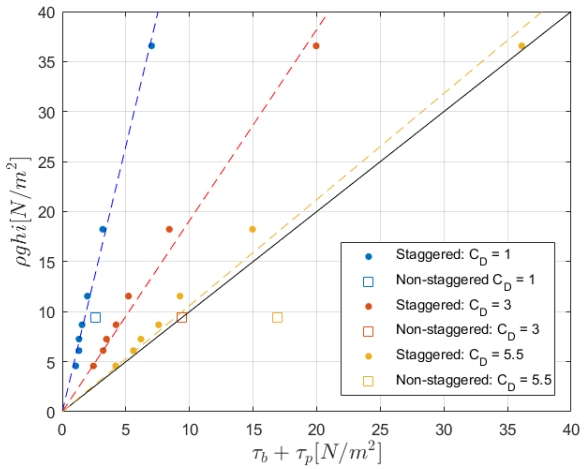

Figure 6.6: Shear difference for non-staggered grid

If the non-staggered grid is compared to the staggered grid it is observed that this method is less effective. The squares in figure 6.6 indicates the non-staggered grid. Clearly it results in significantly less drag and this orientation of the field satisfies the theoretical line with a drag coefficient of 3. The suggestion that the flow is less retarded and affected by a non-staggered grid from section 4.2.2 is strengthened by this finding.

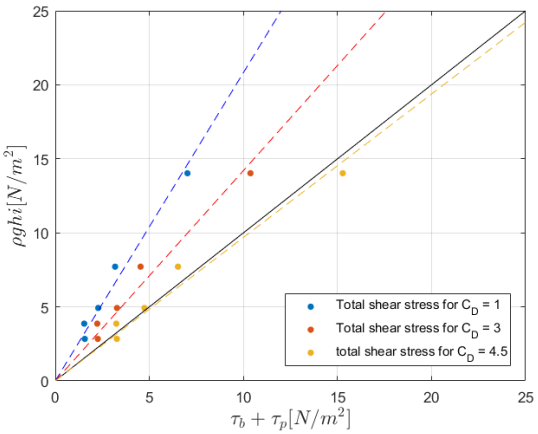

Figure 6.7: Total shear of porcupines dependant on drag coefficient, for experiments with partial blockage

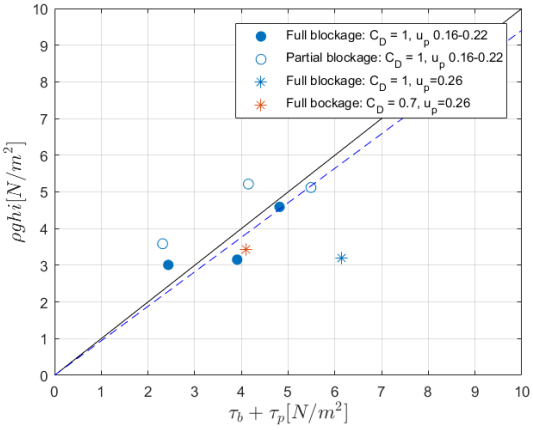

Figure 6.8: Total shear of porcupine fields with sediment bed dependant on drag coefficient, for all experiments

For the experiment with partial blockage it is observed that the total drag is lower in comparison with the same experiments where porcupines are placed over the total width. The trend lines are already closer to the theoretical line for a drag coefficient of 1, and give the best fit for a C_D of 4.5. Although larger deviations from the trend are observed, it becomes clear that the friction for experiments with porcupines over the total width are not the same when porcupines are placed over half the width. However, they have similar effectiveness when compared to a field over the total width with lower densities. This indicates that the friction felt by the flow is not dependent on the position of porcupines over the width, when approximately the same amount of porcupines are used. In figure 6.7 the width average water level gradient is used. The transverse water level gradient results in horizontal mixing, which would eventually lead to the observed energy loss. Therefore it is sufficient to work with the width average gradient.

Finally, in the mobile-bed experiments it is observed that the porcupines result in a significant reduced drag. Although the measurements are less accurate it is clearly observed that the drag coefficient is closer to 1. For experiments with high average flow velocities the results start to deviate. In those experiments a lower drag coefficient is sufficient. The severe reduction in effectiveness is the result of the combine effect that the porcupines sink into the bed as an effect of their self generated turbulence near the bottom, and a reduction in the frontal area due to the coverage of the bottom triangle near the bed. Besides, it was also observed that velocity differences in the porcupine field for mobile-bed experiments were much smaller compared to fixed-bed experiments. The drag coefficient is proportional to the velocity squared which means that a small difference in flow velocity has a large influence on the resulting drag. A higher u_p results in a smaller C_D indicating that velocity averaging inside the porcupine field may result in a significant overestimation of drag coefficients. Since the roughness in mobile-bed experiments is severely hampered by morphological development over time, the remaining part of this analysis focusses on the fixed-bed experiments only. In appendix E, a further elaboration on the mobile-bed experiments will be given.

Table 6.2: Overview of resulting shear stresses and representative roughness described by the formulation of Baptist, for the fixed-bed experiments. Fully blocked experiments: $C_D = 5.5$, partly blocked experiments: $C_D = 4.5$

exp.	h [m]	Q [l/s]	u [m/s]	longitudinal spacing [m]	ΔE [cm]	i_{wl} [-]	u_p [m/s]	τ_b [N/m^2]	τ_p [N/m^2]	τ_t [N/m^2]	C_r [m$^{1/2}$/s]
8	0.114	32.5	0.36	0.01	1.723	0.0327	0.22	0.56	35.56	36.12	6.41
9	0.1732	32.5	0.23	0.01	0.401	0.0068	0.11	0.36	8.89	9.25	9.69
10	0.1968	32.5	0.21	0.01	0.286	0.0045	0.1	0.22	7.35	7.57	10.69
11	0.172	25	0.18	0.01	0.273	0.0043	0.09	0.23	5.95	6.18	9.63
12	0.1705	40	0.29	0.01	0.621	0.0109	0.14	0.56	14.40	14.96	9.57
13	0.173	32.5	0.23	0.02	0.359	0.0036	0.15	0.36	5.23	5.59	12.44*
14	0.1728	32.5	0.24	0.03	0.271	0.0027	0.17	0.36	3.84	4.20	14.19*
15	0.1075	32.5	0.38	0.01	1.107	0.0133	0.22	0.56	14.72	18.56	7.94
16	0.1731	32.5	0.23	0.01	0.248	0.0029	0.12	0.36	4.38	5.71	11.66
17	0.2073	32.5	0.20	0.01	0.156	0.0019	0.1	0.2	3.04	3.92	13.08
18	0.1606	25	0.19	0.01	0.211	0.0018	0.1	0.23	3.04	3.95	11.07
19	0.1673	40	0.30	0.01	0.382	0.0047	0.14	0.56	5.96	7.85	11.41

* Deviating drag coefficients are applied

In table 6.2 an overview of the resulting total shear stress and representative Chézy roughness is given for the fixed-bed experiments. These values follow from equations 6.2, 6.3 and 6.4 with the determined drag coefficients that give the best fit for the theoretical line. In the figures below the dependency between the different settings is given for the resulting porcupine stress and representative roughness.

For the depth dependency of the shear stress it should be kept in mind that the flow velocity is also fluctuating since the discharge remains equal. Therefore a non-linear relation is observed. This is due to the fact that both the water level and the flow velocity have an effect on the porcupine stress. Taking a look at the velocity dependency a more linear relation is observed between the increasing shear stress and flow velocities. Combining this with varying water levels results in non-linear behaviour. For both the fully blocked and partially blocked flow conditions the dependency relations are similar. As was shown in the determination of the drag coefficient, reducing the density of the porcupine field does not give a linear relation for the drag reduction. The same holds for the shear stress. This is clearly illustrated in figure 6.11 where the longitudinal distance is increased in identical steps, however the shear stress is not reduced in identical steps.

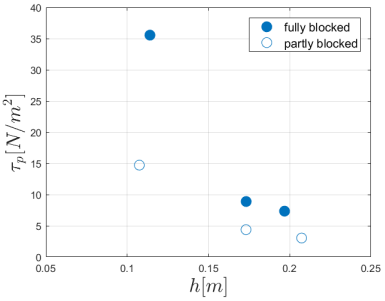

Figure 6.9: Depth dependency of τ_p

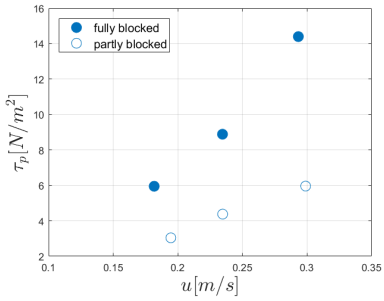

Figure 6.10: Velocity dependency of τ_p

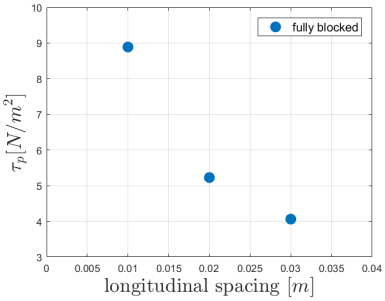

Figure 6.11: Density dependency of τ_p

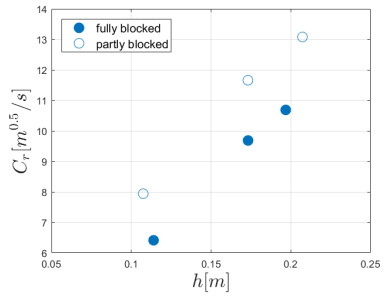

Figure 6.12: Depth dependency of C_r

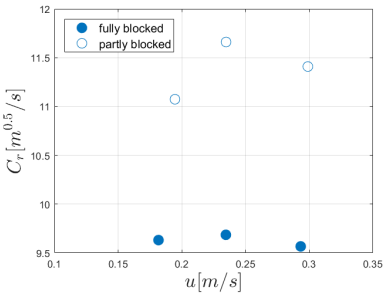

Figure 6.13: Velocity dependency of C_r

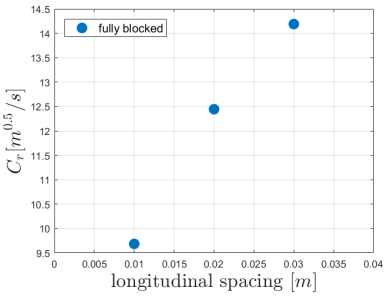

Figure 6.14: Density dependency of C_r

By filling in equation 6.2 the Chézy values in in table 6.2 are obtained. These are plotted in relation to their corresponding variable in the figures 6.12, 6.13 and 6.14. They show a linear relation with the water depth and the density of the field. Smaller depths and denser fields result in higher roughness. However, the flow velocity seems to be of less importance for the roughness. Small differences are observed where flow velocities are varied.

6.1.3. Drag coefficient

In the analysis so far it is assumed that a single drag coefficient can be used to describe the total porcupine field. It is already mentioned that the drag coefficient is highly determined by the flow velocity but since the flow velocity also varies over the depth it is natural to assume that the exerted drag therefore also varies. Sukhodolova & Sukhodolov (2012) have derived a relation in which the drag is described as a function of the gradients in turbulent shear stress and velocity over the vertical given in equation 6.5

$$C_D = \frac{2\left(g i_0 + \frac{1}{\rho}\frac{\mathrm{d}\tau_{xz}}{\mathrm{d}z}\right)}{Au^2(z)} \tag{6.5}$$

Applying this formulation on the measurements from the experiments results in the drag variation over the porcupine height visualised in figure 6.15. Here the equation is is applied for the situation upstream from the porcupines in the undisturbed flow, in the middle of the porcupine field, and just downstream of the porcupine field. Especially in the measurement inside the porcupine field it becomes apparent that the porcupine top significantly increases the drag. Further downstream this effect is not observed that well.

Clearly the mean drag coefficient is lower than the derived coefficients previously. This is partly due to the fact that formulations applied in the method of Baptist assume a fully developed flow field with uniform velocity profiles. This would only be obtained for much larger porcupine fields where the flow on top of the porcupines has fully developed again. In these experiments the porcupine field partly functions as a weir or groyne over which rapid velocity changes are present. Consequently the derivation of drag coefficients with formulations derived for uniform flow do not work accurately. The formulation of Sukhodolova & Sukhodolov (2012) does not require uniform flow since it takes into account velocity measurements at each point individually. The observed values for C_D in figure 6.15 at $x/L = -0.48$ in the middle of the porcupine field are almost all below the physical maximum value of 2 where they are much higher downstream of the porcupine field,

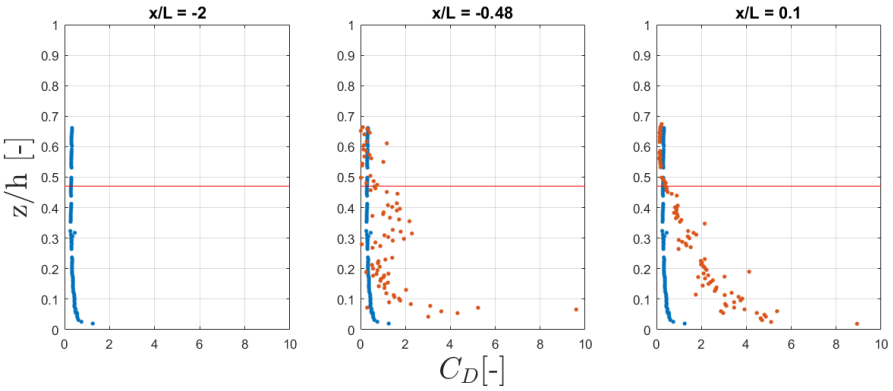

Figure 6.15: Drag coefficient varying over the depth, Experiment 11. Blue indicates the undisturbed profile, red indicates the profile at location $\frac{x}{L}$

indicating that there may be an additional effect downstream from the porcupines that affects the total drag force of the porcupine field. It is assumed that Carnot energy losses behind the porcupine field may interfere in the computations of the drag coefficient. This effect is further elaborated in section 7.1.9.

6.1.4. Water level gradient

To check whether the obtained Chézy values represent the flow correctly the measured water levels are compared to a 1D model calculation with the SOBEK model that takes into account the Belanger equations for backwater effects. In figure 6.16 the modelled water level is plotted over the water level measurements for the calculated Chézy roughness, followed by a best possible fit with different Chézy values. It can be observed that for this particular experiment the initial estimation of the roughness is almost a perfect fit with the observed water level. After a small adjustment the model follows the measurement almost perfectly.

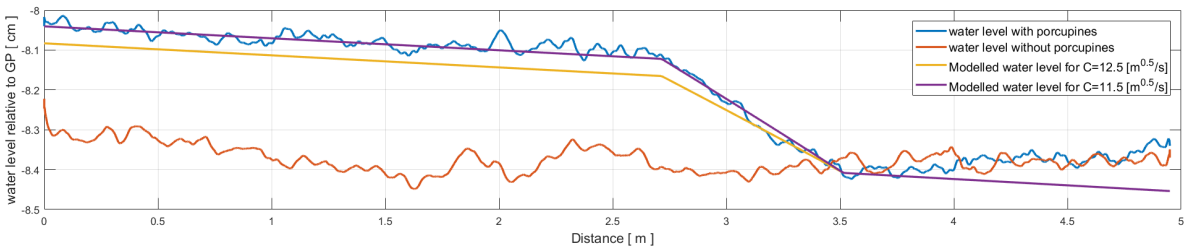

Figure 6.16: Water level comparison with SOBEK, Experiment 13

For other experiments the model deviates more from the observed water levels. In figure 6.17 it is observed that the water level upstream is not reached in the model. This is due to the fact that the estimated Chézy value is already below 10, which is the maximum roughness that can be applied in this model. No fit can be found this way to see for which roughness value the water levels start to match. Besides the deviation in the upstream region of the porcupines there is also a deviation downstream from the porcupines. This deviation is present in all experiments.

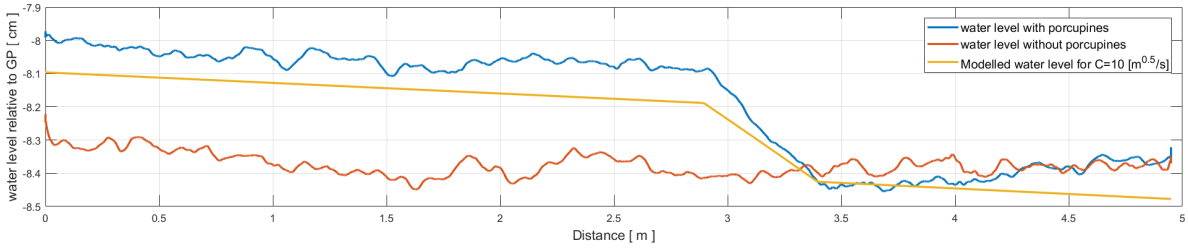

Figure 6.17: Water level comparison with SOBEK, Experiment 9

In section 4.2.4 it was mentioned that due to Bernoulli effects the water experiences an acceleration over the porcupines and deceleration downstream. Besides from the energy loss that is caused by the increased turbulence, there is also a decelerating flow behind the porcupines where pressure restoration occurs. Thus the water level restores partly to its original level minus the loss of energy. However it is observed that the water level upstream follows the computed gradient from the model for both measurements. Downstream however both measurements deviate. It is expected that this is the result of a small backwater that is caused by the weir downstream that controls the water level in the flume.

6.1.5. Bed shear stress

Figure 6.18 gives an overview of the Reynolds shear stresses close to the bottom of the flume for all fixed-bed experiments. it is observed that higher in the water column the shear stresses increase significantly which was also described in section 4.2.5. The most interesting part of these shear stresses are close to the bottom, where the bed shear stress is approximated by this method. It is observed that for almost all experiments the bed shear stress becomes lower compared to the undisturbed velocity profile upstream from the porcupine field. This means that sediment will be transported less quick behind porcupines. Especially if the sediment of a river is less well graded compared to the sediment in these experiments this has a significant effect on the sediment transport.

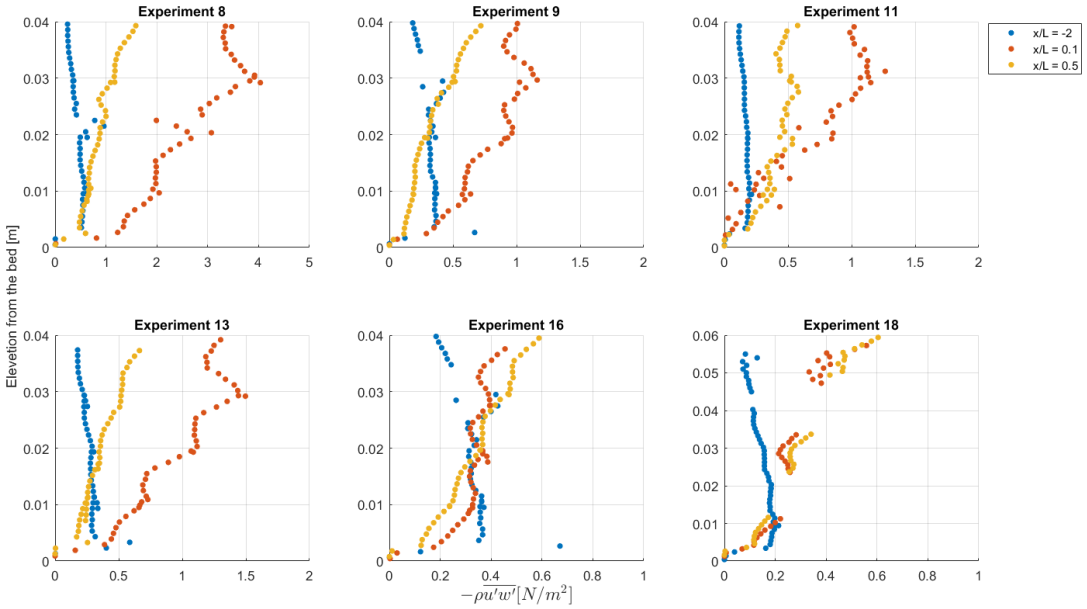

Figure 6.18: Shear stresses close to the bottom for the undisturbed velocit profiles at x/L = -2, directly behind the porcupines at x/L = 0.05 and a little downstream at x/L = 0.5

It is observed that for most experiments the bed shear stress reduces more, further downstream from the porcupines. Apparently the most severe turbulence contribution has been removed after approximately half the porcupine field length. The bed shear stress reduction for experiment 11 with lower discharge is not that large. This indicates that turbulent fluctuations are dissipated faster where flow velocities are lower and that less turbulent mixing occurs. Consequently less dynamic behaviour should be observed which is clearly the case when compared to the same set-up in the mobile-bed-experiment. In case of smaller field densities, experiment 13, the reduction is also less when compared to similar conditions in experiment 9. This is the reason why sedimentation rates are lower for experiments with lower densities. For experiments 16 and 18, the experiments with partial blockage, there is not much difference compared to their corresponding full blockage experiments 9 and 11 respectively. Both experiments show a stronger total shear reduction in the near bed region. This is due to the fact that most of the flow is diverted to the unblocked part, automatically reducing the total shear stress behind the porcupines.

6.2. Morphological processes

6.2.1. Volume

In the mobile-bed experiments it is observed that sedimentation occurs behind the porcupine field up to a certain level. From this moment the sediment does no longer migrate in the vertical direction, but starts migrating downstream in longitudinal direction. Over time the sedimentation front migrates further downstream resulting in a section of the flume with smaller depths and higher flow velocities. To check whether this volume of sediment that is deposited downstream of the porcupines is not only a redistribution of sediment from inside the porcupine field, the volumes are calculated. It is observed that the volume of sedimentation behind the porcupines is higher for all experiments compared to the amount of erosion inside the field. This means that porcupines work in effectively capturing sediment. For experiment 4 with lower porcupine density it is even observed that, on average, sedimentation occurs instead of erosion within the field.

For all volume changes it holds that the computed volume is relative to the measurement at the start of the experiment. The volumes in the figure are therefore the net volume changes since the placement of the porcupines. Consequently, the difference in successive measurements is the volume change in between consecutive measurements in time. In experiment 1 and 3 for instance, it is observed that the volume changes decline over time indicating that they are evolving towards and equilibrium.

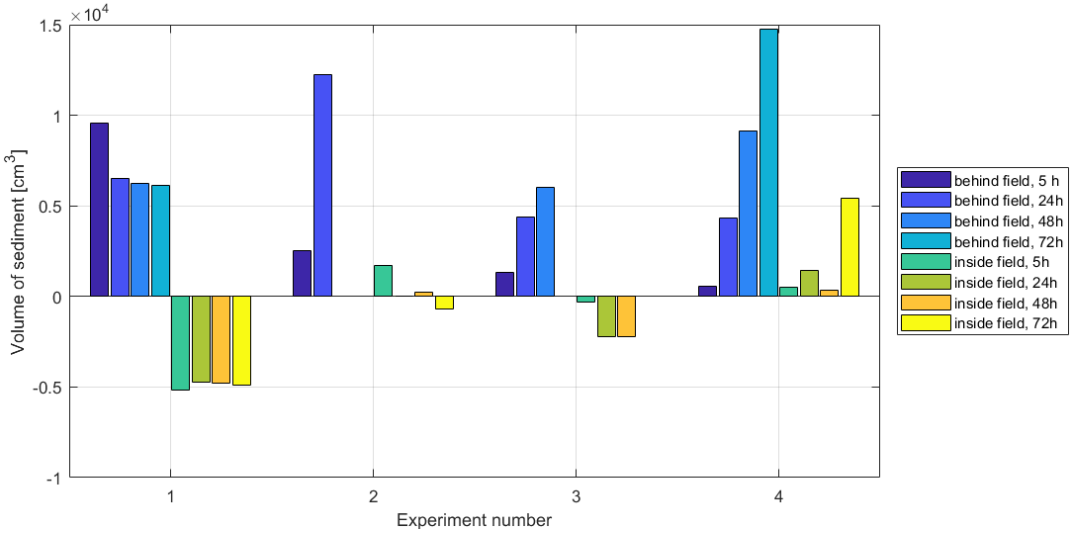

Figure 6.19: Amount of sedimentation and erosion inside and behind the porcupine field for different moments in time. Experiment 1: h=0.11 [m], Q=32.5 [l/s], L=0.5 [m]. Experiment 2: h=0.17 [m], Q=32.5 [l/s], L=0.5 [m]. Experiment 3: h=0.17 [m], Q=25 [l/s], L=0.5 [m]. Experiment 4: h=0.17 [m], Q=32.5 [l/s], L=0.7 [m]

For experiment 2 and 3 data is missing in figure 6.19. The final measurements of experiment 3 are lost and can therefore not be analysed. For experiment 2 it is observed that the final two measurements behind the porcupine field are missing. This is due to the fact that the sedimentation front was already migrated outside the measure domain of the flume. It is observed that the migration has continued further downstream, however this is not captured in any measurement. It does seem that no further erosion inside the porcupine field occurs, while sedimentation clearly continued, indicating that the porcupines efficiently capture sediment in their retardation zone.

6.2.2. Sedimentation rate

In the preceding section it is mentioned that the sedimentation migrates downstream with a sedimentation front. In figure 6.20 the travelled distance of the sediment front from the porcupine field, x_{sf} is given for the four experiments with total blockage. Over time the development is observed, where it can be noted that for experiment 1 with a low water level the migration of the sedimentation front is extremely quick in the first hours. After the first hours however the sediment front seems to migrate back. This explains why the total accreted volume behind the porcupines is also decreasing over time. The height of the sedimentation bar is very limited and therefore it can be expected that porcupines do not work properly in conditions with high flow velocities and low water levels.

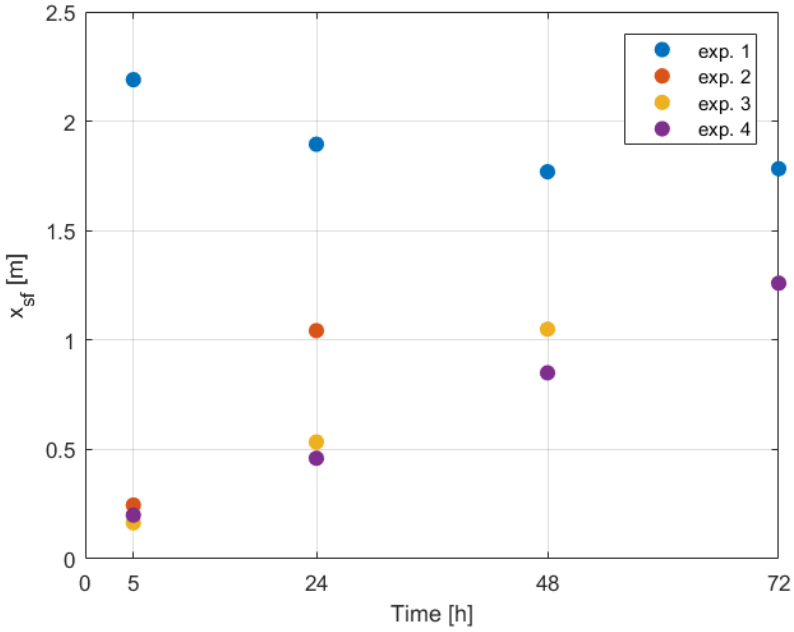

Figure 6.20: Distance travelled by the sedimentation front over time

6.2.3. Sedimentation height

In table 6.3 the maximum height of the sedimentation bar directly behind the porcupine field is given. Furthermore, the relative percentage of accretion is given for the depth and for the porcupine height k itself. Although the hydraulic conditions for experiment 2 and 4 are very similar, the maximum sedimentation height Δz_b for experiment 4 is lower. Even though the flow velocities are slightly lower, for which experiment 3 shows that this has a positive contribution to the bar height. Apparently the lower density fields result in a smaller sedimentation height. Figure 6.20 also indicates that the migration of the sedimentation front for this experiment was the lowest.

Table 6.3: Sedimentation characteristics with maximum acretion height relative to the depth h and porcupine height k

Experiment	h [m]	Q [m^3/s]	u [m/s]	Longitudinal spacing [m]	Δz_b [m]	$\%z_b$ of h	$\%$ z_b of k	i_{bank} [-]
1	0.1121	32.5	0.36	0.01	0.0086	7.67	10.75	0.0044
2	0.1648	32.5	0.25	0.01	0.0199	12.08	24.875	0.0044
3	0.1475	25	0.21	0.01	0.0211	14.31	26.375	0.0176
4	0.1786	32.5	0.23	0.02	0.0175	9.80	21.875	0.00517

The sedimentation heights from table 6.3 are plotted against their corresponding characteristics in figures 6.21 and 6.22. The dimensionless sedimentation height is given relative to the water level. From the table it is observed that the maximum sedimentation height relative to the porcupine height is approximatley 25%. For rivers with a porcupine with dimensions 15 times as large this corresponds to a sedimentation height of approximately 30 centimetres.

It can be observed that there is a maximum sedimentation height for varying water levels. And their is a clear trend observed when the sedimentation height is plotted against their corresponding flow velocities. For experiment 4, with lower porcupine density, it is observed that the sedimentation height is smaller although the flow velocities are lower. The reduction in flow velocities in the retardation zone is smaller and therefore the critical flow velocities that result in sediment transport remain higher behind the porcupines in this case.

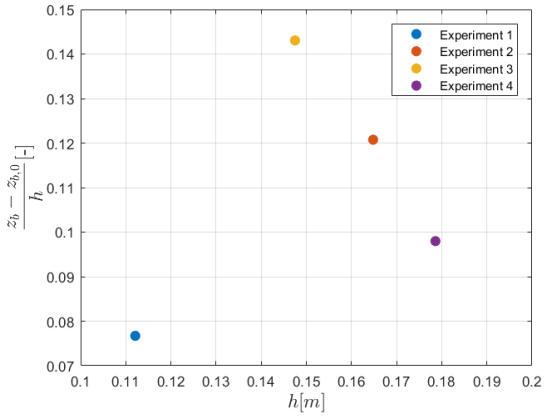

Figure 6.21: Dimensionless sedimentation height as a result of different water levels

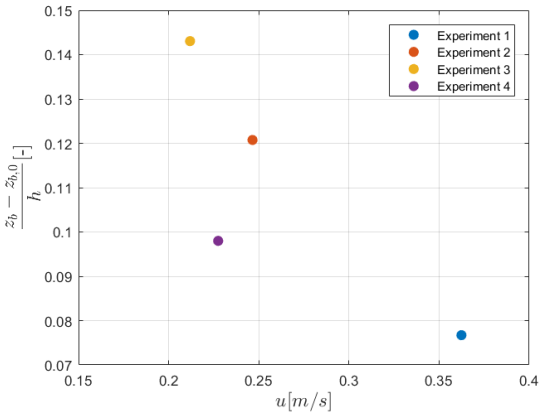

Figure 6.22: Dimensionless sedimentation height as a result of differenct flow velocities

6.2.4. Equilibrium length

In section 6.1.1 an estimation is performed for where the hydraulic effect of porcupines is no longer present. Besides, it is mentioned in section 5.2.1 that the accreted sediment bar behind the porcupines show a decline in height over the longitudinal distance. Figure 6.20 shows the development over time of the sedimentation front, but it does not clearly indicate if it migrates to an equilibrium state.

In table 6.3 the bank slope is given that is present for the sedimentation banks behind the porcupines. In the bed development figures from section 5.2.1 it is observed that these slopes remain constant over time and follow a linear decline downstream. Although it is only observed for experiment 1 that the end of the sedimentation bank is reattached to the initial profile it is expected that other experiments also have a point of reattachment. This point is determined by extrapolation of the bank slope to the point where $\Delta z_b = 0$. A comparison is made between these distances and the deceleration lengths as determined in section 6.1.1.

In table 6.4 below the determined length, $x_{\text{deceleration}}$, for which the flow profile is restored is compared to the length after which the sedimentation bank is reattached to the bed again. Experiments with similar settings are put side by side, and it turns out that for most experiments the length scales are close together. The difference in approximated length scales is in the order of tenths of metres.

Table 6.4: Comparison between deceleration length and sedimentation length

Experiment	λ_0	i_λ	$x_{\text{deceleration}}$	Experiment	Δz_b	i_{bank}	$x_{sf,max}$	Δx
8	0.359	0.085	2.103	1	0.0086	0.0046	1.870	0.233
9	0.553	0.068	4.700	2	0.0199	0.0044	4.523	0.177
11	0.519	0.075	3.443	3	0.0211	0.0176	1.199	2.244
13	0.458	0.090	3.570	4	0.0175	0.0052	3.385	0.185

For experiment 11 and 3 the lengths do not compare really well. These are the experiments with lower discharge, and therefore lower flow velocities. These low flow velocities result in a decreased sediment transport capacity. The development of the sedimentation bar behind the porcupines is not present yet as is illustrated in section 5.2.1. Small ridges of sedimentation humps are developing behind the porcupines, however no clear bank has developed. The bank slope is now determined based on these small ridges, while no actual bar is present resulting in a much steeper gradient. It is assumed that the bank will eventually be present and that it will result in a milder bank slope comparable with the other experiments.

Filling in the approximated length scales in figure 6.20 and extrapolating the migration of the sedimentation front gives an indication of the time scales required to achieve the equilibrium sedimentation pattern. Figure 6.23 illustrates the time required to reach the calculated equilibrium length. Although this is a rough estimation of the time scale it can be observed that there is a certain band width in which the processes take place. Porcupine fields with high densities and normal flow conditions work most efficient, while experiments with low water depths and high flow conditions work least efficient. In between there is a range in which mild flow conditions and lower field densities perform relatively equal in efficiency.

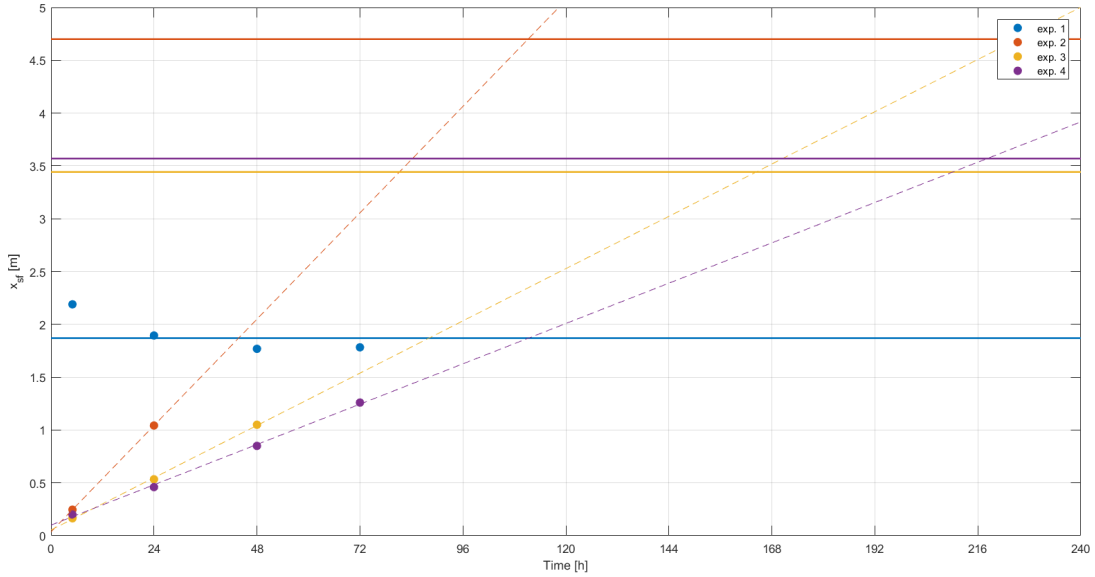

Figure 6.23: Extrapolation of the sedimentation front to the determined reattachment point

6.2.5. Partial blockage

For the mobile-bed experiments with partial blockage the sedimentation patterns are different, and can therefore not be quantified in uniform sedimentation volumes or migrating sedimentation fronts. In the experiments with partial blockage complex flow patterns arise that result in alternating bar patterns. In figure 6.24 the development over time is schematised.

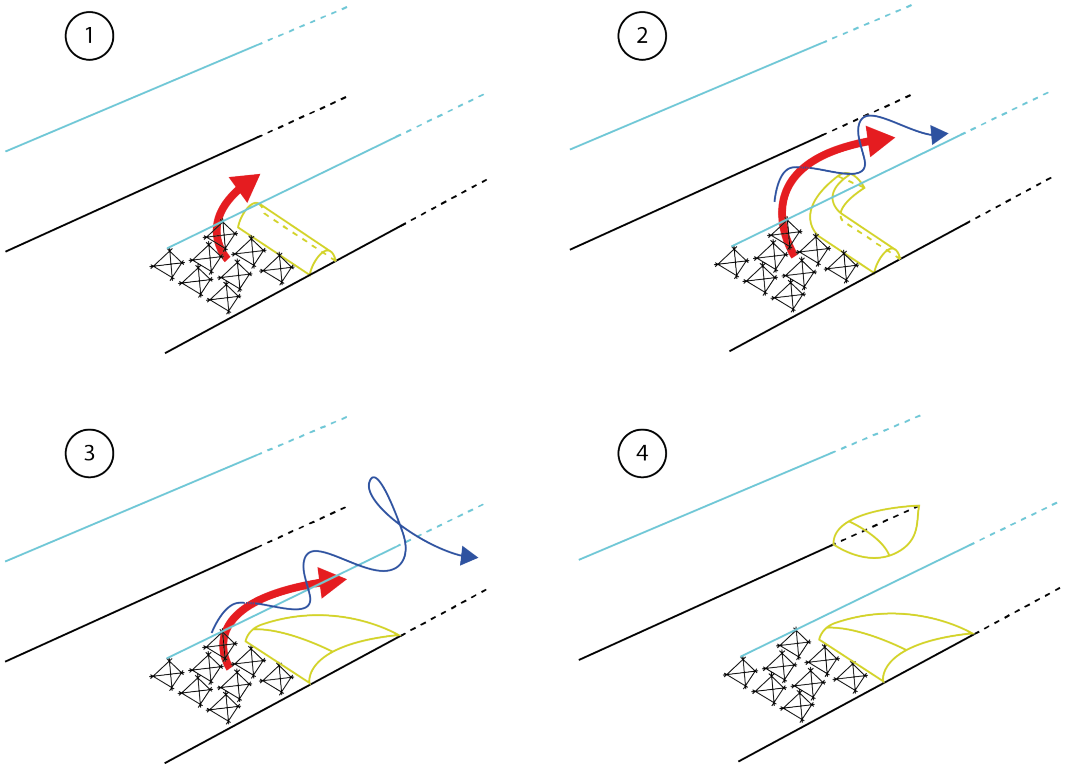

Figure 6.24: Development of the the bed during partial blockage. Red arrow indicates mean flow direction, blue arrow indicates the secondary flow patterns.

In the initial phase bar development behind the porcupine field is observed similarly to the experiments with full blockage of the flow. However, after a while the sediment ridge behind the porcupines will affect the flow itself and start to push the flow away towards the left, indicated with the red arrow. The flow velocities increase towards the gap, and decrease behind the gap again and will therefore extend the ridge in longitudinal direction as described in section 5.2.1. Although this is not indicated in the schematic overview, there is also an increased erosion in the flow path of the red arrow due to the increased flow velocities.
The water level gradient over the width of the flume is not constant as is illustrated in section 4.2.4. The transverse water level gradient causes secondary flow patterns with increased velocity gradients towards the left near the surface, and a return current near the bed. This secondary helical flow pattern behind the porcupines results in the sedimentation shape behind the porcupines as observed in experiments 5 and 6. The sedimentation ridge that is formed in the previous step is now pushed behind the porcupines. In experiment 7 this step is never reached due to the low flow velocities and therefore the low sediment transport capacity. It is hard to predict if this will happen when increasing the experiment duration, however the previous steps have been observed in the other experiments therefore it is assumed that over time the same morphological development will take place.

This increasing sedimentation bar behind the porcupines affect the helical flow patterns even more and the sedimentation bar behind the porcupines is therefore limited to grow any further. However, due to the present bar behind the porcupines flow will be affected further downstream resulting in the generation of alternating hybrid bar patterns. Over time these bars will grow in size and may shift further downstream as the upstream bar grows. The size of the hybrid wave length is dependant on the depth, flow velocities and sediment transport characteristics (Le, 2015).

7

Discussion

In this chapter, the results of the experiments and the practical relevance of the obtained knowledge is discussed. The hypotheses that have been stated are tested and interesting points for further research are highlighted. The chapter is divided in the interpretation of the experimental results in section 7.1 and the comparison between porcupines and vegetation in section 7.2. In section 7.3 the experimental set-up itself is discussed. Finally in section 7.4 the applicability of the results for prototype scale are discussed.

7.1. Interpretation of results

7.1.1. General behaviour

It is an important observation that porcupine partly work as weirs and divert the flow around them. They clearly work in affecting the water level upstream, even when the flume is partly blocked. Considering that a higher water level in a river channel affects an upstream located bifurcation by reducing the discharge to this channel, porcupines may effectively influence bifurcation points in braiding rivers.

In general it was expected that sedimentation would occur within and behind the porcupine field, and that due to the reduction in sediment transport erosion would occur further downstream. However mainly erosion occurred inside the porcupine field and no notable erosion has been identified downstream from the porcupines. Sedimentation inside the porcupine field would probably occur once the field is extended over a longer distance. This was already observed for experiments with lower field densities which were slightly longer.

It remains questionable if significant erosion behind the porcupine field will ever occur. The sedimentation height behind the field reduces in longitudinal distance up until the point where the sedimentation height has reached the original level again where a new balance between erosion and accretion is obtained. From this point the velocity remains constant, and a constant sediment transport rate is assumed to be present again. The amount of sediment that is captured by the porcupines is relatively small related to rest of the flume and therefore the erosion that may be present behind the porcupines is negligible. Besides, the bathymetry update is measured as the mean of the 15 measured transects along the flume, it could therefore be assumed that due to averaging of the bathymetry less accretion and erosion is observed while it may be present.

7.1.2. Effect of water depth

In the conducted experiments that were aimed to identify the relevance of the relative depth of the flume the discharge remained the same. It was chosen to vary as little variables with each different experiment to eliminate secondary interactions. However, in experiments with varying water levels and constant discharges the effective flow velocity changes considerably. This has a significant effect on the sediment transport capacity since the shear velocity, u_*, for the sediment does not change. To quantify the effect of water level differences it is therefore better to achieve a constant critical flow velocities in all experiments with varying water levels, and eliminate the different sediment transport rates. This has not been done in the experiments performed in this research and therefore it is hard to say if water level differences in itself have a significant effect on the morphological behaviour around a porcupine field. It can be observed however that for lower water depths a steeper water level gradient over the porcupines is observed, which indicate that the relative roughness

increases with lower water levels. It does remains uncertain if there is a relation between water levels and sedimentation rates behind the porcupines.

Besides, in mobile-bed experiments it is incredibly difficult to fix the water level to a certain depth. It may be the required water level during the initiation and set-up of the experiment, but during morphological development the water levels change and cannot be controlled precisely during the course of the experiment. Water evaporates, causing lowering of the water level which is mitigated by refilling the flume every once in a while. In the fixed-bed experiments the water level could be determined more accurate, however in this case the bottom of the flume shows significant deviations of approximately 2 centimetres and therefore no constant depth is achieved over the flume.

In section 3.4 the hypothesis was given that experiments with lower water level would result in more sedimentation because a relative larger part of the flow would be affected by the porcupines. While it is indeed observed that a lower water level results in a higher representative porcupine roughness, no additional sedimentation is measured. On the contrary, almost no sedimentation is measured due to the higher flow velocities. This is partly the result of increased flow velocities. It is still expected however that porcupines work better with lower water levels as long as u_* remains constant, based on the findings by (Aamir & Sharma, 2015b).

7.1.3. Effect of velocity

Although the pump can be set to a constant discharge, the value that is measured by the discharge measurement equipment is sensitive to air bubbles. This means that if too much air is trapped in the reservoir at the end of the flume the discharge measurements can give values lower than they actually are. Although the discharge is set to a certain value that is read from the measurement equipment it can still result in deviations in between experiments. Therefore the flow velocity may not be constant for experiments with equal water levels and equal discharge output.

Nevertheless, relations between the flow velocity and sedimentation rates are observed. As expected the sedimentation front migrates faster for higher flow velocities. Something that was not anticipated for is the erosion around the porcupines themselves, which significantly increase for higher velocities. The generated vortices around the bottom triangle result in local scouring resulting in porcupines that 'sink' into the bed. This drastically reduces the effectiveness of the porcupines, therefore it may be interesting to study mitigation measures to prevent the local scour and increase the effectiveness of the porcupines.

7.1.4. Effect of porcupine field density

It was expected that porcupines work significantly less effective for decreasing densities of the field based on the findings of Aamir & Sharma (2015b). However it was observed that for half the density only a small reduction in velocity retardation occurs. Apparently the porcupines still work quite efficiently in retarding the flow with lower densities. The drag, and therefore the effective roughness of the field reduces, but not by a half although the density is reduced by a half. When the density of the field was reduced with 75% the drag only reduced with 45%. These limited drag reductions are supported by the reductions in water level impoundments upstream for lower field densities. With a quarter of the field density the water level upstream is only reduced by approximately 35%. Besides, the amount of sedimentation behind the field for half the density only results in a reduction of approximately 25% in sedimentation volume. In section 3.4 the hypothesis was also given that reducing the porcupine density would not decrease its effect on sedimentation as much, which is confirmed by the measurements. Finally, in the experiments with lower density it is observed that no significant erosion occurs inside the porcupine field whereas in the other experiments this did occur. Due to the larger spacing in between consecutive rows of porcupines there is enough room for initial sedimentation behind the first row of porcupines. This affects the hydrodynamic behaviour further inside the field and results in less turbulent energy near the bed since flow is diverted upward. Measurements of the the turbulence intensities show similar turbulence intensities inside the porcupine field for different densities. Behind the porcupine field more turbulence is even observed for the experiment with lower field densities. However these measurements are from the fixed-bed experiments where morphological developments are not accounted for. More extensive research on the development of turbulence through porcupine fields in required to get more insight in the contribution of density difference on turbulent behaviour.

7.1.5. Effect of staggering

Although no extensive research has been performed on the effect of staggering versus non-staggering it is observed and measured that porcupines are more effective once applied in a staggered grid which was al-

ready assumed based on literature. The amount of drag and roughness is less for non-staggered grids since the flow is not obstructed in between the porcupines. Flow velocities therefore remain relatively high inside the porcupine field and near the bed. Behind the porcupine field it is observed that, due to horizontal turbulent mixing, the velocity profiles still retard significantly. Additional experimental research on the the morphological development behind non-staggered grids is therefore necessary to determine how sensitive the morphological development is for staggering.

7.1.6. Effect of partial blockage

In this experimental research the effect of asymmetrical placement of porcupines along the width of the flume is studied. This is important to understand how porcupines may affect the flow in horizontal direction, and how they can be used as bank protection measures. In the experiments performed with partial blockage alternating banks are generated. It is highly questionable however if similar developments will be present in larger river systems if porcupines are only used as bank protection and therefore partly bock the flow. Multiple pilot studies have been performed on mitigation measures for bank protection with the use of porcupines or jack jetties in which alternating bank patterns are never mentioned or observed (Kharya & Kumar, 2012; Nayak et al., 2016; Sarma & Acharjee, 2012; Shriwastava & Sharmar, 2014). In reality rivers do not have the same width to depth ratio that is present in the flume and therefore the conditions for the generation of alternating banks is probably less favourable. In their studies different porcupine configurations are applied where large longitudinal spacing was present. Although this set-up is not tested in this research it is expected, based on the lower density experiments, that this layout is effective in capturing sediment inside the field. Fewer porcupines over a larger distance could therefore be relatively effective in protecting river banks against severe scour.

7.1.7. Turbulence

From the ADV measurements the Reynolds stresses can be determined over the vertical profile as is illustrated in figure 7.1. It was described that these measurements can be used to determine the bed shear stress for uniform flow, and that the measurements compare relatively well with the determined bed shear stresses from water level gradients. Using this method to effectively quantify porcupine shear stresses however, the measurements start to deviate significantly from the determined porcupine shear stresses as described in section 6.1.2. Baptist et al. (2007) indicates that Reynolds stresses at the maximum vegetation height give a representative indication of the shear stress that vegetation exerts on the flow. Doing this for the measured data from the experiments in this research gives a significant underestimation of the shear stress, and therefore the friction generated by the porcupines. Figure 7.1 shows how the Reynolds stresses developed over the depth and show a maximum value of approximately 4.5 [N/m^2] where the calculations from section 6.1.2 result in a porcupine shear stress of 8.89 [N/m^2] for the same experiment.

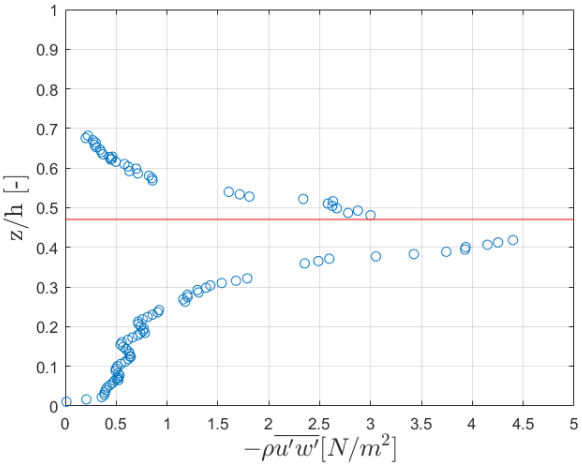

Figure 7.1: Reynolds stresses over the vertical, Experiment 9

This underestimation of the shear stress is due to the fact that the measurement of the velocity fluctuations are not performed directly behind the porcupine but a couple of centimetres further downstream to get a

clearer measurement. This means that some of the turbulent eddies are already dissipated and therefore not captured by the ADV. Furthermore, the ADV measures at a certain frequency and has a limited capability of measuring smaller scale turbulence fluctuations. This leads to the underestimation of the shear stress and possible overestimation of the Chézy roughness.

7.1.8. Roughness

In the determination of the representative roughness based on the method of Baptist et al. (2007) it is assumed that the bed shear stress is the same for a flume without porcupines as for the part within the porcupine field during the experiment. For the fixed-bed experiments this assumption is valid since the bottom does not change, however for the mobile-bed experiment this assumption is no longer valid. The bed shear stress of the flume without porcupines is bases on the water level gradient over the flume where the dimensions of the ripples determine the roughness of the bed. When the porcupines are placed these ripples in the porcupine field are suppressed by the increased turbulence and are therefore no longer present. It is not known how sensitive the resulting drag and representative roughness are for a non-constant bed roughness, and should therefore be studied in more detail. This becomes especially important when porcupines will be placed over a much longer longitudinal distance, which could result in serious overestimation of the roughness of the porcupine field.

The drag has been determined by fitting the momentum balance of resisting forces similar to the method of Luhar & Nepf (2013) to a theoretical line and resulted in a C_D coefficient of approximalty 5. However in the research by Zhu et al. (2009) a drag coefficient of approximately 1.5 was found in numerical studies and confirmed with experimental research on a single element. This deviation is partly due to the fact that form drag for a single element is different compared to the form drag of a field of porcupines. Further discussion on the drag coefficient is provided in the next section. Although the values for the drag may be unrealistic, the determined values for the drag coefficient and the corresponding roughness values in this study have been verified with a computer model and showed promising similarities in the water level behaviour for similar roughness coefficients.

In this research the representative roughness is also determined for the mobile-bed experiments but the results from the mobile-bed experiments show no satisfactory results. Water level measurements show large deviations and velocity profile are highly disturbed by the ripples. This prevents in-depth comparisons with the findings in the fixed-bed experiments for the amount of roughness. The representative Chézy values have been determined but are hard to verify with the measured water levels and SOBEK calculations. Due to the ripple formation, the sediment bed results in higher roughness compared to the concrete bottom. Although the measurements are not that good, it is observed that the additional roughness from the porcupines is significantly less in mobile-bed experiments compared to fixed-bed experiments.

7.1.9. Drag coefficient & Carnot energy loss

The drag coefficient is very sensitive to the applied flow velocity in the formulations. This was already indicated in sections 6.1.2 and 6.1.3, where it becomes apparent that a slight adjustment in flow velocity can already result in a large deviation of the drag coefficient. Since the drag coefficient is proportional to the velocity squared and the flow velocity is variable over the depth it is difficult to derive one drag coefficient that describes the whole porcupine field as one. Besides, the formulations that compute the drag coefficient ar only applied for objects in fully developped flow conditions, which is not the case in this study. Large deviations from the actual drag coefficients may therefore be the results. The formulation of Sukhodolova & Sukhodolov (2012) is used to see how the drag coefficient evolves over the depth behind the porcupines and it is observed that the drag is larger near the bottom. Although it is not clearly observed in all measurements it can also be noted that close to the top of the porcupines, the drag increases as well. This formulation gives some insight in the drag dependency on the flow velocity and depth, it does not explain the high values for the drag coefficient that are found in the analysis. In the analysis it is assumed that the total energy loss can be subscribed to the exerted roughness by the porcupines. Furthermore it is assumed that the formulations can be used that are solely derived for uniform flow conditions in which a fully developed logarithmic flow profile is present. Clearly, these assumptions are not completely correct and result in unrealistic values for the drag coefficient.

There is a large velocity difference between the part within the porcupine field and above. Behind the porcupine field this difference results in additional form drag of the total field where the flow starts mixing the two different layers again. In this extremely turbulent part behind the porcupines it is expected that Carnot energy losses are present that should be excluded from the calculations in the derivation for the drag

of the porcupines. However, it is difficult to calculate the exact Carnot energy loss because porcupines do not result in the same behaviour as a weir. In analogy with the Carnot losses over a weir it is assumed that energy losses only occur behind the weir due to turbulent mixing where a sudden velocity difference is present. They can be computed using the water level at the end of the weir and at some distance downstream form the weir, combined with the flow velocity on top of the weir and the flow velocity downstream.

$$\Delta H = h_2 + \frac{u_2^2}{2g} - h_3 - \frac{u_3^2}{2g} \tag{7.1}$$

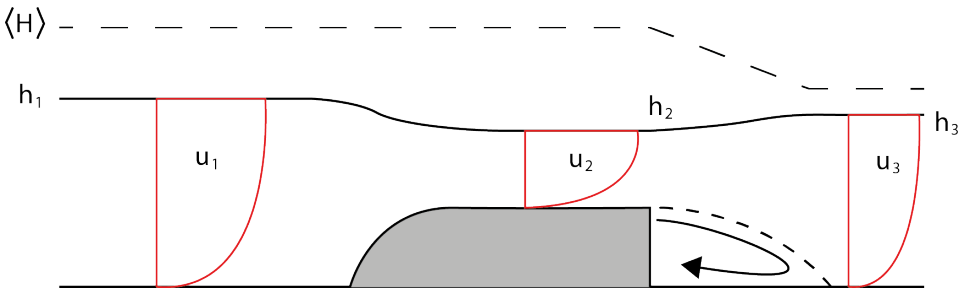

Figure 7.2: Carnot energy losses for a weir

where u_1,h_1 and u_2, h_2 are the flow velocity and water level at the end of the weir and at some distance downstream respectively. However in this highly idealised example the flow velocity on top of the weir is uniformly distributed and no energy loss has yet occurred until the end of the weir. Furthermore the total discharge is present on top of the weir. Porcupines are permeable structures that allow through-flow. This means that it is uncertain which fraction of the discharge passes through the porcupines and which fraction is diverted over the porcupines. Therefore no clear value for the velocity can be subscribed to the velocity that should be applied in equation 7.1.

The flow through a porcupine field is only slightly comparable to the flow over a weir. Figure 7.3 gives a schematic overview of the hydraulic behaviour through a porcupine field for the important parameters that are required in the derivation of Carnot energy losses. Comparing this behaviour with the flow over a weir clearly shows the differences between a short porcupine field and a weir. Water levels on top of the porcupines are not constant and significant velocity differences are present. Clearly the energy losses cannot solely be subscribed to Carnot losses since the porcupines themselves also result in severe energy losses due to increased friction and induced turbulence. They result in an individual porcupine drag, however the field as a whole also results in a form drag that is dependent on the configuration of the total field.

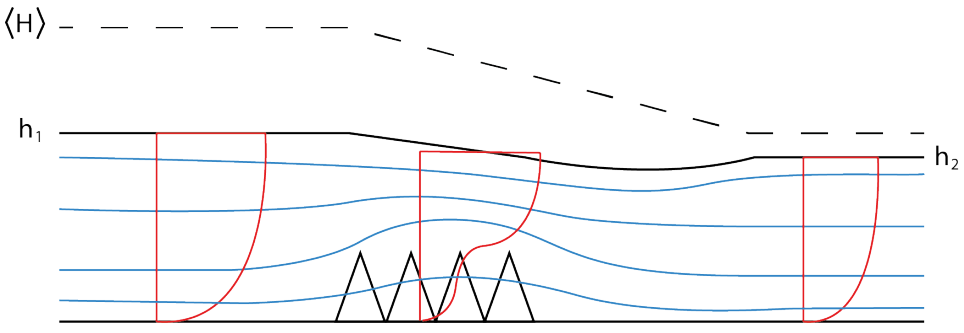

Figure 7.3: Additional Carnot energy losses for porcupines

Calculating the energy losses with equation 7.1 using the velocity profile most downstream from the porcupines, and only taking into account the mean velocity on top of the porcupines overestimates the energy loss. The velocity inside the porcupine field reduces the energy loss downstream since the velocity difference is smaller compared to a weir. Therefore the following equation should be applied to approximate the energy loss, where water level differences are neglected.

$$\Delta H = \frac{\frac{1}{2}(\overline{u}+u_1)^2}{2g} + \frac{\frac{1}{2}(\overline{u}-u_2)^2}{2g} \Longrightarrow \frac{\overbrace{\overline{u}^2 + \overline{u}u_1 - \overline{u}u_2 + \frac{1}{2}u_1^2 + \frac{1}{2}u_2^2}^{\text{Carnot energy loss}}}{2g} \tag{7.2}$$

In which $\overline{u}$ is the mean depth average flow velocity and it is assumed that the porcupine height is half the water depth, which is generally the case in the conducted experiments. Furthermore, u_1 and u_2 are the difference in flow velocity on top of the porcupines and inside the porcupine field relative to the mean flow velocity respectively. This leads to the following description in case $u_1 = u_2$.

$$\Delta H = \frac{\overbrace{\overline{u}^2 + u_1^2}^{\text{Carnot energy loss}}}{2g} \tag{7.3}$$

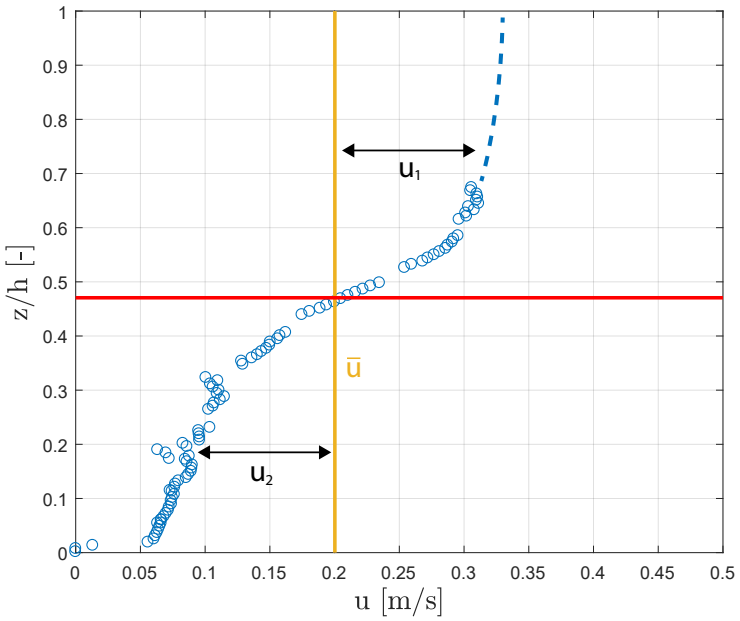

Figure 7.4: Velocity differences that induce Carnot energy losses, Experiment 11

Equation 7.3 indicates that if the flow velocity difference is half the value of the mean flow velocity, the Carnot energy loss is already a quarter of the total energy loss. Figure 7.4 illustrates that this is indeed the case for experiment 11 where the depth average flow velocity is approximatley 0.2 [m/s]. Filling in equation 7.3 with the measured values results in a total energy loss of 0.27 [cm] which corresponds to the energy loss based on the water level differences. Subtracting the Carnot energy losses does reduce the total drag coefficient by 1.5 [-] but still remains larger than 2[-]. For further research it would be interesting to investigate the effect of non-equal velocity differences and different submergence ratio's.

7.2. Porcupines versus vegetation

7.2.1. Velocity profile

Currently porcupines are schematised in numerical models as additional roughness by simulating them as rigid cylinders described, for instance, by the formulations of Baptist et al. (2007). However the question remains if this is valid or that another approach should be used. First of all the velocity profiles that are present in schematic represented vegetation are more or less uniform and continues over the vertical, with a transitional zone near the top and bottom of the vegetation. In the measurements from the experiments performed with porcupines in staggered grid similar profiles are observed although a uniform vertical profile in the porcupine field has not been observed that clearly. The main reason for this is that in the experiments with

porcupines in this study the length of the porcupine field has always been very limited. Only a little amount of porcupines were produced and therefore no clear experiment with porcupines over multiple meters could be performed. It is assumed that if the porcupines are stretched over a longer distance the velocity profile will convert more towards a uniform velocity profile inside the porcupine field.

Velocity profiles behind a row of non-staggered porcupines show different profiles however. They show large similarities with the observed velocity profiles of Lu et al. (2011) where the velocity profiles behind a single element is studied. Apparently the velocity profiles cannot be compared to velocity profiles in vegetation when staggering is not applied. This is due to the fact that the porcupines have an open body where flow is pushed trough with increasing velocities inside the porcupine when applied in non-staggered grid. As a result increased turbulent kinetic energy close to the bed is present. In case of vegetation the turbulence decreases rapidly towards the bottom. Besides, the velocity profile in between the porcupines even show signs of increased velocity near the bottom which is the complete opposite of vegetation.

Although the total field may show similarities for the velocity profile with vegetation measurements, the detailed flow profile through the porcupines is completely different and it is not known how this may effect the schematisation of porcupines as vegetation. Experiments with longer porcupine fields are therefore extremely important to see how the velocity profile evolves once retarded over a longer distance. It is hypothesised that, when enough porcupines are present, the flow will become more or less identical with measurements from vegetation experiments.

While a porcupine field has a much smaller density than a vegetation patch it does show the same defection patterns of the flow around the field. For vegetation it is found that the amount of deflection and the length scale after which turbulent boundary layers will begin to develop again are scalable with the canopy drag (δ_e) defined in the work of Nepf (2012b). It would be interesting to know if these length scales can be determined the same way, or if porcupines work as effective in deflecting the flow.

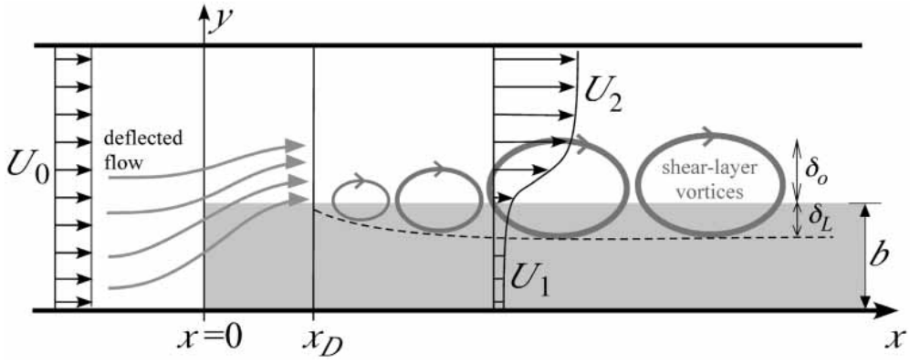

Figure 7.5: Deflection of flow and turbulence development for long vegetation patches, adopted from (Nepf, 2012b)

Figure 7.5 gives a schematic overview of how the velocity is deflected for vegetation and how, after a certain distance, shear-layer vortices with a constant size are generated. These shear vortices dominate the effective roughness of the vegetation and relations are found that determine the scales and growth of these vortices for vegetation (Luhar & Nepf, 2013; Nepf, 2012a,b). In the experiments conducted in this research the porcupine field is to short to observe such behaviour. Dedicated research on the growth of turbulent shear vortices is therefore required to accurately determine the effective roughness of porcupines and identify their effectiveness to extend their vortices into the open channel.

7.2.2. Natural product

Vegetation is a product of nature. It has roots that hold the soil beneath it whereas porcupines immidiatly start sinkin into the bed when increased turbulence occurs around the porcupines. This does not happen for vegetation or at least less significantly. Another extremely important difference is the flexibility of vegetation. Plants and grasses move with the flow which has additional complex effects on the drag, turbulence distribution and shear stresses Luhar & Nepf (2011). This does not apply for porcupines which are rigid structures and should behave the same for different hydrodynamic conditions. The drag should not become significantly different once the flow velocities increase, and the turbulence distribution should remain similar.

7.3. Experimental set-up

7.3.1. Imperfection of measurement results

The measurements obtained in this research are affected by the imperfections of the flume. The flume is constructed out of wood and has been used for a long time already. The wood has started to deform over time since it has become wet and dry many times. Therefore the rails on top of the flume, where the cart with all the measuring equipment is mounted on, is not straight any more. Especially after the extension of the rail, more irregularities have risen in the measurement output. Although error files have been generated multiple times during this research uncertainties remain about the quality of some of the measurements.

In the fixed-bed experiments no flat bed is present. The bottom is made out of concrete blocks that go up and down along the flume. Previous experiments in the flume for a different study required a whole in the bottom which was refilled for this experiment. However this has resulted in more deviations of the concrete bottom. During the experiments for this research water started leaking from the flume, so a part of the concrete bottom had to be removed to fix the problem. By repairing the flume more irregularities in the concrete bottom remained. So it is safe to say that the fixed-bed experiments are far from ideal with a perfectly smooth and straight bottom. From measurements it was already concluded that the flume is in between a hydraulic smooth and intermediate state. Although this is not ideal, the results from the fixed-bed experiments are significantly better compared to the mobile-bed experiments.

In the mobile-bed experiments it was more difficult to get a clear measurement of the hydraulic behaviour due to the disturbance caused by the bedforms. The velocity profiles are plotted relative to the bottom of the mean cross section. If the measurement is not performed at the height of the cross section at the time the cross section was measured it results in vertically shifted velocity profiles. Besides, the individual velocity points in the vertical are plotted relative to the bottom. During experiments with high flow velocities it happens that ripples move underneath the ADV during the measurement and therefore individual points are shifted vertically. Due to the migration of ripples the local flow velocities increase or decrease in the near bed region, resulting in strange velocity profiles where some parts of the profile consist of much higher flow velocities.

7.3.2. Equilibrium conditions

For all mobile-bed experiments hold that 1 day of morphological development has been applied prior to the start of the experiments. This was necessary in order to get a representative bed profile at the start of each experiment. However the bed is still not in morpholocigal equilibrium at the start of the experiment. Based on an estimated transport parameter Φ and a representative roughness coefficient, discharge and water level a morphological equilibrium is estimated to be reached after 8 days of morphological development (van Rijn, 1993). Obviously this is too long in order to perform enough different experiments, which was already difficult since experiments itself took a week as well. Time restrictions have prevented more mobile-bed experiments, if an equilibrium was required for all experiments only half of the experiments could have been performed.

Although an equilibrium bed would be a better starting position for the experiments, the general behaviour and development of the bed would not change that much. In some experiments large scale morphological developments were observed which may have influenced the behaviour of the porcupines although this is questionable.

7.4. Translation to prototype

For the practical applications of the results from this research relations are required that links the scale model to prototype scale. However, there are a number of differences between a flume and a real river branch that complicate the translation of the results from the flume to the river. First of all a flume is much shorter and therefore it is almost never the case that equilibrium conditions in both the hydrodynamics and morphodynamics are present. The velocity profile is not fully developed and equilibrium sediment transport would only be present after a couple of weeks. Besides, a flume is schematised such that the cross section is constant, resulting in a constand width-to-depth ratio along the flume. In a river this is not the case, the cross section varies in lateral direction and completely different width-to-depth ratios are present. Therefore velocity profiles in a river are never constant in both lateral and transverse direction. This variability in hydrodynamic conditions may result in different behaviour of a porcupine field compared to the flume where conditions remain as constant as possible. Finally the sediment composition in the flume has a very steep gradation curve whereas in rivers this is generally less steep. This indicates that there is a larger variation in sediment size which will result in different sediment transport characteristics in rivers than in the flume. Although it

is hard to accurately translate the results obtained in a flume to a river, there are some points that are useful and described in this section.

7.4.1. Roughness

In the analysis the roughness is determined as the Chézy coefficient. This is not a dimensionless friction coefficient that can directly be applied for larger scales. Therefore the coefficient should be written a dimensionless friction factor.

$$c_f = \frac{g}{C^2} \tag{7.4}$$

Assuming that the river width is much larger than the water depth, and assuming that uniform flow is present where a rough regime is dominating the flow the following expression for the dimensionless friction coefficient is valid.

$$\frac{1}{\sqrt{c_f}} = 5.75 \log\left(\frac{12h}{k_r}\right) \tag{7.5}$$

The roughness is usually described in terms of the Nikuradse roughness height, k_r [m], as described in section 2.2.2. From equation 7.5 it becomes clear that the roughness is solely dependent on the ratio of water level over roughness height. This means that for rivers where the water level and porcupines are scaled with similar factors the results from this thesis can be applied on prototype scale without scale effects.

Calculating this roughness height for the determined representative roughness for porcupines results in a roughness height that is approximately 3 times higher than the water level itself. This is a common phenomena for describing vegetation in terms of a representative roughness height. This is due to the fact that the formulations are derived for sand and rock with particles of a certain diameter. The resulting roughness of vegetation is generally much larger than sediment or rock and therefore the resulting representative roughness height described for rocks give rather extreme dimensions. For porcupines hold the same, describing porcupines in terms of Nikuradse roughness results extreme roughness heights. Nonetheless, these values can be used to determine the ratio of roughness height over water level.

Using this ratio an estimate for unequal scaling factors can be provided. If it is assumed that porcupines will be approximately 15 times larger, and water levels are assumed to be 30 times larger the new ratio for $\frac{h}{k_r}$ can be determined. This assumption is valid as long as the roughness heigt scales linearly with the dimensions of the porcupines. Based on the research of Bakker (2017) it is assumed that the flow velocities in the Ayeyarwady river are comparable with the flow velocities in the flume. Mean flow velocities between 0.1 [m/s] to 0.5 [m/s] have been measured in the field study whereas the mean flow velocity in the conducted experiments are in the range of 0.2 - 0.4 [m/s].

Table 7.1: Overview of scaled friction coefficients for a porcupine scale factor of $n_p = 15$ and a water level scale factor of $n_h = 30$

experiment	h [m]	Q [l/s]	u [m/s]	Longitudinal spacing [m]	u_p [m/s]	C_r [$m^{1/2}/s$]	c_f [-]	k_r [m]	$\frac{h}{k_r}$ [-]	$\frac{h}{k_r}_{new}$ [-]	$c_{f\,new}$ [-]	C_{new} [$m^{1/2}/s$]
8	0.114	32.5	0.36	0.01	0.22	6.41	0.238	0.602	0.189	0.378	0.070	11.835
9	0.1732	32.5	0.23	0.01	0.11	9.69	0.105	0.602	0.287	0.575	0.043	15.107
10	0.1968	32.5	0.21	0.01	0.1	10.69	0.086	0.602	0.327	0.654	0.038	16.109
11	0.172	25	0.18	0.01	0.09	9.63	0.106	0.602	0.286	0.571	0.043	15.053
12	0.1705	40	0.29	0.01	0.14	9.57	0.107	0.602	0.283	0.566	0.044	14.988
13	0.173	32.5	0.23	0.02	0.15	12.44	0.063	0.423	0.409	0.818	0.031	17.866
14	0.1728	32.5	0.24	0.03	0.17	14.19	0.049	0.338	0.511	1.023	0.026	19.610
15	0.1075	32.5	0.38	0.01	0.22	7.94	0.155	0.467	0.230	0.460	0.055	13.364
16	0.1731	32.5	0.23	0.01	0.12	11.66	0.072	0.468	0.370	0.740	0.034	17.082
17	0.2073	32.5	0.20	0.01	0.1	13.08	0.057	0.467	0.444	0.887	0.029	18.501
18	0.1606	25	0.19	0.01	0.1	11.07	0.080	0.468	0.343	0.687	0.036	16.496
19	0.1673	40	0.30	0.01	0.14	11.41	0.075	0.467	0.358	0.717	0.035	16.831

Table 7.1 gives an overview of the resulting values for the dimensionless friction factor and corresponding roughness heights. For all experiments with the same configuration of porcupines it is observed that the computed roughness height is similar. For configurations with lower densities the roughness height decreases. Taking into account the new ratios for the water depth over the roughness height results in Chézy values that

are much larger than the observed values in the experiments. For the mobile-bed experiments these new Chézy values are even higher, ranging from 18 to 22 [$m^{1/2}/s$], since the porcupines are less effective when placed on a sediment bottom.

The obtained values in table 7.1 give an indication only for rivers in which the flow conditions are similar to the flow conditions in the flume. Besides the water level should be scaled with a factor 30 where the porcupines should be scaled with a factor 15. For different flow conditions these roughness coefficients are no longer valid. Varying flow velocities on larger scale will probably affect the roughness, however this is extremely difficult to predict since the formulations for the flow velocity relative to the Nikuradse roughness height assume logarithmic velocity profiles which are clearly not present at the porcupine field.

7.4.2. Sedimentation patterns

For the sedimentation patterns behind the porcupines it is possible to quantify the sedimentation lengths for application in larger rivers as long as all conditions are scaled with the same factor. In case the porcupine scale is the normative scale factor all quantities should be multiplied by 15. This means that equilibrium sedimentation length behind the porcupines ranges from 31.5 metre to 70.5 metre. The mean sedimentation height is found to be approximately 25% of the porcupine height. If the sedimentation heights are also scalable with the porcupines this means that the mean sedimentation height in a river becomes 0.3 metre.

Based on the results in the analysis it is observed that there is a significant variation in sedimentation length scales. Therefore a hypothetical description for further research is given in figure 7.6 for the maximum sedimentation length scales behind the porcupines in relation to different variables. From literature it is known that sedimentation may occur inside the retardation zone which is approximately 5-10 time the obstruction height (Schiereck & Verhagen, 2012). However porcupines are permeable structures which results in advection trough the obstruction which will result sedimentation over a longer distance. A lack of measurements and different experiments prevent a conclusive description. This graph may therefore be error-sensitive and should be confirmed or dis-confirmed by additional research. Like described previously it is hard to distinguish the single effect of different water levels or different flow velocities from each other. Therefore they are described as the combined effect. For the individual effect an assumption is made, indicated with the dashed lines.

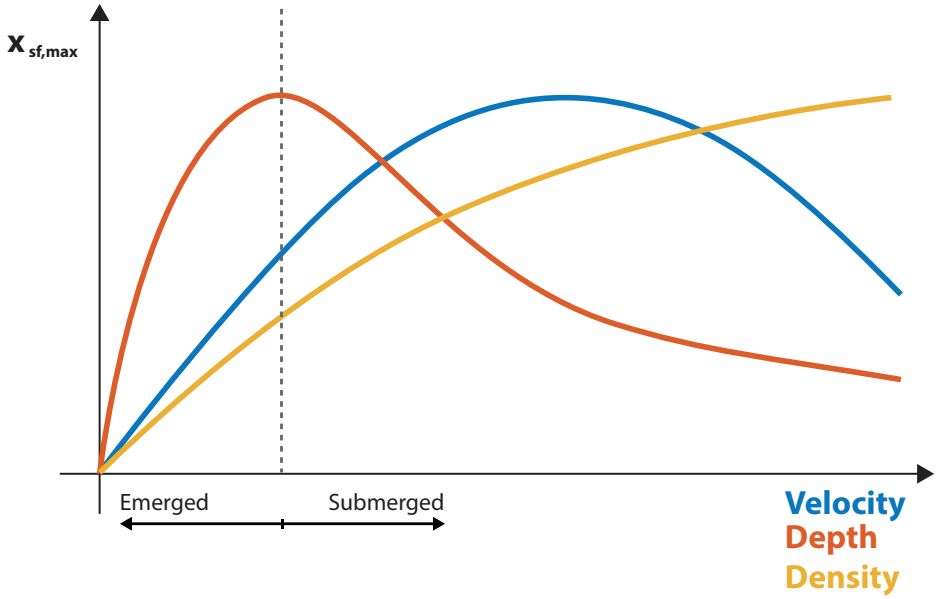

Figure 7.6: Hypotheses for the maximum sedimentation length behind the porcupine field in relation to the flow velocity, water depth, and field density

In the experiments with similar water level it has been observed that for increasing flow velocity the maximum sedimentation length behind the porcupines increases. In the experiment with lower water level but even higher flow velocity the sedimentation length drastically decreased. Based on these findings it is hypothesised that there is an area in which an increasing velocity is beneficial to a longer sedimentation bank since flow retardation is present over a longer distance. This is confirmed by the velocity measurements in the fixed-bed

experiments. However there is a certain point where flow velocities become too high and where porcupines can no longer work effectively in capturing sediment behind them. From the obtained data in this research it is found that for low water levels the porcupines perform less good compared to higher water levels. However in these experiments the flow velocity was also much higher so it is rather difficult to identify which process does what. Findings by Aamir & Sharma (2015b) suggest that porcupines work really effective in capturing sediment with lower water levels. Therefore it is assumed that the sedimentation behind the porcupines increases very rapidly as long as the water level is lower than the porcupines. When the porcupines become submerged the relative effectiveness of porcupines on the flow decreases, and will probably result in smaller sedimentation lengths. It is assumed that there is some sort of equilibrium point where increasing water depths no longer affect the sedimentation lengths. In figure 7.6 it is hypothesised that the effect of water depth is more dominant as long as the porcupines are submerged than the effect of flow velocity. When the porcupines become submerged the relative effect of the porcupines decreases and the flow velocity becomes dominant.

Based on the measurements in both the fixed-bed experiments and mobile-bed experiments it is observed that porcupines become more effective with increasing field densities. What was also observed in the determination of the roughness is that a reduction in density does not result in a similar reduction in porcupine effectiveness. This is confirmed by the maximum sedimentation length in the mobile-bed experiments. A reduction of the density by 50% only reduced the maximum sedimentation length with 25%. Similar effectiveness observations have been found in the fixed-bed experiments.

7.4.3. Applying results for practical purpose

Based on the findings in this study on the effect of porcupines it remains hard to describe design rules for river application, or model approaches for porcupines in Delft3D. Generally it is found that the largest sedimentation bar and largest water level difference upstream is present for high field densities. Therefore high field densities seem profitable. This is confirmed by the findings of (Brown, 1985) who stated that porcupines will become more effective over time as porcupines trap sufficient debris in the river, therefore increasing the effective density of a porcupine field. The downside of a higher field density is the increased rate of erosion within the porcupine field. Larger volumes are eroded and the bed level is lowered significantly more for higher field densities as a result of processes similar to bridge pier scour. This would reduce the effectiveness of porcupines over time. Therefore, for practical application it seems best to apply porcupine fields in a reduced density, with enough spacing between them, but in staggered layout. Lower densities reduce the costs of the field whereas the effect is only slightly reduced. Staggering helps to improve the effectiveness of the field. The flow is retarded over the field as a whole which stimulates the flow reduction and energy dissipation.

Porcupines should not be placed in fast flowing river sections, since they would mainly result in erosion and very little sedimentation and the significant roughness is approximately the same. Porcupines will probably work much better in the shallow part of the river channel where flow velocities are also generally lower. This means the porcupine fields can be used as groyne-like structures that can narrow a river reach and cause enough roughness to affect the water level upstream. If shallow areas in the middle of a river reach are present this would also suffice for a location of a porcupine field.

For modelling the porcupines in a numerical model such as Delft3D, the rigid cylinder approach seems like a valid option. However porcupines are not rigid cylinders. Therefore it is important to change the input of the number of cylinders in the model to number of porcupines. The model still calculates the flow with the description for cylinders, but now the number of porcupines are used. Besides, the frontal area of the cylinders was defined as the diameter of the poles times the height. To determine the representative diameter of a porcupine for the model the following relation can be used.

$$D \approx \frac{5lb}{k} \tag{7.6}$$

Where l, b are the representative length and width of the porcupine beams, and k is the porcupine height. Numerical simualtions should be performed to confirm if these adaptations to the formulation of Baptist (2005) are valid.

8

Conclusions & recommendations

The objective of this research was to gain more insight in the near-field hydrodynamic and morphodynamic responses of porcupines and their effect on the river bed. The research questions stated in section 1.3 are repeated and answered in this chapter. Recommendations for further research and implications for this research context are given in the second section of this chapter.

8.1. Conclusions

What is the hydrodynamic effect of porcupines?

Porcupines generate a lot of additional roughness and effectively push the water upward in front of the field. This induces backwater curves upstream of the field and results in a significantly increased water level gradient over the porcupine field. By approximating this gradient as a straight line the amount of drag can be determined and consequently the representative Chézy roughness can be computed by the equation of Baptist. However this approach in determining the drag is subject to error since Carnot energy losses are not taken into account. Due to the non erodible bed in the fixed-bed experiments high values for the representative roughness were found where it is observed that for the mobile-bed experiments the values are much lower where the porcupines 'sink' into the bed and become less effective.

The porcupines effectively reduce the flow velocities in longitudinal direction revealing that the porcupines can reduce sediment entrainment. The reduction in flow velocities becomes less for lower field densities, however the reduction does not reduce as much as the reduction of the density indicating that porcupines can work effectively with less porcupines present. To reduce the flow velocities as much as possible, staggered grids are required. Non-staggered grids do not reduce the velocities between the porcupines whereas staggered grids do. Besides, non-staggered grids result in less drag and are therefore less effective. The deceleration rates indicate that flow velocities are restored quickest for experiments with higher flow velocities and lower field densities. The distance over which the deceleration restores to its original profile gives an indication for the length of the sedimentation bar that will develop in mobile-bed experiments.

The experimental data shows that as the flow passes through the porcupine frame, the flow vectors behind the porcupine are directed downward within a region from the bed to the top of the porcupine. Furthermore, both the longitudinal and vertical turbulence intensities in this region are larger than those for the undisturbed approach flow. This causes severe energy dissipation, combined with a steep velocity gradient and downward directed flow velocities. The porcupines may reduce the probability of particle suspension or even induce sediment deposition for suspended sediment.

Porcupines that partly block the flow retard the flow velocities similar to a fully blocked flume, but in the unblocked part of the flow the velocities increase due to the deflection in lateral direction. Transverse water level slopes result in secondary flow patterns behind the porcupines, inducing additional energy losses as a result of horizontal mixing. Although not the full channel is blocked, water level differences in longitudinal direction over the total flume are present. This indicates that applying small porcupine patches in river channels may still be feasible to influence bifurcation points upstream of the river channel.

What is the morphodynamic effect of porcupines?

The mobile-bed experiments confirm the findings from the fixed-bed experiments. Sedimentation occurs behind the porcupines. In the retardation zone of the porcupines the flow regime is retarded in such a manner that the deposition of sediment becomes possible. First a sediment hump is generated behind the porcupines that starts migrating downstream once the maximum sedimentation height has been reached. Sedimentation height is approximately up to 25 % of the porcupine height depending on the flow conditions. Although the equilibrium length over which sedimentation occurs was only observed for a single experiment, a relation is found between the deceleration length and the actual sedimentation length. For the experiments performed in this research this leads to a varying length between 4 and 8 times the length of the porcupine field. When this relation can be used for prototype scale this gives an indication of the possible length scale of morphological response in the channel. Applying a scale factor of approximately 15-20 and assuming that flow conditions remain similar to the conditions in the flume, the morphological response can be expected up to 80 metres downstream from the porcupine field.

For experiments with high flow velocities and low water levels the deposition of sediment does not happen so clearly. The high flow velocities are reduced, but due to the significant increase of turbulent energy behind the porcupines sediment does not settle that well. Critical flow velocities remain too high and therefore almost no significant sedimentation is observed. On the contrary, high volumes of erosion within the porcupine field is measured for experiments with high flow velocities as a result of significant increased turbulence. Low flow velocities and lower field densities prevented large volumes of erosion inside the field, but resulted in less sedimentation behind the field. There is an equilibrium point where porcupines become most efficient, both effectively and economically. In high densities they might result in the largest volume of sediment depositions, however larger volumes of erosion will be observed. With less porcupines almost the same amount of friction is obtained and identical sedimentation patterns are measured, the sedimentation processes only occur approximately twice as slow for a density twice as low.

Experiments with partial blockage of the flow show that porcupines clearly work partly as a groyne. Flow is diverted around and the sedimentation patterns that arise behind the field clearly indicate how the flow is affected. In section 6.2.5 the consecutive sedimentation steps for partial blockage are described. In the initial phase of sedimentation the same hump behind the field is generated, although at some point the secondary flow patterns become dominant and will eventually result in alternating bank patterns downstream.

What are the dominant processes that cause sedimentation?

There is no clear process that results in the sedimentation behind the porcupine field but a combination of processes. First and most importantly, the porcupines reduce the flow velocity in the vicinity of the porcupines. If porcupines are placed in a staggered grid, they can effectively reduce the flow velocity in the near-bed region by a factor 1/2 or even more depending on the conditions. Reducing the flow velocity reduces the sediment transport capacity significantly, especially further downstream where the additional effect of the increased turbulence has been dampened out.

Secondly, the significant increase of turbulent kinetic energy results in a lot of energy dissipation through and behind the porcupine field. Combined with the downward directed longitudinal flow velocity, suspended sediments can be captured this way and be deposited on the bed. Energy dissipation in the porcupine region and a steep velocity gradient especially increases the probability of sedimentation for courser sediments. In rivers with a larger variance in sediment size it is therefore expected that sedimentation processes may be more significant when larger particles settle first, and that due to armouring of the bed, larger volumes of sediment are trapped.

Finally, the Reynolds shear stresses are lower in the near-bed region compared to the undisturbed approach flow, indicating that the bottom shear stress is lower behind the porcupines. This is the case for most experiments conducted, where the effect varies for different conditions. The reduction in shear stress close to the bottom, or at least no significant increase, combined with the low velocity drastically reduces the sediment transport in the near-bed region. Bedload sediment transport is largely reduced this way and results in the initial sedimentation hump behind the porcupine field. After such a hump is generated, additional recirculation zones behind the hump stimulate a further decrease of sediment transport.

Can the hydrodynamic effect of porcupines be schematised by the concept of Baptist?

In order to model a river with porcupines in a computer model it would be useful if they can be schematised similar to a situation with rigid cylinders, also used often for vegetation, described by the formulations

of Baptist. The velocity profiles around porcupine field seem rather similar compared with experimental research on vegetation. Furthermore the representative roughness computed with the formulations of Baptist seem to satisfy the water level behaviour in the one dimensional computer model SOBEK. Therefore it seems like the hydraulic behaviour can be schematised by the concept of Baptist. However, in section 7.2 the important differences in behaviour are given. Especially the density differences, turbulence structures and inflexibility of porcupines result in significant different behaviour. The differences are not captured in the equations derived by Baptist and should therefore be used with caution. Although, there are formulations in the momentum equation that describe the turbulence for rigid cylinders in Delft3D it remains unknown if they describe the turbulent behaviour of porcupines correctly.

Moreover, turbulence measurements clearly show that the location of the reduction in bed shear stress corresponds to the location where sediment transport is significantly reduced. The drawback of schematisation of vegetation based formulations such as Baptist is that they parametrise the flow resistance by means of the bed roughness. Consequently, the presence of vegetation, or porcupines, will lead to a higher bed roughness and thus to a higher bed shear stress, where a lower shear stress is measured. The higher bed shear stress that is computed by the model will lead to larger sediment transport rates in case of morphological computations. Therefore an additional term is added in the momentum equation that takes into account the reduced bed shear stress. No validation of the observations of the sediment transport and the computed bed shear stresses are performed with a numerical model. Therefore, it remains unknown if their approximation is valid.

The drag coefficient in the schematisation of Baptist is generally assumed to be close to 1 [-]. In this research it is found that porcupines result in a much larger drag coefficient than physically possible when similar assumptions are applied as in the derivation of the equation of Baptist. Applying the formulation derived by Sukhodolova, that determines the drag coefficient relative to the amount of turbulence and flow velocity over the depth, gives more realistic values. However these are only observed when applied inside the porcupine field, behind the field again larger drag coefficients are found which indicate that there is an effect of the field form drag besides the form drag of an individual porcupine. It is assumed that Carnot energy losses downstream of the porcupines contribute to the overall energy losses and therefore interfere in the calculations of the drag coefficient. From preliminary computations it is observed that when the Carnot energy loss is excluded a reduction in drag is obtained. For the mobile-bed experiments it was observed that the drag significantly reduced, where the amount of deceleration was also smaller. This indicates that Carnot losses could be extremely important for the overall drag and that this effect is less prominent is case of a mobile bed.

Under which conditions is a porcupine field the most efficient to create additional roughness and result in sedimentation?

Porcupines are open permeable structures and do not block the flow completely. Therefore incredibly complex flow structures arise within the porcupine field which cause all kind of turbulent vortices behind the field. In case of high flow velocities the porcupines mainly cause increased erosion within the porcupine field near the bottom of the frame due to self generated turbulence similar to bridge pier scour holes. However, porcupines have no foundation and will therefore sink in their own scour holes, developing the scour even further. Lower flow velocities decrease the amount of erosion, however if the flow velocities are too low also no clear sedimentation patterns behind the porcupines arise. Lowering the field density also lowers the amount of erosion within the field, but the amount of sedimentation is again reduced. If the amount of sedimentation is the dominant requirement to determine the effectiveness of the porcupines a high density field is the best solution as long as the water levels do not become too low and therefore the flow velocities become not to high. However the effectiveness of porcupines can also be measured as the hight of the water level difference upstream from the porcupines.

The height of the water level difference is determined by the exerted roughness of the porcupines. The roughness becomes higher by reducing the water level. By lowering the water level the effect of the porcupines becomes relatively larger over the water depth. The top part of the water column is now also strongly affected by the presence of the porcupines and the relative roughness is therefore much higher for lower water depths. This scenario works the best in pushing the water up whereas it performed least good in providing additional sedimentation behind the field. Higher flow velocities and higher field densities also contribute to a larger roughness and therefore cause larger water level differences.

Finally, the grid should be staggered in order to increase the effectiveness of the porcupines. Non-staggered grids leave room for high flow velocities inside the field, reducing the drag and roughness of the porcupines.

The amount of sedimentation has not been measured since no dedicated experiment on the effect of non-staggered grids on morphology has been performed. However based on observations with dye, velocity measurements and water level gradients it is observed that non-staggered grids are less effective than staggered grids.

For application of the results on prototype scale the roughness can be determined as long as similar flow conditions are present by using the ratio of the water level over the roughness height as described in section 7.4. When all quantities and dimensions are scaled with the same factor, the model results can directly be used for engineering practises in real rivers. Besides in the provided hypothesis in section 7.4.2 the maximum sedimentation length is given as a function of the dominating variables. This summarizes the described processes above and generally indicates that porcupines should be applied in areas with mild flow conditions and relatively shallow parts of a river. When higher porcupine field densities are applied they become more beneficial.

8.2. Recommendations

8.2.1. Context

As described in chapter 1 the context of this research was to identify if porcupines can be used to control large braiding river systems and influence their bifurcation point. Besides, more insight was sought on the application of porcupines as groyne-like structures to prevent bank erosion and narrow the river. Although this research never focussed on the effect of porcupines on bifurcation points it is possible to pronounce an expectation about their effect on such a situation. As clearly measured in the experiments in this research, the porcupines effectively increase the roughness locally and cause backwater curves due to a water level increase upstream of the porcupines. These water level impoundments will affect the discharge distribution over a bifurcation point such that less water will enter the channel with porcupines. If this really results in enough control to maintain the discharge distribution as required remains unknown. Especially the effect of varying flow conditions are not tested in this research, but in real rivers such as the Ayeyarwady river, significant changes in water level, flow velocities and sediment concentrations are observed throughout the year. This makes it incredibility hard to predict how well porcupines will work in large systems like this. Therefore more research is required and will be elaborated on in the next section.

Applying porcupines on a large scale such as in the Ayeyarwady river becomes problematic since the channels are too wide to be fully blocked. In this research only small porcupine fields are applied, where no uniform conditions are present. The derivation of the roughness and drag coefficients therefore remain uncertain however it is observed that even small fields are relatively effective in retarding the flow. Besides it is observed that small patches that partly block the flow can already be effective in influencing the total water level of the flume. This is an important finding for further research where the effect of positioning and sizes of smaller field should be investigated in numerical models. In order for such a study to be possible findings in this research should be validated. The current problem is that it remains unknown if porcupines can be modelled as rigid cylinders with the concept of Baptist. Based on the results from this research it seems likely that this is a valid approach however more knowledge is required on the amount of energy dissipation by porcupines as a result of the Carnot energy losses. Besides the turbulence patterns should be modelled correctly since they may influence the sedimentation patterns behind the porcupine fields significantly. For the water depth, flow velocity and field density hypothetical relations are provided that illustrate their importance on the sedimentation behind short porcupine fields. These should be confirmed by applying more mobile-bed experiments with multiple variations.

8.2.2. Further research

- To get more insight in the exact behaviour of porcupines, and to generate better schematisations for their behaviour it is required to perform more research with porcupine fields that stretch the entire flume. This way uniform flow conditions over the field can be assumed and therefore the derivation of the drag and roughness can be performed much better since their formulations are based on hydraulic conditions with fully developed flow. However, porcupines are also applied in groyne-like structures and therefore the roughness contribution of short fields is extremely important too. For a better understanding of the effect of short porcupine fields a study should be performed to asses the contribution of the Carnot energy losses and its effect on the roughness. This will provide insight in the added value for different field sizes.

- There seem to be large similarities between porcupines and vegetation, however in section 7.2 important differences are mentioned that may result in different schematisations. It is important to get a better understanding of the turbulent length scales and intensity of porcupines compared to vegetation. These should be validated with the model output from numerical computations. Based on the findings in this research it is expected that significant deviations in turbulence intensities may drastically effect the morphological development. It may be interesting to investigate the trade-off between reduced mean velocity and the increased turbulence and test it against the results in this study.
- A pilot study on prototype scale should be applied to eliminate the scale effects from the results in the flume. Differences and similarities between prototype scale and laboratory scale can be assessed which could prove useful for improving numerical models.
- More mobile-bed experiments are required to retrieve more data on the behaviour of the porcupines on the morphology. This way better trend lines can be fitted to the measured data, and a more accurate prediction of their behaviour can be determined. Besides, it is concluded that porcupines might be very effective in capturing suspended sediment but no suspended sediment was present in the experiments conducted. It would be extremely interesting to study the effect of porcupines on suspended material since large river systems usually have a high concentration of suspended sediment.
- It is observed that porcupines dig themselves into the bed due to self-induced scour mechanisms. It would be useful to study the decrease of of effectiveness of porcupines when they sink into the bed, and if they are even a viable option for high discharge river systems, where they are assumed to sink rather quick.
- In this research some comparison of the measured data is performed with the numerical model SOBEK, however this model is fairly limited and due to time restrictions no detailed model study was performed. It would therefore be of much interest to be able to reproduce the experimental research in a model and validate the observed quantities for roughness and sedimentation volumes to improve the computer model. .

Bibliography

Aamir, M., & Sharma, N. (2014). *Sediment Trap Efficiency of Porcupine Systems for Riverbank Protection* (Tech. Rep. No. August).

Aamir, M., & Sharma, N. (2015a). Efficiency of triangular and prismatic Porcupines in capturing sediment. , 17–19.

Aamir, M., & Sharma, N. (2015b). Riverbank protection with Porcupine systems: Development of rational design methodology. *ISH Journal of Hydraulic Engineering*, *21*(3), 317–332.

Ashmore, P., Ferguson, R., Prestegaard, K., Ashworth, P., & Paola, C. (1992). Secondary flow in anabranch confluences of a braided, gravel-bed stream. *Earth Surface Processes and Landforms*, *17*(3), 299–311.

Ashmore, P., & Parker, G. (1983). Confluence Scour in Coarse Braided Streams. *Water Resources Research*, *19*(2), 392–402.

Bakker, T. (2017). *Dispersion in the Ayeyarwady River* (Unpublished master's thesis).

Baptist, M. (2005). *Modelling floodplain biogeomorphology* (Unpublished doctoral dissertation).

Baptist, M., Babovic, V., Rodríguez Uthurburu, J., Keijzer, M., Uittenbogaard, R., Mynett, A., & Verwey, A. (2007). On inducing equations for vegetation resistance. *Journal of Hydraulic Research*, *45*(4), 435–450.

Bristow, C. S., & Best, J. L. (1993). Braided rivers: perspectives and problems. *Geological Society, London, Special Publications*, *75*(1), 1–11.

Brown, S. A. (1985). *Design of spur-type streambanks stabilization structures* (Tech. Rep.). Georgetown Pike: Turner-Fairbank Highway Research Ceter.

Coleman, J. M. (1969). Brahmaputra river: Channel processes and sedimentation. *Sedimentary Geology*, *3*(2-3), 129–239.

Commandeur, A., Sloff, K., & Oo Mon, T. (2017). *AIRBM - Component 3, Engineering, Design, Capacity Building and Construction Supervision for Sub-Project 1* (Vol. 1; Tech. Rep. No. July).

Crosato, A., & Mosselman, E. (2009). Simple physics-based predictor for the number of river bars and the transition between meandering and braiding. *Water Resources Research*, *45*(3), 1–14.

de Vriend, H., Havinga, H., van Prooijen, B., Visser, P., & Wang, Z. (2011). River Engineering. *Collegedictaat CIE4345*.

Duró, G., Crosato, A., & Tassi, P. (2016). Numerical study on river bar response to spatial variations of channel width. *Advances in Water Resources*, *93*, 21–38.

El Kadi Abderrezzak, K., Die Moran, A., Mosselman, E., Bouchard, J.-P., Habersack, H., & Aelbrecht, D. (2014). A physical, movable-bed model for non-uniform sediment transport, fluvial erosion and bank failure in rivers. *Journal of Hydro-Environment Research*, *8*, 95–114.

El Kadi Abderrezzak, K., Die Moran, A., Tassi, P., Ata, R., & Hervouet, J. M. (2016). Modelling river bank erosion using a 2D depth-averaged numerical model of flow and non-cohesive, non-uniform sediment transport. *Advances in Water Resources*, *93*, 75–88.

Engelund, F., & Hansen, E. (1967). A monograph on sediment transport in alluvial streams. *Technical University of Denmark 0stervoldgade 10, Copenhagen K.*.

Grassel, K. (2002). *Taking out the jacks: issues of jetty jack removal in bosque and river restoration planning* (Tech. Rep.). Albuquerque: Water Resources Program, The University of New Mexico.

Hays, J. (2008). *IRRAWADDY RIVER AND RIVER TRAVEL IN MYANMAR | Facts and Details*. Retrieved 2017-10-18, from http://factsanddetails.com/southeast-asia/Myanmar/sub5{_}5f/entry-3539.html

Heller, V. (2011). Scale effects in physical hydraulic engineering models. *Journal of Hydraulic Research*, *49*(3), 293–306.

Hoffmans, G. J. C. M., & Verheij, H. J. (1997). *Scour Manual*. Rotterdam, Netherlands: A.A.Balkema.

Jagers, B. (2003, jun). *Modelling planform changes of braided rivers* (Tech. Rep.). Enschede: University of Twente.

Jansen, P., Van Bendegom, L., Van den Berg, J., De Vries, M., & Zanen, A. (1979). *Principles of river engineering: The non-tidal alluvial river*. Delftse Uitgevers Maatschappij.

Jibon, G. M. (2013). *Poor Navigability on route to Baghabari port: 22 fertiliser-laden vessels stuck in Jamuna River | The Daily Star*. Retrieved 2017-10-18, from http://dev.thedailystar.net/news-detail-265081

Kharya, A., & Kumar, P. (2012). RCC Porcupines An Effective River Bank Protection Measure – A Case Study of Protection of Majuli Island. *India Water Week*(April), 10–14.

Khaund, P., Goswami, R., & Das, G. (2015). A study on the effect of porcupine on the flow velocity in a laboratory tilting type channel using physical modal. In *4th irf international conference 2015* (pp. 105–107). Cochin.

Klaassen, G. J., & Masselink, G. (1992). Planform changes of a braided river with fine sand as bed and bank material. *Proceedings of 5th International Symposium on River Sedimentation*(March 2017), Vol. I, pp. 459–471.

Klaassen, G. J., & Vermeer, K. (1988). Confluence scour in large braided rivers with fine bed material. *Proceedings of the International Conference on Fluvial Hydraulics*(March), 381–394.

Le, T. B. (2015). *Long-term morphological developments of river channels separated by a longitudinal training wall* (Tech. Rep.). Delft: Delft University of Technology.

Ligthart, D. (2017). *The physical processes influencing morphodynamics in braided rivers* (Unpublished master's thesis). Delft University of Technology.

Lu, J. Y., Chang, T. F., Chiew, Y. M., Hung, S. P., & Hong, J. H. (2011). Turbulence characteristics of flows passing through a tetrahedron frame in a smooth open-channel. *Advances in Water Resources*, *34*(6), 718–730.

Lu, J. Y., Hong, J. H., & Ho, S. C. (2009). Scour protection downstream of a grade-control structure using tetrahedron frames. In *Proceedings of 33rd iahr congress: Water engineering for a sustainable environment* (pp. 3596–3603). Vancouver, BC, Canada.

Luhar, M., & Nepf, H. M. (2011). Flow-induced reconfiguration of buoyant and flexible aquatic vegetation. *Limnology and Oceanography*, *56*(6), 2003–2017. doi: 10.4319/lo.2011.56.6.2003

Luhar, M., & Nepf, H. M. (2013). From the blade scale to the reach scale: A characterization of aquatic vegetative drag. *Advances in Water Resources*, *51*, 305–316. doi: 10.1016/j.advwatres.2012.02.002

Meyer-Peter, E., & Müller, R. (1948). Formulas for Bed-Load transport. *IAHSR 2nd meeting, Stockholm, appendix 2*.

Mosselman, E. (2006). Bank protection and river training along the braided Brahmaputra-Jamuna River, Bangladesh. *Braided Rivers: Process, deposits, ecology and management. Special Publication No. 36 of the International Association of Sedimentologists.*, 278–287.

Mosselman, E., Shishikura, T., & Klaassen, G. (2000). Effect of bank stabilization on bend scour in anabranches of braided rivers. *Physics and Chemistry of the Earth, Part B: Hydrology, Oceans and Atmosphere*, *25*(7-8), 699–704.

Nakagawa, H., Teraguchi, H., Kawaike, K., Baba, Y., & Zhang, H. (2011). Analysis of Bed Variation around Bandal-like Structures. *Annuals of Disas. Prev. Res. Inst., Kyoto Univ.*(54 B).

Nayak, A., Sharma, N., Mazurek, K. A., Kumar, A., & =. (2016). Design Development and Field Application of RCC Jack Jetty and Trail Dykes for River Training. *River System Analysis and Management*, 1–417.

Nepf, H. M. (2012a). Flow and Transport in Regions with Aquatic Vegetation. *Annual Review of Fluid Mechanics*, *44*(1), 123–142.

Nepf, H. M. (2012b). Hydrodynamics of vegetated channels Accessed Citable Link. *Journal of Hydraulic Research*, *3*(February), 0–61. doi: 10.1080/00221686.2012.696559

Nortek. (2012). *Acoustic Doppler Velocimetry generically refers to bi-static measurement systems like the Nortek Vectrino and Vectrino II.*

Ostanek Jurina, T. (2017). *Channel closure in large sand-bed braided rivers* (Unpublished master's thesis). Delft.

Partheniades, E. (1965). Erosion and Deposition of Cohesive Soils. *Journal of the Hydraulics Division*, *91*(1), 105–139.

Sarma, J. N., & Acharjee, S. (2012). A GIS based study on bank erosion by the river Brahmaputra around Kaziranga National Park, Assam, India. *Earth System Dynamics Discussions*, *3*(2), 1085–1106.

Schielen, R. R., Doelman, A., & de Swart, H. E. (1993). On the dynamics of free bars in straight channels. *Journal of Fluid Mechanics*, *252*(-1), 325–356.

Schiereck, G. J., & Verhagen, H. J. (2012). *Introduction to Bed, bank and shore protection* (Second edi ed.). Delft: VSSD.

Schuurman, F. (2015). *Bar and channel evolution in meandering and braiding rivers using physics-based modeling* (Unpublished doctoral dissertation). University Utrecht.

Sharma, N., & Nayak, A. (2015). Paper 173 - RCC Jack Jetty and Bamboo Submerged Vanes Application for Navigation Fairway in Ganga River of India. (September), 7–11.

Shields, A. (1936). *Anwendung der Aehnlichkeitsmechanik und der Turbulenzforschung auf die Geschiebebewegung* (Unpublished doctoral dissertation). Technical University Berlin.

Shriwastava, A., & Sharmar, N. (2014). Investigation of RCC Jack Jetty as a Cost Effective River Training Structure.

Struiksma, N., Olesen, K., Flokstra, C., & de Vriend, H. (1985). Bed deformation in curved alluvial channels. *Journal of Hydraulic Research*, *23*(1), 57–79.

Sukhodolova, T. A., & Sukhodolov, A. N. (2012). Vegetated mixing layer around a finite-size patch of submerged plants: 1. Theory and field experiments. *Water Resources Research*, *48*(10), 1–16. doi: 10.1029/2011WR011804

Surian, N. (2015). *Fluvial Processes in Braided Rivers* (P. Rowiński, Ed.). Springer International Publishing.

Tang, H. W., Ding, B., Chiew, Y. M., & Fang, S. L. (2009). Protection of bridge piers against scouring with tetrahedral frames. *International Journal of Sediment Research*, *24*(4), 385–399.

Uijttewaal, W. (2003). Turbulence in hydraulics. *Collegedictaat CT5312*.

Van Rijn, L. C. (1984). Sediment transport, part i: bed load transport. *Journal of Hydraulic Engineering–ASCE*, *110*(10), 1431–1456. doi: 10.1061/(ASCE)0733-9429(1987)113:9(1187)

van Rijn, L. (1993). *Principles of Sediment Transport in Rivers, Estuaries and Coastal Seas.* Amsterdam: Aqua publications.

Vargas-Luna, A., Crosato, A., & Uijttewaal, W. S. (2015). Effects of vegetation on flow and sediment transport: Comparative analyses and validation of predicting models. *Earth Surface Processes and Landforms*, *40*(2), 157–176. doi: 10.1002/esp.3633

Yang, H., Lin, B., & Zhou, J. (2015, apr). Physics-based numerical modelling of large braided rivers dominated by suspended sediment. *Hydrological Processes*, *29*(8), 1925–1941.

Zhu, G. A. O., Xing, L. I., Hong-wu, T., & Zheng-hua, G. U. (2009). Three-dimensional hydrodynamic model of concrete tetrahedral frame revetments. *Journal of Marine Science Applications*, *8*, 338–342.

A

Literature

This appendix presents additional information on the dynamics of braiding rivers and their behaviour in general. Sedimentation and erosion processes are described and numerical complications of modelling such rivers are given. Besides, an elaboration on the derivation of the equations of Baptist are given followed by the theory about sediment transport and transport equations.

A.1. Alternative permeable structures

A.1.1. Bandals

Bandals are groyne-like structures that have a permeable base and impermeable screen at the top. They are designed to guide the sediment-laden water near the bed underneath the structure, while the clearer water near the surface is guided in a direction parallel to the screens (Mosselman, 2006). The separation is meant to induce a sediment overload in the cross-flow direction downstream of the screen. The overload of sediment should result in sedimentation in the area behind the structure. The bandal structure in figure A.1 has been constructed to close off a certain channel, however during high flow conditions a new channel was formed further downstream. To close off a complete channel a larger area should therefore be covered with the bandals, however no attempt has yet been made to test this.

Compared to regular groynes, it can be seen that the bandal-like structures are able to reduce the local scour depth around them(Nakagawa et al., 2011). Conventional groynes protect the bank and ensure a deep enough channel, but bandals can improve the river bank protection due to the increase of sediment deposition downstream of the structure and consequently near the river bank.

Figure A.1: Bandal structure constructed in the Brahmaputra-Jamuna, adopted from (Mosselman, 2006)

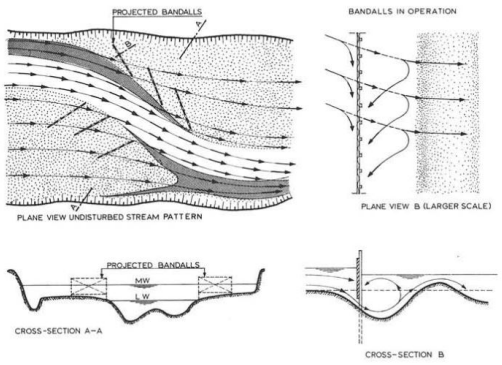

Figure A.2: Bandal applied in the Brahmaputra-Jamuna to create new channels, adopted from (Jansen et al., 1979)

However bandals are designed to result in sedimentation, they are also used to achieve the exact opposite. In the Brahmaputra-Jamuna, bandalling was used as a means to change the local stream pattern. When strategically placed, multiple screens can force the flow in a certain direction and erode a channel. Due to

their flow resistance the discharge can be concentrated in a small area, and a channel will arise automatically which is displayed in figure A.2.

A.1.2. Jack Jetty

Retardation spurs like jack jetties, fences or porcupines are designed to reduce the flow velocity in the vicinity of the channel bank or over the region of influence of the spur scheme (Brown, 1985). Jack jetties are skeletal frames of a number of similar units in triaxial assembly of mutually perpendicular bars tied together by cables. They are connected in the center such that three legs form the triangular base and the other three face sloping upward from the base to an apex. A schematic example of a jack jetty is given in figure A.3 below.

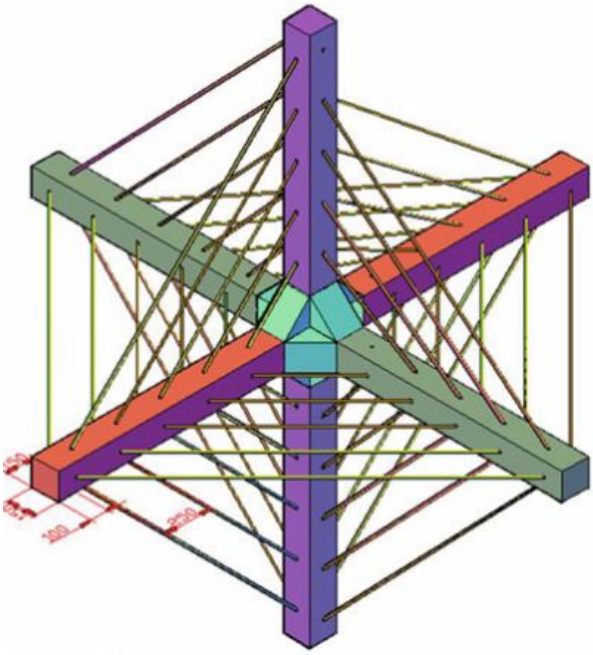

Figure A.3: Jack jetty construction, adopted from (Nayak et al., 2016)

Permeable structures such as jack jetties are best suited for low-threshold and medium-threshold environments, and have been found to be particualarly effective in low-threshold environments (Brown, 1985). A jetty field with lines of jacks in the flow area provide additional resistance to the water passing through the field, which in turn reduces the flow velocity. This reduces the sediment carrying capacity of the flow and sediment is deposited in the field (Nayak et al., 2016). Although the use of jack jetties shows sedimentation in certain conditions, the performance of the jack jetty failed with reduced sediment concentration levels in a river (Grassel, 2002). Since 1950 many jack jetties have been placed along the Rio Grande in lines perpendicular to the flow (retards) and parallel to the flow (diversion lines). They performed extremely well and over 30 years trees and bushes have grown over the jetty fields, and new banks were created. However once dams were constructed along the river reach it reduced the function of the jack jetties dramatically because of the reduction of sediment supply since the jetties require a certain amount of sediment to be effective. There has been a lack of scientific understanding about the design methodology and application of the jetties which leaves them functionless nowadays and because of environmental issues they are being removed (Brown, 1985; Nayak et al., 2016). Despite the lack of understanding back then new research had been performed on the effectiveness of jack jetty fields in India and Bangladesh (Sharma & Nayak, 2015; Shriwastava & Sharmar, 2014) and (Nayak et al., 2016). Both laboratory experiments and application in real rivers have been used to study the effect in more detail

A.2. Braided river morphodynamics

Since this thesis originates from braiding river problems, first some basic insight is gained in the underlying processes that dominate the hydrological and morphological variations. In this section large and complex processes are described together with more fundamental small scale processes that are of importance for

engineering purposes. For engineers the high rates of sediment transport, deposition and erosion combined with frequent channel shifting and rapid bank erosion may pose considerable design problems for both structures within the channel, such as bridge piers, and structures within the braidplain such as roads and railways. More insight in these fundamental processes will be given below.

A.2.1. Bar development

Bars occur in various shapes within a braided river and various distinctions can be made between these different bars based on their origin, size or behaviour. Islands within the river scale with the full width of the river and reach almost floodplain height, whereas bars scale with individual channels. They are flat and highest along the sides and at the bar head. Schielen et al. (1993) defined a stability range in which bar formation starts to occur and from which moment they grow or disappear. This stability range is a function of the wave number 'k' and the width-depth ratio 'B/h' and is displayed in figure A.4.

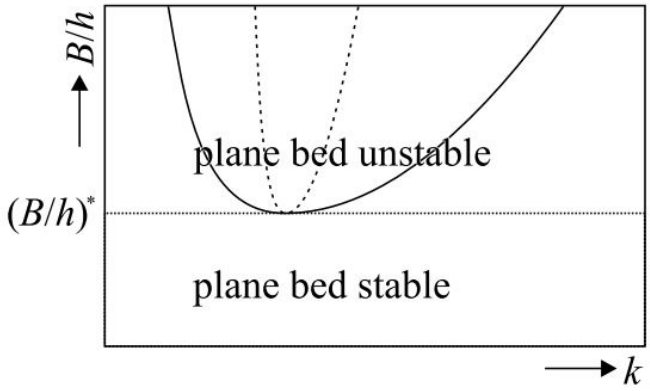

Figure A.4: Stability range for an erodible bed in a straight channel , adopted from (Schielen et al., 1993)

For a straight alluvial channel the longitudinal variation of the near-bank deviations of the flow velocity and bed topography can be described by the physics-based second-order linear equations derived by Struiksma et al. (1985). They are obtained from the steady state 2D depth average continuity and momentum equations for water motion, a sediment balance equation, a sediment transport formula and an equation for the direction of sediment transport. Crosato & Mosselman (2009) developed a method to determine the number of bars in a straight channel based on these equations and can directly estimate the most likely number of bars for certain river planforms. The derived formula performs good for width-to-depth rations up to 100, but deteriorates for ratios higher than 100. The formula is useful for preliminary determination of morphodynamic characteristics of laboratory streams.

$$m^2 = 0.17 g \frac{(b-3)}{\sqrt{\Delta D_{50}}} \frac{B^3 i}{CQ} \tag{A.1}$$

Where,

- m = bar mode [-]
- g = gravitational acceleration [m/s^2]
- b = degree of non-linearity of sediment transport versus depth-averaged flow velocity [-]
- Δ = relative sediment density under water [-]
- D_{50} = median sediment grain seize [m]
- B = river width [m]
- i = longitudinal bed slope [-]
- C = Chézy coefficient [m$^{1/2}$/s]
- Q = discharge [m^3/s]

The formula allows deriving the bar mode m that forms in the flume. The bar mode indicates the number of sand bars in the cross section. An alternating bar pattern will develop for m=1, where only 1 bar exist in a

cross section. From m=2 braidbars will be present and result in multiple channels as illustrated in figure A.5. The different types of bars and their flow pattern will be further explained in appendix A.

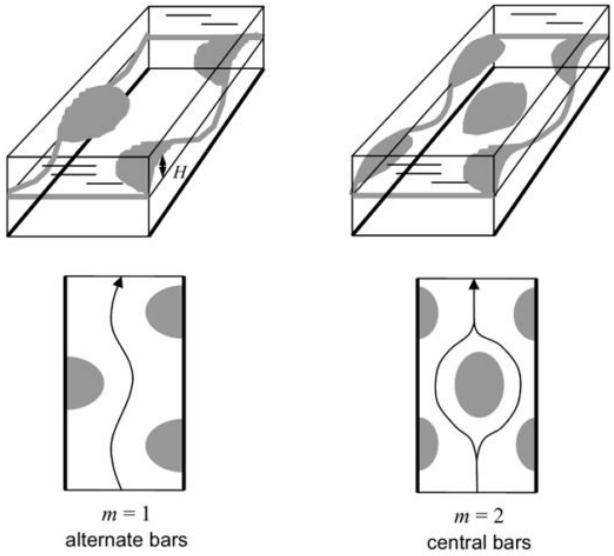

Figure A.5: Bar mode indicates the number of bars in a river, adopted from (Crosato & Mosselman, 2009)

A.2.2. Bifurcations and confluences

Braiding rivers are characterised by multiple channels that bifurcate and rejoin around islands and braid bars again (Jagers, 2003). They are characterized by an unstable network of multiple channels and very active channel processes. In braided rivers the bifurcations and confluences are the basic components of braided rivers (Surian, 2015) and in this report the focus is on the bifurcation and confluence processes. Understanding the dynamics of these processes is therefore of key importance to this thesis.

Confluence

The planform of bifurcations and confluences in a braided river can vary significantly over time due to variations in the discharge ratio and the flow directions of the converging channels. Besides, there are the secondary flow patterns that cause the channels to migrate, rotate, resize and obliterate (Ashmore et al., 1992). Behind the island a region of slack water can be present which may disappear over time due to increased sedimentation. On the other hand large scour holes are observed behind islands as well that can become six times deeper than the channel width itself for gravel-bed braiding rivers. The sediment that is eroded during the formation of the scour hole is often deposited slighly downstream where it starts the initiation of a new bar, which in this case is referred to as a post confluence bar.Ashmore & Parker (1983) found that these types of scour holes are mainly determined by the angle of confluence. Later it was also discovered that secondary helical flow patterns resulted in two helical flow structures that plunge into each other behind the sand bars causing erosion holes as well (Ashmore et al., 1992). For sand-bed braided rivers Klaassen & Vermeer (1988) found scour holes that were less deep which might be attributed to finer sediment and suspended sediment load. Although confluences are relatively stable compared to bifurcations, they can become more dynamic once the channel discharge distribution becomes more asymmetric. When one channel becomes dominant over the other, the confluence moves towards the non-dominant channel by deposition of sediments. The shift of main discharge channel can start a series of events since the direction of the downstream channel usually adapts to the flow upstream. Sedimentation processes behind bars start the formation of bar tail limbs that affect the flow direction as well (Schuurman, 2015). This indicates that small changes at a certain confluence point may already result in a series of morphological changes further downstream.

Bifurcation

For bifurcations the dynamic behaviour is usually less dynamic since it depends only on one inflow magnitude from upstream. In sand bed braided rivers, bifurcations therefore often evolve towards stable symmet-

rical geometries. However, like mentioned above, this single inflow magnitude may be affected by a series of secondary flow patterns and other effects. A summary of possible causes for a transition towards an asymmetrical river bifurcation is given below in figure A.6. The first cause describes an upstream disturbance in the form of a migrating sandbar towards one of the branches. This results in an increased discharge through the other branch, which may eventually result in deepening of this channel and large asymmetry. The second possibility describes an inlet step or bar at the entrance of one of the downstream channels. This effect shows similarities with the previous one and may even result from the previous cause.

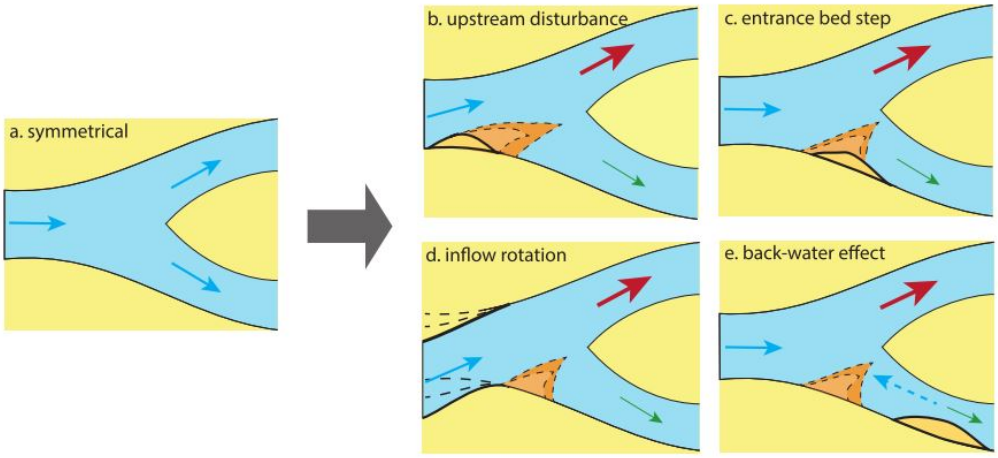

Figure A.6: Possible causes for a transition from a symmetrical to an asymmetrical river bifurcation, adopted from (Schuurman, 2015)

The third reason for asymmetry is due to an upstream inflow rotation. Due to the dynamic behaviour of braiding rivers, the upstream inflow channel can shift and cause a directional shift of inflow conditions. Consequently, the off-take angle into the branches becomes unequal and naturally a higher discharge flows through the branch with the smallest angle. Furthermore a growing point bar, or bar tail limb, will develop which starts closing of the other channel as well. The final mechanism that may result in uneven discharge is the result of a backwater effect due to a downstream bar. Due to the local narrowing of the channel the water level will increase with a resulting backwater curve upstream. This will result in development of a sedimentation front migrating upstream, eventually causing river asymmetry.

Divergent flow patterns like described in this section will also impinge on the banks at an increased angle leading to bank erosion, channel widening and local increase in available sediment, all of which are likely to lead to the development of new braid bars (Bristow & Best, 1993). The deposits of material in confluence and bifurcation points may therefore form the foundation of braided rivers, however there are no known descriptions of these deposits and their internal structure. Where and when the deposits take place exactly remains a highly complicated subject, also stated in the research by Ostanek Jurina (2017) who observed bypass channels, but was not able to predict their location, direction or moment of incision. Researchers up to date still struggle to obtain more insight in the behaviour of the braiding river dynamics.

A.2.3. Channel shifts

Channel shifting in braided rivers is a common but complex process. Normally it is very difficult to determine the exact cause of the shift, and even more difficult to predict the timing and location of a channel shift (Ostanek Jurina, 2017). Usually a small abandoned channel is reclaimed and takes over the main conveyance function. The cause of these shifts is normally due to unstable bifurcations or migration of the upstream channel. An other cause may be the blockage of the current conveyance channel by sedimentation, that forces the flow somewhere else. As described in section A.2.5 the different stages in the hydrograph may also affect the formation of new channels.

The formation of new channels in braided rivers is not fully understood. Observations of cut-off channels in meandering rivers have shown that channels mainly form by upstream erosion, so cut-off channels start at the downstream end of a bar in the form of a headcut. Water flows over the bar and plunges into the channel behind, causing flow acceleration and increased turbulence. Turbulent eddies develop near the bed, and due to the increased sediment transport undercutting takes place near the bank. As the headcut develops, flow

converges and accelerates the erosion even further (Jagers, 2003). However it is found that the cut-of mechanism for channels in a braided river seems to be different. In the study of Jagers (2003) in the Jamuna River, channels often formed from the upstream side (headward erosion). Erosion pattern starts at the upstream end because of an increase in sediment transport once the flow is guided over the bar. Here the flow velocities increase and so does the sediment transport. The process of headward erosion is more dominant in braiding rivers than the cut-of mechanism by a headcut at the downstream end of the bar.

Shifting channels may result in the development of a secondary channel to a dominant discharge channel and vice versa. As long as there are no important harbours or cities connected to one of the channels, such a channel shift does not need to have dramatic consequences. However, if such kind of features are present and also depend on the dominance of the channel, such shifts are highly undesirable. Indirect interventions to control bank retreat and channel shifts were developed and tested in FAP 21/22 projects in the Brahmaputra (Mosselman, 2006). The underlying idea was to influence the morphological development of the river is such a way that erosive channels would be closed by siltation with the use of bandals. However the bandal screen did performed as was intended and the resulting siltation in the area of the measures was substantial, a new entrance channel was formed further downstream. So for large braided rivers it was clear that local solutions should be stretched over a larger area to obtain a more complete closure.

A.2.4. Large-scale erosion and sedimentation

Bank erosion

For braiding rivers to be so dynamic, bank erosion is one of the major principles that enhances this dynamic character. It is one of the main problems in these types of river since it causes large areas to erode, Mosques, temples, schools and hospitals fall into the river and the losses of land often leave not other choice to the riparian population than to move somewhere else (Mosselman, 2006). Bank erosion may occur under relative large erosion rates and erode the river banks between 0 - 500 m/year with larger values up to 1000 m/year observed in the Jamuna river (Klaassen & Masselink, 1992). Banks can also erode several metres at a single moment due to mass erosion. When banks are more cohesive, the main erosion process is undercutting by the flow, which destabilizes the upper part of the bank and results in collapse of river banks. Under alluvial conditions, bank erosion occurs continuously along the outer banks of channels and river bends, and at the upstream end of islands and sand bars. In case of non-cohesive sediment, bank slopes are restricted to an angle of 30-45° and erosion occurs in shallow slides and through fluvial entrainment of particles (Jagers, 2003).

There are mainly three causes to initiate the collapse of banks. First is the undercutting as described above. Second cause of collapse is a geotechnical related failure mechanism caused by saturation of the soil after a long period of high water or heavy rain. After this the long wet period the soil becomes heavier and the pore pressure reduces, which may cause liquefaction of the soil. This often occurs due to a rapid water level decrease. Then the banks are not stabilized by water pressure from the side any more and due to the heavy weight they liquefy or erode very rapidly. Coleman (1969) observed this process in multiple braided rivers and is most common during the falling stage, as highly saturated sediments are more prone to cave than less saturated sediments. Finally, the flow of water through sediment due to piping may destabilize certain sedimentary layers which makes the banks more prone to bank slides. All different types of mass bank failure result in a rapid shift of soil to the toe of the bank, from where the sediment is gradually removed.

Like Ligthart (2017),Schuurman (2015) and Commandeur et al. (2017) have already shown that the implementation of bank erosion in Delft3D is very limited. Bank erosion is simulated in a 2D model by fluvial erosion, which is the removal of bank material by hydraulic forces without taking into account the geotechnical aspects of the bank material. Normally modelled by computing the erosion rate defined by Partheniades (1965):

$$\epsilon = k_d(\tau - \tau_c)^a \tag{A.2}$$

Where:

ϵ = erosion rate [m/s]
k_d = erodibility coefficient [m^{2}s/kg]
τ = shear stress on the bank [N/m^2]
a = an empirically derived parameter (close or equal to 1)

Since this method is very simplified it does not account for the complexity of mass erosion by flooding and drying or other geotechnical related erosion mechanisms described above. These mechanisms depend on

several factors, including the configuration of bank material (whether there is one single type of material or several layers, soil characteristics (cohesive or non-cohesive), bank slope and height, groundwater pressure and vegetation (El Kadi Abderrezzak et al., 2016).

Most of the bank erosion can be prevented by the use of bank protection and stop the supply of sediments to the main channel. But the resulting surplus in the sediment transport capacity will be compensated by the increased erosion of the channel bed and result in bed scour (Mosselman et al., 2000). Surface erosion may be prevented or slowed down by the present vegetation, but the influence of vegetation is negligible for undercutting. The roots do not penetrate deep enough to have and effect on this process (Klaassen & Masselink, 1992). Promising results have been obtained however by applying porcupines in the Brahmaputra river where severe bank erosion has been prevented by the use of porcupines (Sharma & Nayak, 2015)

Scour holes

Just like bank erosion, there are multiple scour mechanisms that affect the river morphology. Below in figure A.7 the main processes that cause scour holes are schematically displayed. Generally scour occurs when the bed shear stress becomes larger than the critical shear stress ($\tau > \tau_c$). This occurs when the flow velocities increase during the rising stage of the hydrograph, however, the largest scour depths occur in general during the last part of the flood during the falling stage as the adaptation of the bed level lags behind.

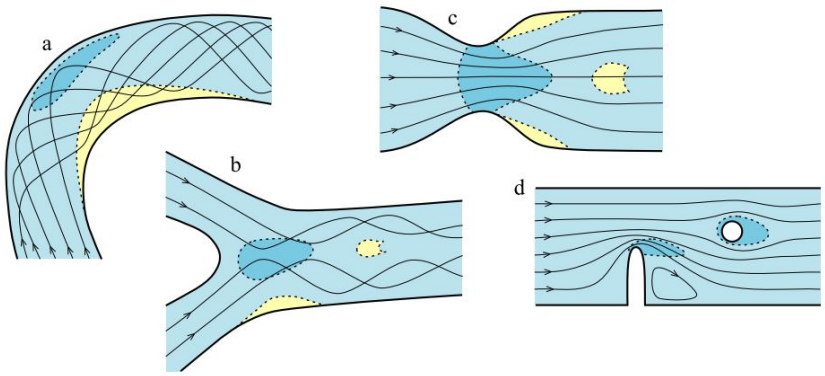

Figure A.7: Scour types:(a) bend scour, (b) confluence scour, (c) constriction scour, (d) Obstruction scour, adopted from (Jagers, 2003)

Jagers (2003) describes the main scour types classified in four different categories. Bend scour is the result of helical flow patterns in the outer bend, where sediment is transported towards the inner bend. This scour hole results in steepening of the bank, thereby increasing the bank erosion probability. Confluence scour is the effect where two or more channels meet and where their flow pattern results in spoon shaped scour holes behind the confluence. The theory behind these so called confluence scour holes is described in section A.2.2. Constriction flow occurs where a channel is constricted to a narrow section. This may be caused by non-erodible ridges or less erodible sediments. The flow velocity increases near the constriction resulting in higher sediment transport capacity, enhancing the erosion. Further downstream the velocity reduces, normally a sand bar develops here again. Obstruction scour is closely related to constriction scour, but is caused by man made structures. The erosion mechanism is the same, due to an increase and decrease of the flow velocity sediment is eroded.

Sedimentation

The eroded sediment by bank erosion or scour holes is deposited as soon as the sediment transport capacity reduces downstream. Large scale erosion in a river dominated by bedload transport is generally associated with significant sedimentation in a downstream area nearby. For suspended sediment this relation only holds to a smaller degree. During flood the finer sediments in suspension are transported higher in the water column and reach the top of the flood plains and large islands, but the coarser sediments remain in the channels. This is also where the sediments are mainly deposited, so fine sediments are found on top of the flood plains while the coarser material is located near the banks and in the channels.

Most sediment, suspended or bedload, is deposited during the falling stage due to the rapid decrease in flow velocity. Coleman (1969) found this in the field and explained that this has consequences for sand bar development. Sand bars develop rather quickly due to increased sedimentation and can block existing channels, resulting in flow deviation which enhances the incision of new channels elsewhere.

Problems related to channel shifts have been treated in section A.2.3, however the problems concerning sedimentation are very similar. Where one channel becomes more dominant, the other becomes less dominant by silting up, which may hinder the navigation towards or along a certain river channel. As long as these channels can be avoided by ships, the problems remain small. However, if large harbours are connected to certain channels that slowly silt-up the problem may be very large. Besides sedimentation of complete channels, local sedimentation can hinder shipping as well. Due to the large morphological activities in braided rivers the navigational thalweg can change very rapidly leaving many ships stranded aground, sometimes for days at a time (Hays, 2008; Jibon, 2013).

A.2.5. Hydrograph

In large braided rivers such as the Ayeyarwady four different hydrograph stages can be distinguished: low, rising, peak and falling stage. They are a consequence of the typical yearly climate circumstances, dependant on the location of these rivers. Low flow conditions coincide with the dry season, whereas the peak discharge conditions coincide with the wet season. All four stages of the hydrograph have their contribution to the morphological development of the river. During the rising stage deepening and widening of the channels take place to increase the conveyance width for the higher discharge. During peak flow all braid bars and sand bars are below water surface so lots of complex processes dominate the system. Peak flow mainly results in most bank erosion, and can completely wash away some of the bed topography Ligthart (2017). Observations by Coleman (1969) and model studies by Ligthart (2017); Yang et al. (2015) indicate that new channels are particularly formed during the falling stage of the hydrograph. Due to a rapid decrease of the water level sediment rapidly deposits and sand bars are formed. These bars may block the flow and push the channel into an alternative direction, forming new channels (Jagers, 2003). Also the probability of bank failure increases during this stage due to outflow of subsurface water. Even during low flow conditions sedimentation and erosion takes place in the dominant channels due to the erosive and sedimentation processes described in section A.2.4.

Different sorts of problems arise with each different phase in the hydrograph. Large erosion and sedimentation result in the problems described earlier, however there is still a major problem that has not yet been mentioned and that occurs during the low flow conditions. During this stage the water level is lowest, and therefore the least available depth is reduced the most during this stage of the season. Navigation along the river becomes more difficult and certain parts of the river may not be accessible any more.

A.3. Bar types

A.3.1. Alternating bars

As mentioned in section A.2, the number of sand bars within a cross section determines the bar mode of that channel. For alternating bars holds that there is always only one bar per cross section, thus m=1 for alternating bars. Below in figure A.8 a schematic overview is given of the most common sand bars that can be distinguished form each other within a braiding river. First of al it is useful to make the phenomenological distinction between local and periodic bars. Local bars are large deposits of sediment, scaling with the river width, which are forced by a permanent deformation of the water flow. These types of deformation can be caused by natural river bends or a man-made structure such as groynes (Duró et al., 2016). From now on these local bars will be referred to as "forced bars" and are, due to their origin, always on fixed locations.

Periodic bars are large deposits of sediment whose formation depends on morphodynamic instability, and they do not arise if the system is outside the instability range. Based on distinguishable mechanisms two types of periodic bars can be defined: "free" and "hybrid" bars.

Free bars arise within the mophodynamic instability range of the system as soon as a perturbation of the flow or bed level is present. They do not require any type of forcing for their formation, and are in general migrating (Duró et al., 2016). They have a wavelength that compares with the channel width and amplitude that compares with the water depth (Le, 2015)

Hybrid bars arise from morphodynamic instability, but they also require the presence of forcing, which has the effect of fixing their phase at a certain location along the river axis. The fixing of phase prevents hybrid bars from migrating and therefore fixes their celerity as zero. The amplitude and wavelength of hybrid bars are not proportional to the forcing, but are determined by the morphodynamic instability (Duró et al., 2016). The wavelength of hybrid alternate bars is generally 2-3 times longer than the wavelength of alternate free

bars (Le, 2015).

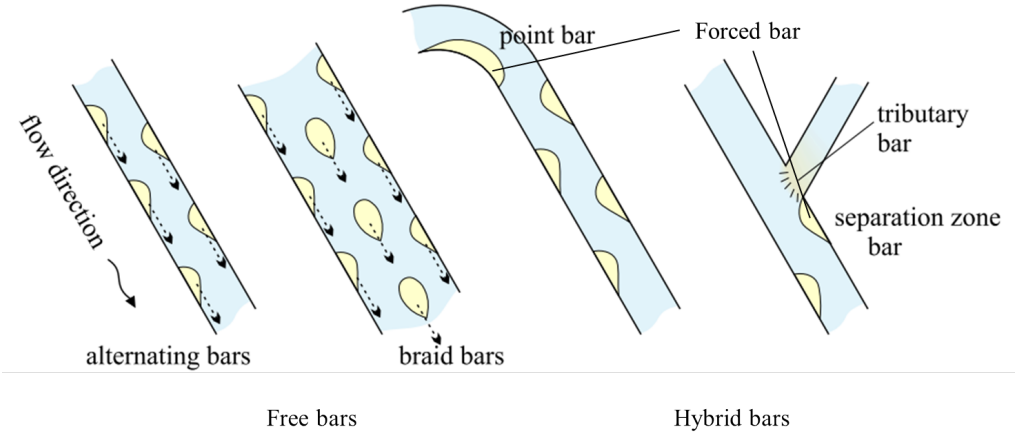

Figure A.8: Most common sand bars present in braided rivers, adopted from (Jagers, 2003)

In figure A.8 a visual summary is given for the above defined types of sand bars. The definition of these bars however still results in confusion sometimes, since hybrid bars are defined as non-migrating. But since their origin lies in the generation of forced bars upstream they may still migrate downstream. Point bars or sand bars behind groynes may namely develop over time and grow larger behind their obstruction. This has consequences for the hybrid alternating bars further downstream because their wavelength and amplitude is still dependent on the forcing. So a growing forced bar results in migrating hybrid bars downstream which may be interpreted as free bars. When we take discharge variation into account as well these bars may also start to migrate upstream or downstream, but will always remain hybrid bars.

A.3.2. Braid bars

Braid bars are sand bars that are not attached to the side walls. Because of their appearance the number of bars per cross section is increased to two, resulting in a bar mode of m=2. If the number of braid bars per cross section increases, consequently the bar mode will increase as well. An example of a braid bar is also given in figure A.8. The generation of braid bars is initiated by sorting mechanisms of the sediment. Due to a smaller transport capacity of the larger particles the courser sediment particles starts to accumulate in the middle of the channel. This small bar of sediment then start to grow by successive accretion at its downstream end (Jagers, 2003). This process continues, resulting in a bar in which the sediments have been sorted on average from coarse at the upstream side and along the outer rim, to fine at the downstream side and inside the bar.

A.3.3. Flow patterns

Flow patterns around alternating bars and braid bars result in the shape of bars and channels within the braiding river. Bars mainly grow during low flow conditions by lateral, downstream and upstream accretion. They mainly grow due to lateral accretion and migrate by upstream erosion and downstream deposition. The upstream end is of a bar is on average higher than the downstream end. The sediment deposition on the downstream end of a bar will sometimes form bar tail limbs which indicate the direction of the braided river-flows. In figure A.9 a schematization of such a bar tail limbs is shown. The larger bar tail indicates the dominant channel (Schuurman, 2015).

Secondary flow (or spiral flow) has a large importance on the dynamics of the bar tail limbs. The specifics of these secondary flow patterns will be elaborated in section A.4, but the general effect is explained here. Due to curvature in the flow direction water is pushed sideways, increasing the water level slightly at the outer bends. This results in a transverse flow component directed to the inner bend near the channel bed due to mass balance. The flow near the bed transports sediment to the inner bend. This mechanism will deepen the outer bend and accrete the inner bend until a new equilibrium is reached between the increasing down slope gravity component and the inward directed force exerted on the sediment by the helical flow. The erodibility of the river banks determine the effect of secondary flow and therefore affect the shape and generation of bar tail limbs.

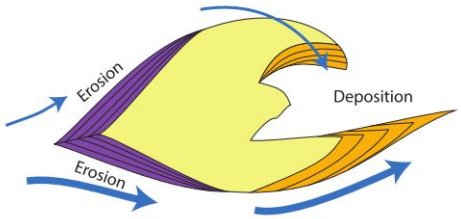

Figure A.9: Evolution of bar tail limbs by erosion and accretion, adopted from (Schuurman, 2015)

A.4. Spiral flow and bed slope effect

As previously mentioned, helical flow or spiral flow is a very important mechanism that highly influences the river morphology. An other important mechanism that can largely effect the morphology is the bed slope effect. Both mechanisms will be discussed below.

A.4.1. Spiral flow

Helical flow patterns are caused by flow curvature that pushes water to the outer bend, resulting in a return flow near the bottom which enhances sediment transport towards the inner bend. The combination of this circulation pattern and the primary flow results in the spiral flow along the curved river course. Due to the curvature and the sediment transport towards the inner bend, the outer bend start to erode. The outer bend becomes deeper and bank erosion starts to occur, which in its turn makes the curvature even larger. In a single channel river this effect is the driving force for meandering, constant eroding outer bends and deposition on the inner bend causing the channel to shift outwards. With multiple channels in a braided river reach the dynamics become increasingly complex. The meandering effect of the channels only occurs during the falling stage and low flow conditions, during high water conditions the hydrodynamics are completely different.

Schuurman (2015) found that the the secondary flow effect enhanced the development of the braided pattern in a self-formed braided river. The equations used in the Delft3D model to describe the deflection of sediment transport due to helical flow are listed below. However, Ligthart (2017) found that these equations do not represent the hellical flow accurate enough. In a depth-averaged computation really rough assumptions are performed by the model to simulate some general effects based on spiral flow. However these assumptions are made for a perfect symmetrical curve and perfect flow conditions which do practically never occur in braided rivers in nature. Therefore the use of these equations is useful for a first assessment but are not accurate enough to give a correct result.

$$\tan(\phi_\tau) = \frac{v - \alpha_I \frac{u}{U} I_s}{u - \alpha_I \frac{v}{U} I_s} \tag{A.3}$$

$$\alpha_I = \frac{2}{\kappa^2} E_{spir} \left(1 - \frac{1}{2} \frac{\sqrt{g}}{\kappa C}\right) \tag{A.4}$$

in which

ϕ_τ = direction of bed load transport relative to primary flow direction due to secondary flow [°]
u = flow velocity in the x direction [m/s]
v = flow velocity in the y direction [m/s]
I_s = spiral flow intensity [m/s]
C = Chézy roughness coefficient [$m^{1/2}/s$]
h = water depth [m]
κ = the von Karman constant [-]
E_{spir} = calibration coefficient of the spiral flow [-]

A.4.2. Bed slope effect

The bed slope effect is a mechanism in which the gravitational force becomes important for the sediment transport. In the scenario that sediment is positioned on a slope, the gravitational forces downslope enhances or reduces sediment transport rates. The steeper the slope, the higher its effect. Furthermore, the sediment transport direction is also deflected by the presence of a slope. This effect is shown in figure A.10 in which the

sediment particle is moved by the flow in flow direction, but also down the slope due to the gravitational pull. Due to this effect sharp gradients are avoided and an overall flatter bed topography is achieved.

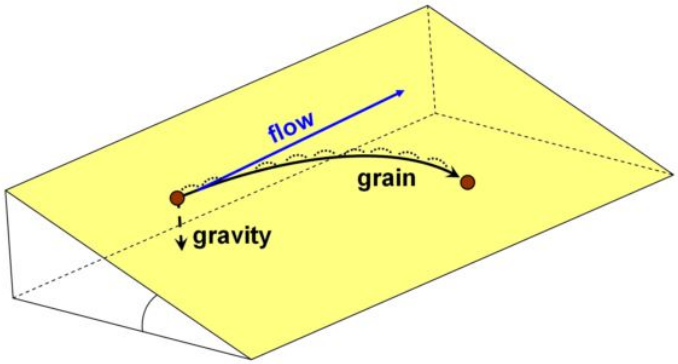

Figure A.10: Transverse bed slope effect: deflection of sediment due to gravity, adopted from (Schuurman, 2015)

For numerical modelling numerous parametrizations for the bed slope effect have been used, however accurate representation of the effect is difficult to obtain and mainly dependent on arbitrary calibration parameters. Schuurman (2015) found that varying the parameters for the bed slope effect significantly influences the braiding intensity, dimensions of the channels and bar height. Therefore a verification of river models is always required. The equations used by Delft3D for the bed slope effect are the following.

$$\tan(\phi_s) = \frac{\sin(\phi_\tau + \frac{1}{f(\psi)}\frac{dz_b}{dy}}{\cos(\phi_\tau + \frac{1}{f(\psi)}\frac{dz_b}{dx}} \tag{A.5}$$

$$f(\theta) = A_{shield}\psi^{B_{shield}}\left(\frac{D_i}{h}\right)^{C_{shield}}\left(\frac{D_i}{D_{50}}\right)^{D_{shield}} \tag{A.6}$$

in which

ϕ_s	= the direction of sediment transport due to bed slope effect [°]
ϕ_τ	= direction of shear stress (sediment transport before the bed slope effect) [°]
z_b	= bed level [m]
$A_{shield}, B_{shield}, C_{shield}\&D_{shield}$	= calibration parameters [-]
ψ	= Shields mobility parameter [-]
D_i	= median grain size of the fraction [m]
D_{50}	= median grain size of the bed [m]

A.5. Roughness

In equation A.7 the representative roughness for vegetation is schematized. This equation is valid for uniform flow conditions. A constant uniform velocity is assumed inside the vegetation and a logarithmic velocity profile is assumed on top of the vegetation, this is illustrated in the figure below. In this research the analogy between the effect of vegetation an the effect of porcupines is found and therefore it is tried to determine the amount of roughness based on this equation.

$$C_r = \sqrt{\frac{1}{\frac{1}{C_b^2} + \frac{C_D m A}{2g}}} + \frac{\sqrt{g}}{\kappa}\ln\left(\frac{h}{k}\right) \tag{A.7}$$

in which

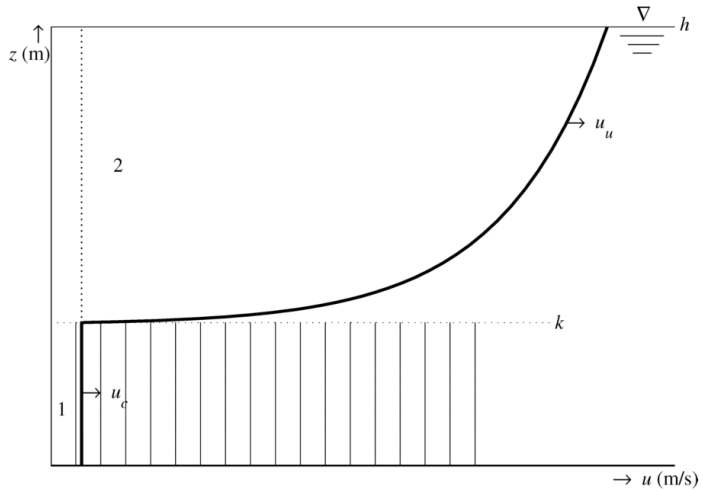

Figure A.11: Assumed velocity profile for applicability of the formulation

C_r = representative Chézy value [$m^{1/2}/s$]
C_b = bed resistance [$m^{1/2}/s$]
C_D = drag coefficient [-]
m = number of porcupines [$1/m^2$]
κ = Von Kármán constant (≈ 0.4) [-]
h = water depth [m]
k = porcupine height [m]

To be able to compute the representative Chézy value by the formulation described it is first required to determine the drag coefficient for porcupines. In order to do so it is assumed that the total shear stress is composed out of the bed shear stress and the porcupine shear stress.

$$\tau_t = \tau_b + \tau_p \tag{A.8}$$

in which

τ_t = total shear stress [N/m^2]
τ_b = bed shear stress [N/m^2]
τ_p = additional porcupine shear stress [N/m^2]

In the derivation by Baptist et al. (2007) it is assumed that the total shear stress can be computed since a constant water level slope is present. This constant slope is present since the vegetation stretches over a distance long enough for an equilibrium of forces. Therefore the total shear stress is described as:

$$\tau_t = \rho g h i \tag{A.9}$$

Furthermore it is assumed that the bed shear stress is determined by the uniform velocity through the vegetation, u_c:

$$\tau_b = \frac{\rho g}{C_b^2} u_c^2 \tag{A.10}$$

where C_b is the Chézy bed roughness which is known. The uniform velocity profile in the vegetated layer follows from the momentum balance for flow through and over vegetation. For a uniform flow profile over the vegetation height, k (m), the drag force becomes:

$$\tau_p = \frac{1}{2} \rho C_D m A u_p^2 \tag{A.11}$$

in which

ρ = density of water [kg/m^3]
C_D = drag coefficient of porcupines [-]
m = number of porcupines [1/m^2]
A = frontal area of porcupine(=$3 \cdot 0.1 \cdot 0.007 \cdot \cos(30)$) [m^2]
u_p = flow velocity in porcupine field [m/s]

By filling in equation A.8 the following description is given for the flow velocity through the vegetation:

$$u_c = \sqrt{\frac{hi}{\frac{1}{C_b^2} + \frac{C_D m A}{2g}}} \tag{A.12}$$

Combining this equation with equation A.10 yields an expression for the vegetated bed shear stress, or porcupine shear stress, written as a reduction factor times the well known equation of the total shear stress.

$$\tau_p = \frac{1}{1 + \frac{C_D m A C_b^2}{2g}} \rho g h i \tag{A.13}$$

Equation A.12 only describes the flow velocity through the vegetated part, however there is also a logarithmic velocity profile on top of the vegetation. However after a mathematical analysis and data fitting with measurements Baptist ended up with equation A.7 where the logarithmic velocity profile on top of the vegetation is also taken into account. With this formulation the representative roughness of the vegetation can be computed.

A.6. Drag force

The drag on a certain object in the flow determines the roughness of that object. The amount of drag corresponding to an object is described as the pressure difference over that object. For flow conditions with high Reynolds numbers it is observed that the drag force is proportional to the velocity squared as given by equation A.14.

$$F_D = \frac{1}{2} \rho u^2 C_D A \tag{A.14}$$

in which,

F_D = drag force [N]
ρ = density of water [kg/m^3]
u = flow velocity [m/s]
C_D = drag coefficient [-]
A = frontal area [m^2]

A larger area over which the pressure does not restore to its initial pressure results in a drag force. For many objects the corresponding drag coefficient is determined, and the maximum drag force where no pressure is restored at all results in the largest drag coefficient of 2. In this case the pressure difference is twice $\frac{1}{2}\rho u^2$. However, if the Reynolds numbers are very small, the drag is no longer proportional to the velocity squared but to the velocity itself. This means that if we still write the drag force in terms of a drag coefficient the following relation arises.

$$F_D \sim \eta u l = C_D \frac{1}{2} u^2 l \rightarrow C_D \sim \frac{\eta}{\rho u l} = \frac{1}{Re} \tag{A.15}$$

This relation writes a viscous dominated flow in terms of an inertia dominated flow. However it is observed that in these scenarios the drag coefficient can be much larger than 2 which is illustrated in figure A.12. In reality however this is physically not possible where high Reynolds numbers are present.

A.7. Sediment transport

A.7.1. Shields

Sediment transport is the result of an interaction between water and sediment. The flow of water exerts a force on the sand bed, resulting in a shear stress that causes the sediment to move. Probably the best-known formula for sediment transport is the one by Shields (1936) who describes the incipient motion of non-cohesive sediments. He gives a relation between a critical shear stress (τ_c) and the so-called particle

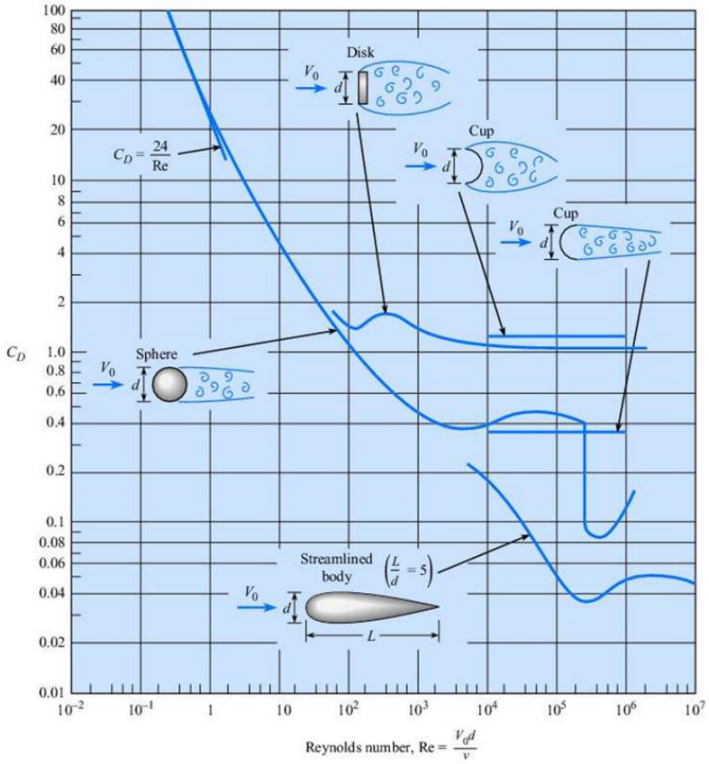

Figure A.12: Drag relation with Reynolds number

Reynolds-number (Re_*). Particle movement will occur when the instantaneous fluid force on a particle is just larger than the instantaneous resisting force from the particle. Instability, followed by movement of grains, occurs when the bed shear stress is larger than the instantaneous critical shear stress. Shields focussed on the incipient motion of a complete sand bed with the bed shear stress as active force. He defined a mobility parameter for different particle diameters dependent on the particle Reynolds number as illustrated below.

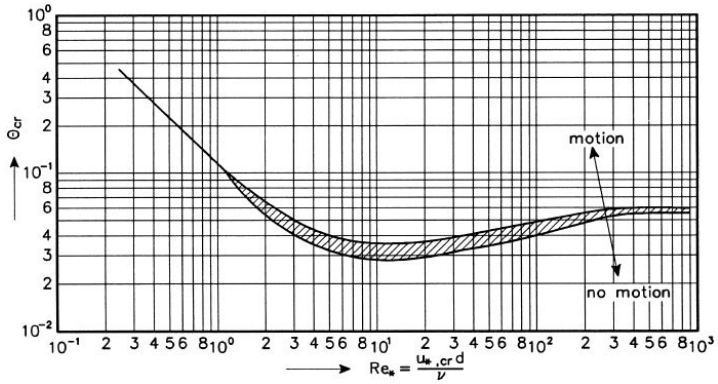

Figure A.13: Critical mobility parameter according to Shields, adopted from (van Rijn, 1993)

The figure represents the following equation of the mobility parameter given as equation A.16, which is described as θ_{cr} in the graph but as ψ_c in this thesis. Besides, in the description for the Reynolds number the notation for the shear velocity (u_*) is given which is calculated by equation A.17 and is only valid if Chézy is valid, so only with uniform flow conditions. This notation differs from the notation used by van Rijn (1993) for the critical shear velocity ($u_{*,c}$).

$$\psi_c = \frac{\text{Load}}{\text{Strenght}} = \frac{\tau_c d^2}{(\rho_s - \rho_w) g d^3} = \frac{\tau_c}{(\rho_s - \rho_w) g d} = \frac{u_{*c}^2}{\Delta g d} = f(Re_*) = f\left(\frac{u_{*c} d}{\nu}\right) \tag{A.16}$$

in which

τ_c = critical bed shear stress (=ρu_{*c}^2) [N/m^2]
d = sediment diameter [m]
ρ_s = density of sediment [kg/m^3]
ρ_w = density of water [kg/m^3]
g = gravitational acceleration [m/s^2]
u_{*c} = critical shear velocity [m/s]
Δ = relative density [-]
Re_* = particle Reynolds number [-]
ν = kinematic viscosity [m^2/s]

$$u_* = \sqrt{\frac{\tau}{\rho_w}} = \overline{\overline{u}}\frac{\sqrt{g}}{C} \tag{A.17}$$

in which

$\overline{\overline{u}}$ = depth- and time averaged flow velocity [m/s]
C = Chézy coefficient [m$^{1/2}$/s]

The particle Reynolds-number indicates whether the grain protrudes into the turbulent boundary layer or stays within the viscous sub-layer. For high Re^* numbers (large grains, larger than the viscous sub-layer, turbulent flow around the grain) the mobility parameter, ψ_c, is no longer dependent on Re_* and becomes constant with a value of about 0.055.

To determine the critical flow velocity using the method of Shields, one has to perform a number of iterations to arrive at the final values for Re_*,ψ_c and u_{*c}. This iteration can be avoided by using the modified approach by Van Rijn (1984). Here the particle Reynolds number is replaced by a dimensionless particle diameter, d_*, defined as:

$$d_* = d\left(\frac{\Delta g}{\nu^2}\right)^{1/3} \tag{A.18}$$

in which

d_* = dimensionless particle diameter [-]
d = (d_{50}) median particle diameter [m]

Once the particle diameter is known, using this equation the dimensionless diameter can easily be computed. Using the Van Rijns presentation of the shields relation one can immediately find the corresponding mobility parameter, obeying the following conditions:

Table A.1: Empirical relations for ψ_c, adopted from (Van Rijn, 1984)

ψ as function of D_*	Condition for D_*
$\psi_c = 0.24D_*^{-1}$	$D_* \leq 4$
$\psi_c = 0.14D_*^{-0.64}$	$4 \leq D_* \leq 10$
$\psi_c = 0.04D_*^{-0.1}$	$10 \leq D_* \leq 20$
$\psi_c = 0.013D_*^{0.29}$	$20 \leq D_* \leq 150$
$\psi_c = 0.055$	$D_* \geq 150$

Combining equations A.16 and A.17, and the obtained mobility parameter, an expression for the critical flow velocity can be found for which the critical bed shear stress is exceeded and incipient sediment transport is induced.

$$u_c = \sqrt{\Delta d \psi C^2} \tag{A.19}$$

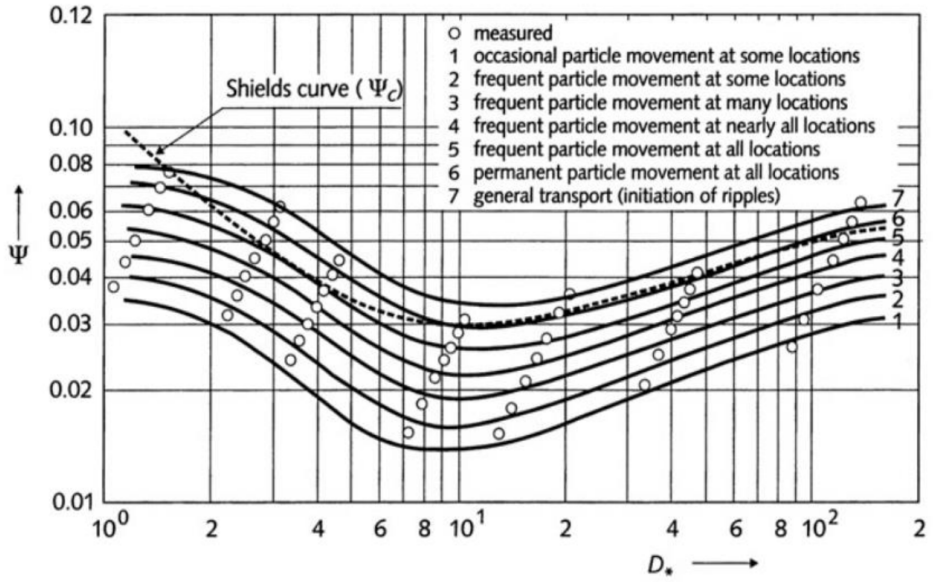

Figure A.14: Critical mobility parameter according to Shields with the dimensionless partical diameter of Van Rijn, adopted from (Hoffmans & Verheij, 1997)

A.7.2. Transport equations

Sediment transport can be categorised in three types of load, namely as bed load transport, suspended load transport and washload. Specifically bedload transport, is a key process to understand morphodynamics in braided rivers (Surian, 2015). Suspended load and bedload transport dominate large sand-bed braided rivers and together they form the so called total or material load. Bed load is usually defined as the sliding and rolling of particles close to the bed, while suspended load is defined as the transport of sediment that is suspended in the fluid for some time (de Vriend et al., 2011). Particles get into suspension once the upward turbulent forcing is larger than the submerged particle weight. Although this theoretical difference is clear, in reality it is hard to differentiate between both categories. Further complexity is due to the nature of suspended load, since a part of the suspended load can be washload. Washload is the suspension of very small particles with very large adoption lengths. This material does, by definition, not interact with the bed and has therefore no influence on the bed development. A summary of the sediment transport can be given in the following figure, where transport can be defined according to the origin or the transport mechanism.

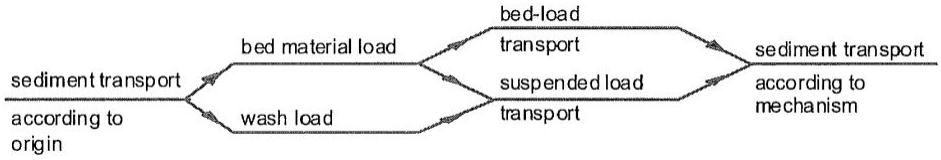

Figure A.15: Classification of sediment transport, adopted from (de Vriend et al., 2011)

Bedload is highly determined by the amount of bed roughness exerted by the bed, which is determined by the composition of the bed. Different sizes or types of sediment have a different influence on the bed roughness. Large gravel particles induce more bed resistance than fine clays. This resistance causes a shear stress on the bed that determines the amount sediment transport. An increasing bed shear stress does not automatically mean an increase or decrease of sediment transport. Larger bed shear stresses result in lower flow velocities and therefore enhance sedimentation. On the other hand, the larger bed shear stress acts as larger forces on the bed which has an increasing effect on the sediment transport. So, the amount of sediment transport is not only determined by the shear stress, but also depends on other parameters.

Bed roughness can be described with different parameters such as the Chézy parameter, that describes the bed roughness as a uniform value independent of water depth. Other options are the use formulations that describe the Chézy roughness coefficient related to water depth, such as the Manning or White-Colebrook formulations. The formulation for Manning reads:

$$C = \frac{h^{1/6}}{n} \tag{A.20}$$

and for White-Colebrook:

$$C = 18\log\left(\frac{12h}{k_s}\right) \tag{A.21}$$

in which

C = Chézy roughness coefficient [$m^{1/2}/s$]
n = Manning coefficient [-]
h = water depth [m]
k_s = Nikuradse roughness height [m]

The amount of transport and also the type of transport depends on the sediment characteristics and the amount of generated roughness, but also on the flow conditions. Shields (1936) has specified a relation between the critical dimensionless shear stress and the particle Reynolds number. The formula to calculate this parameter, ψ, is derived from an equilibrium of forced on the bed an reads as follows:

$$\tau_* = \psi = \frac{\tau}{(\rho_s - \rho_w)gD} \tag{A.22}$$

in which

ψ = Shields mobility parameter [-]
τ = bed shear stress [N/m^2]
ρ_s = density of sediment [kg/m^3]
ρ_w = density of water [kg/m^3]
g = gravitational acceleration [m/s^2]
D = sediment particle diameter [m]

Incipient motion of sediment is observed once the shields parameter becomes higher than the critical shear stress, ψ_{cr}, for that specific type of sediment. This ψ_{cr} can be determined from the Reynolds number, and indicates that for movement of a particle a certain stress is necessary. The shear stresses are a function of the flow velocity and bed roughness and are used in numerous sediment transport estimator equations for river modelling. Frequently used formulas that describe the sediment transport in rivers are the Engelund and Hansen formula (Engelund & Hansen, 1967), the Meyer-Peter & Müller formula (Meyer-Peter & Müller, 1948) and the formula of van Rijn (van Rijn, 1993). Generally, all sediment transport equations state that the sediment transport s per unit width is a function of the gravitational field (g), the fluid attributes (ρ, ν), the sediment attributes (ρ_s, d) and one or more parameters regarding the influence of the flow (τ_b).

$$s = f(g, \rho, \nu, \rho_s, d, \tau_b) \tag{A.23}$$

A more common description of a sediment transport formula is given below where the variables of the previous equation are summarized in a single parameter (m). Here the sediment transport formula is described as a specific dependent coefficient times the flow velocity to a certain power.

$$s = m \cdot u^n \tag{A.24}$$

in which

s = specific sediment discharge [$m^3/s/m$]
m = sediment transport dependent coefficient
u = flow velocity [m/s]
n = coefficient determining the power above the velocity [-]

By means of dimensional analysis the parameters that determine the sediment tranport can be combined into different non-dimensional variables. In most of the existing transport formulas only the flow parameter (Ψ) and the transport parameter (Φ) are used.

$$\Phi = \frac{s}{\sqrt{\Delta g d^3}} \tag{A.25}$$

$$\Psi = \frac{\mu\tau}{(\rho_s - \rho_w)gD} = \mu\psi \tag{A.26}$$

in which

Ψ = flow parameter
Φ = transport parameter [-]
μ = ripple factor

The ripple factor represents the influence of the bed forms and is denoted by equation A.27 where the Chézy coefficient (C_{90}) is related to D_{90} as given by equation A.28.

$$\mu = \left(\frac{C}{c_{90}}\right)^{3/2} \tag{A.27}$$

$$C_{90} = 18\log\frac{12h}{D_{90}} \tag{A.28}$$

Below the sediment transport equations described by Meyer-Peter & Müller and Engelund and Hansen will be given. The Meyer-Peter-Müller formula formula is derived from purely bed-load transport with a $\mu\psi$ of 0.2 and a sediment diameter of maximum 0.4 mm. The Meyer-Peter & Müller formula in terms of Ψ and Φ reads:

$$\Phi = 8(\Psi - 0.047)^{3/2} \tag{A.29}$$

or in terms of the variables with dimensions:

$$s = 8D_{50}\sqrt{\Delta g D_{50}}(\mu\psi - \xi\psi_{cr})^{3/2} \tag{A.30}$$

The sediment transport of the Engelund-Hansen formula concerns the total load. So the calculated sediment transport includes both bed-load and suspended load excluding wash load. The formula in terms of Ψ and Φ reads:

$$\Phi = 0.05\Psi^{5/2} \tag{A.31}$$

and in terms of the variables with dimensions, the equation reads:

$$s = \frac{0.05u^5}{\sqrt{g}C^3\Delta^2 D_{50}} \tag{A.32}$$

in which

q = discharge [m^2/s]
Δ = relative density $(\rho_s - \rho_w)/\rho_w$ [-]
C = Chézy roughness coefficient [m$^{1/2}$/s]
α = calibration coefficient [-]
μ = ripple factor or efficiency factor [-]
θ_{cr} = critical mobility parameter (0.047) [-]
ξ = hiding and exposure factor for the sediment fraction [-]

A.7.3. Compensation for vegetation

In numerical computations, the sediment transport is determined partly by the bed-shear stress as is described in the previous section. However computer models schematise vegetation as increases roughness, consequently the presence of vegetation in a model will lead to higher bed roughness. The downside of this method is that this will increase the bed shear stress and therefore increase the sediment transport rates for morphological computations. Although the shear stress behind porcupines or vegetation indeed increases on average, close to the bed the bed shear stress actually decreases, but this is not taken into account by the model. Therefore, a compensation term has been included in the momentum equations for Delft3D, $-\frac{\lambda}{2}u^2$, in which λ represents the flow resistance of the vegetation.

B

Experimental set-up

This appendix elaborates on the choice of sediment for the conducted experiments based on the theory of Van Rijn and the Rouse number. Furthermore, the sieve curve of the sediment with additional information is presented.

B.1. Sediment choice

To choose the right sediment for the experiments there have been two separate tests to determine the amount of suspension of the sediment and the size of the bed forms. In scale models it is of importance that scale effects are minimal, so to model the real river as accurate as possible the sediment should be as small as possible as well. However, scaling down sediment is possible to a certain extend before it starts to show cohesive behaviour. For this experiment three different sediment sizes have been compared to each other; M32, M34 and AF100. In table B.1 an overview is given of the difference in required critical flow velocity to get sediment transport.

In this table k_s is assumed to be $3.5 \times d_{50}$ and ψ is calculated by using the relations from table A.1. The Chézy value is computed by using the formula for the intermediate chezy roughness. And finally, the equations for the critical velocity and critical bed shear velocity are given below.

$$u_c = \sqrt{\Delta d_{50} \psi C^2} \tag{B.1}$$

$$u_{*,c} = \sqrt{\psi \Delta g d_{50}} \tag{B.2}$$

in which

u_c = critical flow velocity [m/s]
Δ = relative density [-]
d_{50} = median grain size [m]
ψ = Shields parameter [-]
C = Chézy coefficient [$m^{1/2}/s$]
$u_{*,c}$ = critical bed-shear velocity [m/s]

Table B.1: Sediment characteristics

Sediment type	d_{50} [μm]	k_s [μm]	d_* [-]	ψ [-]	C [$m^{1/2}/s$]	$u_{*,c}$ [m/s]	u_c [m/s]
M32	260	910	6.58	0.042	57.4	0.013	0.244
M34	170	595	4.30	0.055	59.7	0.012	0.235
AF100	130	455	3.29	0.073	61.1	0.012	0.242

It can be noted that all three critical velocities are more or less equal to each other, and that no distinct decision can be made on based on these characteristics. Therefore insight is sought on the size of the dunes and ripples that will develop during the model test. These bed forms should be as small ass possible to prevent

inference on the results. In reality these bed forms will be present but their size is much smaller compared to the size of the porcupines, in the flume this relation quickly becomes much larger and should be avoided.

In order to determine the size of the ripples and dunes the bed-shear stress parameter (T) should be determined as described below. The results of these computations have been summarised in table B.2. For the computations a flow velocity of approximately 0.36 m/s has been applied.

$$T = \frac{\tau'_{b,c} - \tau_c}{\tau'_{b,c}} \tag{B.3}$$

$$\tau_c = \rho u^2_{*,c} \tag{B.4}$$

$$\tau'_{b,c} = \rho g \left(\frac{\overline{\overline{u}}}{C'} \right)^2 \tag{B.5}$$

$$C' = 18 \log \left(\frac{12h}{3d_{90}} \right) \tag{B.6}$$

in which

T = bed-shear stress parameter [-]
$\tau'_{b,c}$ = grain-related bed-shear stress [N/m^2]
τ_c = critical bed-shear stress [N/m^2]
$\overline{\overline{u}}$ = time-and depth averaged velocity [m/s]
C' = grain-related Chézy coefficient [m$^{1/2}$/s]
d_{90} = sediment size for which 90% is smaller [m]

Table B.2: Computation for ripple factor

Sediment type	d_{50} [μm]	d_{90} [μm]	ψ [-]	τ_c [N/m^2]	C' [m$^{1/2}$/s]	$\tau'_{b,c}$ [N/m^2]	T [-]
M32	260	340	6.58	0.176	58.440	0.380	1.155
M34	170	215	4.30	0.151	62.023	0.338	1.230
AF100	130	165	3.29	0.154	64.092	0.316	1.059

Again, the values for the three different sediment sizes do not differ that much, and all computed values result in mini-ripples based on the theory of van Rijn (1993). In table B.3 an overview is given for the resulting ripples or dunes based on the value of T and d_*. For the flume experiment all three sediment sizes result in low transport regime with small ripples because the d_* is never larger than 10.

Table B.3: Ripple factor, adopted from (van Rijn, 1993)

Transport regime		Particle size	
		$1 \leq d_* \leq 10$	$d_* > 10$
Lower	$0 \leq T \leq 3$	mini-ripples	dunes
	$3 < T \leq 10$	mega-ripples and dunes	dunes
	$10 < T \leq 15$	dunes	dunes
Transition	$15 < T \leq 25$	washed-out dunes, sand waves	
Upper	$T \geq 25$, Fr < 0.8	(symmetrical) sand waves	
	$T \geq 25$, Fr ≥ 0.8	plane bed and/or anti-dunes	

Finally, the amount of suspended sediment is determined. For the experiments the aim is to have as less suspended sediment as possible. In contrast to the small influence of different grain sizes on the critical flow velocity and ripple size, significant difference in types of transport are present with different grain sizes. The amount of suspended sediment is expressed as the Rouse number (Z). It expresses the importance of suspended load transport as a ratio between the turbulent fluid forces and gravitational forces (van Rijn, 1993).

The different Rouse numbers have been computed in table B.4, and this time the differences are very clear. By using table B.5 with general conditions it becomes clear that finer sediment results in more suspension. Since suspended sediment is to be avoided as much as possible the choice has been made to use the M32 sediment for the flume experiments.

$$Z = \frac{w_s}{\kappa u_*} \tag{B.7}$$

$$w_s = \frac{10\nu}{d_{50}}\sqrt{1+\left(\frac{0.01\Delta g d_{50}^3}{\nu^2}\right)} \qquad \text{if} \qquad 100 < d \leq 1000\mu m \tag{B.8}$$

in which

Z = Rouse number [-]
w_s = fall velocity [m/s]
κ = Von Kármán constant (≈ 0.4) [-]
u_* = bed-shear velocity [m/s]
ν = kinematic viscosity [m^2/s]
d_{50} = median grain size [m]
Δ = relative density [-]
C = Chézy coefficient [$m^{1/2}/s$]

Table B.4: Rouse number

Sediment type	d_{50} [μm]	ψ [-]	C [$m^{1/2}/s$]	w_s [m/s]	u_* [m/s]	u_*/w_s [-]	Z [-]
M32	260	0.042	57.4	0.037	0.020	0.537	4.656
M34	170	0.055	59.7	0.020	0.019	0.954	2.620
AF100	130	0.073	61.1	0.013	0.019	1.475	1.695

Table B.5: The amount of suspended sediment related to the Rouse number, adopted from (van Rijn, 1993)

Z	$\frac{u_*}{w_s}$	Suspended sediment distribution over the depth
5	0.5	suspended sediment in near-bed layer ($z < 0.1h$)
2	1.25	suspended sediment up to mid depth ($z < 0.5h$)
1	2.5	suspended sediment up to water depth
0.1	25	suspended sediment almost uniformly distributed over depth

B.2. Sieve curve

The selected sediment M32 has been sieved to check the values for the d_{50} and d_{90}. In this simple experiment it turned out that they were both somewhat lower than was expected. However it does not affect the sediment choice because the Rouse number remained the highest since the particles were still much larger compared to the others. Therefore not much suspended sediment was expected and the sediment was used in the experiments.

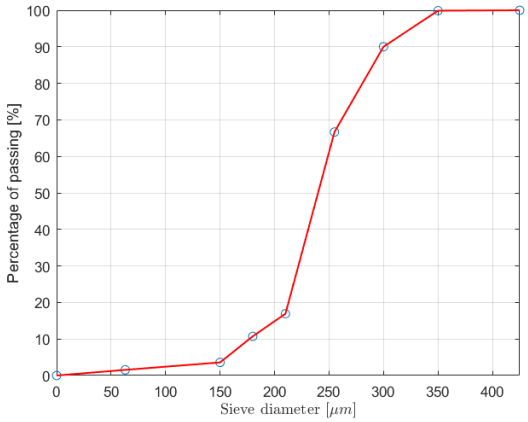

Figure B.1: Sieve curve of experimental sediment

After sieving the sediment it was observed that the curve steepness was very sharp, indicating a really uniform sediment size. In reality the curve is less steep since a larger variety of sediment fractions is present. This means that sediment in reality is probably less mobile than the sediment in the experiments. This could mean that the ripple formation in the experiments are less extreme in reality and will therefore affect the behaviour around porcupines less. This was also mentioned in the work of Vargas-Luna et al. (2015) who experienced difficulties with the ripple formation of too uniform sediment.

C

Fixed-bed experiments

This appendix provides additional information on the fixed-bed experiments. First the velocity profiles are given, followed by the water level measurements. Finally, some information is provided on the amount of turbulence along the flume for different experiments.

C.1. Velocity profiles

The figures below illustrate the flow velocity and directions in longitudinal direction in the near field of the porcupine field. Clearly the porcupines divert the flow around them, and especially in figure C.1 it is observed that porcupines affect the water levels also. In all figures the bottom profile and water level downstream from x=5 [m] has not been measured due to the configurations of the measurement set-up but the flow profiles were measured. Therefore an extrapolated water level and bed profile are given but not actually measured.

C.1.1. Fully blocked

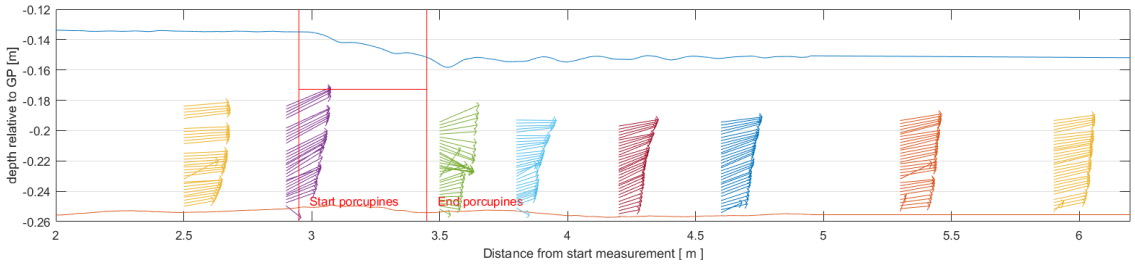

Figure C.1: Vector plot of velocity profiles, Experiment 8: h=0.11 [m], Q=32.5 [l/s], L=0.5 [m]

In experiment 8 it is observed that downstream of the porcupines flow velocities are directed upward, something that is not observed in other experiments. This indicates a larger probability of downstream erosion. In experiment 1 (mobile-bed experiment) this is also observed slightly, indicated in figure D.16. This is probably the result of the strongly diverted flow velocities around the porcupines such that they plunge down stronger than in other experiments and attack the bottom of the flume with larger velocities

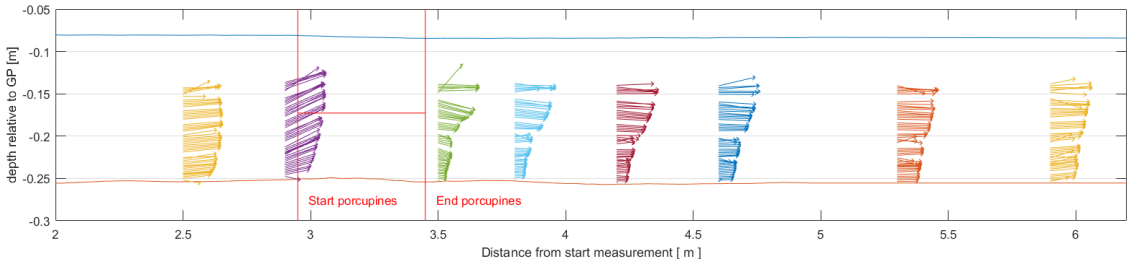

Figure C.2: Vector plot of velocity profiles, Experiment 9: h=0.17 [m], Q=32.5 [l/s], L=0.5 [m]

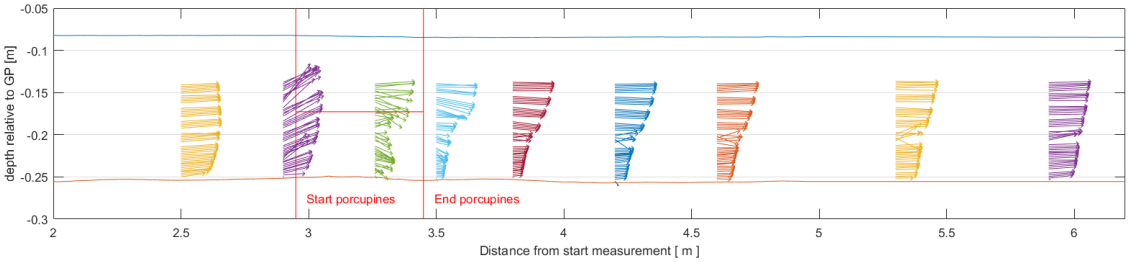

Figure C.3: Vector plot of velocity profiles, Experiment 11: h=0.17 [m], Q=25 [l/s], L=0.5 [m]

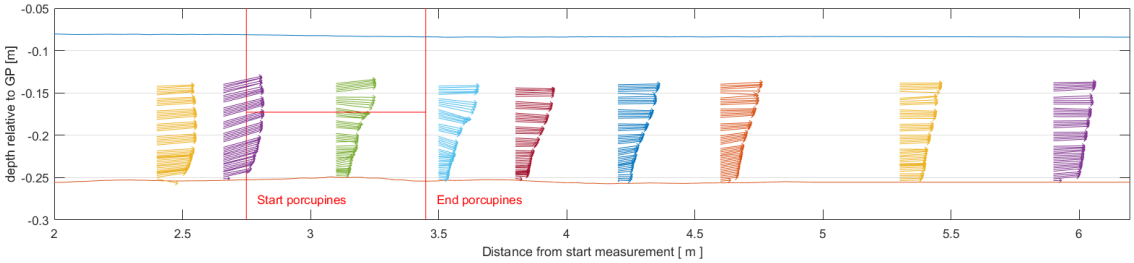

Figure C.4: Vector plot of velocity profiles, Experiment 13: h=0.17 [m], Q=32.5 [l/s], L=0.7 [m]

C.1.2. Partly blocked

The velocity measurements for the partially blocked flow have been measured at fixed distances along the width of the flume and at the same longitudinal distances as the measurements with fully blocked flow. Figure C.5 gives a schematic overview where the velocity measurements have been performed. Both the actual distance and relative distances have been indicated.

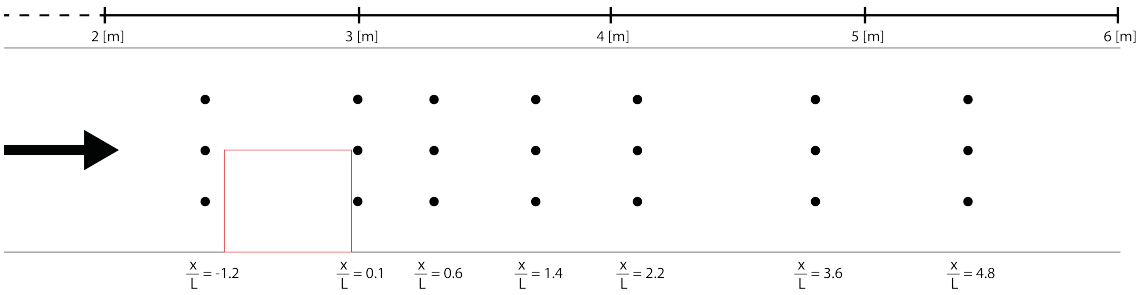

Figure C.5: Position of velocity measurements in the experiments with partially blocked flow

The velocity measurements of experiment 18 are less extensive due to the time restrictions of the experiments. As explained in chapter 3 the velocity measurements of each profile consists of approximately 10 individual measurements that require a measurement time of 3 minutes per measurement. Therefore each individual

profile takes approximately half an hour to measure. One can assume that performing these extensive measurements is very time consuming and therefore it is chosen to decrease the amount of measurements for experiment 18 as is clearly observed in figure C.7.

Although the profiles are less dense, the same behaviour is clearly observed and no distinct differences between the two experiments can be observed. The flow velocities are lower but the direction are mostly the same, except for the direction of the first two profiles in the blocked part of the flume. The profile at $[x/L]$=-1.2 is directed towards the right. The following profile at $[x/L] = 0.1$ is directed towards the left. This is completely opposite compared to experiment 16 but no explanation could be given.

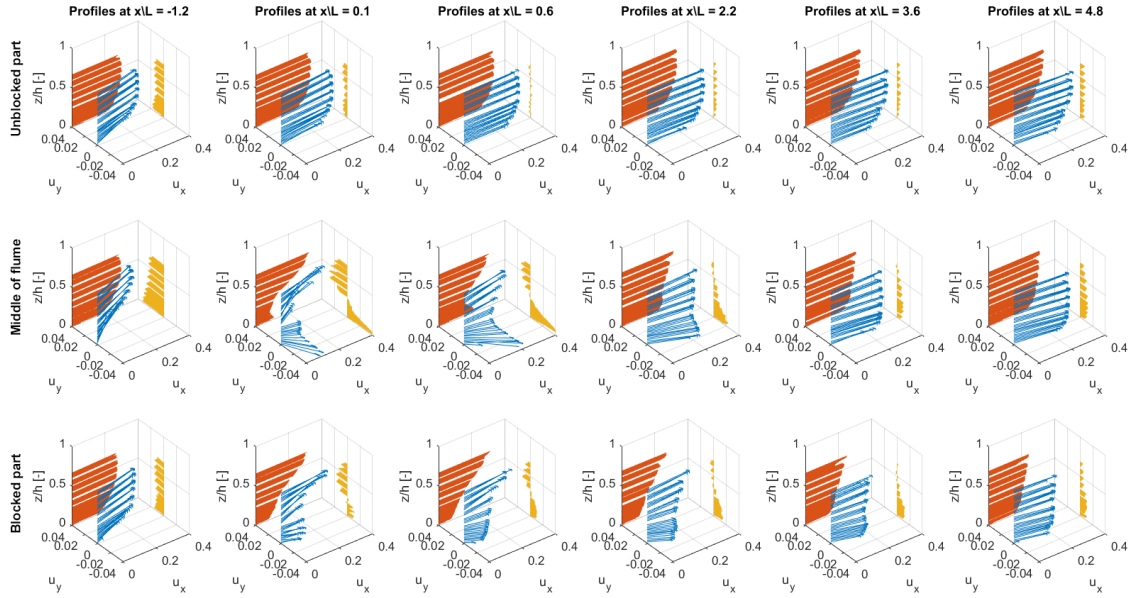

Figure C.6: Vector plot of velocity profiles, Experiment 16: h=0.17 [m], Q=32.5 [l/s], L=0.5 [m]

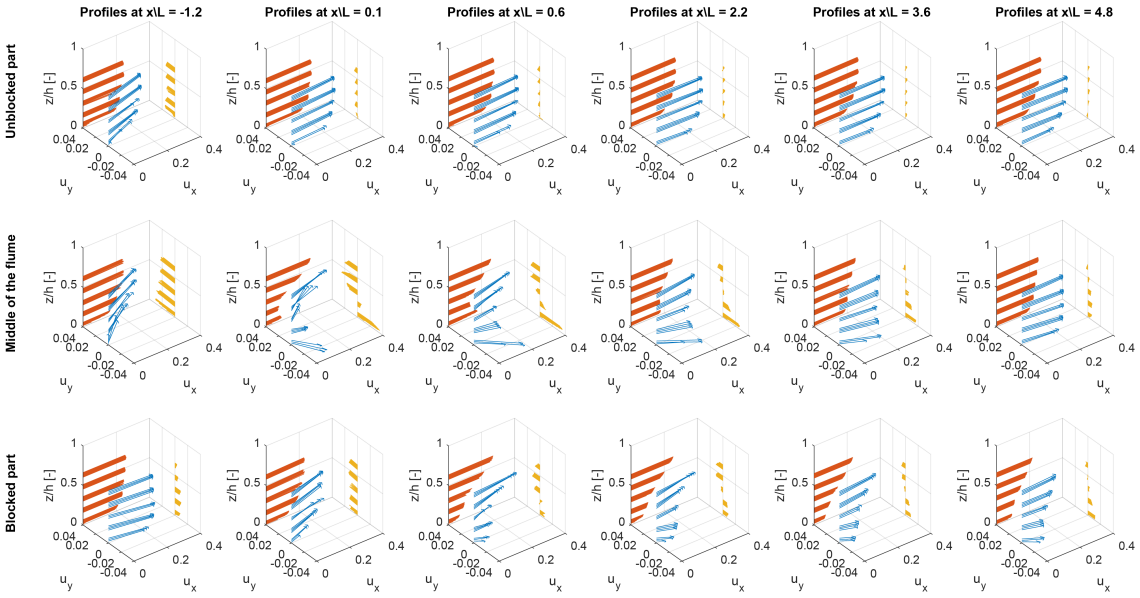

Figure C.7: Vector plot of velocity profiles, Experiment 18: h=0.17 [m], Q=25 [l/s], L=0.5 [m]

C.2. Water levels

C.2.1. Fully blocked

As was explained in section 4.2.4 the energy losses over the porcupines are larger for experiments with smaller depths, higher discharges and higher field densities. The figures below give all measured water levels of all performed experiments with a fully blocked flow. As can be observed not all measurements show the same measurment error, but for all experiments in hold that the error is in the order of tenths of millimetres.

Water level difference

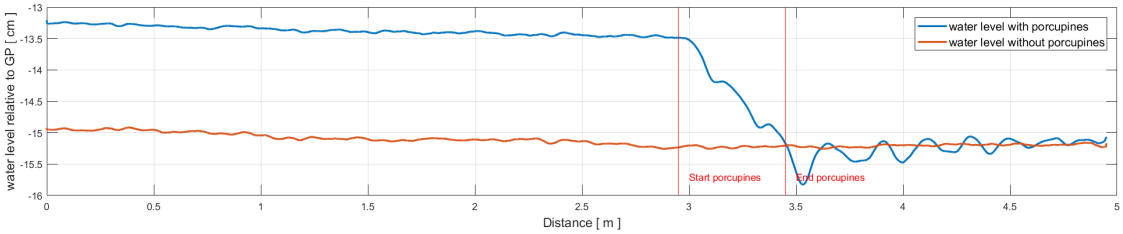

Figure C.8: Vector plot of velocity profiles, Experiment 8: h=0.11 [m], Q=32.5 [l/s], L=0.5 [m]

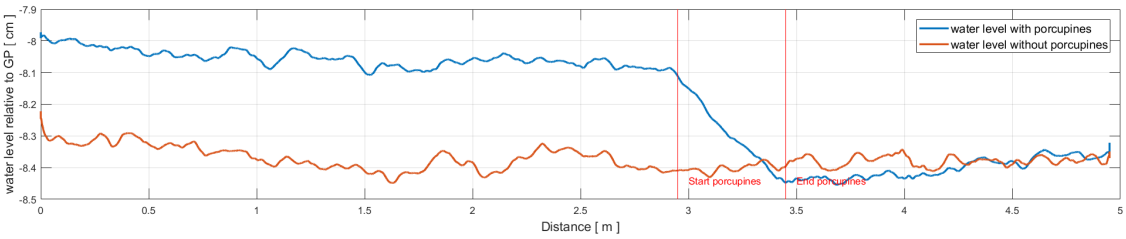

Figure C.9: Vector plot of velocity profiles, Experiment 9: h=0.17 [m], Q=32.5 [l/s], L=0.5 [m]

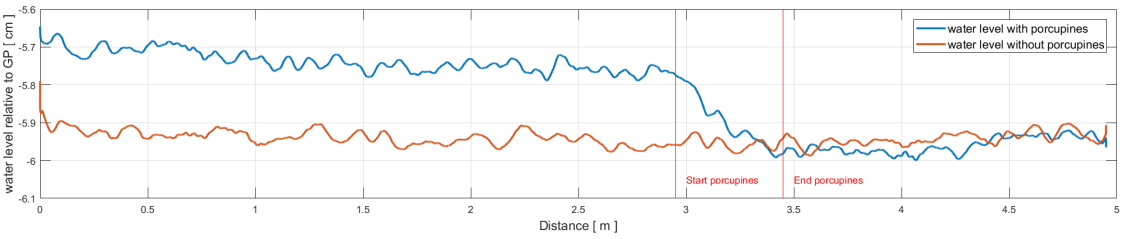

Figure C.10: Vector plot of velocity profiles, Experiment 10: h=0.20 [m], Q=32.5 [l/s], L=0.5 [m]

Discharge difference

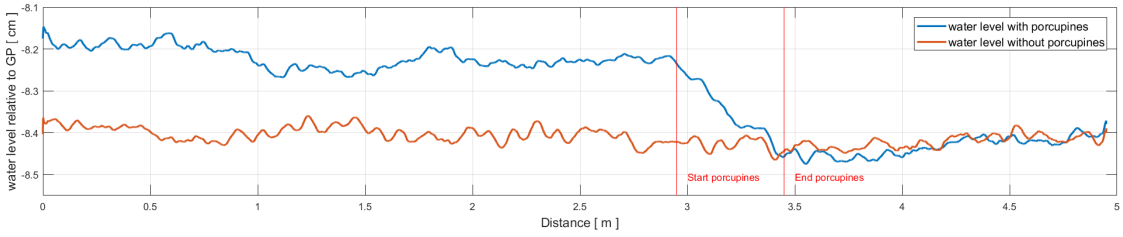

Figure C.11: Vector plot of velocity profiles, Experiment 11: h=0.17 [m], Q=25 [l/s], L=0.5 [m]

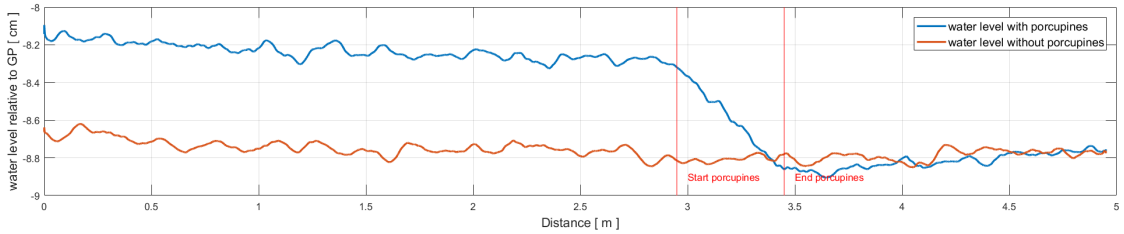

Figure C.12: Vector plot of velocity profiles, Experiment 12: h=0.17 [m], Q=40 [l/s], L=0.5 [m]

Density difference

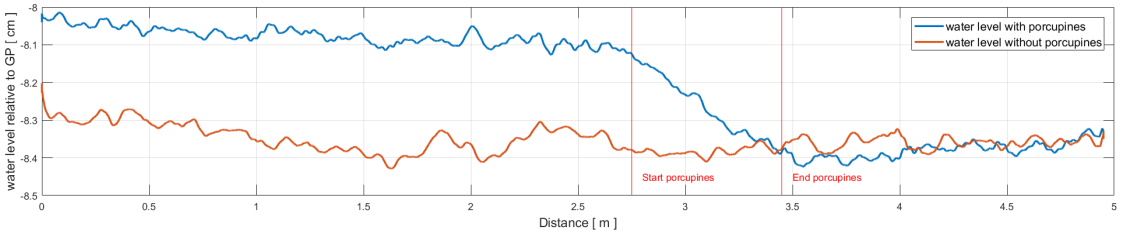

Figure C.13: Vector plot of velocity profiles, Experiment 13: h=0.17 [m], Q=32.5 [l/s], L=0.7 [m]

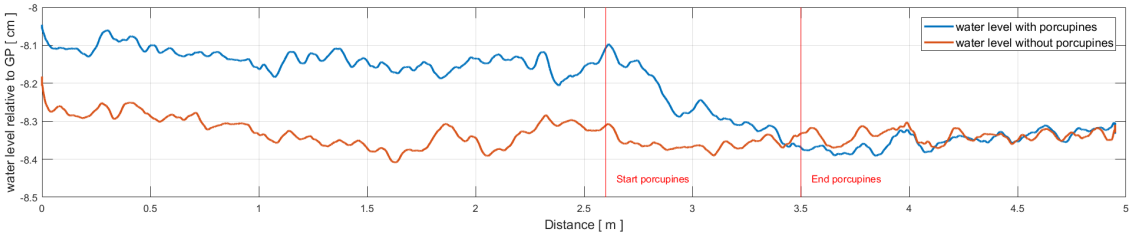

Figure C.14: Vector plot of velocity profiles, Experiment 14: h=0.17 [m], Q=32.5 [l/s], L=0.9 [m]

C.2.2. Partly blocked

The water levels in the partially blocked experiments is less affected than the fully blocked experiments which has also been elaborated in section 4.2.4. Interestingly however, it is observed that for increasing water depths, the effect on the water level is stretched over a longer distance for the partially blocked experiments. This can clearly be observed in figures C.15, C.16 and C.17.

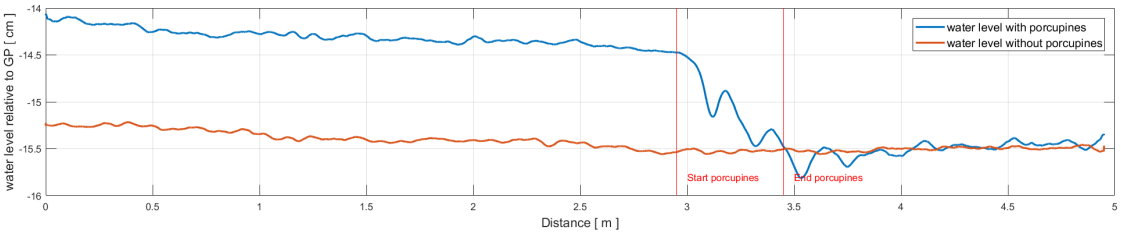

Figure C.15: Vector plot of velocity profiles, Experiment 15: h=0.11 [m], Q=32.5 [l/s], L=0.5 [m]

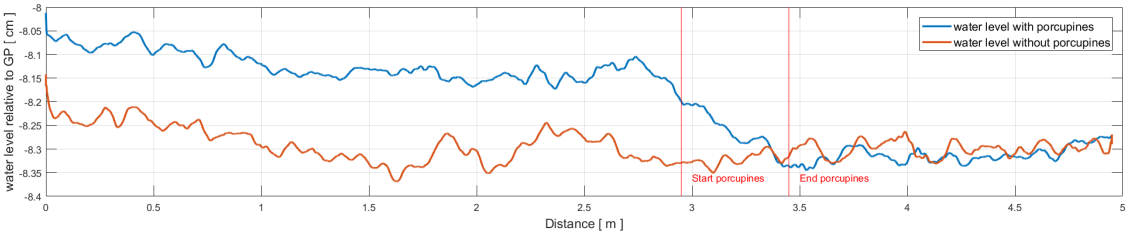

Figure C.16: Vector plot of velocity profiles, Experiment 16: h=0.17 [m], Q=32.5 [l/s], L=0.5 [m]

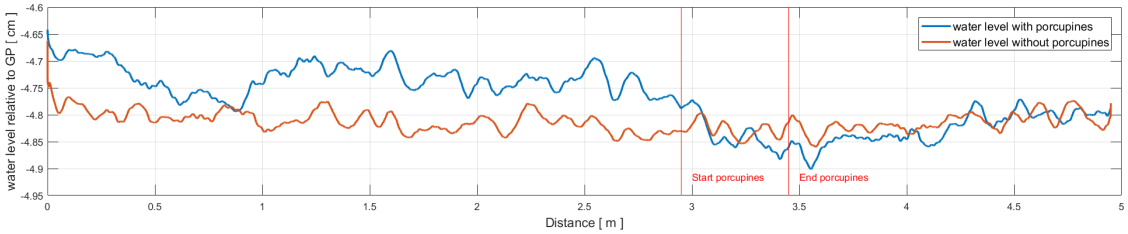

Figure C.17: Vector plot of velocity profiles, Experiment 17: h=0.20 [m], Q=32.5 [l/s], L=0.5 [m]

Like in the fully blocked experiments, increasing discharges also increase the energy losses. Similar to the observations with varying water levels with partially blocked flows, the effect is stretched over a longer distance with increasing flow velocities. This indicates that the deflection effect of porcupines is felt further upstream with increasing flow velocities in case of partly blocked flow. This effect is not observed in fully blocked flow.

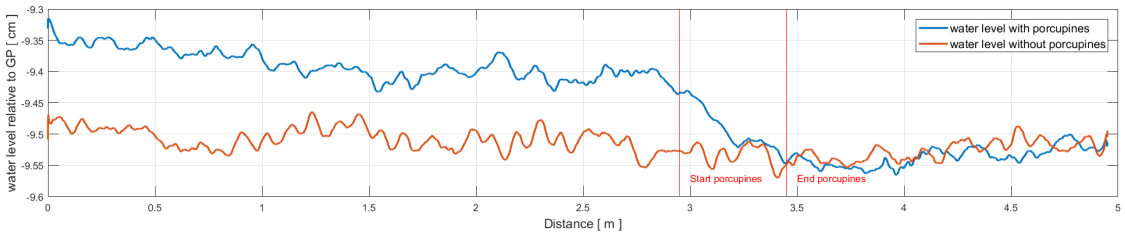

Figure C.18: Vector plot of velocity profiles, Experiment 18: h=0.17 [m], Q=25 [l/s], L=0.5 [m]

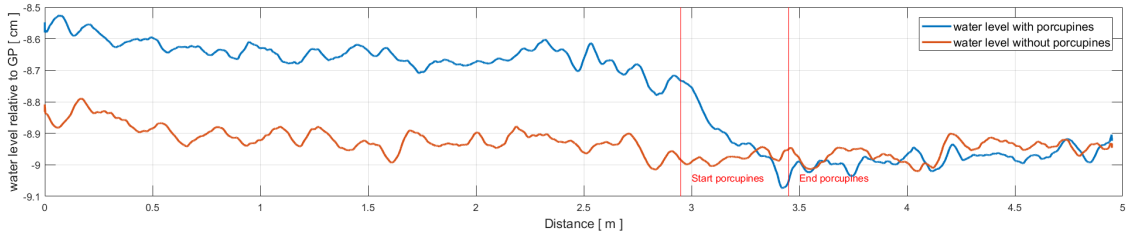

Figure C.19: Vector plot of velocity profiles, Experiment 18: h=0.17 [m], Q=40 [l/s], L=0.5 [m]

C.3. Turbulence

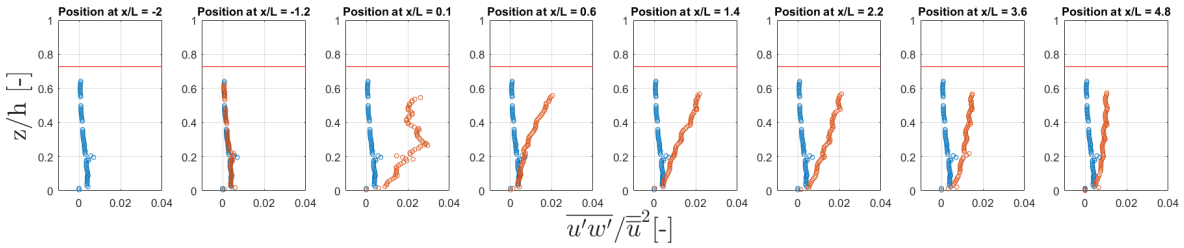

Figure C.20: Turbulence intensities, Experiment 8: h=0.11 [m], Q=32.5 [l/s], L=0.5 [m]

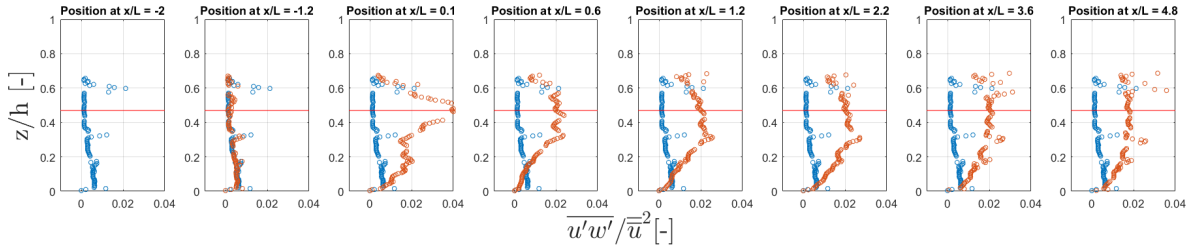

Figure C.21: Turbulence intensities, Experiment 9: h=0.17 [m], Q=32.5 [l/s], L=0.5 [m]

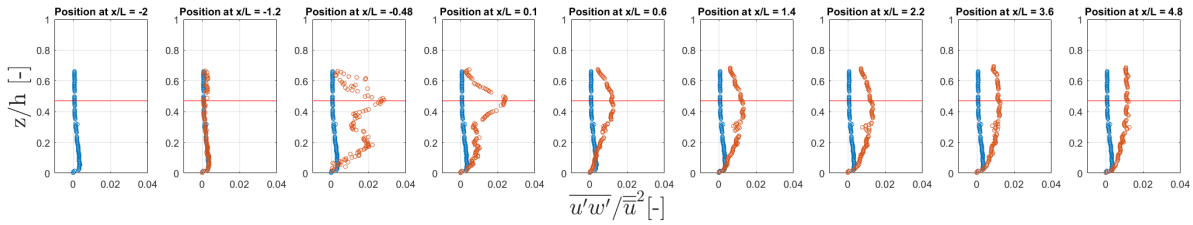

Figure C.22: Turbulence intensities, Experiment 11: h=0.17 [m], Q=25 [l/s], L=0.5 [m]

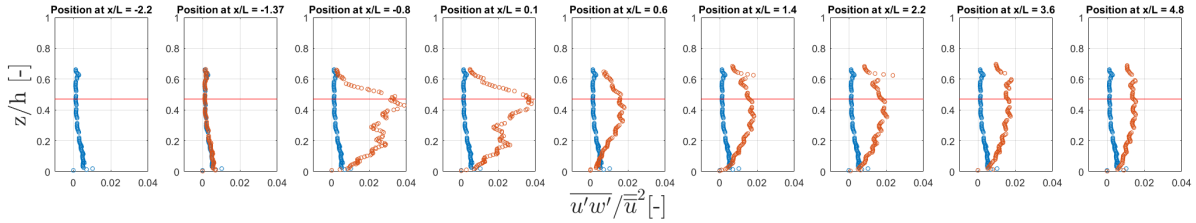

Figure C.23: Turbulence intensities, Experiment 13: h=0.17 [m], Q=32.5 [l/s], L=0.7 [m]

D

Mobile-bed experiments

In this appendix the results from the mobile-bed experiments are given. First the velocity profiles are given for only the fully blocked experiments for multiple moments in time. In the second section the bathymetry update over time for all experiments are presented to illustrate morphological developments. This is shown for both the fully blocked and partly blocked experiments.

D.1. Velocity profiles

D.1.1. Fully blocked

Experiment 1

In section 5.1 it was already mentioned that measurement errors occurred in the mobile-bed experiments due to migration of bedforms. Especially in experiment 1 where high flow velocities resulted in fast migration rates the velocity profiles are significantly retarded by the flow deflection over ripples. Besides, the measurements are vertically shifted if, during the measurement of a single profile, a ripple has migrated directly below the ADV. The result is that almost no profiles end at the same level in the plots, while in reality they have al been measured until the exact same level in the flume.

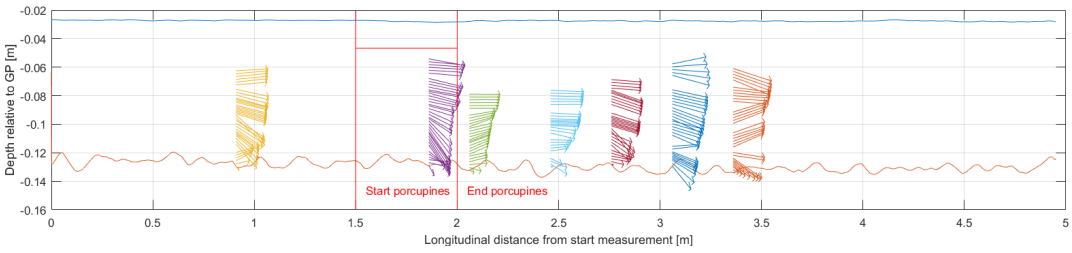

Figure D.1: Vector plot of velocity profiles at start of experiment 1: h=0.11 [m], Q=32.5 [l/s], L=0.5 [m]

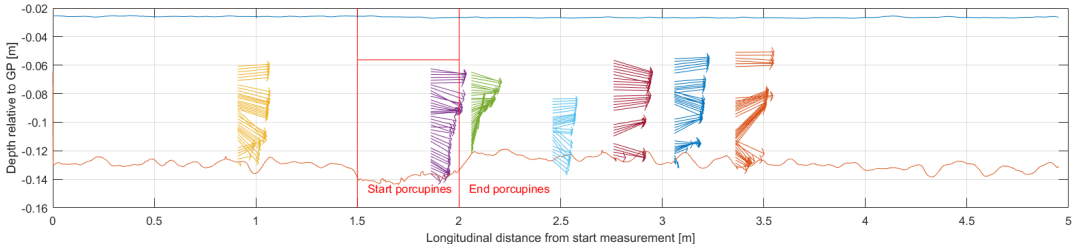

Figure D.2: Vector plot of velocity profiles after 24 hours, Experiment 1: h=0.11 [m], Q=32.5 [l/s], L=0.5 [m]

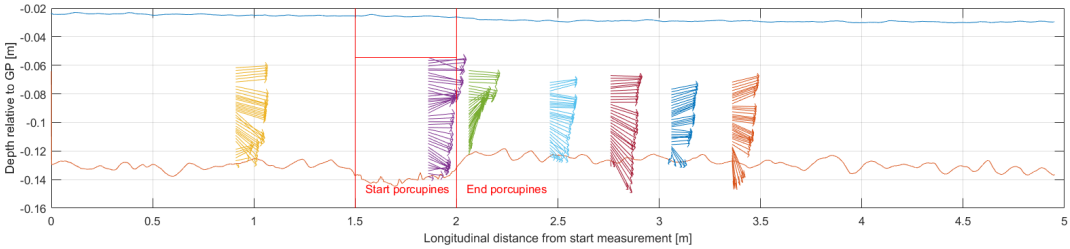

Figure D.3: Vector plot of velocity profiles after 72 hours, Experiment 1: h=0.11 [m], Q=32.5 [l/s], L=0.5 [m]

Experiment 2

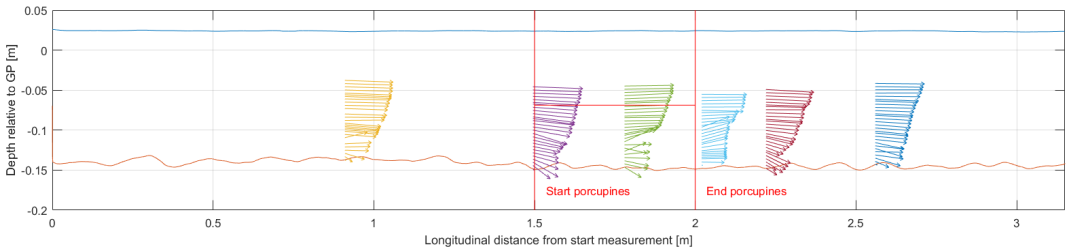

Figure D.4: Vector plot of velocity profiles at start of experiment 2: h=0.17 [m], Q=32.5 [l/s], L=0.5 [m]

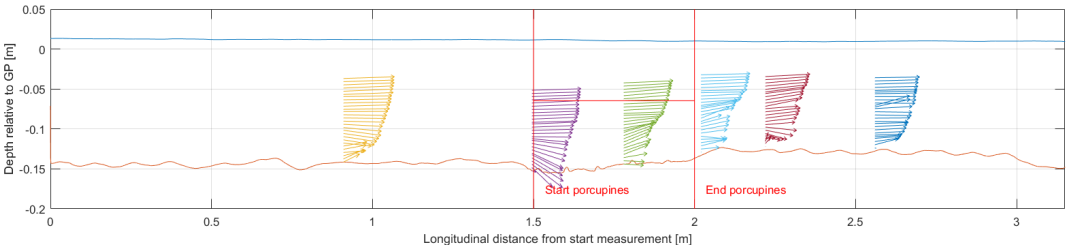

Figure D.5: Vector plot of velocity profiles after 24 hours, Experiment 2: h=0.17 [m], Q=32.5 [l/s], L=0.5 [m]

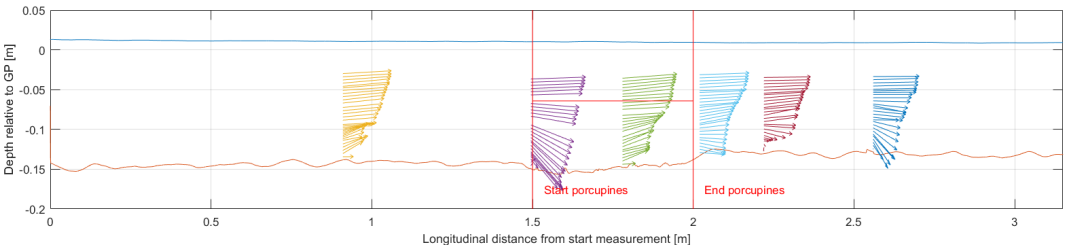

Figure D.6: Vector plot of velocity profiles after 72 hours, Experiment 2: h=0.17 [m], Q=32.5 [l/s], L=0.5 [m]

Experiment 3

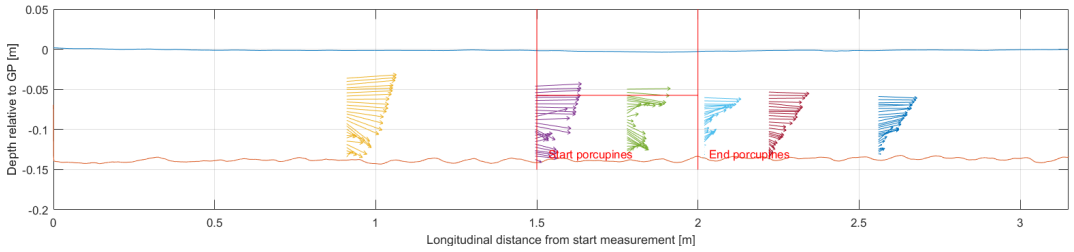

Figure D.7: Vector plot of velocity profiles at start of experiment 3: h=0.17 [m], Q=25 [l/s], L=0.5 [m]

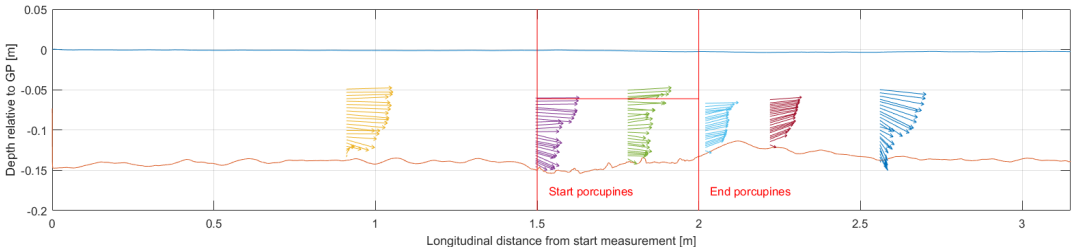

Figure D.8: Vector plot of velocity profiles after 24 hours, Experiment 3: h=0.17 [m], Q=25 [l/s], L=0.5 [m]

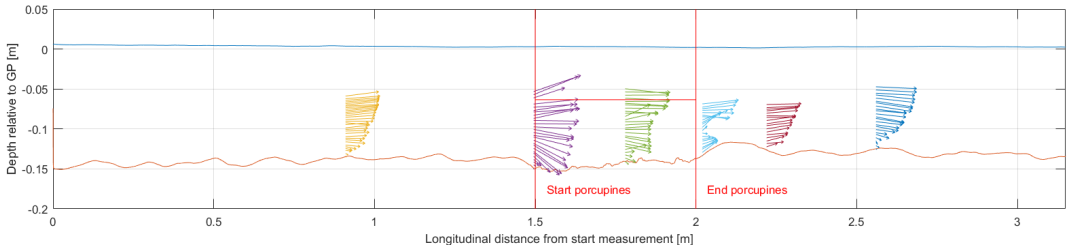

Figure D.9: Vector plot of velocity profiles after 48 hours, Experiment 3: h=0.17 [m], Q=25 [l/s], L=0.5 [m]

Experiment 4

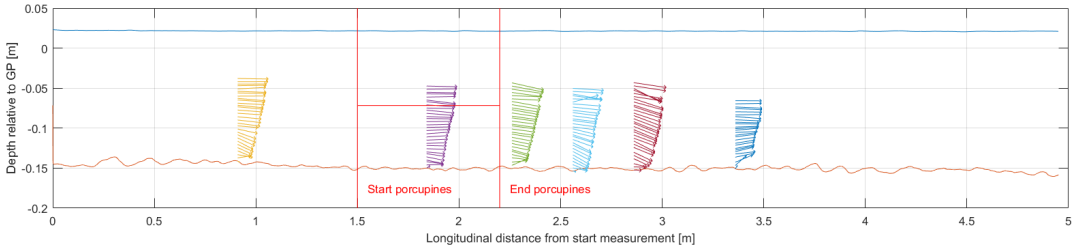

Figure D.10: Vector plot of velocity profiles at start of experiment 4: h=0.17 [m], Q=32.5 [l/s], L=0.7 [m]

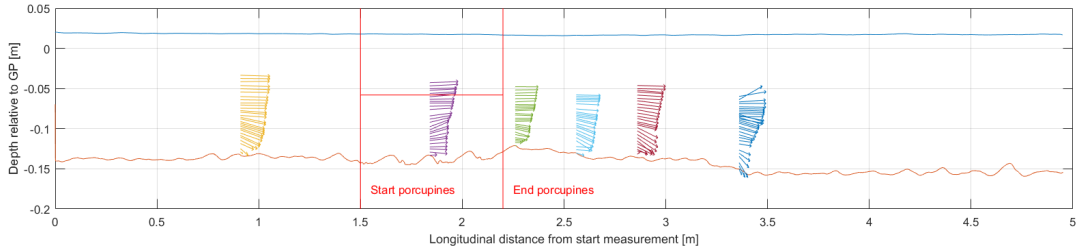

Figure D.11: Vector plot of velocity profiles after 72 hours, Experiment 4: h=0.17 [m], Q=32.5 [l/s], L=0.7 [m]

D.2. Bathymetry

D.2.1. Fully blocked

Experiment 1

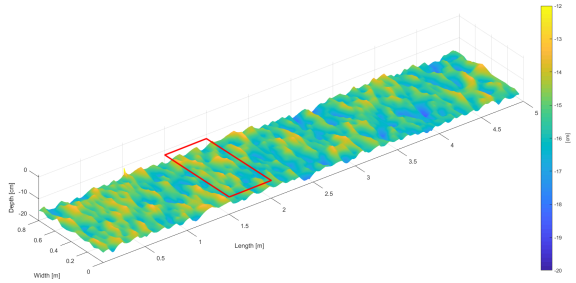

Figure D.12: Initial bathymetry of experiment 1

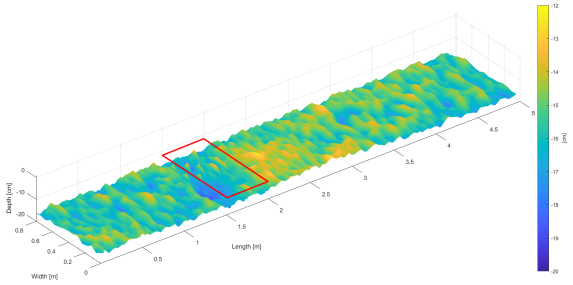

Figure D.13: Bathymetry after 5 hours of experiment 1

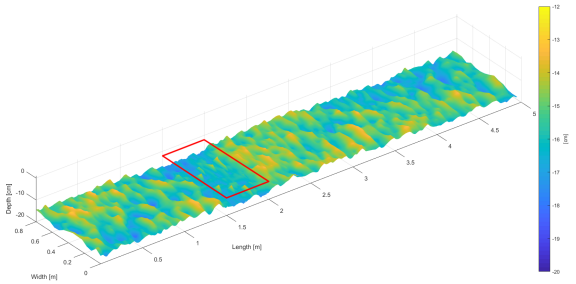

Figure D.14: Bathymetry after 24 hours of experiment 1

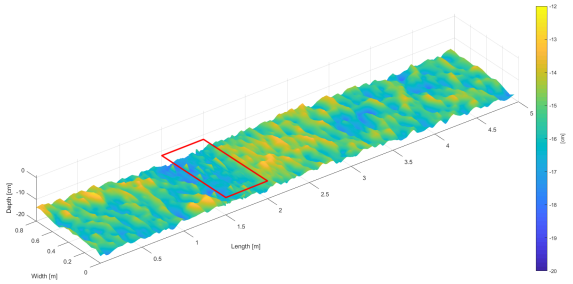

Figure D.15: Bathymetry after 48 hours of experiment 1

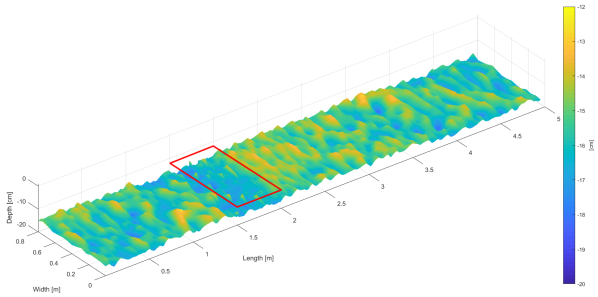

Figure D.16: Bathymetry after 72 hours of experiment 1

As was stated in section 5.2.1 the amount of sedimentation in experiment 1 was decreasing. The sedimentation volume also decreased and this is also observed in these figures. In chapter 7 it is discussed whether any form of erosion downstream of the porcupines is observed. For most experiments it holds that this is not the case, however for experiment 1 it is noted that some erosion is measured. Although this is no significant

erosion, figures D.14 and D.15 indicates a dark blue area at a length of approximately 3.5 metres. However after 72 hours this erosion spot is removed again.

Experiment 2

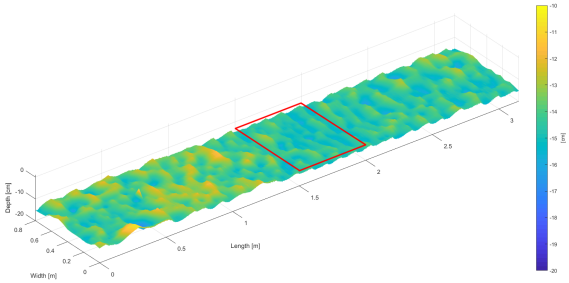

Figure D.17: Initial bathymetry of experiment 2

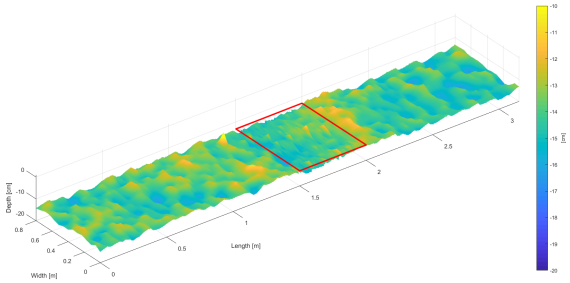

Figure D.18: Bathymetry after 5 hours of experiment 2

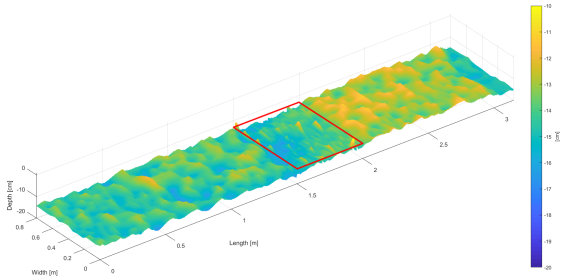

Figure D.19: Bathymetry after 24 hours of experiment 2

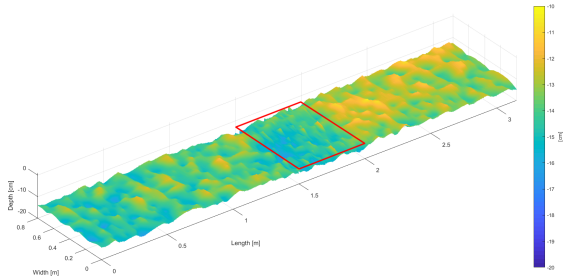

Figure D.20: Bathymetry after 48 hours of experiment 2

Experiment 3

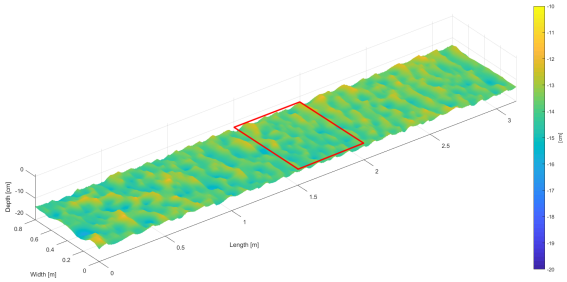

Figure D.21: Initial bathymetry of experiment 3

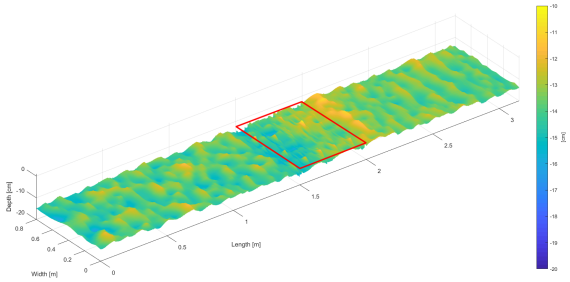

Figure D.22: Bathymetry after 5 hours of experiment 3

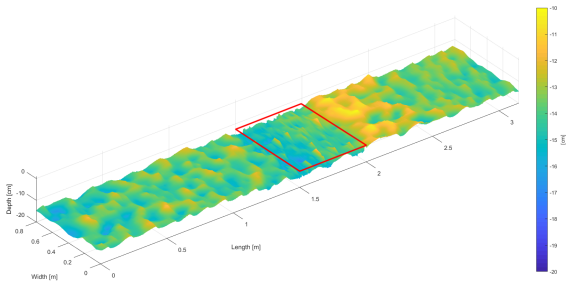

Figure D.23: bathymetry after 24 hours of experiment 3

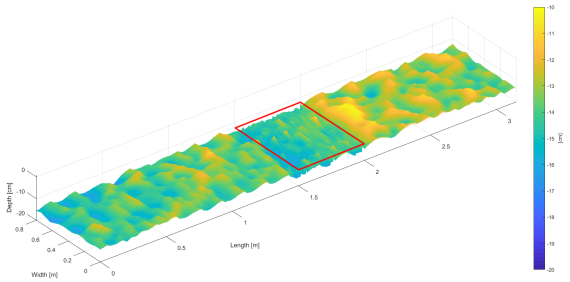

Figure D.24: Bathymetry after 48 hours of experiment 3

Experiment 4

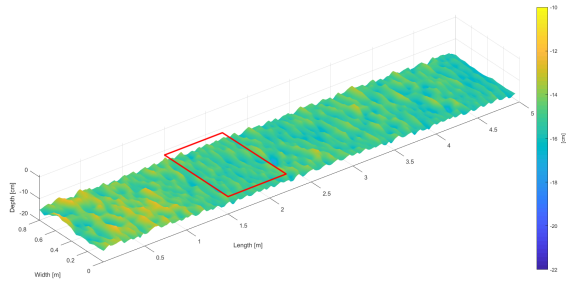

Figure D.25: Initial bathymetry of experiment 4

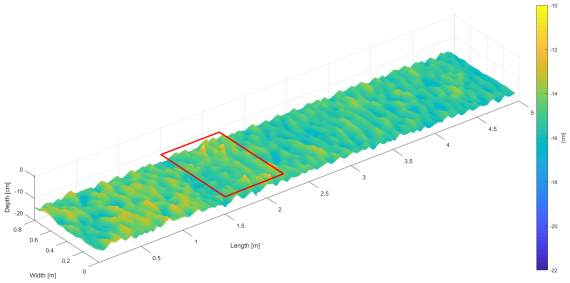

Figure D.26: Bathymetry after 5 hours of experiment 4

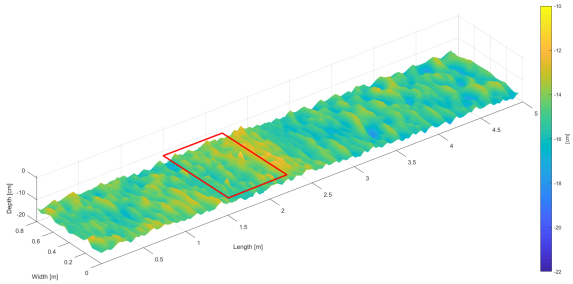

Figure D.27: Bathymetry after 24 hours of experiment 4

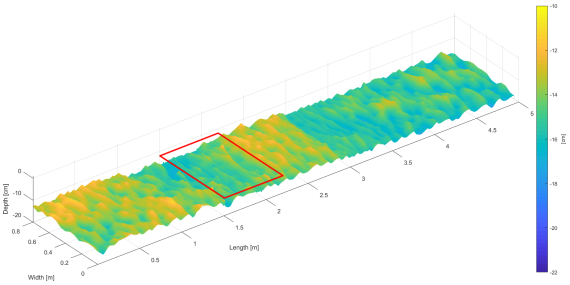

Figure D.28: Bathymetry after 48 hours of experiment 4

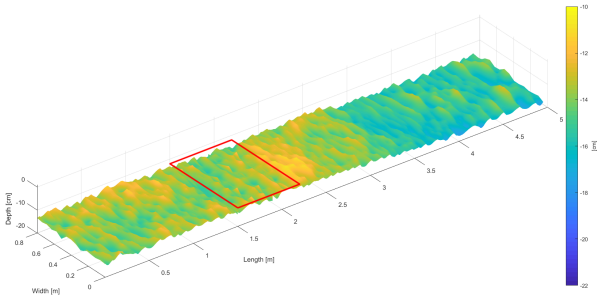

Figure D.29: Bathymetry after 72 hours of experiment 4

D.2.2. Partly blocked

Experiment 5

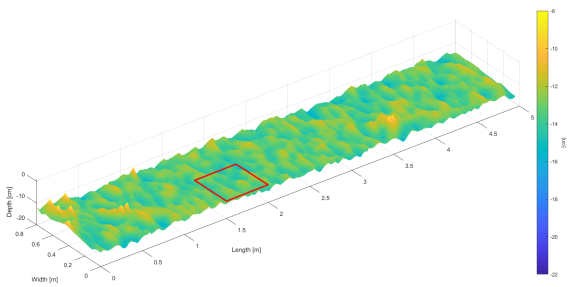

Figure D.30: Initial bathymetry of experiment 5

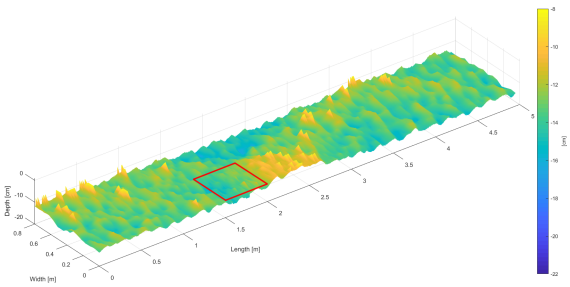

Figure D.31: Bathymetry after 5 hours of experiment 5

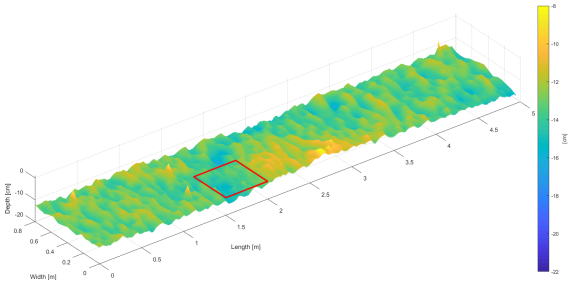

Figure D.32: Bathymetry after 24 hours of experiment 5

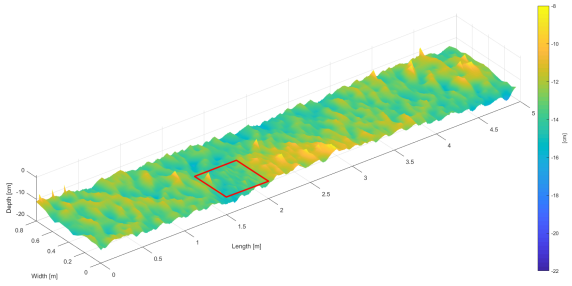

Figure D.33: Bathymetry after 48 hours of experiment 5

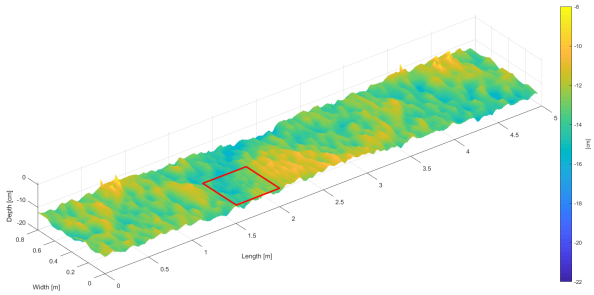

Figure D.34: Bathymetry after 72 hours of experiment 5

Experiment 6

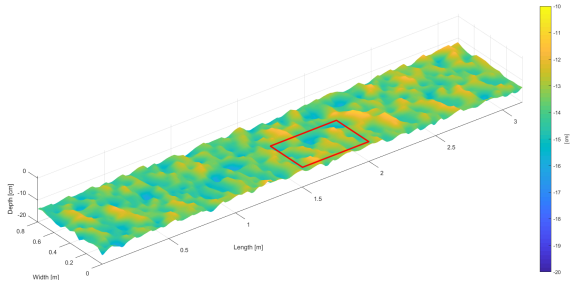

Figure D.35: Initial bathymetry of experiment 6

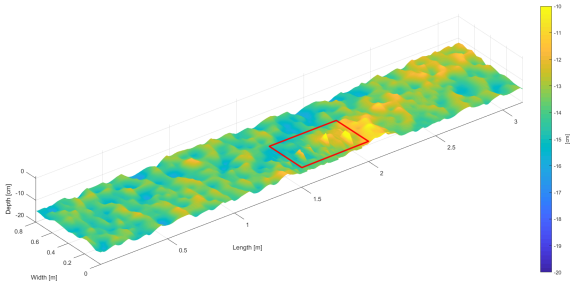

Figure D.36: Bathymetry after 5 hours of experiment 6

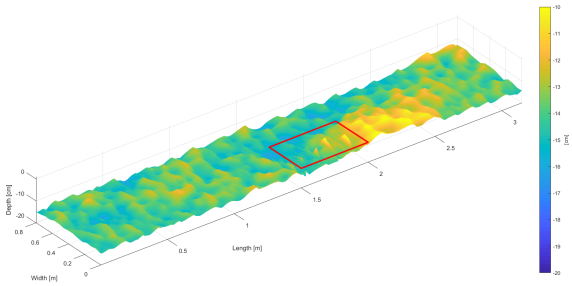

Figure D.37: Bathymetry after 24 hours of experiment 6

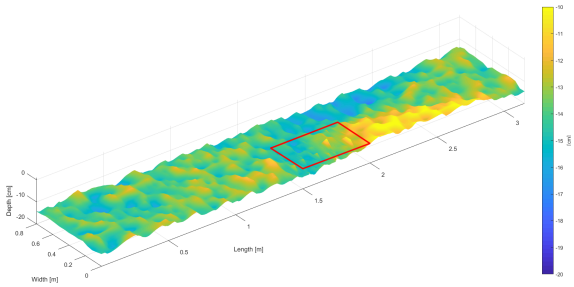

Figure D.38: Bathymetry after 48 hours of experiment 6

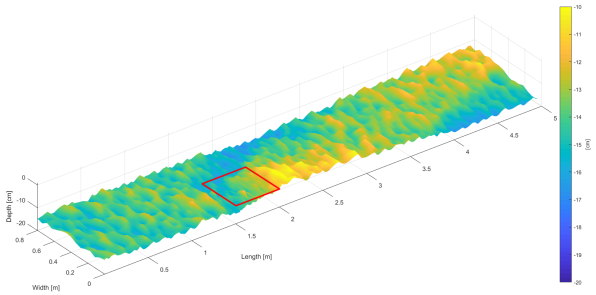

Figure D.39: Bathymetry after 72 hours of experiment 6

Experiment 7

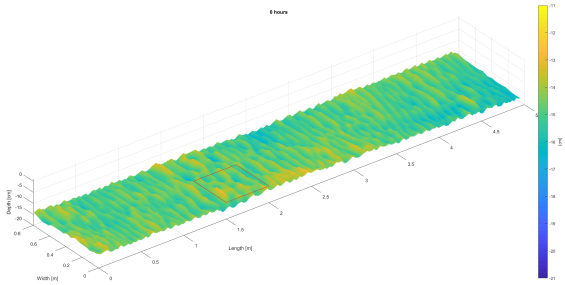

Figure D.40: Initial bathymetry of experiment 7

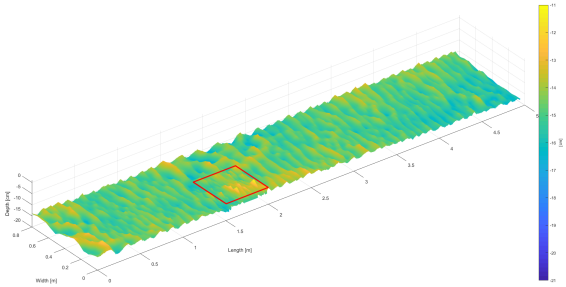

Figure D.41: Bathymetry after 5 hours of experiment 7

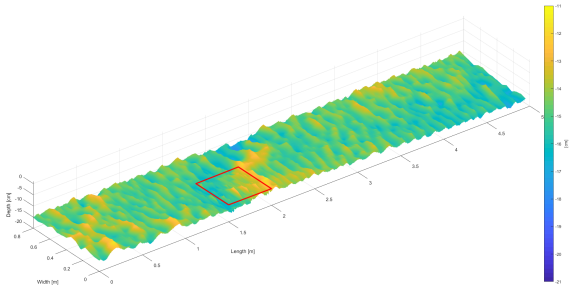

Figure D.42: Bathymetry after 24 hours of experiment 7

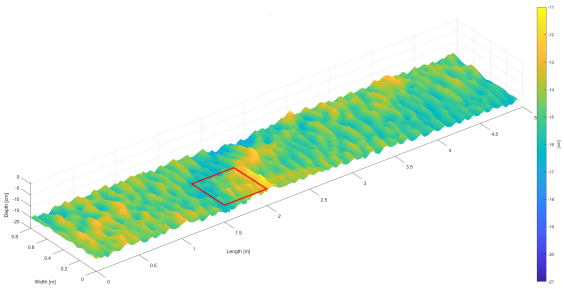

Figure D.43: Bathymetry after 48 hours of experiment 7

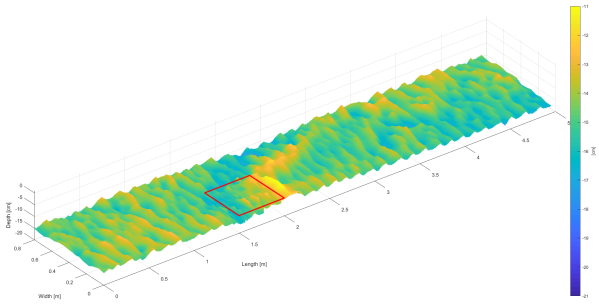

Figure D.44: Bathymetry after 72 hours of experiment 7

E

Additional analysis

In this appendix complimentary analysis are provided for all experiments that have not been shown in the main report. The computed Chézy values are applied in SOBEK and compared to all measured water levels, also for the mobile-bed experiments although the quality of the data is limited.

E.1. Water level fit to model outcomes

As was mentioned in section 6.1.4 not all water levels could be fitted to the computed water levels by the computer model SOBEK due to a roughness restriction in the model. Especially for experiments with higher flow velocities a large deviation from the maximum roughness by the model is therefore observed. However, for experiments where the Chézy coefficient was higher than 10 relative good water level fits were obtained.

E.1.1. Fixed-bed experiments

Water level difference

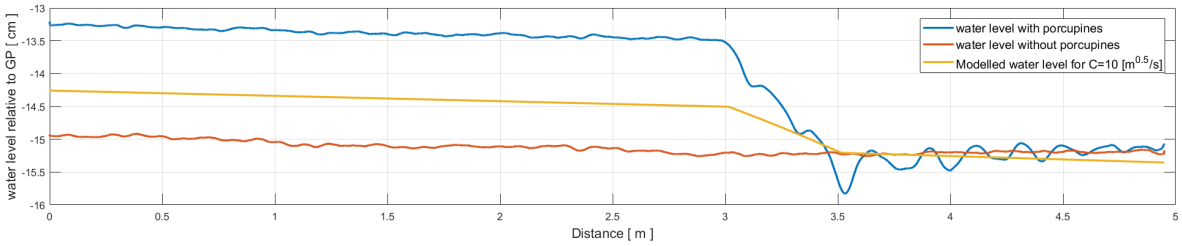

Figure E.1: Water level comparison with SOBEK, Experiment 9: h=0.11 [m], Q=32.5 [l/s], L=0.5 [m]

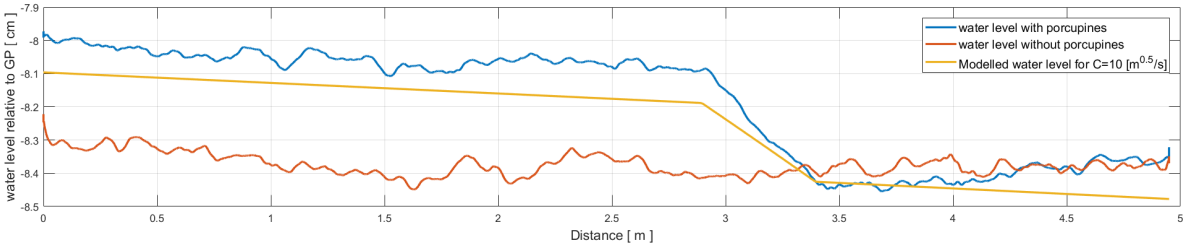

Figure E.2: Water level comparison with SOBEK, Experiment 9: h=0.17 [m], Q=32.5 [l/s], L=0.5 [m]

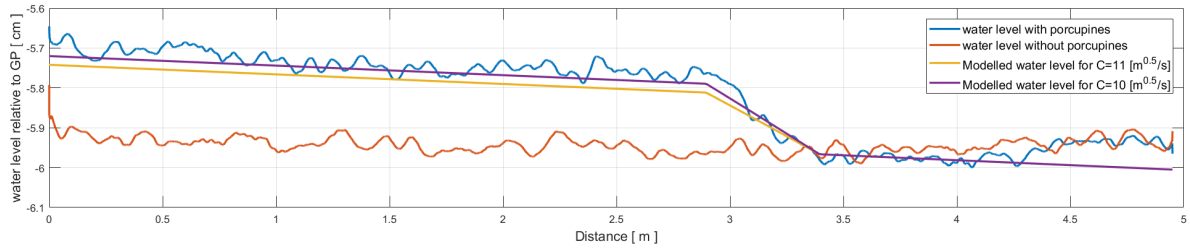

Figure E.3: Water level comparison with SOBEK, Experiment 10: h=0.20 [m], Q=32.5 [l/s], L=0.5 [m]

Discharge difference

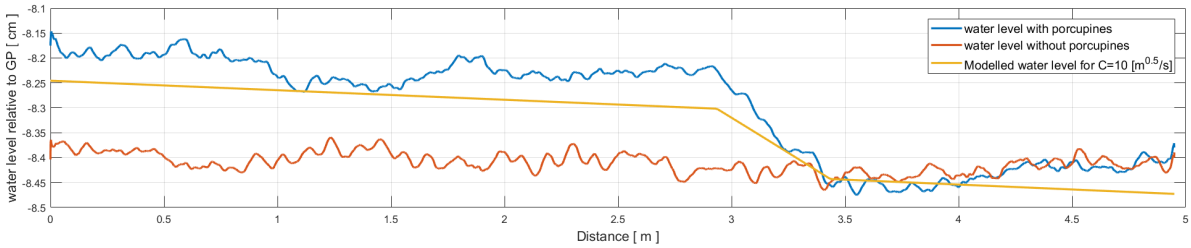

Figure E.4: Water level comparison with SOBEK, Experiment 11: h=0.17 [m], Q=25 [l/s], L=0.5 [m]

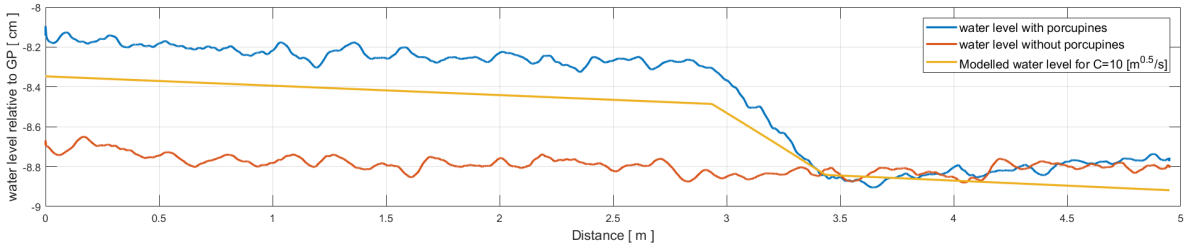

Figure E.5: Water level comparison with SOBEK, Experiment 12: h=0.17 [m], Q=40 [l/s], L=0.5 [m]

Although the formulation for the representative roughness of porcupines does not include the flow velocity it is observed that higher flow velocities result in a larger roughness of the porcupines. Indirectly the flow velocities are incorporated in the formulation by means of the drag coefficient which is dependent on the flow velocity. However, the drag coefficient is determined by fitting all measurements on a single line from which individual experiments may deviate. This data fitted line is used to determine the drag coefficient for all experiments with the same density. This way the effect of different flow velocities is partly eliminated, resulting in a mismatch between the calculated roughness and the measured water levels. Unfortunately the roughness is limited in SOBEK, so it is not possible to find the correct Chézy roughness for varying flow velocities.

Density difference

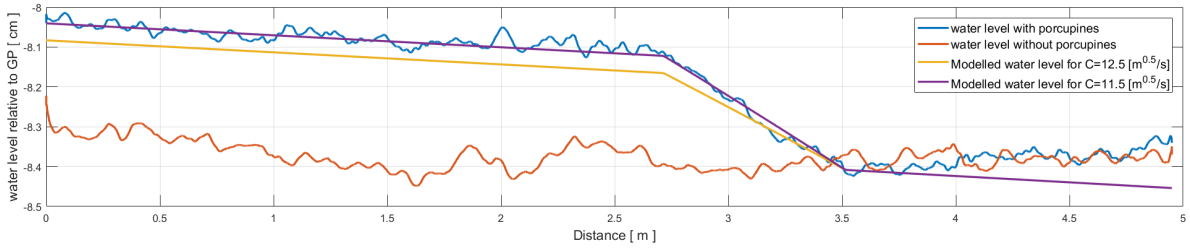

Figure E.6: Water level comparison with SOBEK, Experiment 13: h=0.17 [m], Q=32.5 [l/s], L=0.7 [m]

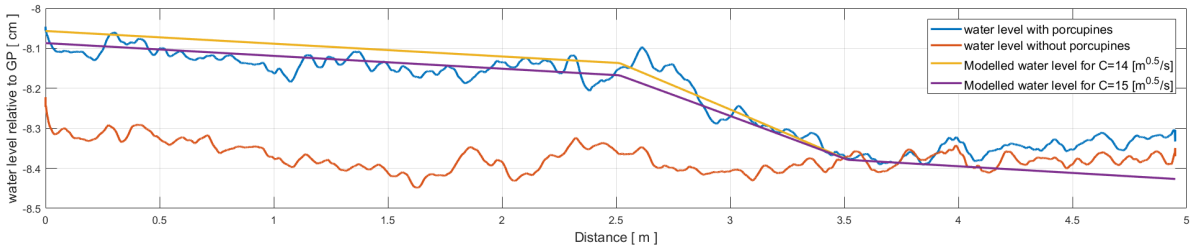

Figure E.7: Water level comparison with SOBEK, Experiment 13: h=0.17 [m], Q=32.5 [l/s], L=0.9 [m]

E.1.2. Mobile-bed experiments

In section 6.1.2 the representative roughness is determined for the fixed-bed experiments since the measurements of the mobile-bed experiments are relatively poor. Here an overview will be given of the determined roughness for the mobile-bed experiments and their comparison with the SOBEK model. Table E.1 gives an overview of the representative roughness values for the different experiments performed. Looking at the bed roughness it becomes clear that not all experiments were identical, and that bedforms affected the water differently in different experiments.

Table E.1: Representative roughness for mobile-bed experiments

Exp.	h [m]	Q [m^3/s]	u [m/s]	Longitudinal spacing [m]	ΔE [cm]	i_{wl} [-]	u_p [m/s]	τ_b [N/m^2]	τ_p [N/m^2]	τ_t [N/m^2]	C_b [m$^{1/2}$/s]	C_r [m$^{1/2}$/s]
1	0,1121	32,5	0,36	0,01	0,145	0,0029	0,26	1,04	3,061	4,101	34,59	16,185
2	0,1648	32,5	0,25	0,01	0,142	0,0028	0,23	0,82	3,993	4,817	27,28	16,178
3	0,1475	25	0,21	0,01	0,104	0,0021	0,16	0,50	1,932	2,435	34,9	15,628
4	0,1786	32,5	0,23	0,02	0,126	0,0018	0,21	0,58	3,328	3,908	30,02	16,946
5	0,1305	32,5	0,31	0,01	0,2	0,004	0,25	0,77	4,717	5,487	34,59	14,660
6	0,1601	32,5	0,25	0,01	0,166	0,0033	0,21	0,82	3,328	4,148	27,28	15,951
7	0,1618	25	0,19	0,01	0,113	0,0023	0,15	0,62	1,698	2,313	24,28	15,834

In experiment 1 it is observed that the bottom roughness reduces due to a lower water level and increased flow velocity. Although the derivation for the bottom roughness by the water level gradient resulted in a C_b of 34.5 [m$^{1/2}$/s], the model required a bottom roughness of 42 [m$^{1/2}$/s] to approximately match the measured water level slope. Besides the calculated Chézy roughness coefficient did not satisfy the measured local gradient over the porcupines. By trial and error a value of 13 [m$^{1/2}$/s] gave a satisfying fit for the porcupine roughness. This indicates that the porcupines indeed work less good compared to the fixed-bed experiments, but still result in a significant local roughness increase for low water level conditions.

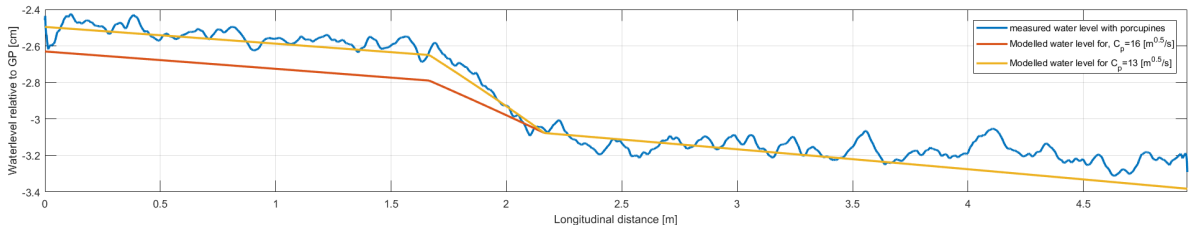

Figure E.8: Water level comparison between measurement and model outcome, with model $C_b = 38\text{m}^{1/2}$/s, Experiment 1

The water level measurements for experiment 2 were less accurate and therefore larger errors in the measurement are present. The bottom roughness seems to be calculated relatively well, and is much rougher compared to experiment 1. However no clear fit could be obtained for the porcupine roughness it is approximated to be in the order of 12 [m$^{1/2}$/s]. This is again lower than calculated in table E.1, which indicates that the velocity measurements inside the porcupine field are less accurate. This was indeed observed and explained in section 7.1.3 and limits the usefulness of the mobile-bed experiments.

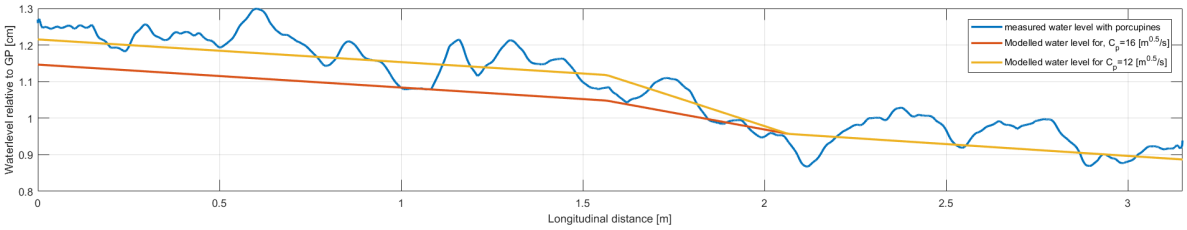

Figure E.9: Water level comparison between measurement and model outcome, with model $C_b = 27\mathrm{m}^{1/2}/\mathrm{s}$, Experiment 2

Experiment 4 gave a relatively good fit to the measurements however the bed roughness has been reduced to match the observed water levels slightly. Furthermore, the observed and calculated roughness of the porcupine field gave a real good match with the calculated water level profile by SOBEK.

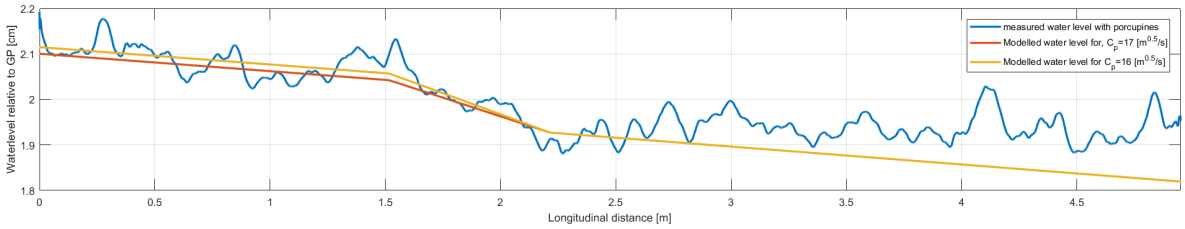

Figure E.10: Water level comparison between measurement and model outcome, with model $C_b = 34\mathrm{m}^{1/2}/\mathrm{s}$, Experiment 4

Based on these measurements it is clear that porcupines work less good in case of a mobile bed. The roughness is significantly lower in case of fixed-bed experiments. Still, the porcupines show an increased roughness and will affect the water level but far less than in the fixed-bed experiments. Taking a look at ΔE in table E.1 it is can be noted that the water level differences over the porcupine field are much smaller than compared to the water level differences as given for the fixed-bed experiments in table 6.2.